

COLLECTED PAPERS
ON
COHERENT QUANTUM OPTICS AND TECHNOLOGY

Volume 8

August 1992—July 1993

Professor

Motoichi OHTSU

TOKYO INSTITUTE OF TECHNOLOGY

Interdisciplinary Graduate School of Science and Engineering

4259 Nagatsuta, Midori-ku, Yokohama,

Kanagawa 227, JAPAN

各位殿

拝啓 時下ますますご清祥のこととお慶び申し上げます。

さて、このたび、前回に引き続きまして、最近の私どもの発表論文をまとめましたので、ここにお送り致します。よろしくご査収下されば幸いです。いずれも未熟な論文ばかりでございますので、ご意見、ご批評を賜ればと、お待ちしております。

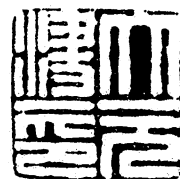
なお、本年度より（財）神奈川科学技術アカデミー（KAST）において「フォトン制御」プロジェクトが発足しました。5年間は東京工業大学とKASTとを兼務致します。高コヒーレントレーザシステム、フォトンSTMシステムの基礎と応用に関してKASTでも研究に従事致しますので今後ともご指導ご鞭撻のほど、宜しくお願い申し上げます。

敬具

平成5年8月

東京工業大学総合理工学研究科

大津 元一



PREFACE

In order to realize the ultimate status of light and matter, M. Ohtsu aims at the following three research subjects:

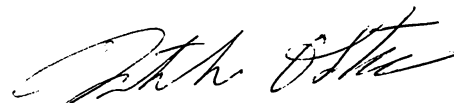
- (1) Laser frequency control.
- (2) Application of highly coherent semiconductor lasers.
- (3) Photon scanning tunneling microscope.

The papers related to the subject (1) cover several progresses in the study on one Peta-Hertz hyper-coherent optical frequency sweep generator, optical frequency comb generator for highly accurate optical frequency counting, nonlinear optical frequency conversion, high- T_c oxide super-conducting film for an ultrafast photo-detector, and frequency stabilization of a LD-pumped YAG laser for gravitational wave detection. The subject (2) is for developing commercial products of a passive ring resonator-type fiber gyroscope and a LD-pumped rubidium atomic clock, which are supported by Research Development Corporation of Japan (JRDC) with the cooperation of industries. The subject (3) is for developing a chemical etching technology of optical fiber probes, study on local photo-induced chemical reaction and its application to high density optical storage, and proposal of virtual photon model for analyzing primary process of a photon STM. The final goal of the subject (3) is the manipulation of a single neutral atom by using an optical fiber probe as an optical tweezer. The results of its preliminary experiment will be reviewed in the forthcoming volume.

A "PHOTON CONTROL" project, directed by M. Ohtsu, started at April, 1993 as an five-year research project of the Kanagawa Academy of Science and Technology^(*). The research subjects of this project covers (1) and (3) described above. The main mission of this project is not only the basic research but also the technical transfer of the result of the basic research to the industry. Six research staff members including three visiting

scientists from industry are engaged in these subjects in cooperation with M. Ohtsu's coworkers of Tokyo Institute of Technology.

August 1993



Motoichi OHTSU

(*) Address: Kanagawa Academy of Science and Technology
3-2-1 Sakado, Takatsu-ku, Kawasaki-shi, Kanagawa
213, Japan

Phone: 044-819-2071

Fax: 044-819-2072

(**) Back numbers of the collected papers are still available on request.

MEMBERS

Professor

Motoichi OHTSU (Dr. Eng.)^{a)}

Research Associate

Ken'ichi NAKAGAWA (Dr. Sci.)^{b)}

Motonobu KOUROGI (Dr. Eng.)^{b)} (04/1993 -)

Graduate Students (Doctor Candidates)

Motonobu KOUROGI (M. Eng.) (- 03/1993)

Mituru MUSHA (M. Sci.)

Togar PANGARIBUAN (M. Eng.)

Weizhi WANG (M. Eng.)

Yoshinari AWAJI (M. Eng.) (04/1993 -)

Yasunobu TODA (M. Eng.) (04/1993 -)

Graduate Students (Master Course)

Yoshinari AWAJI (B. Eng.) (- 03/1993)

Yasunobu TODA (B. Eng.) (- 03/1993)

Yukitaka SHIMIZU (B. Eng.)^{c)} (- 03/1993)

Madoka KAWAI (B. Eng.)^{d)} (- 03/1993)

Takeshi KATSUTA (B. Sci.)

Mikio KOZUMA (B. Sci.)

Shuji SAYAMA (B. Eng.)

Yutaka IMAI (B. Sci.)

Takashi ENAMI (B. Eng.)

Bambang WIDIYATMOKO (B. Eng.)

Undergraduate Students

Takeshi YAMASHITA^{e)} (- 03/1993)

Takeo UENO

Junichi ICHIHASI^{f)} (- 03/1993)

Takeshi ENAMI (- 03/1993)

Kazuhiro IMAI (04/1993 -)
Takeshi NAKATA (04/1993 -)
Takuya MATSUMOTO (04/1993 -)

Research Students

Toru IMAI^{g)}
Naoto KITABAYASHI^{h)} (- 03/1993)
Yoshito KOYAMAⁱ⁾ (- 03/1993)

Visiting Scientists

Shudong JIANG
Hisao OHSAWA^{j)} (- 03/1993)
Michel DE LABACHELERIE^{k)}
Vladmir Anatolyevich ALEKSEEV^{l)} (- 12/1992)
Alexander Michailovich AKULSHIN^{l)} (- 07/1993)
Vyacheslav Nikolayevich BARYSHEV^{m)}
Andrei Vasilyevich ZVYAGIN^{m)}
Alexander Sergeevich SHELKOVNIKOV^{l)} (04/1993 -)

Secretaries

Sanae OKAMOTO
Kaoru OGURA

- a) Also with Kanagawa Academy of Science and Technology
(Director, "Photon Control" Project)
- b) Also with Kanagawa Academy of Science and Technology
(Research staff member, "Photon Control" Project)
- c) Presently with Sharp Corp.
- d) Presently with Konica Corp.
- e) Presently with Graduate School, Tokyo Institute of Technology.
- f) Presently with Graduate School, Tokyo University.
- g) Permanent affiliation : Tokyo Aircraft Instrument Co. Ltd.,
Tokyo, Japan.

- h) Permanent affiliation : Nihon Musen Co. Ltd., Saitama, Japan.
- i) Permanent affiliation : Fujitsu Corp., Kanagawa, Japan.
- j) Permanent affiliation : Nikon Co. Ltd., Tokyo, Japan.
- k) Permanent affiliation : Laboratoire de l'Horloge Atomique/CNRS
Orsay, France.
- l) Permanent affiliation : P.N. Lebedev Physical Institute,
Moscow, Russia.
- m) Permanent affiliation : Institute of Metrology for Time and
Space (VNIIFTRI), Moscow, Russia.
- n) Permanent affiliation : Communications Research Laboratory,
Tokyo, Japan.

LIST OF PAPERS

[I] LASER FREQUENCY CONTROL

(a) Journal Papers

[1] W. Wang, K. Nakagawa, Y. Toda, and M. Ohtsu, "1.5 um diode laser-based nonlinear frequency conversions by using potassium titanyl phosphate", Appl. Phys. Lett., Vol.61, No.16, Oct. 1992, pp.1886-1888

[pp.1 - 3]

[2] M. Kozuma, M. Kourogi, and M. Ohtsu, "Frequency stabilization, linewidth reduction, and fine detuning of a semiconductor laser by using velocity-selective optical pumping of atomic resonance line", Appl. Phys. Lett., Vol.61, No.16, Oct. 1992, pp.1895-1897

[pp.4 - 6]

[3] W. Wang, K. Nakagawa, S. Sayama, and M. Ohtsu, "Coherent addition of injection-locked high-power AlGaAs diode lasers", Opt. Lett., Vol.17, No.22, Nov. 1992, pp.1593-1595

[pp.7 - 9]

[4] C.-H. Shin and M. Ohtsu, "Homodyne Optical Phase Locking of Resonant Cavity Coupled Semiconductor Lasers", IEEE J. Quantum Electron., Vol.29, No.2, Feb. 1993, pp.374-385

[pp.10 - 21]

[5] Y. Awaji, S. Sayama, H. Suzuki, M. Ohtsu, and Y. Teramachi, "Generation of Phase Conjugate Wave from a Visible InGaAlP Laser", Jpn. J. Appl. Phys., Vol.32, Part 1, No.3A, March 1993, pp.1107-1111

[pp.22 - 26]

[6] W. Wang and M. Ohtsu, "Continuous-wave optical parametric amplifier that uses a diode laser for a wideband coherent optical frequency sweep generator", Opt. Lett., Vol.18, No.11, June 1993, pp.876-878

[pp.27 - 29]

[7] M. Ohtsu, K. Nakagawa, M. Kouroggi, and W. Wang, "Frequency control of semiconductor lasers", J. Appl. Phys., Vol.73, Vol.12, June 1993, pp.R1-R17 (Review paper)

[pp.30 - 46]

(b) International Conferences

[1] Y. Harada, K. Narushima, M. Sano, M. Sekine, Y. Higashino, and M. Ohtsu, "Optical Response of $\text{YBa}_2\text{Cu}_3\text{O}_{7-x}$ Epitaxial Thin Films", Advances in Superconductivity IV [Proc. 4th Int. Symposium on Superconductivity, pp.763-766 (Oct. 14-17, 1991, Tokyo)], ed. by H. Hayakawa and N. Koshizuka, Springer-Verlag, Tokyo 1992

[pp.47 - 50]

[2] E. Kawate, K. Tanaka, K. Mizobushi, Y. Higashino, M. Okaji, and M. Ohtsu, "Nonbolometric Optical Response of $\text{YBa}_2\text{Cu}_3\text{O}_x$ Epitaxial Thin Films", Advances in Superconductivity V [Proc. 5th Int. Symposium on Superconductivity, pp.1165-1168 (Nov.16-19, 1992, Kobe)], ed. by Y. Band and H. Yamauchi, Springer-Verlag, Tokyo 1993

[pp.51 - 54]

[3] K. Nakagawa, Y. Shimizu, T. Katsuda, and M. Ohtsu, "Highly stable and high power Nd:YAG lasers", Proc. of SPIE Symposium on Frequency-Stabilized Lasers and Their Applications, pp.40-48 (Nov.16-18, 1992, Boston), ed. by Y. Chung (SPIE Vol.1837)

[pp.55 - 63]

[4] M. Kouroggi, K. Nakagawa, and M. Ohtsu, "A highly accurate frequency counting system for 1.5 μm wavelength semiconductor lasers", Proc. of SPIE Symposium on Frequency-Stabilized Lasers and Their Applications, pp.205- 215 (Nov.16-18, 1992, Boston), ed. by Y. Chung (SPIE Vol.1837)

[pp.64 - 74]

[5] W. Wang and M. Ohtsu, "Continuous-wave optical parametric amplifier by using diode laser for wideband coherent optical frequency sweep generator", Tech. Digest of Conference on Lasers and Electro-Optics, (Opt. Soc. Am. and IEEE/Lasers and Electro-Optics Soc., Washington, D.C., 1993) (May 2-7, 1993, Baltimore, MA), paper number CThS24, pp.506-507

[pp.75 - 76]

[6] Y. Awaji, M. Kouroggi, K. Nakagawa, T. Enami, and M. Ohtsu, "Nonlinear optical frequency conversion of a 1.5 um wavelength diode laser for frequency linking to the 0.6 um optical frequency standard", Tech. Digest of Quantum Electronics Laser Science, (Opt. Soc. Am., Washington, D.C., 1993) (May 2-7, 1993, Baltimore, MA), paper number QThE7, p.213

[p.77]

[II] A PHOTON SCANNING TUNNELING MICROSCOPE

(a) Journal Papers

[1] T. Pangaribuan, K. Yamada, S. Jiang, H. Ohsawa, and M. Ohtsu, "Reproducible Fabrication Technique of Nanometric Tip Diameter Fiber Probe for Photon Scanning Tunneling Microscope", Jpn. J. Appl. Phys., Vol.31, Part ", No.9A, Sept. 1992, pp.L1302-L1304

[pp.78 - 80]

[2] M. Ohtsu, "What are the Limits of Controlling Lights and Atoms", J. Inst. Electron., Information, and Commun. Eng., Vol.75, No.8, Aug. 1992, pp.870-873 (Review paper, in Japanese)

[pp.81 - 84]

[3] M. Ohtsu and H. Hori, "Atomic-Level Measurements and Control by Light", J. Soc. Instrum. and Control Eng., Vol.31, No.9, Sept. 1992, pp.943-948 (Review paper, in Japanese)

[pp.85 - 90]

[4] M. Ohtsu and H. Hori, "Experiment and Theory of Photon STM", Jpn. J. Opt., Vol.21, No.11, Sept. 1992, pp.780-788 (Review

paper, in Japanese)

[pp.91 - 99]

[5] M. Ohtsu, "Photon Scanning Tunneling Microscope: Beyond the Diffraction Limit", Butsuri (Monthly Publication of Phys. Soc. Jpn.), Vol.48, No.1, Jan. 1993, pp.25-28 (Review paper, in Japanese)

[pp.100 - 103]

[6] M. Ohtsu, "A Photon Scanning Tunneling Microscope with Atomic-Level Resolution: For Atomic-Level Measurements and Fabrication", J. Inst. Electrical Eng. Jpn., Vol.113, No.5, May 1993, pp.381-384 (Review paper, in Japanese)

[pp.104 - 107]

[7] M. Ohtsu, "Controlling Zero: New "Vacuum" Technology by Light", J. Vacuum Soc. Jpn., Vol.36, No.5, May 1993, pp.461-470 (Review paper, in Japanese)

[pp.108 - 117]

(b) International Conferences

[1] H. Hori and M. Ohtsu, "Quantum Optical Aspects on Single-Atom Manipulation by a Photon STM Probe", Quantum Control and Measurement [Proc. ISQM Sattelite Workshop (Aug.28-29, 1992, ARL, Hitachi, Hatoyama, Saitama)] , ed. by H. Ezawa and Y. Murayama, North-holland, Amsterdam/London/New York/Tokyo, 1993, pp.197-202

[pp.118 - 123]

[2] M. Ohtsu, S. Jiang, T. Pangaribuan, and M. Kozuma, "Nanometer Resolution Photon STM and Single Atom Manipulation", Proc. Workshop on Near Field Optics, Oct.26-28, 1992, Besancon, France, paper number 5 pp.131-139

[pp.124 - 132]

[3] M. Kozuma, S. Jiang, T. Pangaribuan, M. Ohtsu, and H. Hori, "Analysis and experimental evaluation of a localized evanescent field by using Yukawa potential", Tech. Digest of Quantum Elec-

tronics Laser Science, (Opt. Soc. Am., Washington, D.C., 1993)
(May 2-7, 1993, Baltimore, MA), paper number QThH7, pp.227-228
[pp.133 - 134]

PUBLISHED BOOKS

- [1] M. Ohtsu, Laser Frequency Fluctuations, Chapter 1 in Fluctuations, Vol.2, ed. by T. Musha, Morikita Publishing, Tokyo, 1992, pp.1-52 (in Japanese)
- [2] M. Ohtsu, COHERENT QUANTUM OPTICS AND TECHNOLOGY, KTK Scientific Publishers, Tokyo (branch of Kluwer Academic Publishers, Dordrecht/Boston/London), 1992

PRESENTED PH.D. THESIS

- [1] M. Kouroggi, "Study on Highly Coherent Optical Frequency Synthesizer", Jan. 1992 (in Japanese)
- [2] H. Okamura, "Studies on the Construction Methodology of Interferometric Optical Fiber Sensors Based on Optical Amplifiers", March 1993

1.5 μm diode laser-based nonlinear frequency conversions by using potassium titanyl phosphate

Weizhi Wang, Ken'ichi Nakagawa, Yasunori Toda, and Motoichi Ohtsu
Graduate School at Nagatsuta, Tokyo Institute of Technology, 4259, Nagatsuta-cho, Midori-ku, Yokohama 227, Japan

(Received 20 April 1992; accepted for publication 4 August 1992)

Both second harmonic and sum-frequency generations by using 1.5 μm diode lasers in a type II phase matched potassium titanyl phosphate are demonstrated for the first time. A maximum second harmonic output power of 1.0 μW is obtained with the use of an external buildup cavity, and a 0.23 μW sum-frequency output power at 0.54 μm is obtained by using 1.5 and 0.82 μm diode lasers.

For many fields such as high resolution laser spectroscopy and precision optical measurements, a coherent optical frequency sweep generator (OFSG) with the frequency coverage from ultraviolet to infrared is required as a coherent light source. A diode laser-based OFSG with a Peta-Hz frequency sweep range, which involves multiple diode lasers and nonlinear frequency conversions by means of organic and nonorganic nonlinear crystals, has been proposed for its wide tunable range and hyper-coherent property.^{1,2} In the OFSG system, various frequency conversions and frequency links between diode lasers and frequency standards are indispensable. The second harmonic (SH) generation of a 1.5 μm diode laser provides a link between the 1.5 μm region and the 0.78 μm region for which a Rb atomic absorption line has been widely utilized to serve as the frequency standard to lock the diode laser frequency. The internal SH generation of a 1.5 μm diode laser can be used for this purpose,³ however, the weak SH power hindered the performance.

Because the present available power of the diode laser at 1.5 μm is low, the 1.5 μm diode laser-based nonlinear frequency conversions, as we have known, have been rarely investigated. On the other hand, diode laser sources for generating green lights through direct SH generation are unavailable, and the green output from the all diode laser-based nonlinear frequency conversion has not yet been obtained.

In this letter, we report two experiments on the nonlinear frequency conversions of the 1.5 μm diode lasers by using potassium titanyl phosphate (KTiOPO₄, KTP). One is the SH generation of a 1.5 μm diode laser with the use of an external buildup cavity. The other one is the sum-frequency (SF) generation of a 1.5 and a 0.82 μm diode lasers for generating a green light.

The KTP crystal is chosen for its large nonlinear coefficients, large acceptance angle, low loss in both visible and infrared region and large temperature tolerance. We used the same crystal for our two experiments at room temperature. The crystal, sized $3 \times 3 \times 10 \text{ mm}^3$, is cut with faces 54° to the crystallographic z axis, and in the xz plane ($\phi=0^\circ, \theta=54^\circ$), and is coated with AR films at both 1.5 and 0.8 μm on both end faces.

The experimental setup for the SH generation is shown in Fig. 1. The laser source for the fundamental wave is a multielectrodes corrugation-pitch-modulated MQW-DFB

laser diode with a wavelength of 1.54 μm and a 350 kHz free-running linewidth.⁴ The y axis of the KTP crystal was in the vertical direction and the incident angle of the laser beam was changed in the θ direction as shown in Fig. 1. The output polarization from the laser lies in the xz plane or perpendicular to the y axis. A Faraday rotator was used to rotate 45° of the incident polarization for satisfying the type II phase matching condition. The angular phase matching is obtained at $\theta=53^\circ$. The polarization of the SH output is along the y direction. Several nanowatts of the single-pass SH wave was measured as the incident power of the fundamental wave was 8 mW. For enhancement of the generated SH wave, an external buildup ring cavity was employed. The laser beam was collimated with a collimating lens CL and was then focused into the ring cavity using a lens ML with a focusing length of 400 mm for the cavity mode matching while the laser beam waist was adjusted to near the midst of the crystal with the size of about 100 μm . The enhancement factor of the fundamental wave by the cavity was estimated as 12 from the transmission and reflection resonance curves, which is limited by the imperfection of the mode matching. The maximum SH output power was 1.0 μW as the input laser power was 8 mW. Figure 2(a) shows the measured SH output by an optical spectrum analyzer (Anritsu, MS9030A).

Although the axis of the cavity is not coincident with

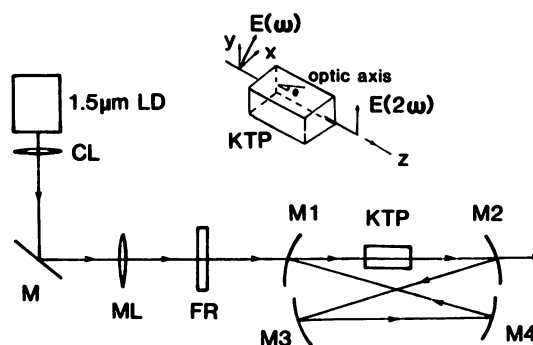
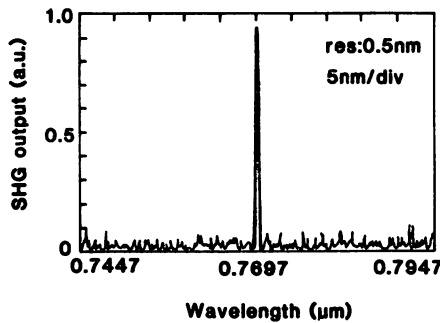
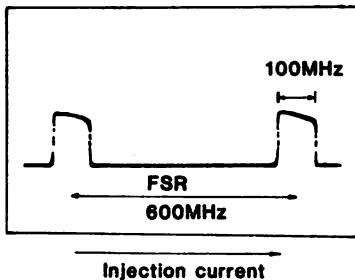


FIG. 1. Experimental setup for the SH generation with an external buildup ring cavity. CL, collimating lens; M, reflecting mirror; ML, mode-matching lens; FR, Faraday rotator; The four mirrors, M1–M4, for the ring cavity have the same curvature radii of 80 mm, M1 and M2 have the reflectivities of 97% at 1.5 μm and transmission of 80% at 0.78 μm , M3 and M4 have the reflectivities of 99.9% at 1.5 μm . The round-trip length of the ring cavity is about 520 mm.



(a)



(b)

FIG. 2. (a) Measured spectral profile of the SH output. (b) Transmission resonance curve of the built-up ring cavity. FSR, the free-spectral range of the cavity.

the normal of the crystal end facet, there is still a weak optical feed back to the laser cavity resulting from the backward scattering on the cavity mirrors, which can be used to lock the frequency of the semiconductor laser to the resonant frequency of the cavity as described by Hemmerich

*et al.*⁵ This is confirmed, in our case, from the resonance characteristics of the cavity by modulating the frequency of the diode laser as shown in Fig. 2(b). It was seen from this figure that the locking range of this optical feedback was about 100 MHz. Therefore a short-term stable SH output was obtained due to the optically locking of the diode laser. The further FM noise reduction of the sub-MHz linewidth 1.5 μm diode laser was achieved by this feedback and its linewidth was estimated to be several tens kHz. The linewidth of the generated SH wave was increased by a factor of 2 as has been pointed out in Ref. 6 and estimated to be less than 100 kHz, although such a linewidth cannot be resolved in the spectrum profile of Fig. 2(a) which was limited by the instrument resolution.

The KTP crystal used in the experiment above is also suitable for the SF generation of 1.5 and 0.8 μm lasers in the case of the type II phase matching. Figure 3 shows our experimental setup for generating the green SF wave. A 1.5 μm diode laser (OKI Optoelectronic Device OL503A-65) with the maximum output power of 50 mW and a 0.82 μm AlGaAs laser (Spectra Diode Labs, SDL-5311-G1) with the maximum single mode output power of 100 mW were employed as the laser sources. The KTP was fixed with the

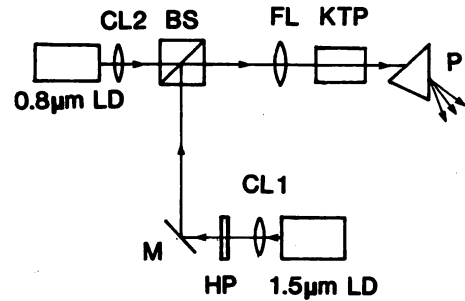


FIG. 3. Experimental setup for the SF generation. CL1, CL2, collimating lenses; M, reflecting mirror; BS, beam splitter; FL, focusing lens; P, prism. The half-wave wavelength plate, HP, was used to rotate 90° of the output polarization from the 1.5 μm laser for satisfying the type II phase matching condition.

y axis in the vertical direction. The two laser beams were focused into the crystal by the FL lens with a focusing length of 100 mm and the angular phase matching was obtained at $\theta=47^\circ$ which is in accordance with the calculated result using the Sellmeier equation given by Bierlein,⁷ while the 1.5 and 0.82 μm laser beams correspond to the ordinary and extraordinary waves inside the crystal. The used beam splitter has a transmission of 98% at 0.8 μm for p -polarization and a transmission of 46% at 1.5 μm for s -polarization so as to permit us to use fully the high power from the 0.82 μm . The SF output has a wave length of 0.54 μm with the polarization along the y axis.

The output power of the generated SF wave can be expressed as $P_{\text{out}}=1.1 \times 10^{-4} P_1 P_2 [W]$, by using the method developed by Boyd and Kleinman,⁸ where P_1 and P_2 represent the input powers of the two lasers in units of watt. The reduction factor due to the walkoff effect, which was included in the coefficient of the expression, was estimated as 0.07 when the beam walkoff angle was 1.5° and the beams waists were about 20 and 40 μm for 0.82 and 1.5 μm diode lasers, respectively. The relation between the SF output power and the input power of the 0.82 μm diode laser is shown in Fig. 4 by fixing the input power of the 1.5 μm diode laser at 8 mW. The solid line gives the theoret-

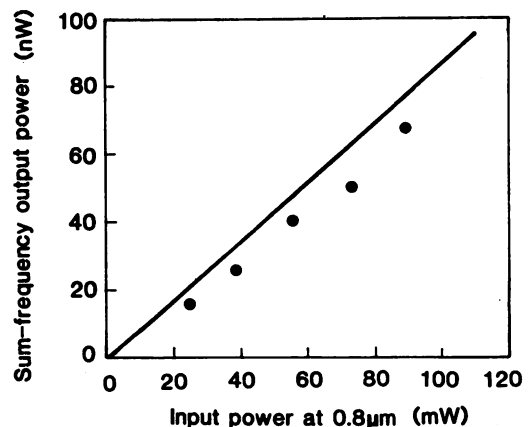


FIG. 4. Relation between the input power of the 0.82 μm diode laser and the SF output power at 0.54 μm as the input power of the 1.5 μm diode laser was 8 mW. The solid line is the calculated result, and the filled circles are measured values.

ically calculated result and the filled circles in the figure represent the measured values. The green light output power varies linearly with the input power of one of the lasers as expected. The slight deviation of the experimental values from the calculated values was attributed to the imperfect overlap of the two beams in the crystal. The maximum output power of $0.23 \mu\text{W}$ was obtained as the $1.5 \mu\text{m}$ laser was operated in its maximum output power.

As the KTP crystal has a large acceptance angle for phase matching, a tuning range of the sum frequency output about 15 nm can be expected with a tuning angle of 1° .

Because the optical heterodyne signal by measuring the beat note has been obtained successfully for the optical phase locking (OPL) while both participants having sub-MHz linewidths and an average power of μW order or even lower,^{6,9} our experimental result in the SH generation has demonstrated the possibility of obtaining enough power to establish a frequency link even for a mW order laser source so as to enable an OPL between 1.5 and $0.78 \mu\text{m}$ diode lasers. It is also seen from Fig. 4 that a highly coherent SF wave with a sub- μW order output power, by replacing the high power multimode diode laser in the SF generation with the MQW-DFB laser used in the SH generation, can be realized to be ready for an OPL, in which the linewidth of the generated light would be increased by a factor of $\sqrt{2}$ resulted from the two uncorrelated lasers assuming that the two lasers have the same linewidth.⁶

At present, a semiconductor laser with a hertz-order linewidth has been achieved by using both optical and electrical feedback,¹⁰ therefore, the nonlinear frequency con-

versions can be realized to generate the highly coherent light in our diode laser-based optical frequency sweep generator by using efficient nonlinear crystals.

In conclusion, we have performed both SH and SF generations by using $1.5 \mu\text{m}$ diode lasers in one KTP crystal. A maximum SH output power of $1.0 \mu\text{W}$ at $0.77 \mu\text{m}$ with a linewidth less than 100 kHz and a SF output power of $0.23 \mu\text{W}$ at $0.54 \mu\text{m}$ have been obtained. The green SF output by using two diode lasers is reported, to our knowledge, for the first time.

The authors would like to thank Dr. M. Okai of Hitachi Corp. and Dr. Y. Kawai of Oki Electric Corp. for providing diode lasers, and Dr. C-H. Shin of National Mokpo Merchant Marine College, Korea, for his helpful discussions.

¹M. Ohtsu, K. Nakagawa, C-H. Shin, H. Kusuzawa, M. Kourogi, and H. Suzuki, *Technical Digest Series, CLEO'90* (Optical Society of America, Washington, DC, 1990), paper CME5, p. 22.

²H. Kusuzawa, E. Ikegami, H. Furuta, K. Nakagawa, and M. Ohtsu, *Technical Digest OEC'90* (Institute of Electronics, Information, and Communication Engineers, Makuhari Messe, Japan, 1990), paper 12D2-1, p. 174 (1990).

³M. Ohtsu and E. Ikegami, *Electron. Lett.* **25**, 22 (1989).

⁴M. Okai, T. Tsuchiya, K. Uomi, N. Chinone, and T. Harada, *IEEE Photon. Technol. Lett.* **2**, 529 (1989).

⁵A. Hemmerich, D. H. McIntyre, C. Zimmermann, and T. W. Hänsch, *Opt. Lett.* **15**, 372 (1990).

⁶H. R. Telle, D. Meschede, and T. Hänsch, *Opt. Lett.* **15**, 532 (1990).

⁷J. D. Bierlein and H. Vanhezeele, *J. Opt. Soc. Am. B* **6**, 622 (1989).

⁸G. D. Boyd and D. A. Kleinman, *J. Appl. Phys.* **39**, 3597 (1968).

⁹M. Kourogi and M. Ohtsu, *IQEC'92* (American Physical Society and European Physical Society, Vienna, 1992), paper TuM5.

¹⁰C-H. Shin and M. Ohtsu, *Opt. Lett.* **15**, 1455 (1990).

Frequency stabilization, linewidth reduction, and fine detuning of a semiconductor laser by using velocity-selective optical pumping of atomic resonance line

M. Kozuma, M. Kourogi, and M. Ohtsu

Graduate School at Nagatsuta, Tokyo Institute of Technology, 4259 Nagatsuta, Midori-ku, Yokohama 227, Japan

H. Hori

Faculty of Engineering, Yamanashi University, 4 Takeda, Kofu-shi, Yamanashi 400, Japan

(Received 10 February 1992; accepted for publication 10 August 1992)

A novel optical feedback technique for a semiconductor laser has been used successfully in stabilizing the laser frequency to a hyperfine transition frequency of the $\text{Rb}^{87}\text{-D}_2$ line ($F=2-3$) and simultaneously reducing the laser field spectral linewidth 20-times that of the free-running laser. The locking range of this feedback was 200 MHz. The possibility of continuous detuning of the stabilized frequency as large as $\pm\gamma/2$ (half of the natural linewidth of the atomic resonance) was demonstrated.

Frequency-stabilized semiconductor lasers have been used as indispensable light sources for a variety of quantum optical experiments and coherent optical sensing systems, such as laser cooling of neutral atoms,¹ optical pumping of atomic clocks,² and a passive resonator-type fiber gyroscope.³ In the case of laser cooling experiments, the semiconductor laser has to meet at least the following three requirements: (1) The laser frequency must be stable and reproducible, (2) the field spectral linewidth $\Delta\nu$ must be narrower than the natural linewidth γ of the atomic resonance line, and (3) the stabilized laser frequency must be detuned from the atomic resonance frequency ν_r with a magnitude of about $\pm\gamma/2$, i.e., $\nu \sim \nu_r \pm \gamma/2$.

Narrow-band optical feedback, using the reflected beam from a reference Fabry-Perot cavity,⁴ has been used as an effective method to decrease $\Delta\nu$, by which requirement (2) can be met. However, since ν is locked to one of the resonance frequencies of the Fabry-Perot cavity, high reproducibility of ν is not expected even though it is stabilized. Therefore, in order to meet requirement (1), this cavity-locked laser frequency has to be stabilized to ν_r by an additional electrical feedback loop. Furthermore, to meet requirement (3), additional frequency-offset locking techniques should be used. However, these optical and electrical feedback control systems could make the system complicated.

In order to overcome this difficulty, we proposed a novel optical feedback method to control a semiconductor laser frequency by utilizing a velocity-selective optical pumping (VSOP)⁵ and polarization spectroscopy⁶ of a rubidium (Rb^{87}) atomic vapor to meet the three requirements presented above. In this method, the light possessing the information of the Doppler-free atomic resonance spectral profile is injected into the laser. As compared with the method using a Fabry-Perot cavity and the methods previously reported,^{7,8} the present method has several advantages. They are: (1) The three requirements presented above are easily met, and the setup is simple and compact. (2) An optically thick atomic vapor cell is not required to obtain high signal-to-noise ratios in the Doppler-free sig-

nal. (3) For frequency detuning, a strong magnetic field is not required.

Figure 1 shows the experimental setup. The total length of this system was as short as 300 mm. The ^{87}Rb cell was 35 mm long and was used at room temperature. The output beam of the semiconductor laser (HITACHI HL7802, 0.78 μm wavelength) was divided into two beams by a beam splitter (BS1). One beam (4.0 mW) was used for pumping and the other (0.8 mW) was for probing the Rb^{87} vapor. The angle between pump and probe beams was so small that the residual Doppler broadening was negligible.

The VSOP and its detection are realized by the following processes. The polarization of the probe beam was converted from linear to elliptic by passing through the Rb^{87} cell due to the circular dichroism induced in the Rb^{87} vapor by a nonlinear interaction with the strong pump beam. Furthermore, the circularly polarized strong pump beam produces velocity-selective polarization in the Rb vapor and induces velocity-selective circular dichroism and birefringence in the probe beam reflected by a mirror M3. In order to inject the spectral selective probe beam to the laser, a Faraday rotator with a rotation angle of 45° was used. For the optical feedback the polarizer also serves as an analyzer.

Figure 2(a) shows the Doppler-free $\text{Rb}^{87}\text{-D}_2$ spectral profile line due to hyperfine transitions from the $F=2$ level in the ground state. It was measured by a photodiode (PD) by sweeping the laser injection current. In this case, the reflected probe beam was not injected into the laser, i.e., the laser was in the free-running condition.

The labels for the various peaks in Fig. 2(a) were determined as follows. By a nonlinear interaction with the pump beam, the strongest orientation of the atomic spin is induced at the transition from $F=2$ to $F=3$ in the $\text{Rb}^{87}\text{-D}_2$ line. It is because the hyperfine pumping was not caused in this transition. For this reason the strongest VSOP signal was obtained at the transition frequency from $F=2$ to $F=3$. We estimated the frequencies of the other peaks by comparing with this signal.

Since this spectral profile exhibited a peak at ν_r , stable

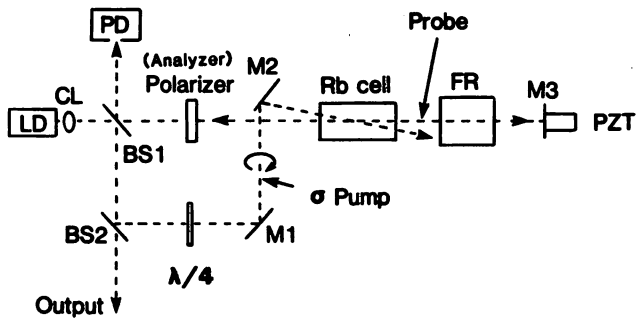


FIG. 1. Experimental setup of optical feedback laser. LD: semiconductor laser. CL: collimating lens. BS1, BS2: beam splitters. M1, M2, M3: mirrors. FR: Faraday rotator. PD: photodiode.

resonant optical feedback was achieved by injecting the reflected probe beam into the laser. As a result, the laser frequency ν was locked to ν_r . Figure 2(b) shows the deformed Doppler-free spectral profile measured as a result of this injection, i.e., the laser was in the optical feedback condition. The plateau at the center of the profile suggests that the ν was locked to ν_r (the transition between $F=2$ to $F=3$). The locking range was as wide as 200 MHz as the laser frequency would change by about 200 MHz by changing the injection current by the magnitude of $80 \mu\text{A}$.

Because the high reproducible atomic resonance line was utilized for a frequency reference, the reproducibility of the laser cavity frequency is expected to be high in principle. The estimation of the laser frequency stability of the present method can be carried out by comparing with another independent frequency reference.

Although the control of the optical path length between the laser and the mirror M3 is required for stable optical feedback by a slow electrical feedback to the PZT on which M3 was mounted, our optical feedback was maintained stable without controlling the PZT for longer than several minutes because of a compact and rigid experimental setup.

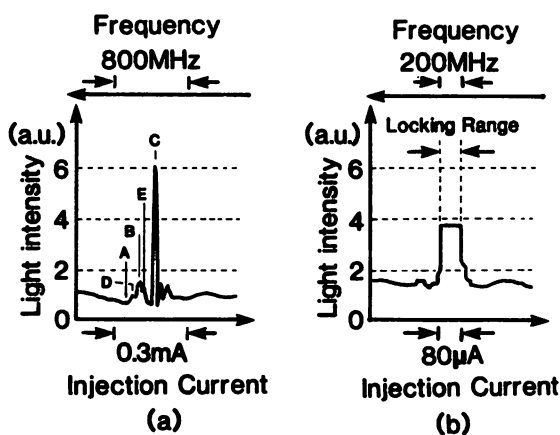


FIG. 2. Doppler-free spectral profile of Rb^{87} vapor measured as a function of the laser injection current. (a) Measured circular dichroic spectral profile by using a free-running laser. Spectral lines A, B, C correspond to the transitions $F=2-1$, $2-2$, $2-3$, respectively. Spectral lines D and E correspond to the crossover resonances. (b) The profile measured by injecting the reflected probe beam into the laser.

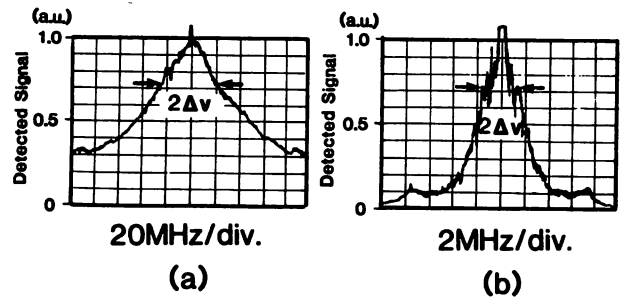


FIG. 3. The laser spectral profiles resulting from the delayed self-homodyne method with 4-km-long single-mode fiber. The ordinate represents the amplitude of the self-homodyne beat signal measured by linear scale. The peaks which extend well above the border of the graph represent the spectral line of the local oscillator in the spectrum analyzer. They are not from the laser FM noise. $\Delta\nu$: The field spectral linewidth of the optically stabilized laser was determined by fitting the spectral profile to the Lorentzian and measuring the half-linewidth at the $(1/2)^{1/2}$ of the maximum. (a) Free-running condition. $\Delta\nu=20$ MHz. (b) Optical feedback condition. $\Delta\nu=1$ MHz.

The electrical feedback experiment and the estimation of the influence of optical path length on the frequency stability, which have been performed, will be published elsewhere.⁹

Figures 3(a) and 3(b) show the field spectral profiles of the laser under free-running and optical feedback conditions, respectively, obtained using the delayed self-homodyne method¹⁰ with a 4-km-long single-mode fiber. The half-linewidth $\Delta\nu$ was reduced to 1 MHz by the optical feedback, which was 20 times narrower than that of the free-running laser. By these experimental results, it was confirmed that the present method could meet requirements (1) and (2).

The advantage of the present optical feedback is that the stabilized laser frequency can be detuned continuously from ν_r with a magnitude of about $\pm\gamma/2$, i.e., $\nu_r - \gamma/2 < \nu < \nu_r + \gamma/2$.

By changing the Faraday rotation angle from 45 deg, the spectral profile of the reflected probe beam was deformed from absorptive to dispersive due to the circular birefringence of the Rb vapor as is depicted by Figs. 4(a) and 4(b). And the peak of the dispersive profile appears approximately at ν_r to $\gamma/2$, depending on the Faraday rotation angle.

Figure 4(c) shows the spectral profile of the Rb^{87} vapors, measured while injecting the reflected probe beam to the laser. The laser frequency ν was locked at the plateau of this profile, which suggests that the stabilized laser frequency ν was detuned from ν_r , i.e., $\nu \sim \nu_r + \gamma/2$ by changing the Faraday rotation angle from 45° to 22.5°.

By this result, it was confirmed that requirement (3) was met. The Faraday rotator can be replaced by a polarizer whose optical axis is fixed to be 45° with respect to the analyzer, which can make the system simpler.

In summary, we have succeeded, by using a novel optical feedback technique for a semiconductor laser, in stabilizing the laser frequency to a resonance frequency of a hyperfine transition of the $\text{Rb}^{87}\text{-D}_2$ line ($F=2-3$) and simultaneously reducing the laser field spectral linewidth 20-

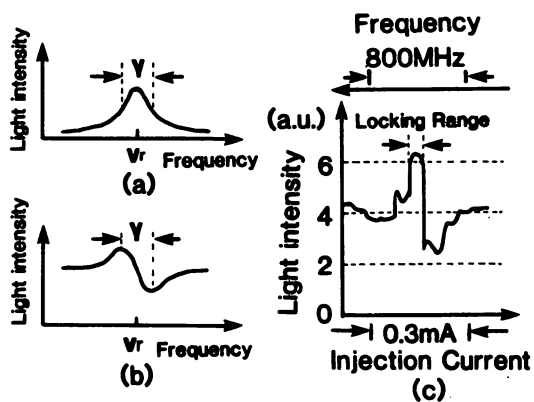


FIG. 4. Typical absorptive and dispersive profiles, and experimental results obtained to demonstrate the possibility of detuning the stabilized laser frequency. (a) A typical absorptive profile. (b) A typical dispersive profile. (c) Measured dispersive spectral profile while injecting the reflected probe beam into the laser. The Faraday rotation angle was changed to about 22.5° .

times that of the free-running laser. The locking range of this feedback was 200 MHz. The possibility of continuous detuning of the stabilized frequency as large as $\gamma/2 \pm \gamma$ (half of the natural linewidth of the atomic resonance) was

demonstrated. It can be expected that this optically stabilized laser is used as a stable light source for laser cooling experiments.

The authors wish to thank Dr. L. Hollberg (NIST) and Dr. K. Nakagawa (TIT) for their valuable comments and discussions. A part of this work was supported by the Grant-in-Aid (No. 03555006) from Ministry of Education, Science and Culture.

¹D. Sesko, C. G. Fan, and C. E. Wieman, *J. Opt. Soc. Am. B* **5**, 1225 (1988).

²M. Hashimoto and M. Ohtsu, *IEEE Trans. Instrum. Meas.* **39**, 458 (1990).

³M. Ohtsu and S. Araki, *Appl. Opt.* **26**, 464 (1987).

⁴B. Dahmani, L. Hollberg, and R. Drullinger, *Opt. Lett.* **12**, 876 (1987).

⁵M. Oria, D. Bloch, and M. Ducloy, Abstract of the 10th International Conference on Laser Spectroscopy, cosponsored by International Union of Pure and Applied Physics, Ministère de la Recherche de la Technologie, June 1991, Font-Romeu, France, p. 38.

⁶C. Wieman and T.W. Hansch, *Phys. Rev. Lett.* **36**, 1170 (1976).

⁷W. D. Lee and J. C. Campbell, *Appl. Phys. Lett.* **58**, 995 (1991).

⁸M. Pinard, C. G. Aminoff, and F. Lae, *Phys. Rev. A* **19**, 2366 (1979).

⁹H. Hori (private communication).

¹⁰T. Okoshi, K. Kikuchi, and A. Nakayama, *Electron. Lett.* **16**, 630 (1980).

Coherent addition of injection-locked high-power AlGaAs diode lasers

W. Wang, K. Nakagawa, S. Sayama, and M. Ohtsu

Graduate School at Nagatsuta, Tokyo Institute of Technology, 4259, Nagatsuta-cho, Midori-ku, Yokohama 227, Japan

Received June 15, 1992

Coherent addition with the use of injection-locked AlGaAs high-power diode lasers has been performed. The linewidths of the master and slave lasers were narrowed to less than 30 kHz by using the optical feedback from an off-axis confocal Fabry-Perot resonator. The coherently added output power of two diode lasers was increased up to 110 mW, which corresponds to an addition efficiency of 0.85. The residual phase fluctuation of the system was controlled within 0.25 rad. Addition of three high-power diode lasers has been also demonstrated for the first time to our knowledge, and a total output power of 150 mW with an addition efficiency of 0.68 was obtained.

A highly coherent and high-power laser source is indispensable for optical nonlinear frequency conversions such as pumping of an optical parametric oscillator and detection of gravitational wave. Since there is a limit in power or coherence for a single laser device, pioneering research to obtain high output power by adding multiple laser outputs coherently of various laser devices has been carried out,¹⁻⁵ and monolithic arrays with an output coherent power of as much as 1 W have been achieved.⁵ However, there remain problems of low addition efficiency as in the case of the utilization of a spatial filter and an external cavity,¹ the complexity of a system as in the case of the addition of phase-locked gas lasers,² and unsatisfactory output beams with multilobe spatial pattern as in the case of the phase-locked diode-laser arrays of antiguides.⁵ On the other hand, diode lasers of the single-stripe type can be considered as a promising candidate for this aim because of their convenience in electrical and optical feedback control, wide frequency tuning range, and availability of direct modulation.

The injection locking of the 1.5- μm diode lasers and the coherent addition between master and slave lasers have been reported by us.⁴ In this Letter we report the experimental results of coherent addition by using injection-locked high-power AlGaAs diode lasers with much improved results in both coherence and addition efficiency and also demonstrate multiple laser addition by using three diode lasers.

The experimental setup is shown in Fig. 1; all three diode lasers were Spectra Diode Laboratories SDL-5311 AlGaAs single-mode lasers with a 0.82- μm wavelength and a maximum output power of 100 mW. The lasers were installed on copper blocks whose temperature fluctuations were controlled within 1 mK. All diode lasers were operated with drive currents in the range of 5.8–7.0 times the threshold value. An optical isolator (isolation ratio >30 dB) was used to prevent the master laser from being injected by slave lasers and the reflections of optical components. The principle of the coherent addition of injection-locked lasers involves two steps.

The first is to use the master laser to inject a part of its output power into the slave laser, by which the laser frequency of the slave laser is locked to that of the master laser. The second is to use a beam splitter to add the incident powers from the two lasers at which the in-phase interference condition between the two laser beams is maintained by control.

In the experiment, laser beams were collimated with the same type of collimating lenses to match the wave fronts. Wedge plates were used as beam splitters to keep sufficiently high power of the master laser for coherent addition after its beam was injected into the slave laser and an off-axis confocal Fabry-Perot (CFP) resonator. The off-axis CFP resonator with a finesse of 75 and a free spectral range of 1.5 GHz was used as an optical feedback resonator to reduce the laser frequency noise. This optical feedback scheme is the same as the one proposed by

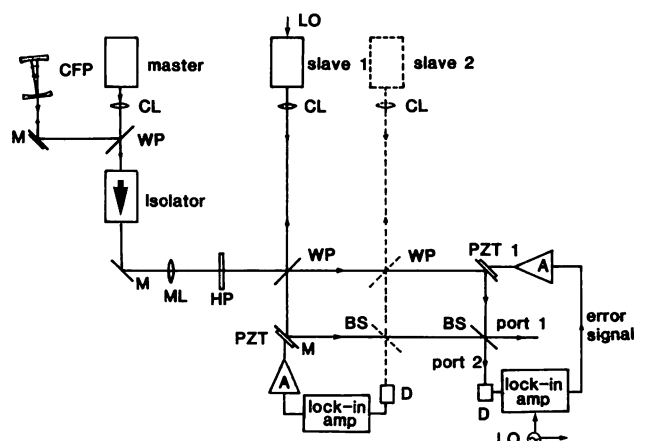


Fig. 1. Experimental setup of the coherent addition by using injection-locked diode lasers. WP's, wedge plates; M's, reflecting mirrors; BS's, beam splitters; PZT's, piezoelectric transducers; CL's, collimating lenses; CFP, confocal Fabry-Perot resonator; HP, half-wave plate for keeping the polarization of the master laser the same as that of the slave laser; ML, mode-matching lens; A's, amplifiers for driving the PZT's; D's, photodetectors; LO, local oscillator.

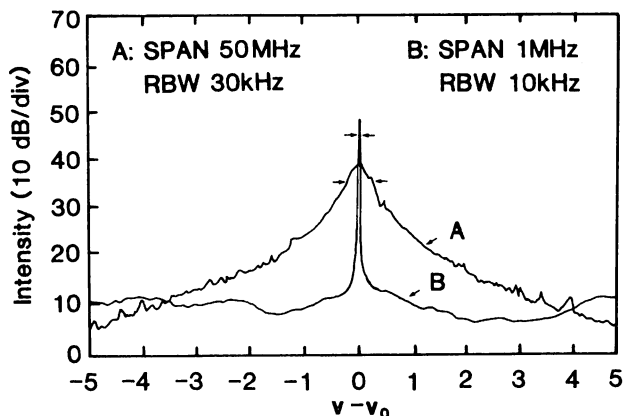


Fig. 2. Field spectral profiles of the master laser under free-running conditions (curve A) and with optical feedback from the CFP resonator (curve B). RBW, resolution bandwidth.

Dahmani *et al.*⁶ Figure 2 gives the measured field spectral profiles by the delayed self-homodyne method with a 4-km optical fiber. The 3-dB linewidth of the free-running master laser was ~ 2 MHz, and the linewidth was reduced to below the resolution limit of the 4-km optical fiber delay line when the laser frequency was locked to the CFP resonator and was estimated to be less than 30 kHz. The locking range of 300–500 MHz was observed with an optical feedback power ratio of 10^{-5} . When the slave laser was injection locked by the master laser, the linewidth of the locked slave laser was also measured by the delayed self-homodyne method and the field spectral profile was observed to be the same as that of the master laser, which means that the highly coherent properties of the master laser were transferred to the slave laser. The injection-locking range was measured as 8.4 ± 0.3 GHz by using an optical wavelength meter and tuning the drive current of the slave laser when the injection power was estimated to be 0.7 mW. This locking range, corresponding to a current range of 3.8 mA, can be easily confirmed as the interference fringes at the output port of the beam splitter disappeared when the drive current was tuned out of the locking range. The output intensities at the two output ports of the beam splitter can be expressed as $I_1 = r^2 I_m + t^2 I_s + 2rt(I_m I_s)^{1/2} \cos \delta$ and $I_2 = t^2 I_m + r^2 I_s - 2rt(I_m I_s)^{1/2} \cos \delta$, where I_m and I_s represent the optical intensities of the master and slave lasers, r and t represent the amplitude reflection and transmission coefficients, respectively, and δ represents the phase difference between master and slave laser beams. The coherent addition was realized as δ was controlled to be kept at zero. The addition efficiency can be defined as the ratio of the obtained output power to the ideal output power and is expressed as $\eta = I_{\text{out}} / (I_m + I_s)$, where I_{out} represents the experimentally available output power.

Since the phase difference between the two lasers was also locked to a certain value by the injection locking, the stability of the output power was limited by the phase fluctuations involving the fluctuation of the optical path length of the laser beams and the residual phase fluctuation in the injection locking. Because the contrast of the interference fringes can

be considered as the representation of the phase correlation between master and slave lasers, two methods, which gave the same result, were used to measure the fringe contrast. One method was to put a pinhole in front of the photodetector, and the another method was to couple the two beams into a single-mode fiber so as to obtain the complete matching of the two wave fronts, while the phase difference between the two beams was varied by changing the voltage applied to piezoelectric transducer PZT 1 in Fig. 1. The maximum measured contrast was 0.94, which corresponds to a theoretical value of 0.97 for the currently used beam splitter ratio of $r/t = (6/4)^{1/2}$. Such a result implies that the residual phase noise in this case was reduced to a nearly ideal level by the injection locking.

Figure 3 shows the interference pattern from both output ports of the beam splitter. It can be seen clearly that the powers from the two lasers were canceled at one port and were added at the other port. For obtaining a maximum stable output power, the locked slave laser was modulated by sweeping the drive current within the locking range so as to modulate the phase difference between the two laser beams. The phase difference thus was locked by using the phase-sensitive detection technique through a lock-in amplifier to feedback a voltage to PZT 1, i.e., the output at port 2 was locked to the dark fringe. The modulation frequency was 5 kHz, and the error signal from the output of the lock-in amplifier was recorded as is shown in Fig. 4. This figure shows that the external influences, mainly from the mechanical vibration, on the phase difference were reduced to less than 0.25 rad or $\lambda/25$ (where λ is the laser wavelength). An output power of 110 mW was obtained as the two laser powers incident upon the beam splitter were 67 and 68 mW, respectively. This corresponded to an addition efficiency $\eta = 0.85$, which is much improved compared with the previously reported values.⁴

To demonstrate experimentally the feasibility of the coherent addition of multiple injection-locked lasers, we also carried out coherent addition of two

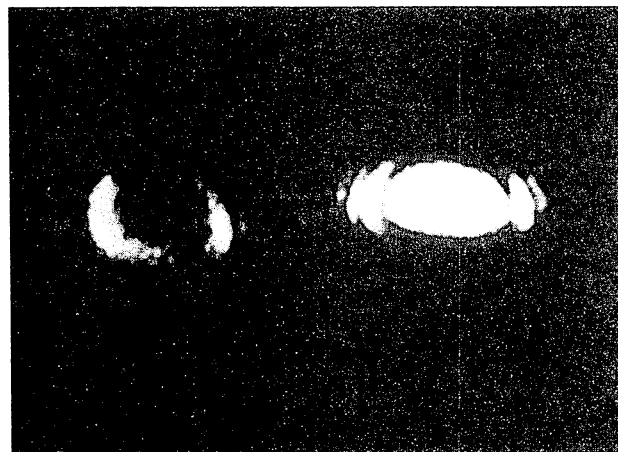


Fig. 3. Interference patterns between the master laser and the injection-locked slave laser. The bright fringe on the right side is from port 1 in Fig. 1, and the left image is the dark fringe from port 2.

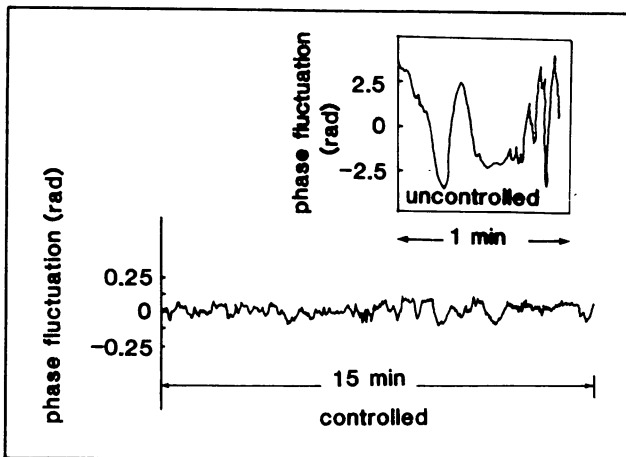


Fig. 4. Error signals from the output of the lock-in amplifier. The inset gives the phase fluctuation of the system in the uncontrolled state.

injection-locked slave lasers and the master laser. The experimental setup was changed by adding the part depicted by the dashed lines in Fig. 1. An output power of 150 mW was obtained, corresponding to a total addition efficiency of 0.68. The degradation of the addition efficiency was attributed to the difficulty of the spatial mode matching and also to the practical experimental situation in which the third laser hardly oscillated with the sufficiently high longitudinal-mode stability. More careful selection of the laser device could be expected to improve the result.

Because the laser beams in our method are added coherently, both spatially and temporally, the present experiment has shown that coherent addition can be used as an efficient technique for obtaining high output power while maintaining the diffraction-limited single spatial mode beam of each diode laser and the low FM noise determined by the optically fed back master laser. It can also be advantageous over the scheme of the conventional laser amplifier because of the absence of the excess noise that is due to the spontaneous emission. Moreover such a method is compatible with construction of an injection chain to add coherently multiple diode lasers directly, rather than the diode-pumped solid-state lasers,⁷ to realize an all-diode-laser-based coherence source for making full use of the merits of diode lasers in applications.

In the case of multiple diode lasers with identical intensities, namely, I , assuming that all the additions are with the same efficiency η , we can add 2^n diode lasers by using beam splitters with $r/t = 1$ and obtain $I_{\text{out}} = (2\eta)^n I$, whereas for addition of arbitrary n diode lasers we obtain $I_{\text{out}} = [(\eta + \eta^{n-1} - 2\eta^n)/(1 - \eta)]I$ by using the beam splitters with $r/t = (1/n)^{1/2}$ at which the outputs from the reflecting ports are locked to the dark fringes. As an example, for $\eta = 0.85$, $n = 8$, the output powers of these two schemes will be $4.9I$ and $4.2I$, respectively. The latter has a lower output power, however, it can be used for any number of diode lasers.

In conclusion, we have carried out coherent addition by using injection-locked high-power AlGaAs lasers. An addition efficiency as high as 0.85 in the addition of two lasers with a total output power of 110 mW was obtained. The linewidths of the master and slave lasers were reduced to less than 30 kHz by using optical feedback from an off-axis CFP resonator. Such a result, in both addition efficiency and coherence, is to our knowledge the best that has been reported in experiments using various lasers. We have also demonstrated the addition of three high-power diode lasers for the first time to our knowledge, and the total output power and the addition efficiency were 150 mW and 0.68, respectively. The residual phase fluctuations of the system were controlled within 0.25 rad.

This research is supported by a Grant-in-Aid (no. 04234204) for science research from the Ministry of Education, Science and Culture of Japan.

References

1. C. J. Corcoran and R. H. Rediker, *Appl. Phys. Lett.* **59**, 759 (1991).
2. G. A. Kerr and J. Hough, *Appl. Phys. B* **49**, 491 (1989).
3. J. Harrison, G. A. Rines, and P. F. Moulton, *Opt. Lett.* **13**, 111 (1988).
4. K. Nakagawa, M. Teshima, and M. Ohtsu, *Opt. Lett.* **16**, 1590 (1991).
5. L. J. Mawst, D. Botez, M. Jansen, T. J. Roth, C. Tu, and C. Zmudzinski, *Electron. Lett.* **27**, 1586 (1991).
6. B. Dahmani, L. Hollberg, and R. Drullinger, *Opt. Lett.* **12**, 876 (1987).
7. E. A. P. Cheng and T. J. Kane, *Opt. Lett.* **16**, 478 (1991).

Homodyne Optical Phase Locking of Resonant Cavity Coupled Semiconductor Lasers

Chul-Ho Shin and Motoichi Ohtsu, *Senior Member, IEEE*

Abstract—Two confocal Fabry–Perot cavity coupled semiconductor laser diodes (CFP-LD) have been constructed for the use in optical phase-locking experiments. Their FM noise suppression characteristics are precisely evaluated by measurements of FM noise by using an optical resonator as the optical frequency discriminator (FM noise suppression ratio 39 dB), spectral linewidth by heterodyning of two CFP-LD's (6.5 kHz) and frequency drift of a heterodyne signal in the time domain (20 kHz/s) and calculations by using a proposed simple linearized model of optical feedback system. Using two CFP-LD's, we carried out homodyne optical phase-locking experiments. Performance of the optical phase-locked loop (OPLL) was evaluated with measured phase error variance and the calculated one considering the actual power spectral density of FM noise of the lasers employed in the OPLL. Phase error variance of the OPLL considering infinite bandwidth was $2.26 \times 10^{-2} \text{ rad}^2$. Total phase-locked power concentration ratio of the slave laser in the OPLL was 97.7%. In other words, 97.7% of temporal coherence of the master laser was transferred to the slave laser by this OPLL.

I. INTRODUCTION

OPTICAL phase locking is an important basic technology for the following applications.

- 1) Coherent optical communication systems employing coherent homodyne/heterodyne detection of PSK (phase shift keying) and ASK (amplitude shift keying) modulation format. [Homodyne and heterodyne optical phase-locked loops (OPLL's).]
- 2) Precise optical measurements such as high resolution spectroscopy, frequency chain for frequency measurement [1], interference pattern measurement [2] and so on. [Heterodyne and homodyne OPLL's.]
- 3) Optical frequency sweep generator (optical frequency synthesizer) with very precise frequency tracking performance. [Heterodyne OPLL.]
- 4) Frequency stabilization of a laser by locking to a stable master laser. [Homodyne and heterodyne OPLL's.]

- 5) Coherent pulse generation by multiple frequency offset locking [3]–[5]. [Heterodyne OPLL.]
- 6) Timing stabilization of mode-locked laser [6]. [Pulsed OPLL.]

The pioneering optical phase lockings by He–Ne lasers have been demonstrated in the 1960's [7] (and listed in [4] of [8]). In the 1980's, extensive studies on homodyne and heterodyne optical phase-locking experiments have been started for applications to coherent optical communications and applications to high resolution spectroscopy and optical frequency measurement.

Experiments of heterodyne OPLL have been carried out by using optically or electrically frequency stabilized semiconductor laser diodes (LD's) [9]–[13], free running LD's [14]–[17], Nd:YAG lasers [18], He–Ne lasers [8], a dye laser, and a He–Ne laser [19]. Experiments of homodyne OPLL have been carried out by using He–Ne lasers [7], CO₂ lasers [20], free running LD's [21], [22], LD-pumped Nd:YAG lasers [23], [24], optically frequency stabilized LD's [25], He–Ne laser and optically stabilized LD [26], and electrically stabilized LD's [22]. Except for [21] and [22], optical phase locking could be achieved by a loop natural frequency smaller than 100 kHz because of the low magnitude of FM noise of the lasers used in the experiments. In the case of free running LD's, the loop natural frequency employed was more than 10 MHz. The maximum loop bandwidth was 134 MHz [22], and even in this case the phase error variance was considerable because of the large wideband FM noise in free running LD's. Frequency stabilized semiconductor lasers must be therefore employed for achieving an OPLL with a small phase error.

In this connection, we have constructed resonant cavity coupled semiconductor lasers as the frequency stabilized lasers by optical feedback. In optical feedback methods, there are several kinds of external reflectors, e.g., one mirror [11], [27]–[29], two mirrors (LD is located between them) [30], an optical grating [31]–[33], a fiber cavity [34]–[36], a tilted high finesse resonant cavity [37]–[40], a photorefractive phase conjugate mirror [41], and so on. In the case of one mirror, the reflection coefficient of the mirror must be carefully selected and feedback phase matching is very important for stable operation under optical feedback condition. In this type of external reflector, the optical feedback system is very sensitive to tilting angle, tolerance of which is the order of 10 μrad

Manuscript received January 31, 1992; revised August 4, 1992. This work was supported in part by the Grant-in-Aid for Scientific Research from the Japanese Ministry of Education, Science, and Culture by Grant 01850015.

C.-H. Shin was with Interdisciplinary Graduate School of Science and Engineering, Tokyo Institute of Technology, Midori-ku, Yokohama, Kanagawa 227, Japan. He is now with Mokpo National Maritime University, Mokpo, Chun-Nam, Republic of Korea.

M. Ohtsu is with Interdisciplinary Graduate School of Science and Engineering, Tokyo Institute of Technology, Midori-ku, Yokohama, Kanagawa 227, Japan.

IEEE Log Number 9205902.

[42]. The optical feedback by using an optical grating requires an antireflection (AR) coating on the coupling facet of the semiconductor laser for sufficient optical feedback because of low reflectivity of the optical grating and to avoid multicavity operation. Then, one or more etalons for external mode selection is required to avoid the mode hopping between external cavity modes, because there are many external cavity modes with a strong magnitude due to strong optical coupling between the laser and the external cavity. For this method, commercially available semiconductor lasers are not directly used without applying AR coating on a facet. In case of the optical feedback method by using a fiber cavity, the mode matching between the laser cavity and the fiber cavity is difficult, because the reflection mode of the fiber cavity is used for optical feedback. It is therefore difficult to use a high finesse fiber cavity.

On the other hand, optically frequency-stabilized semiconductor laser diodes by using a tilted external resonant cavity shows high spectral purity with relatively long-term frequency stability by using a high finesse and frequency-stable CFP cavity, and frequency modulation (FM) capability without any AR coating on a facet of the LD's. Any commercially available semiconductor lasers can thus be directly used for this method without any structural change of laser device itself. Frequency noise characteristics of semiconductor lasers coupled to a resonant external cavity have been theoretically analyzed [38], [43] and experimentally evaluated [38], [39]. FM noise reduction and the frequency modulation characteristics of a semiconductor laser diode coupled to a tilted CFP cavity (CFP-LD) has also been evaluated precisely [40].

In this paper, we propose a simple linearized model of the optical feedback system for FM noise reduction. Using this model, FM noise reduction characteristics is calculated and compared with the measured results. Furthermore, frequency drift in the time domain was precisely measured, and the spectral line shape of the LD with optical feedback was also measured and evaluated.

Using these CFP-LD's as low FM noise lasers, we carried out experiments of the homodyne OPLL, which confirmed their excellent frequency and phase tracking capability between two CFP-LD's. This is the first homodyne optical phase-locking experiment by CFP-LD's. Previously, we have reported a heterodyne OPLL by CFP-LD's with a very low frequency tracking error of 0.4 mHz between two lasers [9].

The line shapes of semiconductor lasers frequency stabilized by optical or electrical feedback are non-Lorentzian due to a limited stabilization bandwidth and a noise peak at the relaxation oscillation frequency of the free running LD. For the precise evaluation of the loop performance of an OPLL, by semiconductor lasers in particular, actual FM noises of the slave and the master lasers have to be taken into account. The phase error performances of OPLL's in experiments reported so far, have however been discussed with an assumption that the FM noise of the lasers is white, i.e., the line shape of the

lasers is perfectly Lorentzian. For a relatively narrow band system, narrower than those of the stabilization bandwidth of the optical or negative electrical feedback and of the relaxation oscillation frequency of the semiconductor laser, such an approximation can be acceptable. However, in the case that an OPLL is applied for phase noise rejection, i.e., frequency stabilization of the slave laser by locking to a stable master laser, precisely measured phase error variance can be utilized as a measure of the total stabilized power of the slave laser. For this purpose or a system with a wider bandwidth, precise determination of the phase error variance is indispensable. In this paper, performance of the loop was evaluated with the measured phase error variance and the calculated one considering the actual power spectral density of FM noise of the lasers employed in the OPLL.

II. RESONANT CAVITY-COUPLED SEMICONDUCTOR LASERS

A. Principles of CFP-LD

Fig. 1 shows the schematic diagram of a CFP-LD. The tilted CFP cavity acts as an optical band pass filter for the laser light field which is spectrally purified in the cavity. A part of the cleaned light field built within the cavity returns to the laser through the cavity input mirror at resonance. The oscillation frequency of the laser is then locked to the resonance of this CFP cavity, i.e., optical self-locking takes place. By this process, the spectral linewidth becomes very narrow, and the center frequency is also stabilized substantially. The free spectral range (FSR) and the finesse of the CFP cavity were 1.5 GHz and 50, respectively, which means that the linewidth of the CFP cavity $\Delta\nu_{CFP}$ was 30 MHz. The LD's used in this experiment were commercially available CSP-type AlGaAs lasers (Hitachi 8314E). The longitudinal side mode suppression ratio of the LD without optical feedback was about 30 dB. In this paper, we have neglected longitudinal side modes in discussions as a matter of convenience.

The center frequency of the laser oscillation can be swept by changing the length of the cavity since laser frequency is locked to the resonance frequency of the CFP cavity. For this purpose, the PZT-C (ceramic actuator, capacitance 497 nF, length 2.6 mm, inner diameter 12 mm ϕ , outer diameter 18 mm ϕ) of Fig. 1 was used. The displacement coefficient was 1.7 $\mu\text{m}/150\text{ V}$ under unloaded condition. The change of the resonance frequency $d\nu$ of the tilted CFP cavity by the change of the length dl is given by

$$d\nu = - \frac{2FSR(2dl)}{\lambda} \quad (1)$$

where λ is the wavelength of the laser. Note that the factor 2 of $2dl$ in (1) means two times change of the cavity spacing because of the tilted CFP cavity as shown by Fig. 1. Using this equation and the displacement coefficient of the PZT-C, the frequency tuning coefficient of the laser is calculated as 82.5 MHz/V. The measured frequency

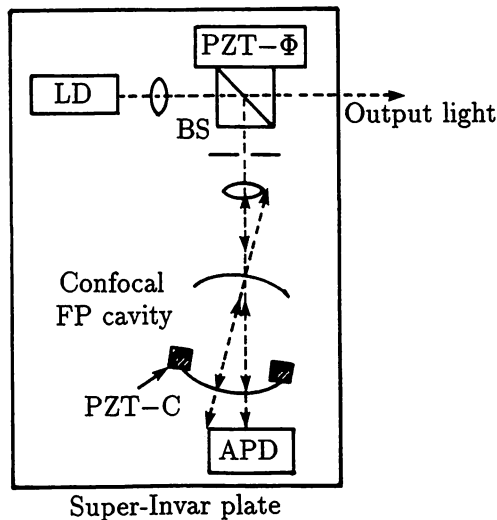


Fig. 1. Schematic diagram of the confocal Fabry-Perot cavity coupled semiconductor laser diode (CFP-LD). BS and APD are a beam splitter and avalanche photo diode, respectively. PZT- Φ and PZT-C are piezoelectric transducers used for optimizing the phase of the feedback light and the fine control of the laser oscillating frequency under optical feedback condition, respectively. The lens located in front of the CFP cavity is used for the mode matching of the cavity.

tuning coefficient was 79 MHz/V at the bias voltage to the PZT-C of about 70 V. These measured and calculated values show a good agreement with each other.

We observed the resonance spectral profiles of the CFP cavity, which was detected by the APD shown in Fig. 1, by sweeping the injection current, of which the frequency tuning coefficient was about -3.0 GHz/mA. Fig. 2 shows such profiles with little feedback (a) and moderate feedback (b) conditions. The resonance profile of the CFP cavity shows a conventional one under little feedback condition. By increasing the feedback power, the range of laser frequency locked to the peak of the resonance frequency of the CFP cavity is increased as can be seen by Fig. 2(b). This frequency locking range of the CFP-LD was in the range of 500 MHz \sim 1.5 GHz, which depends on feedback power. The system could, therefore, endure fluctuations of the injection current and the temperature variation of the laser mount, which was suppressed within 1 mK with the temperature control circuit consisting of Peltier coolers and thermistor sensors. Stable locking was maintained upto about 1 hour without any other additional stabilizing circuits. This period could be extended by using a simple electrical feedback loop to control the feedback phase by using PZT- Φ of Fig. 1 [44], or by miniature packaging [40]. As can be seen by comparing (a) with (b) in Fig. 2, the resonance peak is not located in the center of the locking range because of α parameter. Using this asymmetry, the value of α parameter has been measured to be 3.1 [45].

To confirm magnitude of the external cavity mode, the spectral line shape was observed with 2.2 GHz span as shown by Fig. 3. If there is any external cavity mode, it must be shown in this span because the external cavity mode spacing, i.e., the FSR of the CFP cavity was 1.5

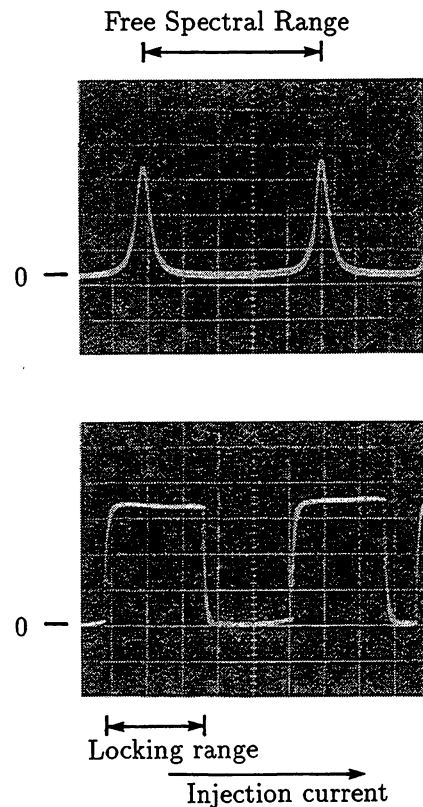


Fig. 2. Resonance profiles of the CFP cavity with little feedback power (a) and moderate feedback power (b). The laser frequency was swept by injection current with the rate of -3 GHz/mA.

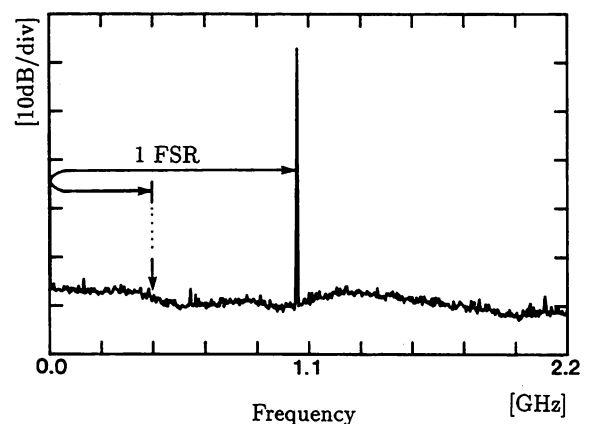


Fig. 3. Spectral profile of the heterodyne signal between two CFP-LD's measured to confirm magnitude of the external cavity mode. The FSR is the free spectral range of the CFP cavity of Fig. 1.

GHz. However, no side mode could be observed. From this measurement, it was confirmed that the side mode suppression ratio of this external cavity semiconductor laser was at least 50 dB, which proves a reliable single external cavity mode oscillation. The longitudinal side mode suppression ratio of the laser itself was, at least, not affected by this optical feedback. This was confirmed by monitoring the spectrum of an optical spectrum analyzer.

There are many stable locking points for this type of optical feedback. When the separation between the LD and the CFP cavity L_S is an odd number times the length

of cavity L_{CFP} , the stable locking takes place on every mode of the CFP cavity, while on every other mode in case of an even number [38]. In our laser, the separation and the length of cavity were about 25 and 5 cm, respectively. Therefore, the frequency of the laser can be stably locked to an every resonance peak of the CFP cavity.

To get a flat resonance profile such as in Fig. 2(b), optical feedback phase must be properly selected by adjusting L_S and L_{CFP} so as to satisfy

$$2L_{CFP} = n\lambda \quad (2)$$

and

$$2L_S + \delta L = n\lambda \quad (3)$$

simultaneously, where δL corresponds to the phase change in the process of coupling between the internal light of the LD and the external feedback light, due to the α parameter [46], [47]. Note that δL can not be experimentally adjusted, while L_{CFP} and L_S can be adjusted by using PZT-C and PZT- Φ , respectively.

B. FM Noise Reduction Characteristics

The FM noise reduction and spectral behavior of semiconductor laser with an external cavity have been investigated with the complex electric field equation of the laser, adding an external feedback term, and the rate equation for the carrier density [34], [38], [43], [46]–[49]. A linearized model of the optical feedback system can be depicted as shown by the Fig. 4. By this model, the relation between the FM noise under free running condition $N_{FR}(s)$ and under feedback condition $N_{FB}(s)$ can be simply expressed. The transfer function of the optical feedback system $H_{OFB}(s)$ is given by

$$\begin{aligned} H_{OFB}(s) &= \frac{N_{FB}(s)}{N_{FR}(s)} \\ &= \frac{1}{1 + K_{OFB}[1 - H_{CFP}(s) \exp(-\tau_D s)]} \quad (4) \end{aligned}$$

where K_{OFB} is total optical feedback gain, which is proportional to the feedback power, $H_{CFP}(s)$ is the transfer function of transmission mode of the CFP cavity, τ_D is the feedback time delay due to the round trip of L_S , and is given by

$$\tau_D = \frac{2L_S}{c} \quad (5)$$

where c is the speed of light.

If the amplitude reflection coefficients of the two mirrors comprising the CFP cavity are the same, $H_{CFP}(s)$ is given by

$$H_{CFP}(s) = \frac{r(1 - r^2)}{1 - r^4 \exp(-\tau_{CFP} s)} \quad (6)$$

where r is the amplitude reflection coefficient of the cavity mirrors, and τ_{CFP} is the time delay in the cavity, which is

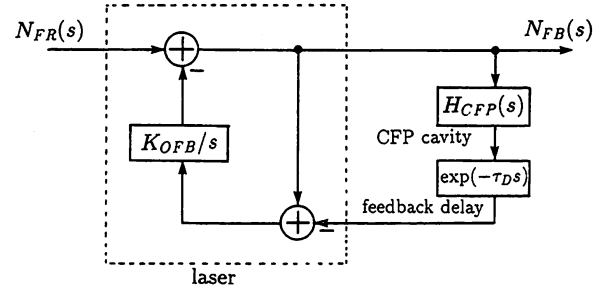


Fig. 4. A linearized model of the optical feedback system. For details, see text.

given by

$$\tau_{CFP} = \frac{4L_{CFP}}{c} = \frac{1}{FSR} \quad (7)$$

where L_{CFP} is the CFP cavity length.

Introducing some approximations and using experimental parameters, (4) can be expressed by

$$\begin{aligned} H_{OFB}(s) &= \frac{N_{FB}(s)}{N_{FR}(s)} \\ &= \frac{1}{1 + \frac{X_0}{\tau_X s} \left[1 - \frac{\exp(-\tau_D s)}{1 + \frac{F}{\pi} \{1 - \exp(-\tau_{CFP} s)\}} \right]} \quad (8) \end{aligned}$$

where X_0 and F are experimentally obtained dc gain for FM noise suppression and the finesse of the CFP cavity, respectively and τ_X is a normalized parameter for introducing the experimental parameters, and given by

$$\tau_X = \tau_D + \frac{F}{\pi} \tau_{CFP}. \quad (9)$$

If $H_{CFP}(s) = 1$, (4) is just for the optical feedback system of an LD with a mirror or an optical grating as the external reflector. Removing the terms relating CFP cavity, (8) is then reduced to

$$H_{OFB}(s) = \frac{N_{FB}(s)}{N_{FR}(s)} = \frac{1}{1 + \frac{X_0}{\tau_D s} [1 - \exp(-\tau_D s)]} \quad (10)$$

The power spectral density (PSD) of FM noise under optical feedback condition S_{OFB} is given by

$$S_{OFB}(f) = |H_{OFB}(j2\pi f)|^2 S_{FR}(f) \quad (11)$$

where $S_{FR}(f)$ is the PSD of FM noise under free running condition. The PSD S_{FR} including relaxation oscillation resonance effect and $1/f$ noise component can have an approximated form given by

$$\begin{aligned} S_{FR}(f) &= \frac{\xi}{f} + \frac{\Delta\nu_{ST}}{\pi} \left[1 + \frac{\alpha^2 \nu_{RF}^4}{(\nu_{RF}^2 - f^2)^2 + (\gamma_e/2\pi)^2 f^2} \right] \\ &[\text{Hz}^2/\text{Hz}] \quad (12) \end{aligned}$$

where ξ , ν_{RF} , α [50], γ_e [51]–[53], and $\Delta\nu_{ST}$ are magnitude of $1/f$ FM noise at the Fourier frequency of 1 Hz, the relaxation oscillation frequency, the linewidth enhancement factor, the damping constant of the laser and the linewidth of the laser given by the Schawlow–Townes' formula, respectively.

The frequency responses of the open loop transfer function of the optical feedback system of Fig. 4 is shown by Fig. 5. These frequency responses are same as those of the reflection mode of the FP interferometer [54] except contribution of the time delay component due to the separation between LD and the CFP cavity. As can be seen by this figure, 3 dB bandwidth of this optical feedback system is a half linewidth of the CFP cavity, and the phase change over the 3 dB bandwidth approaches to 90° except for Fourier frequencies near every integer multiples of the FSR of the CFP cavity. FM noise magnitudes under optical feedback conditions for these areas are larger than that under a free-running condition with peaks at every integer multiple of the FSR of the CFP cavity. This is because positive feedback is made by drastic phase changes at these areas. Magnitudes of these peaks depend on the finesse of the CFP cavity as is described below.

Curve A of Fig. 6 shows the PSD of FM noise normalized to that under free running condition which was measured by using the reflection mode of another FP cavity as a frequency discriminator. The result calculated by using (4) corresponding to the experiment is also shown by curve B in Fig. 6. This shows good agreement. The measured FM noise suppression ratio within the control bandwidth of the optical feedback system was 39 dB. In the calculation, this suppression ratio was used as the feedback gain for the comparison with the experimental results.

Fig. 7 shows FM noise reduction depending on the finesse of the CFP cavity. As can be seen by this figure, lower finesse CFP cavity is better for wideband FM noise suppression if the same feedback gain can be secured. However, it must be noted that optical feedback from a higher finesse gives higher dc gain if the same power from the cavity is fed back to the laser [38]. By decreasing the value of the finesse, the oscillation peak by the positive feedback at the Fourier frequency corresponding to the resonance frequency of the CFP cavity is increased, thereby decreasing the merit of this type of optical feedback with respect to single external cavity mode operation.

Fig. 8 shows the FM noise reduction characteristics of a miniature packaged hemispherical microoptic cavity coupled LD (HMC-LD) [40], which has been developed by the authors as an application of the CFP-LD for the use in an experiment with an optical fiber gyroscope. In this calculation, the finesse and the FSR were 10 and 10 GHz, respectively, the FM noise suppression ratio in the lower Fourier frequency region was 30, and the separation between LD and HMC was 5 cm. There were measured values. Comparing this result with that of curve C in Fig. 7, wideband noise suppression characteristics of

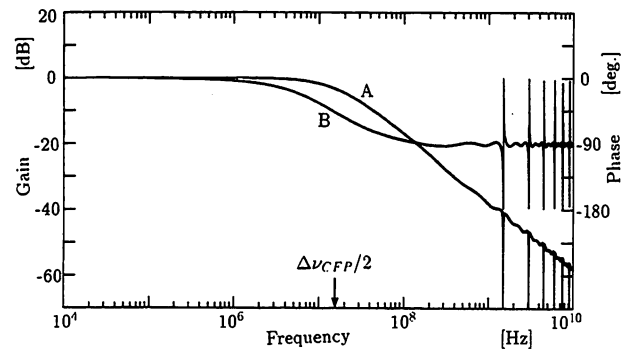


Fig. 5. Frequency responses of the open loop transfer function of optical feedback system of a CFP-LD with the finesse of 50 and the FSR of 1.5 GHz. Curves A and B represent the amplitude and the phase responses, respectively. $\Delta\nu_{CFP}$ is the linewidth of the CFP cavity.

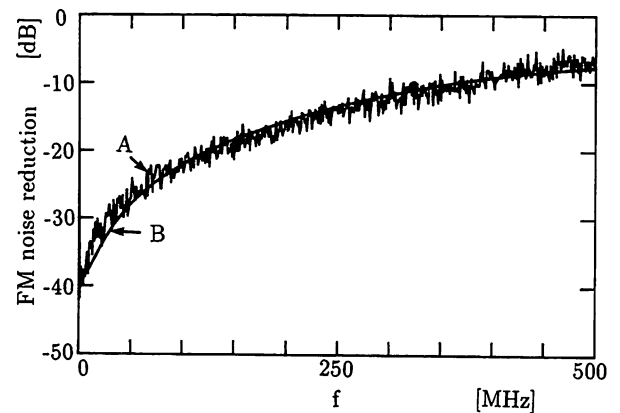


Fig. 6. Measured (curve A) and calculated (curve B) power spectral densities (PSD's) of FM noise under optical feedback condition normalized by that under free running condition.

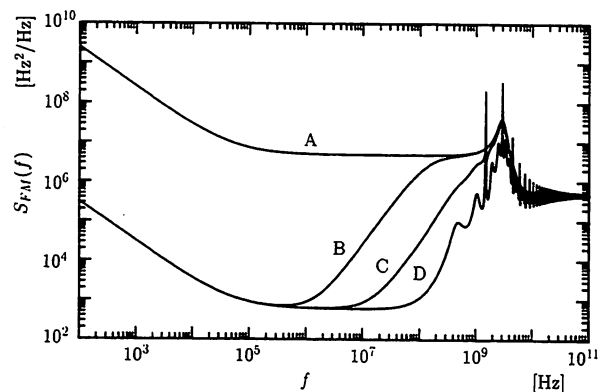


Fig. 7. FM noise suppression characteristics of the CFP-LD. Finesses of the CFP cavity used in this calculation were 500 (B), 50 (C) and 5 (D). Curve A represents FM noise PSD of the free-running condition. Curve C corresponds to that of the actual system used in the experiment.

this practical HMC-LD module is superior to that of a CFP-LD with a higher finesse cavity. Because the noise suppression bandwidth of the HMC-LD is wider than the relaxation oscillation frequency of the LD, the FM noise peak at this frequency is also considerably suppressed as can be seen by Fig. 8. From Figs. 7 and 8, we find that the finesse and the FSR are important factors for the FM noise suppression bandwidth and magnitude of FM noise

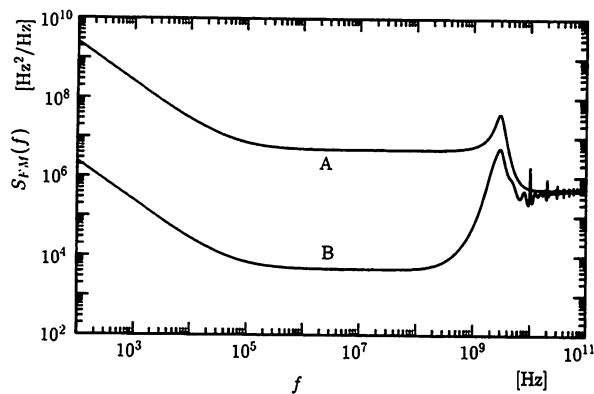


Fig. 8. FM noise suppression characteristics of a hemispherical micro-optic cavity coupled semiconductor laser (HMC-LD). Curves A and B are FM noise PSD's for a free-running LD and the HMC-LD, respectively.

peaks at integer multiple Fourier frequencies of the FSR of the CFP cavity. So, the finesse and the FSR of the cavity must be selected by considering the system bandwidth.

C. Linewidth and Frequency Stability

To measure the linewidth under optical feedback condition, a heterodyne spectrum between two CFP-LD's was observed with the frequency span of 2 MHz as shown by Fig. 9. The spectral linewidths at 3 dB down and 30 dB down are almost the same because of center frequency drifts due to acoustics, temperature variation, and $1/f$ characteristics of FM noise at lower Fourier frequencies.

To confirm the long term frequency stability, the frequency drift of the heterodyne signal of two CFP-LD's in the time domain has been measured by using a commercial time interval analyzer. A measured result is shown in Fig. 10. The heterodyne frequency drift was about 40 kHz/s, which means that the center frequency drift of a CFP-LD was about 20 kHz/s. The CFP-LD was operated in a normally air-conditioned room. The frequency drift direction in Fig. 10 was changed by the long term variation of the room temperature. This is because temperature of the laser mount was well controlled as was described in Section II. However optical paths of the optical feedback loop and the CFP cavity were opened to the air.

The spectral linewidth reduction ratio is roughly equal to the FM noise suppression ratio. If there is no $1/f$ noise and the FM noise spectrum is white, they are exactly the same because the spectral linewidth with the Lorentzian line shape is proportional to the PSD of the FM noise. As can be seen by curve A of Fig. 7, the short-term linewidth under free running condition is not affected by $1/f$ noise since a normally measured short term linewidth is mainly determined by the FM noise magnitude of Fourier frequency corresponding to the linewidth, which was about 15 MHz. The FM noise suppression ratio within the control bandwidth was 39 dB as can be seen by Fig. 6 and the curve C of Fig. 7. The linewidth under optical feedback condition would be about 1.9 kHz. However, FM noise magnitude at Fourier frequency of 1.9 kHz was

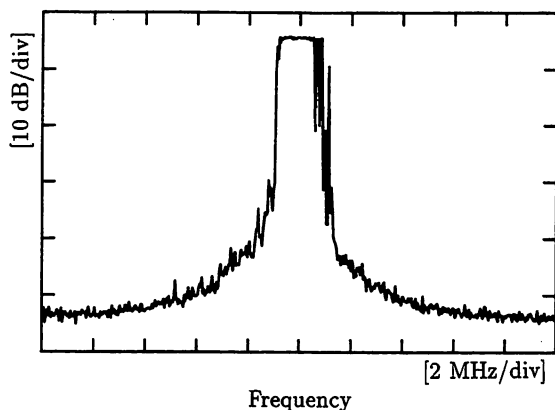


Fig. 9. Field spectrum of a heterodyne signal between two CFP-LD's. The frequency span and the total sweep time were 20 MHz and 100 s, respectively.

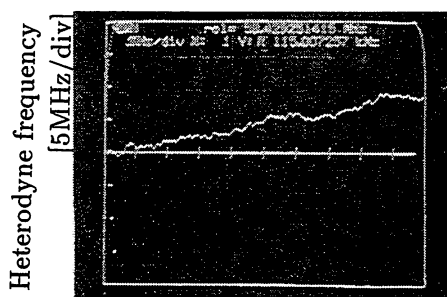


Fig. 10. Measured frequency drift of the heterodyne signal of two CFP-LD's in the time domain.

about 1.3×10^4 [Hz²/Hz], which corresponds to the level of 41 kHz Lorentzian linewidth, because $\Delta\nu_L = \pi S$, where $\Delta\nu_L$ and S are the linewidth and the PSD of FM noise, respectively. This means that the linewidth under optical feedback condition is strongly affected by $1/f$ component of FM noise. To suppress this component, negative electrical feedback using a stable optical frequency reference could be a best solution. By using a negative electrical feedback method with a MHz order bandwidth, the linewidth of a CFP-LD could be reduced to 7 Hz, and the PSD of the FM noise was suppressed to lower than 1 Hz²/Hz in the Fourier frequency range from 10 Hz to about 1 MHz [55].

To observe the short term spectral line shape by suppressing this frequency drift, a heterodyne signal between two CFP-LD's has been locked to a 150 MHz microwave signal from an RF synthesizer by using the heterodyne OPLL technique [9]. The control bandwidth for this loop was about 1 kHz. The result is shown by Fig. 11. The half linewidth, which corresponds to the linewidth of a CFP-LD, at 40 dB down was 650 kHz. If this spectrum is a Lorentzian, the full width at half maximum of a CFP-LD is estimated to be 6.5 kHz. It is expected that the actual linewidth is broader than this value due to $1/f$ FM noise component, because the suppressed FM noise is non-white as can be seen from Fig. 7.

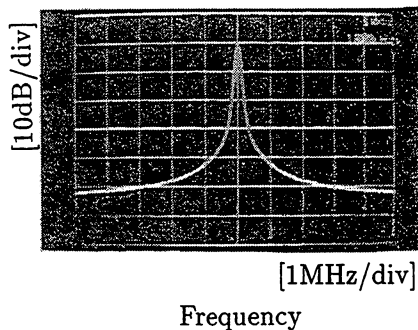


Fig. 11. Spectrum of the heterodyne signal between two CFP-LD's. Two CFP-LD's was frequency offset-locked with a 150 MHz microwave signal from an RF synthesizer by using the heterodyne optical phase-locked loop (OPLL) technique. The locking bandwidth was about 1 kHz.

III. OPTICAL PHASE-LOCKED LOOP

A. Experiments

The experimental arrangement of the homodyne OPLL is shown by Fig. 12. In this experiment, two CFP-LD's with performances as was described in Section II were used as the master and the slave lasers. The phase error between the master and the slave lasers is detected by the optical phase detector which consisted of a beam splitter, two mirrors, an optical power attenuator, and two pin photodiodes as shown in Fig. 12. This is a balanced detector [56]–[60] to reject IM noise component of the slave laser, IM noise power of which is much larger than that of the master laser which can thus be neglected. This is because a small portion of power from the master laser (tens nW to tens μ W) was used in the optical phase detection, while the slave laser was the order of a mW. Optical path lengths and electrical path lengths of the two mixed beam at the beam splitter were adjusted to be the same. The balance of powers of the two beams was adjusted by using the optical power attenuator. The IM noise suppression ratio was measured by an RF network analyzer and by direct intensity modulation of the slave laser. The result is shown by Fig. 13, from which it was confirmed that the intensity noise suppression ratio of the balanced phase detector was 30 to 40 dB up to the frequency of 3 MHz. However, dc drift was still observed, which may be due to the optical path length drift induced by the ambient temperature variation and acoustics. It can be improved by using a monolithically fabricated balanced detector or compactly and rigidly packaged balanced dual-detector modules [25], [61]. In this figure, IM noise suppression ratio is decreased in the frequency range of $f < 1$ kHz because the lower frequency cutoff of the bias-T, to which the intensity modulation signal was applied, was about 1 kHz. IM noise suppression ratio is also decreased in the frequency range of $f > 3$ MHz, because the laser mount and the optical phase detector used in this experiment were not designed for wide bandwidth operation. However, their bandwidths were wide enough for optical phase-locking control.

The detected phase error signal was fed back to the slave laser after low-pass filtering by a standard first-order

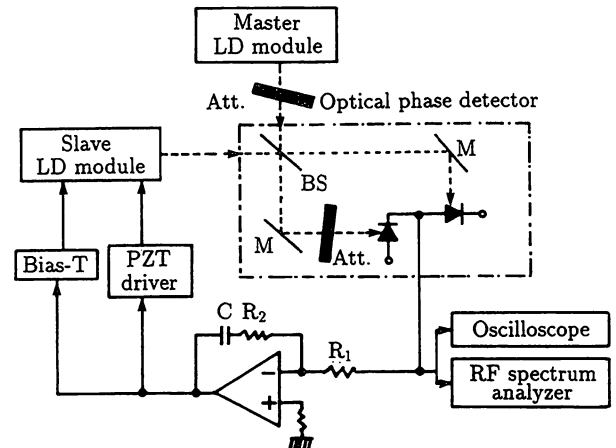


Fig. 12. Schematic diagram of the experimental setup of the homodyne OPLL. LD module: confocal Fabry-Perot cavity coupled semiconductor laser diode (CFP-LD). BS: beam splitter. M: 100% reflection mirror. Att.: optical power attenuator.

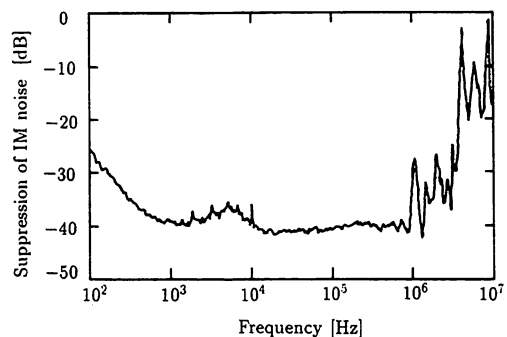


Fig. 13. IM noise suppression characteristics of the optical phase detector.

active loop filter consisted of an operational amplifier, resistors, and a capacitor. In this feedback, two control routes were employed for securing a wide control bandwidth. One is the external cavity length control for slower components of the phase error signal with a 1 kHz bandwidth and the other is the injection current control for faster error signal. The frequency tuning coefficients of the laser were 79 MHz/V by applied voltage to PZT-C for the CFP cavity length control as described in Section II and 31 MHz/mA by the injection current control.

The natural frequency of the loop was selected from several tens kHz to 2 MHz by adjusting the power of the master laser using an optical power attenuator, and resistors and a capacitor of the loop filter shown in Fig. 12. By this adjustment, the loop gain is changed and thereby varying the natural frequency and the damping factor of the OPLL (For details, see Appendix A).

The phase error was measured at the output of the optical phase detector by an oscilloscope to measure the rms phase error and an RF spectrum analyzer for the measurement of power spectral density (PSD) of phase error.

B. Results and Discussions

We measured the phase error comparing the rms voltage value in a phase-locked state with the peak-to-peak

amplitude of the beat signal under unlocked state. Fig. 14 (a) and (b) shows output signals from the optical phase detector measured by an oscilloscope with a 150 MHz bandwidth. In this figure, (a) and (b) are those under unlocked and phase-locked conditions, respectively. In the unlocked state, there are a frequency difference between two lasers, so a beat waveform can be found in the output from the optical phase detector. When two optical signals from the master and the slave lasers are homodyne phase-locked together, the frequency difference became zero and then only the phase errors appeared in the output as shown by Fig. 14(b). The peak-to-peak value of (a) corresponds to 2 rad phase error. Then, the rms phase error $\sigma_{\phi, rms}$ [rad] (square root of phase error variance σ_{ϕ}^2) can easily be determined by measuring the rms voltage of (b) and dividing it by [peak-to-peak value of (a)]/2. The measured rms phase error by this method under the locking condition of the Fig. 14(b), the rms phase error was 4.54×10^{-2} rad ($\sigma_{\phi}^2 = 2.06 \times 10^{-3}$ rad²).

However, the σ_{ϕ}^2 was calculated to be 1.11×10^{-2} rad² by using the loop parameters, i.e., the natural frequency of 1.5 MHz and the damping factor 0.3, and the estimated beat linewidth of 20 kHz with an assumption that the line shape of the lasers are Lorentzian. The fact that the measured values of phase errors were smaller than the calculated values, suggests that the estimated linewidth contained not only Lorentzian phase noise components but also $1/f$ components of FM noise within the FM noise suppression bandwidths of the optical feedback. However, these noise components within the loop bandwidth can be negligible. Furthermore, the measured bandwidth was 150 MHz, whereas the calculated value takes infinite bandwidth. Therefore, the actual FM noise spectrum has to be used to evaluate the phase error of an OPLL.

Fig. 15(a) shows the PSD of phase error of the homodyne OPLL under the same phase locked condition as Fig. 14(b). The break point of the PSD is about 1.5 MHz, which corresponds to the natural frequency of the loop. The PSD's of phase error under phase-locked condition $S_{PE}(f)$, phase noises of the master laser $S_{PH,M}(f)$, and the slave laser $S_{PH,S}(f)$ are related as

$$S_{PE}(f) = [S_{PH,M}(f) + S_{PH,S}(f)] |1 - H(j2\pi f)|^2 \quad (13)$$

where $H(j2\pi f)$ is the transfer function of the OPLL, which is given in Appendix A. Fig. 15(b) is the calculated PSD's $S_{PE}(f)$ (curve B) and $[S_{PH,M}(f) + S_{PH,S}(f)]$ (curve A). The measured and the calculated results show good agreement as can be seen by comparing Fig. 15(a) with the curve B of Fig. 15(b). The phase error of the OPLL is mainly determined by the shot noise as well as phase noises of the lasers. As can be seen from the (19), the phase error by the phase noise is decreased by increasing the bandwidth of the loop, while that by the shot noise is increased. The optimal natural frequency of the loop is therefore the point where these two components are equal to each other. Since the natural frequency of the OPLL in

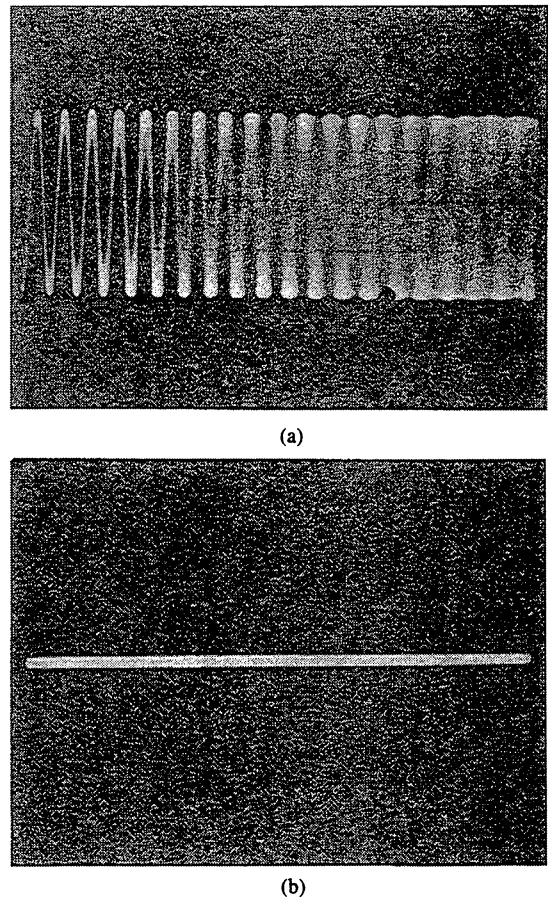


Fig. 14. Output of the optical phase detector under unlocked (a) phase-locked condition (b) measured by a 150 MHz bandwidth RF oscilloscope.

this experiment was far lower than the optimal natural frequency, i.e., over 10 MHz depending on the power of the master laser used in phase error detection, the phase error component due to the shot noise was negligibly small compared with that due to the laser phase noises. So, the shot noise component was not used in this calculation.

Fig. 16 shows calculated power spectral densities of phase error under phase-locked condition (curve B) and the sum of PSD's of phase noises of the master and the slave lasers (curve A). For comparison, the sum of PSD's of phase noises of two free running LD's (curve C) are also shown. The calculation procedure of curves A and C were described in Section II. The curves A and B of this figure are the same ones of curves A and B in Fig. 15(b). Experimentally measured parameters were used in these calculations. The broken curve D in this figure represents the phase noise corresponding to a 20 kHz linewidth, which is the estimated linewidth sum of the master and the slave lasers. As can be seen by comparing this with curve A, the actual phase noise spectrum must be used to evaluate the loop performance.

The phase error variance σ_{ϕ}^2 with a measurement bandwidth B_M of the phase error is calculated by

$$\sigma_{\phi}^2 = \sigma_{\phi, rms}^2 = \int_0^{B_M} S_{PE}(f) df. \quad (14)$$

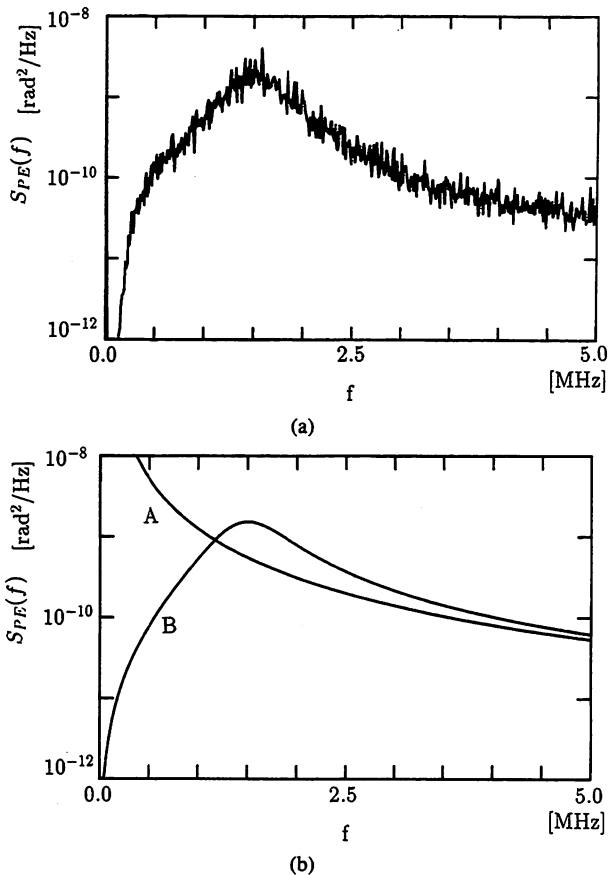


Fig. 15. Power spectral densities of phase error under phase-locked condition. (a) Measured result. (b) Calculated result (curve B). Curve A in (b) is the sum of PSD's of phase noises of the master and the slave lasers. The natural frequency of the loop was 1.5 MHz, which corresponds to a breakpoint found in the spectra under phase-locked condition.

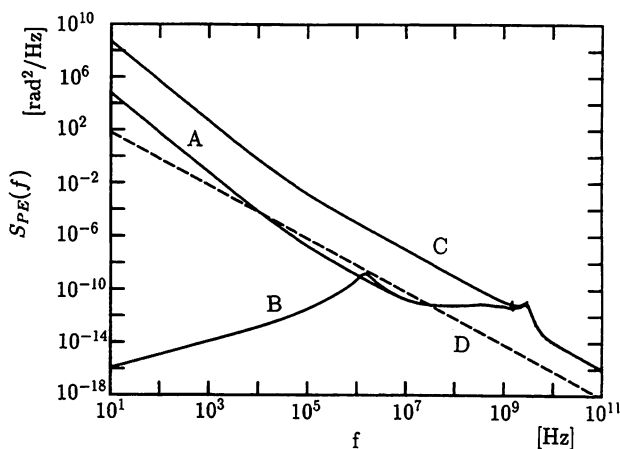


Fig. 16. Calculated power spectral densities of phase error under phase-locked condition (curve B) and the sum of PSD's of phase noises of the master and the slave lasers (curve A). For comparison purpose, the sum of PSD's of phase noises of two free running LD's (curve C) is also shown. The broken curve D represents the phase noise corresponding to a 20 kHz linewidth, which is the estimated linewidth sum of the master and slave lasers.

To compare with the measured phase error by an oscilloscope, phase error variance with a 150 MHz bandwidth was calculated by this equation. The calculated σ_ϕ^2 was $2.98 \times 10^{-3} \text{ rad}^2$, while the measured result was $2.06 \times$

10^{-3} rad^2 . The difference between them is negligibly small. As can be seen by the curve B of Fig. 16, a large amount of phase noise power are remained in the range of $f > 150 \text{ MHz}$. The phase error variance due to phase noises within that range was calculated as $2.05 \times 10^{-2} \text{ rad}^2$. Then, the phase error variance considering a infinite bandwidth is $2.26 \times 10^{-2} \text{ rad}^2$. Using this value and (30) or (31) in Appendix B, the total phase locked power concentration ratio of the slave laser is estimated to be 97.7%. This means that 97.7% of the temporal coherence of the master laser was transferred to the slave laser by this OPLL. Therefore, the OPLL can be used to frequency stabilization of slave lasers with a highly stable master laser.

V. SUMMARY

Optical phase-locking experiments have been carried out using two confocal Fabry-Perot cavity coupled semiconductor laser diodes (CFP-LD's). Their spectral and FM noise suppression characteristics have been precisely evaluated by measurements and calculations.

For the evaluation of the frequency stabilization experiment of semiconductor lasers by optical feedback from the resonant cavity, a simple transfer function of the frequency stabilization scheme with an optical feedback was proposed. FM noise reduction characteristics were calculated by using the proposed model and compared with the measured results. A good agreement between them was confirmed. FM noise suppression ratio within the control bandwidth was 39 dB. Spectral characteristics and the frequency drift in the time domain were evaluated by precise measurements. The short term spectral linewidth and the frequency drift were 6.5 kHz and 20 kHz/s, respectively.

Using two CFP-LD's a homodyne OPLL was constructed. The power spectral density of phase error of the OPLL was measured and compared with the calculated one. They showed a good agreement with each other. The phase error variance with the infinite bandwidth was estimated as $2.26 \times 10^{-2} \text{ rad}^2$ using measured and calculated results. The total phase-locked power concentration ratio of the slave laser was 97.7%. The phase error of the OPLL was low enough for highly coherent application systems listed in Section I.

APPENDIX A

THEORETICAL CONSIDERATIONS OF OPLL

The transfer function of the OPLL $H(s)$ is given by [44], [62], [63]

$$H(s) = \frac{K_{OPD} K_O F(s)}{s + K_{OPD} K_O F(s)} \quad (15)$$

where K_{OPD} , K_O , and $F(s)$ are the gain of the optical phase detector, i.e., a photodetector or a balanced detector consisted of two photo detectors, the loop gain and the transfer function of a loop filter. We choose a standard first

order active loop filter as shown in Fig. 12 with the transfer function

$$F(s) = \frac{1 + \tau_2 s}{\tau_1 s} \quad (16)$$

where $\tau_1 (= R_1 C)$ and $\tau_2 (= R_2 C)$ are time constants of the loop filter. The natural angular frequency ω_N and the damping factor ζ of the homodyne OPLL are then defined as

$$\omega_N = \sqrt{\frac{K_{OPD} K_O}{\tau_1}}, \quad [\text{rad/s}] \quad (17)$$

and

$$\zeta = \frac{\omega_N \tau_2}{2}. \quad (18)$$

The phase error variance σ_ϕ^2 of the homodyne OPLL is given by

$$\sigma_\phi^2 = \int_0^\infty \{ |1 - H(j2\pi f)|^2 [S_{PH,M}(f) + S_{PH,S}(f)] + |H(j2\pi f)|^2 S_{SN}(f) \} df, \quad [\text{rad}^2] \quad (19)$$

where $S_{PH,M}(f)$, $S_{PH,S}(f)$, and $S_{SN}(f)$ are the PSD's of the phase noise of the master and the slave lasers, and phase noise translated shot noise, respectively.

APPENDIX B

POWER CONCENTRATION RATIOS

Power concentration ratio of a laser within a certain bandwidth B is a useful information for users. As an example, we consider a laser with the Lorentzian spectral profile. The line shape function $g(\nu)$ of a Lorentzian spectrum is given by

$$g(\nu - \nu_0) = \frac{\Delta\nu}{2\pi} \frac{1}{(\nu - \nu_0)^2 + (\Delta\nu/2)^2} \quad (20)$$

where $\Delta\nu$ is the spectral linewidth, ν_0 is the center frequency of oscillation, and $g(\nu)$ is normalized by

$$\int_{-\infty}^{\infty} g(\nu - \nu_0) d\nu = 1. \quad (21)$$

Then the power concentration ratio R_{PC} within $\nu_0 \pm B$ can be obtained as

$$R_{PC} = \int_{\nu_0 - B}^{\nu_0 + B} g(\nu - \nu_0) d\nu = \frac{2}{\pi} \arctan\left(\frac{2}{\Delta\nu} B\right) \quad (22)$$

which is graphically shown by the broken line of Fig. 17.

Since the signal with the Lorentzian spectral profile can be regarded as the superposition of a zero-linewidth signal and modulated side frequency components by phase noise, the power concentration ratio R_{PC} of the main spectrum of the phase modulated signal is given by

$$R_{PC} = |J_0(\beta)|^2 \quad (23)$$

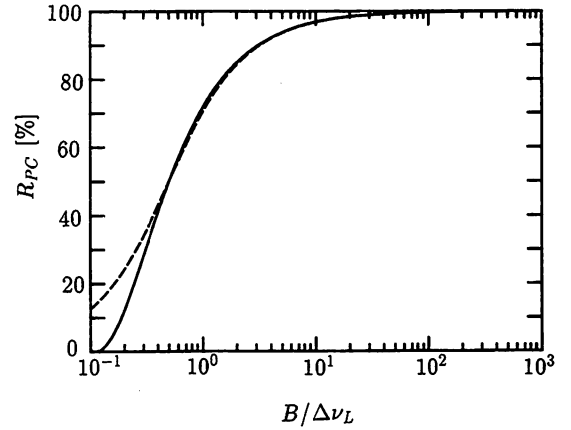


Fig. 17. Power concentration ratio R_{PC} of the laser with the Lorentzian spectral line shape for the considered bandwidth B normalized to the linewidth $\Delta\nu$. The broken line shows the result obtained by an exact calculation. The solid line is obtained by an approximated calculation.

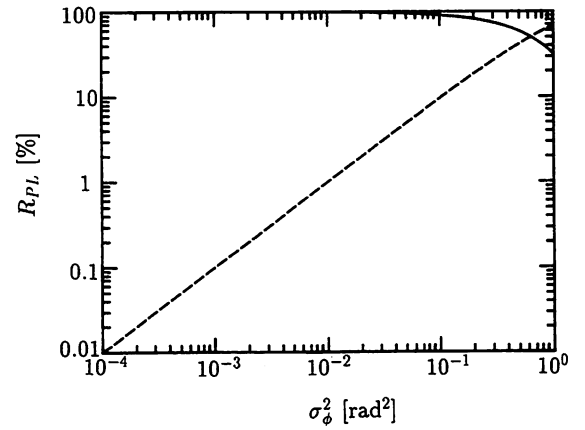


Fig. 18. Total phase-locked power concentration ratio R_{PL} of the slave laser for the phase error variance σ_ϕ^2 . The solid and broken lines are the total phase-locked power and unlocked power, respectively.

where $J_0(\cdot)$ and β are the Bessel function of the first order and the modulation index, respectively, and the value of β is given by

$$\beta = \sum_{k=B}^{\infty} \beta_k \quad (24)$$

where

$$\beta_k = \sqrt{2S_{PH}(k)} \quad (25)$$

which is the zero-to-peak value of the phase fluctuation component at the Fourier frequency k . β can also be expressed as

$$\beta = \sqrt{2} \cdot \sigma_\phi|_B^\infty \quad (26)$$

where

$$\sigma_\phi|_B^\infty = \int_B^\infty S_{PH}(f) df = \int_B^\infty \frac{S_{FM}(f)}{f^2} df, \quad [\text{rad}^2] \quad (27)$$

where $S_{FM}(f)$ is the power spectral density of the FM noise. For the signal with a Lorentzian line shape, (27)

can be simply expressed as

$$\sigma_{\phi}^2|_B^{\infty} = \frac{\Delta\nu}{\pi B}. \quad [\text{rad}^2]. \quad (28)$$

To satisfy preceding discussions, the following equation must be valid:

$$1 - |J_0(\beta)|^2 = \sum_{k=B}^{\infty} \{1 - |J_0(\beta_k)|^2\}. \quad (29)$$

The calculated R_{PC} by using (23) and (26) of the laser with the Lorentzian spectral line shape for the considered bandwidth B normalized to the linewidth $\Delta\nu$ is shown by the solid line of Fig. 17. Comparing the solid line with the broken line, we found that the relation given by (23) can be an acceptable approximation under the condition of $B/\Delta\nu_L > 0.5$, i.e., $\beta < 1.13$.

By following above discussions, the total phase-locked power R_{PL} of the slave laser can be given by

$$R_{PL} \approx |J_0(\sqrt{2} \cdot \sigma_{\phi})|^2 \quad (30)$$

for $\sigma_{\phi} < 0.8$ rad. Fig. 18 shows the calculated results by using (30). From Fig. 18 further approximation can be obtained as

$$R_{PL} \approx 1 - \sigma_{\phi}^2 \quad (31)$$

for $\sigma_{\phi}^2 < 0.1$ rad². A simple relation between the total phase-locked power concentration ratio and the phase error variance was derived. This consideration is important for applications such as noise reduction of the slave laser by phase locking to an highly stable master laser and so on. Furthermore, the phase-locked power concentration ratio of the slave laser can be considered as a comprehensive measure representing the degree of temporal coherence transfer from the master laser to the slave laser, i.e., the frequency stabilization by optical phase locking.

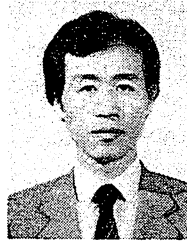
ACKNOWLEDGMENT

The authors would like to thank M. Kouroggi and M. Teshima of Tokyo Institute of Technology, and T. Imai of Tokyo Aircraft Instrument Co. Ltd., for their assistance in preparing the lasers and some calculations. They also thank Dr. K. Nakagawa of Tokyo Institute of Technology for his helpful discussions.

REFERENCES

- [1] H. R. Telle, D. Meschede, and T. W. Hänsch, "Realization of a new concept for visible frequency division: phase locking of harmonic and sum frequencies," *Opt. Lett.*, vol. 15, no. 10, pp. 532-534, 1990.
- [2] S. E. Moran, R. L. Law, P. N. Craig, and M. Goldberg, "Optically phase-locked speckle pattern interferometer," *Appl. Opt.*, vol. 26, no. 3, pp. 475-491, 1987.
- [3] C. L. Hayes and L. M. Laughman, "Generation of coherent optical pulses," *Appl. Opt.*, vol. 16, no. 2, pp. 263-264, 1977.
- [4] M. Ohtsu, "Realization of ultrahigh coherence in semiconductor lasers by negative electrical feedback," *J. Lightwave Technol.*, vol. 6, pp. 245-256, 1988.
- [5] H. E. Hagemeyer and S. R. Robinson, "Field properties of multiple coherently combined lasers," *Appl. Opt.*, vol. 18, no. 3, pp. 270-280, 1979.
- [6] S. P. Dijaili, J. S. Smith, and A. Dienes, "Timing synchronization of a passively mode-locked dye laser using a pulsed optical phase lock loop," *Appl. Phys. Lett.*, vol. 55, no. 5, pp. 418-420, 1989.
- [7] L. H. Enloe and J. L. Rodda, "Laser phase-locked loop," *Proc. IEEE*, vol. 53, pp. 165-166, 1965.
- [8] J. L. Hall, L. S. Ma, and G. Kramer, "Principles of optical phase-locking: application to internal mirror He-Ne lasers phase-locked via fast control of the discharge current," *IEEE J. Quantum Electron.*, vol. QE-23, pp. 427-437, Apr. 1987.
- [9] C. H. Shin and M. Ohtsu, "Heterodyne optical phase-locked loop by confocal Fabry-Perot cavity coupled AlGaAs lasers," *IEEE Photon. Technol. Lett.*, vol. 2, pp. 297-300, Apr. 1990.
- [10] R. C. Steele, "Optical phase-locked loop using semiconductor laser diodes," *Electron. Lett.*, vol. 19, no. 2, pp. 69-71, 1983.
- [11] J. Harrison and A. Mooradian, "Linewidth and offset locking of external cavity GaAlAs lasers," *IEEE J. Quantum Electron.*, vol. 25, pp. 1152-1155, June 1989.
- [12] H. R. Telle and H. Li, "Phase-locking of laser diodes," *Electron. Lett.*, vol. 26, no. 13, pp. 858-859, 1990.
- [13] E. A. Swanson, S. B. Alexander, and R. S. Bondurant, "Wideband frequency noise reduction and FM equalization in AlGaAs lasers using electrical feedback," *Opt. Lett.*, vol. 16, no. 18, pp. 1403-1405, 1991.
- [14] K. Kuboki and M. Ohtsu, "Frequency offset locking of AlGaAs semiconductor lasers," *IEEE J. Quantum Electron.*, vol. QE-23, pp. 388-394, Apr. 1987.
- [15] K. Kuboki, C. H. Shin, T. Kato, and M. Ohtsu, "Performance and its evaluation of optical tracking generator/optical frequency synthesizer by semiconductor lasers," in *Tech. Dig., 1988 Conf. Precision Electromag. Meas. (CPEM)*, S. Suematsu, Ed., June 1988, pp. 24-25.
- [16] K. Kuboki and M. Ohtsu, "A synthesized method to improve coherence in semiconductor lasers by electrical feedback," *IEEE J. Quantum Electron.*, vol. 25, pp. 2084-2090, Oct. 1989.
- [17] O. Ishida, H. Toba, and Y. Tojmorii, "0.04 Hz relative optical-frequency stability in a 1.5 μm distributed-Bragg-reflector (DBR) laser," *IEEE Photon. Technol. Lett.*, vol. 1, pp. 452-454, 1989.
- [18] T. J. Kane, A. C. Nilsson, and R. L. Byer, "Frequency stability and offset locking of a laser-diode-pumped Nd:YAG monolithic non-planar ring oscillator," *Opt. Lett.*, vol. 12, no. 3, pp. 175-177, 1987.
- [19] J. L. Hall, M. Zhu, F. Shimizu, and K. Shimizu, "External frequency stabilization of a commercial dye laser at the sub-hertz level," in *Tech. Dig. 16th Int. Conf. Quantum Electron., (IQEC'88)*, 1989, paper 19A3-3.
- [20] W. R. Leeb, H. K. Phlipp, A. L. Scholtz, and E. Bonek, "Frequency synchronization and phase locking of CO₂ lasers," *Appl. Phys. Lett.*, vol. 41, pp. 592-594, 1982.
- [21] G. Wenke and S. Saito, "Phase locking of semiconductor lasers using homodyne detection and negative electrical feedback," *Japan. J. Appl. Phys.*, vol. 24, no. 12, pp. L908-L910, 1985.
- [22] M. Kouroggi, C. H. Shin, and M. Ohtsu, "A 134 MHz bandwidth homodyne optical phase-locked loop of semiconductor lasers," *IEEE Photon. Technol. Lett.*, vol. 3, pp. 270-272, Mar. 1991.
- [23] T. J. Kane and E. A. P. Cheng, "Fast frequency tuning and phase locking of diode-pumped Nd:YAG ring lasers," *Opt. Lett.*, vol. 13, no. 11, pp. 970-972, 1988.
- [24] L. G. Kazovsky and D. A. Atlas, "A 1320 nm experimental optical phase-locked loop," *IEEE Photon Technol. Lett.*, vol. 1, pp. 395-397, Nov. 1989.
- [25] J. M. Kahn, B. L. Kasper, and K. J. Pollock, "Optical phaselock receiver with multigigahertz signal bandwidth," *Electron Lett.*, vol. 25, no. 10, pp. 626-628, 1989.
- [26] D. J. Malyon, D. W. Smith, and R. Wyatt, "Semiconductor laser homodyne phase-locked loop," *Electron. Lett.*, vol. 22, no. 8, pp. 421-422, 1986.
- [27] C. J. Nielsen and J. H. Osmundsen, "Linewidth stabilization of semiconductor lasers in an external cavity," *J. Opt. Commun.*, vol. 5, no. 2, pp. 42-45, 1984.
- [28] D. Lenstra, B. H. Verbeek, and A. J. Bon Boef, "Coherence collapse in single-mode semiconductor lasers due to optical feedback," *IEEE J. Quantum Electron.*, vol. QE-21, pp. 674-679, June 1985.
- [29] J. M. Kahn, C. A. Burrus, and G. Raybon, "High-stability 1.5 μm external-cavity semiconductor lasers for phase-lock applications," *IEEE Photon. Technol. Lett.*, vol. 1, pp. 159-161, July 1989.
- [30] G. Wenke, R. Gross, P. Meissner, and E. Pazak, "Characteristics of a compact three cavity laser configuration," *J. Lightwave Technol.*, vol. LT-5, pp. 608-615, 1987.

- [31] A. Schremer and C. L. Tang, "Single-frequency tunable external-cavity semiconductor laser using an electro-optic birefringent modulator," *Appl. Phys. Lett.*, vol. 55, no. 1, pp. 19-21, 1989.
- [32] M. Ohtsu, H. Suzuki, K. Nemoto, and Y. Teramachi, "Narrow-linewidth tunable visible InGaAlP laser, application to spectral measurements of lithium, and power amplification," *Japan. J. Appl. Phys.*, vol. 29, no. 8, pp. L1463-L1465, 1990.
- [33] N. A. Olsson and J. P. Van Der Ziel, "Performance characteristics of 1.5- μm external cavity semiconductor lasers for coherent optical communication," *J. Lightwave Technol.*, vol. LT-5, pp. 510-515, Apr. 1987.
- [34] F. Favre and D. LeGuen, "Spectral properties of a semiconductor laser coupled to a single mode fiber resonator," *IEEE J. Quantum Electron.*, vol. QE-21, pp. 1937-1946, Dec. 1985.
- [35] F. Favre, D. LeGuen, and J. C. Simon, "Optical feedback effects upon laser diode oscillation field spectrum," *IEEE J. Quantum Electron.*, vol. QE-18, pp. 1712-1717, Oct. 1982.
- [36] A. G. Bulushev, Y. V. Gurov, E. M. N. Dianov, A. V. Kuznetsov, and V. M. Paramonov, "All-fiber reflector for selection of semiconductor laser modes," *Sov. J. Quantum Electron.*, vol. 18, pp. 698-700, May 1988.
- [37] B. Dahmani, L. Hollberg, and R. Drullinger, "Frequency stabilization of semiconductor lasers by resonant optical feedback," *Opt. Lett.*, vol. 12, no. 11, pp. 876-878, 1987.
- [38] P. Laurent, A. Clairon, and C. Bréant, "Frequency noise analysis of optically self-locked diode lasers," *IEEE J. Quantum Electron.*, vol. 25, pp. 1131-1142, June 1989.
- [39] H. Li and H. R. Telle, "Efficient frequency noise reduction of AlGaAs semiconductor lasers by optical feedback from an external high-finesse resonator," *IEEE J. Quantum Electron.*, vol. 25, pp. 257-264, Mar. 1989.
- [40] C. H. Shin, M. Teshima, M. Ohtsu, T. Imai, J. Yoshida, and K. Nishide, "FM characteristics and compact modules for coherent semiconductor lasers coupled to an external cavity," *IEEE Photon. Technol. Lett.*, vol. 2, pp. 167-169, Mar. 1990.
- [41] M. Segev, S. Weiss, and B. Fisher, "Coupling of diode laser arrays with photorefractive passive phase conjugate mirrors," *Appl. Phys. Lett.*, vol. 50, no. 20, pp. 1397-1399, 1987.
- [42] D. S. Seo, J. D. Park, J. G. McInerney, and M. Osinski, "Effects of feedback asymmetry in external-cavity semiconductor laser systems," *Electron. Lett.*, vol. 24, no. 12, pp. 726-728, 1988.
- [43] H. Li and N. B. Abraham, "Analysis of the noise spectra of a laser diode with optical feedback from a high-finesse resonator," *IEEE J. Quantum Electron.*, vol. 25, pp. 1782-1793, Aug. 1989.
- [44] C. H. Shin, "Optical phase-locking of semiconductor lasers," Ph.D. dissertation, Tokyo Instit. Technol., 1991.
- [45] C. H. Shin, M. Teshima, and M. Ohtsu, "Novel measurement method of linewidth enhancement factor in semiconductor lasers by optical self-locking," *Electron. Lett.*, vol. 25, no. 1, pp. 27-28, 1989.
- [46] R. Lang and K. Kobayashi, "External optical feedback effects on semiconductor injection laser properties," *IEEE J. Quantum Electron.*, vol. QE-16, pp. 347-355, Mar. 1980.
- [47] B. Tromborg, J. H. Osmundsen, and H. Olesen, "Stability analysis for a semiconductor laser in an external cavity," *IEEE J. Quantum Electron.*, vol. QE-20, pp. 1023-1032, Sept. 1984.
- [48] P. Spano, S. Piazzolla, and M. Tamburrini, "Theory of noise in semiconductor lasers in the presence of optical feedback," *IEEE J. Quantum Electron.*, vol. QE-20, pp. 350-357, Apr. 1984.
- [49] D. R. Hjelme and A. R. Mickelson, "On the theory of external cavity operated single-mode semiconductor lasers," *IEEE J. Quantum Electron.*, vol. QE-23, pp. 1000-1004, June 1987.
- [50] C. H. Henry, "Theory of the linewidth of semiconductor lasers," *IEEE J. Quantum Electron.*, vol. QE-18, pp. 259-264, Feb. 1982.
- [51] K. Vahala and A. Yariv, "Semiclassical theory of noise in semiconductor lasers—Part II," *IEEE J. Quantum Electron.*, vol. QE-19, pp. 1102-1109, June 1983.
- [52] P. Spano, S. Piazzolla, and M. Tamburrini, "Phase noise in semiconductor lasers: A theoretical approach," *IEEE J. Quantum Electron.*, vol. QE-19, pp. 1195-1199, July 1983.
- [53] K. Kikuchi and T. Okoshi, "Measurement of FM noise, AM noise, and field spectra of 1.3 μm InGaAsP DFB lasers and determination of the linewidth enhancement factor," *IEEE J. Quantum Electron.*, vol. QE-21, pp. 1814-1818, Nov. 1985.
- [54] M. Ohtsu, M. Murata, and M. Kourogi, "FM noise reduction and subkilohertz linewidth of an AlGaAs laser by negative electrical feedback," *IEEE J. Quantum Electron.*, vol. 26, pp. 231-241, Feb. 1990.
- [55] C. H. Shin and M. Ohtsu, "Stable semiconductor laser with a 7-hz linewidth by an optical-electrical double-feedback technique," *Opt. Lett.*, vol. 15, no. 24, pp. 1455-1457, 1990.
- [56] H. P. Yuen and V. W. S. Chan, "Noise in homodyne and heterodyne detection," *Opt. Lett.*, vol. 8, no. 3, pp. 177-179, 1983.
- [57] G. L. Abbas, V. W. S. Chan, and T. K. Yee, "Local-oscillator excess-noise suppression for homodyne and heterodyne detection," *Opt. Lett.*, vol. 8, no. 8, pp. 419-421, 1983.
- [58] —, "A dual-detector optical heterodyne receiver for local oscillator noise suppression," *J. Lightwave Technol.*, vol. LT-3, pp. 1110-1122, May 1985.
- [59] N. Singh, H. M. Gupta, and V. K. Jain, "Design considerations in dual-detector receiver," *J. Opt. Commun.*, vol. 9, no. 4, pp. 150-154, 1988.
- [60] S. B. Alexander, D. Welford, and D. vL. Marquis, "Passive equalization of semiconductor diode laser frequency modulation," *J. Lightwave Technol.*, vol. 7, pp. 11-23, Jan. 1989.
- [61] P. P. Smyth, A. A. Sayles, N. R. Back, A. P. McDonna, and M. J. Creaner, "High performance balanced dual-detector GaAs IC receiver for 565 Mbit/s optical heterodyne detection," *Electron. Lett.*, vol. 25, no. 21, pp. 1414-1416, 1989.
- [62] L. G. Kazovsky, "Balanced phase-locked loops for optical homodyne receivers: performance analysis, design considerations, and laser linewidth requirements," *J. Lightwave Technol.*, vol. LT-4, pp. 182-195, Feb. 1986.
- [63] T. J. Hodgkinson, "Phase-locked-loop analysis for pilot carrier coherent optical receivers," *Electron. Lett.*, vol. 21, nos. 25-26, pp. 1202-1203, 1985.



Chul-Ho Shin was born in Chun-Nam, Republic of Korea, in September 1952. He received the B.S. and M.S. degrees from the Korea Maritime University in 1976 and 1985, respectively, and the Ph.D. degree in coherent quantum optics and technology from the Tokyo Institute of Technology in 1991.

He was a navigation officer of ocean-going vessels from 1976 to 1980. He became a lecturer and an assistant professor at the National Mokpo Merchant Marine College, Korea, from 1982 and 1984. He is currently an associate professor at the same college from 1992. His interests include coherent optical communications, frequency/phase control and stabilization of semiconductor lasers, optical frequency conversion using optical phase-locked loops or nonlinear optics, the laser spectroscopy, and the electronics navigation.

Dr. Shin is a member of the Korean Institute of Telematics and Electronics, the Optical Society of Korea, the Japan Society of Applied Physics, and the Korea Institute of Navigation.



Motoichi Ohtsu (M'88-SM'90) was born in Kanagawa, Japan, on October 5, 1950. He received the B.S., M.S., and Ph.D. degrees in electronics engineering from the Tokyo Institute of Technology, Tokyo, Japan, in 1973, 1975, and 1978, respectively.

In 1978 he was appointed as a Research Associate and in 1982 became an Associate Professor with the Tokyo Institute of Technology. From September 1986 to July 1987, while on leave from the Tokyo Institute of Technology, he joined the

Crawford Hill Laboratory, AT&T Bell Laboratories, Holmdel, NJ. In 1991, he became a Professor at the Tokyo Institute of Technology. Currently, his main fields of interest are the frequency control of lasers, photon scanning tunneling microscopy, and its application to atom manipulation.

Dr. Ohtsu has written over 100 papers, received two patents, and 20 pending patents. He is the author and coauthor of 11 books including two in English, entitled *Highly Coherent Semiconductor Lasers* (Boston: Artech House, 1991) and *Coherent Quantum Optics and Technology* (Tokyo: Kluwer Academic). He has been a tutorial lecturer of the SPIE. He has been awarded eight prizes from academic institutions including the Issac Koga Gold Medal of URSI in 1984, Japan IBM Science Award in 1988, and the awards of the Japanese Society of Applied Physics in 1987 and 1990. He is a member of the Institute of Electronics, Information and Communication Engineering of Japan, the Institute of Electrical Engineering of Japan, the Japan Society of Applied Physics, and the Optical Society of America.

Generation of Phase Conjugate Wave from a Visible InGaAlP Laser

Yoshinari AWAJI, Shuji SAYAMA, Hiromasa SUZUKI, Motoichi OHTSU and Yasumasa TERAMACHI¹

*Interdisciplinary Graduate School of Science and Engineering, Tokyo Institute of Technology,
4259 Nagatsuta, Midori-ku, Yokohama 227*

¹*Department of Information Engineering, University of Industrial Technology,
4-1-1 Hashimoto-dai, Sagami-hara, Kanagawa 229*

(Received July 14, 1992; revised manuscript received November 30, 1992; accepted for publication December 19, 1992)

This paper presents the first quantitatively measured results of detuning and spatial characteristics of the phase conjugate wave which is emitted from a Fabry-Perot cavity-type InGaAlP laser. Bandwidth of a nearly-degenerate four-wave mixing was confirmed to be due to the relaxation oscillation frequency of the laser. The reflectivity of the phase conjugate mirror and the amplification gain were larger than 10 and 100, respectively. By the off-axial injection of the probe beam to a broad stripe laser, the emitted phase conjugate wave was separated spatially from the pump beam. Non-degenerate four-wave mixing characteristics of an AlGaAs laser were also measured for the first time. Its 3-dB cutoff frequency was as large as 0.1 THz, which was determined by the reciprocal of the half-cycle time of the intracavity light-wave.

KEYWORDS: phase conjugate wave, semiconductor laser, InGaAlP laser, four-wave mixing, waveguide

1. Introduction

Phase conjugate wave (PCW) generation from semiconductor lasers has been intensively studied. This is not only due to scientific interest but also to technical requirements, *e.g.*, to reduce channel-crosstalk when these devices are used as optical amplifiers in a frequency-division multiplexing coherent optical transmission system.¹⁾ It has been known that the semiconductor laser, as a four-wave mixing (FWM) material for generating a PCW, has several notable characteristics as compared with those of conventional photorefractive materials. They are:^{2,3)}

1. the third-order nonlinear optical coefficient takes a large value due to the saturation of the carrier density in the active waveguide;
2. refractive index-induced diffraction grating is generated simultaneously with the gain-induced diffraction grating.
3. FWM bandwidth is wide due to a short interband relaxation time of the carrier;
4. FWM efficiency is large because of the high power density of the intracavity lasing light, which is used as a pump beam for the FWM.

These characteristics can be advantageous when one uses semiconductor lasers as efficient phase conjugate mirrors (PCM). However, spatial characteristics of the PCW, emitted from the narrow-stripe laser cavity, are degraded due to the diffraction because the active waveguide of this laser has sub-wavelength cross-sectional dimensions. This could be disadvantageous to optical measurements, optical information processing, and so on in which the spatial characteristics of the PCW from the narrow-stripe laser are utilized. On the other hand, since the frequency characteristics of the PCW are preserved in the free space even after it is emitted from the narrow-stripe laser, two of the authors (M.O. and Y.T.) have proposed utilizing the semiconductor laser as an external PCM of optical feedback system to reduce the wideband FM noise from another semiconductor laser.⁴⁾ Furthermore, it has been pointed out that these characteristics can be used

to realize an optically controlled lightwave frequency shifter.⁵⁾

Although Fabry-Perot cavity-type visible InGaAlP lasers with 0.67 μm wavelength have already been used for several optical measurement systems, characteristics of the PCW emitted from these lasers, especially its detuning characteristics, have not yet been quantitatively evaluated. This paper presents for the first time the results of three kinds of quantitative evaluation utilizing the experimental techniques for the preliminary evaluations of the PCW characteristics of the 0.83 μm AlGaAs lasers.⁴⁾ They are: (1) dependence of the PCW characteristics on detuning; (2) spatial characteristics of the PCW emitted from a broad-stripe InGaAlP laser; and (3) PCW characteristics of a 0.83 μm wavelength AlGaAs laser being used as a reference laser device in this work, especially its nondegenerate FWM characteristics. This is the first report, as far as we know, about quantitative and systematic measurement of nondegenerate FMW. According to preceding research,⁶⁾ it has been predicted that the bandwidth of nondegenerate FMW is restricted by intraband relaxation time of carrier; however, we discovered that the cycle time within the intracavity exerts more influence on the band width. The results of (1) and (2) will be described in §3.1 and 3.2, respectively, and (3) will be described in the Appendix.

2. Experimental

Figure 1 shows an experimental setup which is almost the same as that used in the preliminary study.⁴⁾ PL and IL represent 0.67 μm -wavelength Fabry-Perot cavity-type InGaAlP lasers used as a FWM medium for PCW generation and as a light source for the probe beam, respectively. They were used under the condition of single longitudinal mode oscillation. Here, the single longitudinal mode oscillation was defined as the state in which the power of the main longitudinal mode was more than 10 dB larger than those of other unwanted longitudinal modes when they were measured by a grating monochromator with 0.1 nm resolution.

For the PL, injection current I was fixed to be larger

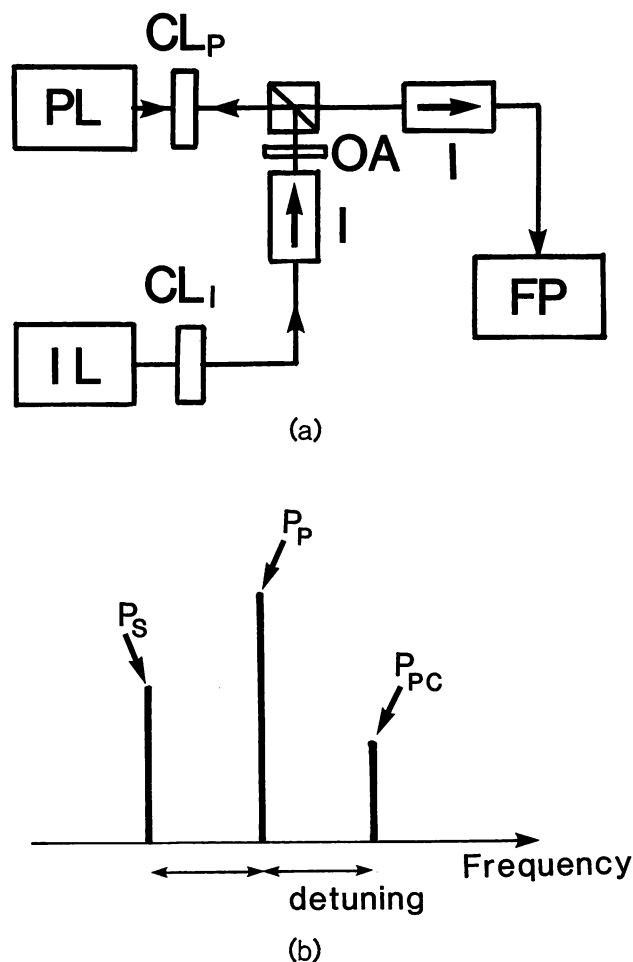


Fig. 1. (a) Experimental setup. PL: laser for generating PCW. IL: laser for emitting the probe beam which is injected into the PL. CL_P , CL_I : collimating lenses. I: optical isolator. OA: variable optical attenuator. FP: Fabry-Perot interferometer. (b) The position corresponding to P_p , P_s and P_{pc} in the observed spectrum. The vertical axis represents arbitrary intensity. The center peak is pump beam P_p and the left peak is P_s , which is incident beam P_{in} amplified in active region of semiconductor laser. Phase conjugation beam P_{pc} appears symmetrically with P_s .

than its threshold value I_{th} such that the CW lasing beams could work as high-power density pump beams for the FWM. Narrow- and broad-stripe lasers were used, and are denoted as PL1 and PL2, respectively in this paper. A Toshiba TOLD9215 laser with $5\ \mu\text{m}$ stripe width was used as the PL1. The PL2 had almost the same structure as that of the PL1, except that the stripe width was as large as $30\ \mu\text{m}$. Although the PL2 usually exhibited the multilongitudinal mode oscillation, it oscillated with a single longitudinal mode when its heat sink temperature was 17°C and the injection current was fixed within the range of $88\ \text{mA} < I < 105\ \text{mA}$. Experiments were carried out under these conditions. The threshold injection current I_{th} was $88\ \text{mA}$ at this temperature, and the lasing output power was $20\ \text{mW}$ at $I=105\ \text{mA}$.

A Toshiba TD9215 laser was also used as the IL. The value of the probe beam power incident into the PL was adjusted by a variable optical attenuator. A Fabry-Perot interferometer was used to separately

measure the powers of the signal beam P_s (i.e., the probe beam P_{in} amplified in the active waveguide of the PL), pump beam P_p of the PL, and the PCW P_{pc} emitted from the PL. Figure 1(b) shows the dependence of P_s , P_{pc} and P_p on frequency, as observed by a Fabry-Perot interferometer. Both P_s and P_{pc} appear symmetrically around P_p . These measured powers were calibrated by using the measured value of the pump beam power that emitted P_{in} from the PL as a reference.

3. Results and Discussions

3.1 Characteristics under the normal injection of the probe beam

Curves A and B of Figs. 2(a) and 2(b) represent the experimental results for the PL1 and PL2, respectively, obtained by injecting the probe beam under a normal incidence to the waveguide facet. Curve C will be explained later. The horizontal axis represents the detuning Δf between the probe and pump beams. Vertical axes represent the PCM reflectivity $R (=P_{pc}/P_{in})$ and the gain $G (=P_s/P_{in})$ of the signal power amplification. Here, $P_{in}=3\ \mu\text{W}$ and $7\ \mu\text{W}$, and $I/I_{th}-1=0.30$ and 0.34 for the PL1 and PL2, respectively. Since the pump beam was found to be injection-locked to the probe beam at $\Delta f < 80\ \text{MHz}$, no measurement was carried out in this detuning range.

It is found that the curves in this figure have the profiles with peaks at several GHz of Δf . The value of Δf at this peak was found to be equal to the relaxation oscillation frequency f_r of the PL by several experimental results, e.g., this value was measured to be proportional to $(I/I_{th}-1)^{1/2}$. This fact means that the dependency of the nearly-degenerate FWM efficiency on the detuning has a bandwidth which is determined by f_r .⁷⁾ However, since such a bandwidth is much larger than that of conventional dielectric photorefractive materials,⁸⁾ these wide bandwidth characteristics could lead to a wide variety of applications of the nearly-degenerate FWM phenomenon. The curves in this figure are nonsymmetric with respect to $\Delta f=0$, and the values of R and G for $\Delta f < 0$ are always larger than those for $\Delta f > 0$. This is due to the nonsymmetric gain which is characterized by the value of the α -parameter, as has been described in ref. 3, i.e., this feature corresponds to the second semiconductor laser characteristics listed in §1. The values of R and G of PL1 and PL2 are larger than 10 and 100, respectively, for $\Delta f < f_r$. Furthermore, comparison between curves A and B confirmed that there are no significant differences in the values of R and G between the narrow- and broad-stripe lasers.

Curves A and B of Fig. 3 represent the measured results of the dependencies of R and G on $I/I_{th}-1$ of the PL1 and PL2, respectively. The values of P_{in} and Δf were fixed to be equal to those in Fig. 2 and to f_r , respectively. It can be seen from this figure that the values of R for the PL1 and PL2 increased with increasing $I/I_{th}-1$ while values of G decreased. Since the values of R and G in Fig. 2 had similar dependencies on Δf , the reason why R and G have opposite dependencies on $I/I_{th}-1$ cannot be stated directly. However, there can be several plausible reasons for the increase or

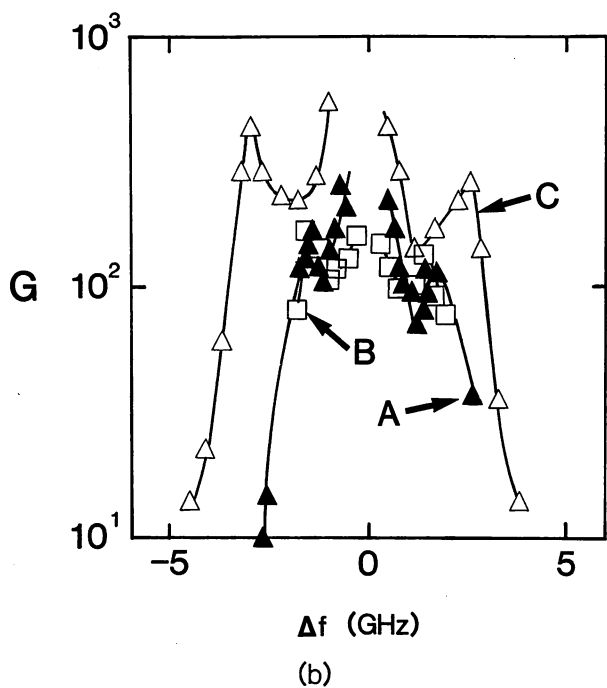
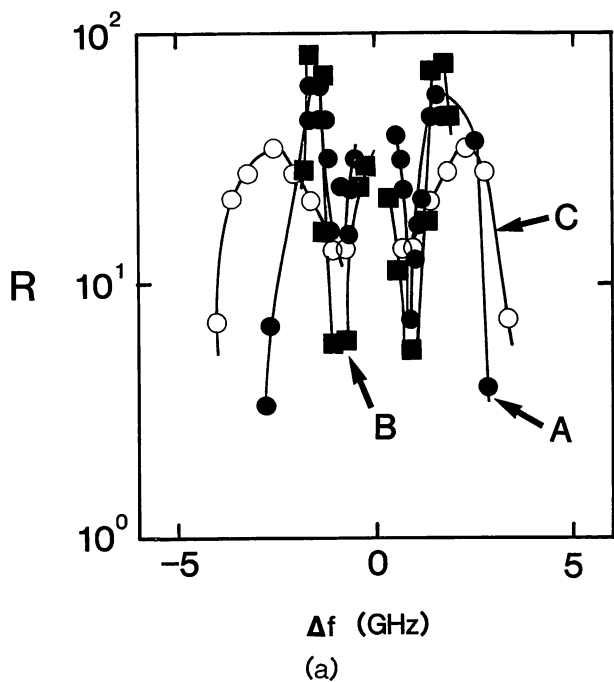


Fig. 2. Dependencies of the PCM reflectivity R (a) and the gain G of the probe beam amplification (b) on the detuning Δf between probe and pump beams. Curves A and B represent the measured results for a narrow-stripe laser (PL1) and a broad-stripe laser (PL2), respectively. Curve C is the measured result for a narrow-stripe AlGaAs laser with $0.83 \mu\text{m}$ wavelength, used as a reference.

decrease of these values, and all of these reasons could contribute to the results shown by Fig. 3. Plausible reasons for the increase are: (1) power density of the pump beam is increased by increasing $I/I_{th} - 1$, and (2) corrugation depth of the diffraction grating induced by intracavity lights is increased by the increase of the pump beam power, and thus, spatial modulation index of the carrier density is increased. A plausible reason for the decrease is the carrier density is increased and

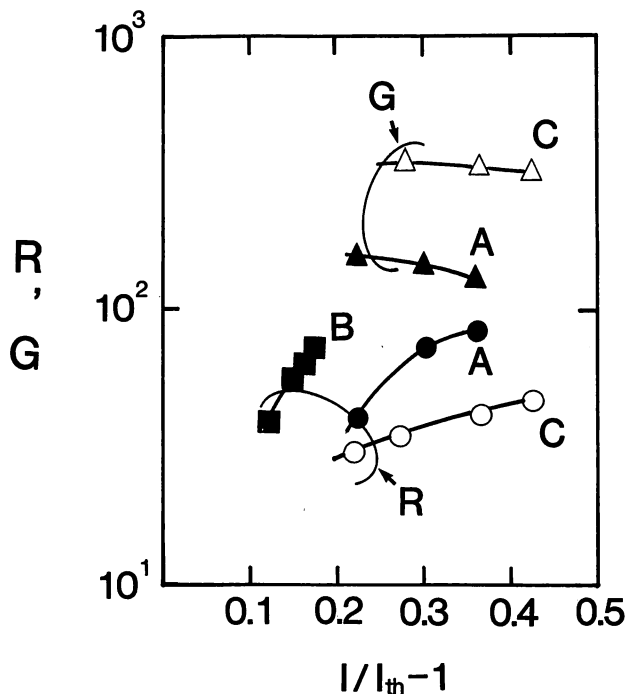


Fig. 3. Dependence of the reflectivity R and the gain G on the normalized bias level $I/I_{th} - 1$. Curves A, B and C represent the results for PL1 and PL2, and a narrow-stripe AlGaAs laser, respectively.

asymptotically approaches its threshold value, by which the spatial modulation index of the carrier density is decreased.

For comparison, the same measurements as those of Figs. 2 and 3 were carried out by using two narrow-stripe Fabry-Perot cavity-type AlGaAs lasers as the IL and PL ($0.83 \mu\text{m}$ -wavelength, Hitachi 8312E, $5 \mu\text{m}$ -stripe width). The results are summarized by curves C of Figs. 2 and 3, where $P_{in} = 1 \mu\text{W}$ and $I/I_{th} - 1 = 0.25$, in Fig. 2, which were almost equal to those for curves A and B. The measured values of R and G , and furthermore, the dependencies of R and G on the normalized bias level were similar to those of curves A and B. Thus, similarity of the nearly-degenerate FWM characteristics between the InGaAlP and AlGaAs lasers was confirmed.

3.2 Characteristics under the off-axis injection of the probe beam

It is usually difficult to spatially separate the PCW from the probe beam because of the small numerical aperture of the active waveguide facet of the narrow-stripe PL. In order to overcome this difficulty, the broad-stripe laser PL2 was employed and its characteristics of the PCM reflectivity were studied under the condition of the off-axis injection of the probe beam. That is, the value of R was measured by realizing the spatial separation when the probe beam was injected off-axially to the active waveguide of the PL2.

As is shown by Fig. 4(a), the value of the injection angle θ was adjusted by the off-axis incidence of the probe beam to the collimation lens CLp (Pentax VS303, 5 mm focal length, 0.35 numerical aperture) in the plane of the planar active waveguide of the PL2. It was

confirmed by geometrical calculations and preliminary measurements that the incident angle was expressed as $\theta [\text{degree}] = \tan^{-1}(x/15)$, where x (mm) is the displacement of the incident probe beam from the active waveguide axis of the PL2. The adjustable range of θ was limited by the geometrical configuration of the CLP, which was $\theta < 11^\circ$. Furthermore, the measurable value of R was limited by the measurement sensitivity of the present experimental setup, which was $R > 3.7$. Figure 4(b) shows the relationship between θ and R measured by fixing $I/I_{\text{th}} - 1 = 0.30$ (i.e., $P_p = 13.5$ mW) and $\Delta f = f_r$. Monotonous decrease in R is seen from this figure by increasing θ . Even though the coupling efficiency of the incident probe beam to the active waveguide of the PL2 was not calibrated, this figure shows that R took values larger than unity, which means that the present broad-stripe laser can be used

as an efficient FWM medium. Especially, it was clearly observed at $\theta = 5^\circ$ that the pump beam and the PCW emitted from the PL2 were separated spatially, and the emitted PCW propagated counter-linearly to the probe beam in the free space.

In the previous report of experiment on the measurement of the relationship between θ and R for a broad-stripe AlGaAs laser (Fig. 3 of ref. 9), the bias level of the PL was fixed below the threshold in order to avoid clamping the carrier density to its threshold value. However, in the present study, it was demonstrated for the first time that a broad-stripe visible semiconductor laser can generate the PCW even though it was biased above the threshold. As were confirmed by these measurements, it can be claimed that the broad-stripe visible semiconductor laser is used as a highly efficient PCM for several applications, *e.g.*, optical measurements and optical information processing. In addition, the wide bandwidth of the nearly-degenerate FWM makes it possible to utilize this laser as a fast external optical-feedback reflector for reducing the wideband FM noise of another semiconductor laser, as has been pointed out by the authors.⁴⁾

4. Conclusions

This work evaluated the characteristics of the phase conjugate wave generated from Fabry-Perot cavity-type visible semiconductor lasers. It was found that the bandwidth of the nearly-degenerate four-wave mixing was determined by the relaxation oscillation frequency. The value of the phase conjugate mirror reflectivity and the gain of the probe beam amplification took values larger than 10 and 100, respectively, within this bandwidth. The phase conjugate wave and emitted pump beam were spatially separated in the free space when the probe beam was incident at some angle to the axis.

The appendix of this paper describes for the first time the characteristics of the nondegenerate four-wave mixing of the $0.83 \mu\text{m}$ -wavelength AlGaAs laser quantitatively and systematically. It was found that the bandwidth was determined by the inverse of the half cycle time of the intracavity light where the measured 3-dB cutoff frequency was 0.1 THz. It was confirmed by these evaluations that semiconductor lasers can be used as high-reflectivity and wide-bandwidth phase conjugate mirrors, which have not been realized by using conventional dielectric photorefractive materials.

Acknowledgements

A part of this work was supported by TEPCO Research Foundation.

Appendix: Characteristics of Nondegenerate Four-Wave Mixing in an AlGaAs Laser

This appendix is devoted to the description of the FWM characteristics of an AlGaAs laser in the detuning range of $\Delta f \gg f_r$, which can be called the nondegenerate FWM. The laser used is exactly the same as that used for a reference laser in §3.1. The experimental setup was the same as that in Fig. 1 except that the

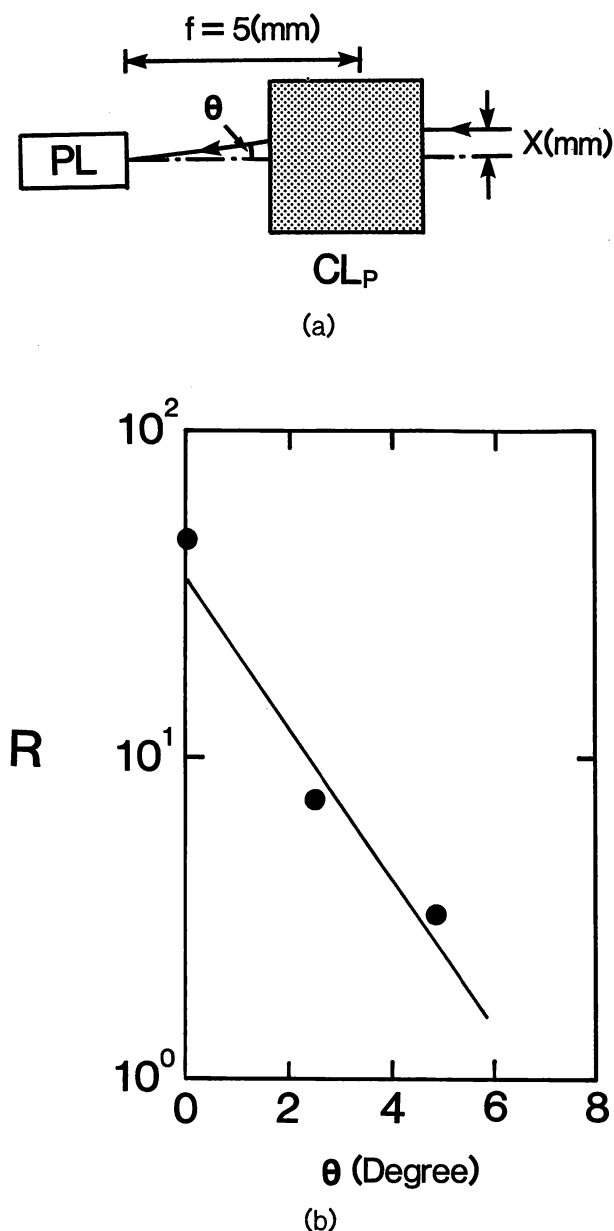


Fig. 4. Dependence of the reflectivity R of PL2 on the incidence angle θ . (a) Schematic explanation of θ determined by off-axial displacement x . (b) Measured results.

Fabry-Perot interferometer was replaced by a type of monochromator called an optical spectrum analyzer (Anritsu MS9030A/9702B). The probe beam frequency was tuned to one of the longitudinal mode frequency of the PL for resonance amplification of the powers of the signal beam and the PCW, because the PCW power generated by the nondegenerate FWM was expected to be very small.

Figures A·1(a) and A·1(b) show the experimental results for $0.5 \text{ mW} < P_{\text{in}} < 1.5 \text{ mW}$ and $I/I_{\text{th}} - 1 = 1.0$. Figure A·1(a) is the spectral profiles of the pump

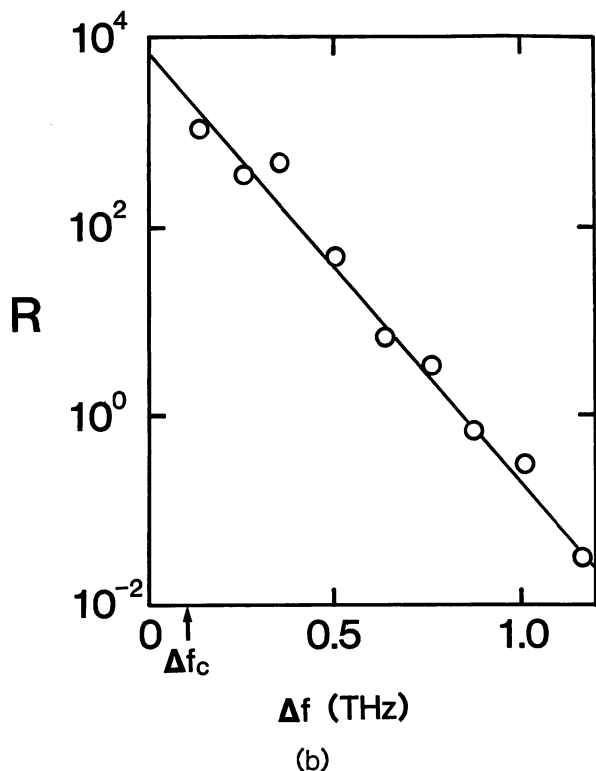
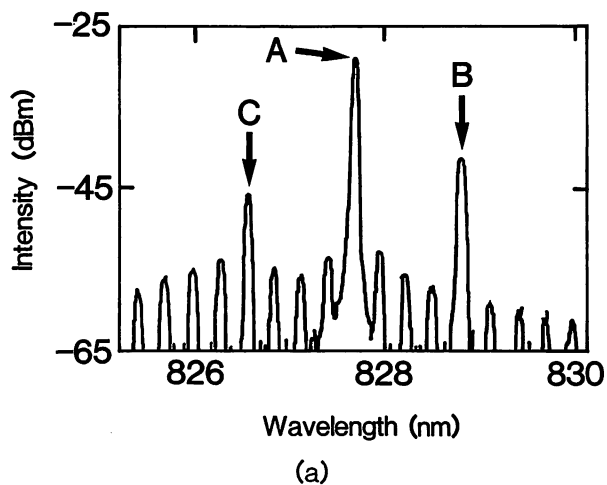


Fig. A·1. Measured characteristics of the nondegenerate four-wave mixing of the AlGaAs laser used for the experiments and shown in of Figs. 2 and 3. Horizontal and vertical axes are the same as in Fig. 2(a). Δf_c represents the 3-dB cutoff detuning frequency.

beam, signal beam and PCW, which are denoted by A, B and C, respectively. It can be seen from this figure that the probe beam and, thus, the signal beam, are resonant to one longitudinal mode of the PL and that the probe beam and the PCW are located symmetrically on the frequency axis with respect to the pump beam. Figure A·1(b) shows the measured relationship between Δf and the PCM reflectivity R . Reproducible measurements were carried out for a wide detuning range of $\Delta f < 1.2 \text{ THz}$. This figure shows that the nondegenerate FWM has the bandwidth in its detuning characteristics and its 3-dB cutoff frequency Δf_c is 0.1 THz. This high-frequency cutoff could be explained as the deviation from the phase matching condition for the FWM, which has been investigated for $1.5 \mu\text{m}$ wavelength InGaAlP lasers.¹⁰ The measure of this deviation can be represented as $|\Delta k L| = 1$, where Δk is the difference in the wavevectors between the probe and pump beams, and L is the active waveguide length of the PL. This expression can be transformed by using detuning Δf as $|\Delta f T| = 1$, where T is half of the cycle time of the probe beam in the active waveguide of the PL. The value of Δf_c can be derived from this expression as $\Delta f_c = 0.1 \text{ THz} (= 1/T)$ by using $T = 3.5 \text{ (ps)}$ of the PL employed for the measurements. This value agrees with the value shown by Fig. A·1(b). It can be concluded that the bandwidth of the nondegenerate FWM is determined by T because this time constant takes a larger value than other time constants such as the intraband relaxation time of the carrier ($= 0.1 \text{ (ps)}$).

Although ref. 9 claimed that the nondegenerate FWM characteristics were measured for the AlGaAs laser, the bandwidth determined by T has not yet been evaluated. The present study gives, for the first time, the evaluation of the nondegenerate FWM characteristics in AlGaAs laser discussed in ref. 10 and the quantitative measurement of R for the range of Δf up to 1.2 THz.

- 1) G. P. Agrawal: *Electron. Lett.* **23** (1987) 1175.
- 2) G. P. Agrawal: *Opt. Lett.* **12** (1987) 260.
- 3) K. Inoue, T. Mukai and T. Saitoh: *Appl. Phys. Lett.* **51** (1987) 1051.
- 4) M. Ohtsu, I. Koshiishi and Y. Teramachi: *Jpn. J. Appl. Phys.* **29** (1990) L2060.
- 5) G. Großkopf, R. Ludwig and H. G. Weber: *Electron. Lett.* **24** (1988) 1106.
- 6) R. Nietzke, P. Panknin, W. Elsasser and E. O. Gobel: *IEEE J. Quantum Electron.* **25** (1989) 1399.
- 7) By these bandwidth characteristics, the FWM phenomenon observed for $\Delta f < f_c$ is called the nearly-degenerate FWM in this paper, as has been denoted in ref. 3. For $\Delta f > f_c$, it is called the nondegenerate FWM, as will be described in the Appendix.
- 8) J. Feinberg: *Optical Phase Conjugation*, ed. R. A. Fisher (Academic Press, New York, 1983) Chap. 11, p. 434.
- 9) M. Lucente, J. G. Fujimoto and G. M. Carter: *Appl. Phys. Lett.* **53** (1988) 1897.
- 10) S. Murata, A. Tomita, J. Shimizu, M. Kitamura and A. Suzuki: *Appl. Phys. Lett.* **58** (1991) 1458.

Continuous-wave optical parametric amplifier that uses a diode laser for a wideband coherent optical frequency sweep generator

Weizhi Wang and Motoichi Ohtsu

Interdisciplinary Graduate School of Science and Engineering, Tokyo Institute of Technology, 4259, Nagatsuta-cho, Midori-ku, Yokohama 227, Japan

Received December 16, 1992

Continuous-wave optical parametric amplification by using a 1.5- μm diode laser and a Ti:sapphire laser has been performed for the first time to our knowledge to generate highly coherent tunable infrared light in a KTP crystal. Tunable output from 1.38 to 1.67 μm with microwatt power was obtained. We also propose a scheme for a precision frequency-tunable light source in the 1.5- μm region with an expected frequency tuning range of 4 THz by using an optical frequency comb generator and the phase-locking technique.

Highly coherent tunable light sources are essential tools in applications from basic physical investigation to precision measurements. In many cases in which highly coherent lasers are used, such as precision spectroscopy and multichannel coherent optical communication, an accurate frequency is required. To realize a tunable light source that can cover a wide frequency range, nonlinear frequency conversions have been popularly utilized for various lasers. We have proposed a diode-laser-based optical frequency sweep generator (OFSG) to cover the tunable frequency range of approximately 1 PHz from the ultraviolet to the near-infrared regions¹ and reported some experimental results toward the realization of the OFSG.^{1,2} Among various frequency conversions, optical parametric amplification (OPA) is important for generating tunable output in the near-infrared region for the OFSG. In this Letter we demonstrate, for the first time to our knowledge, the experimental result of cw OPA by using a 1.5- μm multiple-quantum-well distributed-feedback diode laser and an argon-ion-laser-pumped Ti:sapphire laser in a KTP crystal. The highly coherent light source in the 1.5- μm region that we have focused on is important not only for optical fiber communication but also for the application of high-resolution spectroscopy. On the other hand, a detailed understanding of the OPA process in this region is useful for the design of an optical parametric oscillator (OPO) by which the frequency link between the promising candidate of rubidium absorption lines (0.78 μm) for the frequency reference and the output in the 1.5- μm region can be established. Furthermore, establishing links to some absolute frequency references by using the atomic or molecular absorption lines and high-resolution spectroscopy techniques is one of the essential tasks of the OFSG system. We also propose here a scheme for a precision frequency-tunable light source in the 1.5- μm region based on our previous experiments.¹⁻³

Figure 1(a) shows the experimental setup for OPA of a diode laser by using a Ti:sapphire laser as a

pump source, and Fig. 1(b) shows the relation between the pump power of λ_1 and the output power of λ_3 ($\lambda_3^{-1} = \lambda_1^{-1} - \lambda_2^{-1}$, where the subscripts 1, 2, and 3 denote the pump, the input signal, and the output idler waves, respectively) at $\lambda_2 = 2\lambda_1 = 1.54 \mu\text{m}$, while the input power from the 1.5- μm diode laser was fixed at 5 mW. The KTP crystal (3 mm \times 3 mm \times 10 mm, cut with $\phi = 0^\circ$, $\theta = 54^\circ$) was used for its relatively large nonlinear coefficient and availability of room-temperature operation. The KTP crystal was mounted in the θ plane, and the incident angle of the laser beam was changed in the

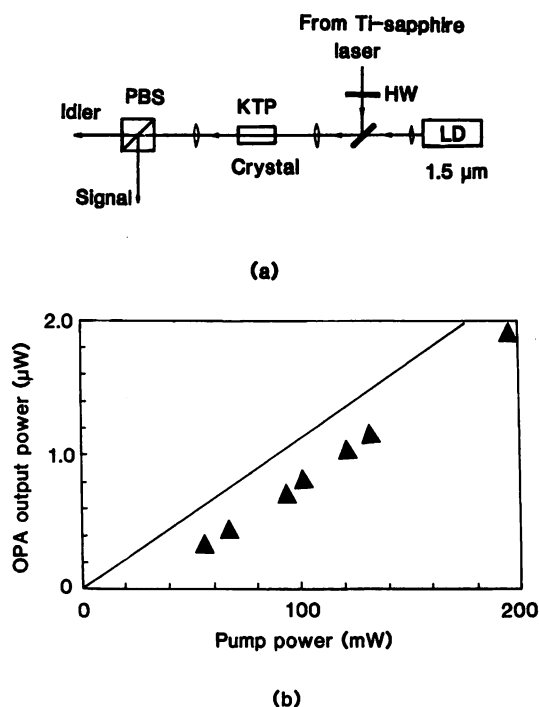


Fig. 1. (a) Experimental setup. PBS, polarized beam splitter; HW, half-wave plate; LD, laser diode. (b) Measured relation between the output power of OPA and the pump power at $\lambda_2 = 2\lambda_1$ while the signal power was fixed at 5 mW. The solid line shows the calculated value.

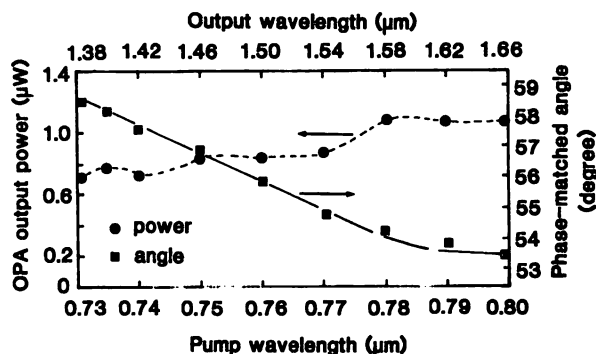


Fig. 2. Measured dependence of the phase-matched crystal angle on the wavelength and the relation between output power and the wavelength. Pump power, 100 mW; diode laser power, 5 mW. The solid and dashed curves are used only for distinguishing the two sets of data.

θ direction for tuning. The polarizations of the two lasers lay orthogonally so as to satisfy the type II phase matching. Since the polarization of the output light was orthogonal to that of the diode laser, we can separate the two infrared light beams by using a polarized beam splitter. From Fig. 1(b) we can see that the output power at the difference frequency between the pump laser and the diode laser was proportional to the pump power. The degenerate optical parametric gain was estimated to be 5×10^{-4} when the pump power was 200 mW and the beam waist was $15 \mu\text{m}$ by using the small gain formula⁴ $g = 8\pi^2 d_{\text{eff}}^2 l^2 P_1 h / \epsilon_0 c \lambda_2 \lambda_3 n_1 n_2 n_3 A$, with $d_{\text{eff}} = d_{24} \sin \theta \approx 6 \text{ pm/V}$ and $l = 10 \text{ mm}$, where h is the reduction factor that is due to the double refraction of the crystal, in the theory of Boyd and Kleinman,⁵ l is the crystal length, n is the refractive index, P is the power, and A is the pump beam cross section. The reduction factor of KTP in our case was estimated to be 1/10 to 1/15, which was subject to deviation from the ideal collimation of the diode laser beam. The output power, $P_3 = gP_2$, was calculated to be $2.5 \mu\text{W}$. The obtained value was lower than the calculated one because of the imperfect mode matching of the experimental condition and also because the practical nonlinear coefficient of the KTP was not known precisely. Although some recent measurements have shown that the nonlinear coefficients of the KTP seem to be smaller than the values reported many years ago,⁶ the dispersion in the crystal growth brings us both optimistic and pessimistic cases.

The tuning of the OPA output was carried out by tuning the input lasers and the angle of the crystal simultaneously. Although the wavelength of the pump source is fixed while the signal is tuned to obtain a tunable output in the conventional case of OPA, we used the tunability of the pump laser to extend the tuning range of the output while the fine tuning was performed by the diode laser. Figure 2 shows the measured output power and the phase-matched angle θ as functions of the pump wavelength. The obtained tunable range was from 1.38 to $1.67 \mu\text{m}$ (i.e., 38 THz), which corresponded to a pump wavelength from 0.73 to $0.80 \mu\text{m}$. The output power in Fig. 2 was calibrated with a pump power of 100 mW, while the power from the Ti:sapphire

laser could not be kept constant during the tuning. The obtained phase-matched angle agreed with the calculation using the dispersion relation in Ref. 7, except for the wavelength near $0.8 \mu\text{m}$. The reason for this discrepancy is unclear and is under investigation. The maximum available tuning range can be as wide as 600 nm near $1.54 \mu\text{m}$ (65 THz), which is limited only by the present crystal size when the Ti:sapphire laser was used. Since both lasers used in this frequency conversion are highly coherent (their linewidths were measured to be less than 500 kHz), the linewidth of the output at the difference frequency was estimated to be less than 1 MHz. From this experimental result, we can conclude that OPA by using two diode lasers with an output power higher than $1 \mu\text{W}$ is also feasible when the Ti:sapphire laser is replaced by a high-power, highly coherent AlGaAs laser diode that has been realized by using a coherent addition technique.⁸ Further improvement of the output power can be realized by using an external built-up cavity for OPA.

The parametric gain obtained in our experiment also provided us the practical information for designing the resonator of the OPO in this wavelength region. In the case of a doubly resonant OPO, the relation $\alpha_i \alpha_s \leq g$ should be satisfied, where α_i and α_s represent the single-trip cavity losses of the idler and

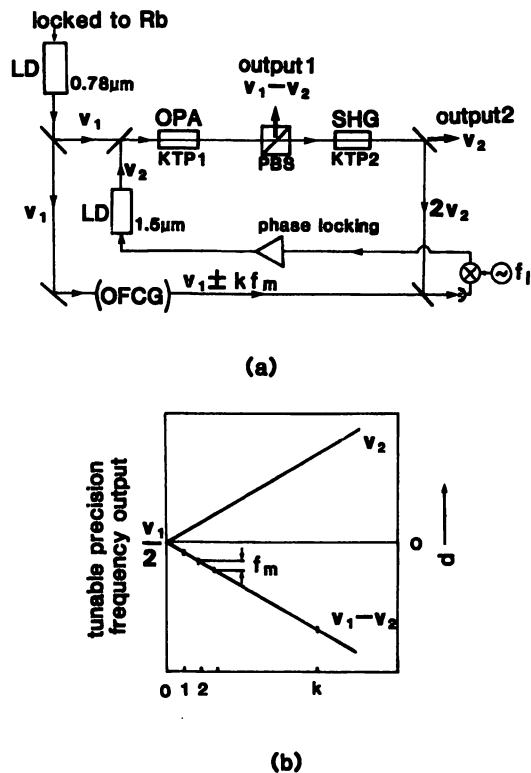


Fig. 3. (a) Proposed scheme of an OPA-based precision frequency-tunable source in the $1.5\text{-}\mu\text{m}$ wavelength region that uses an OFCG and the phase-locking technique: LD's, laser diodes; SHG, second-harmonic generation; PBS, polarized beam splitter; f_m , modulation frequency of the OFCG; k , order of the sideband; f_1 , frequency of the local oscillator. (b) Explanation of the frequency tuning of the system. k represents the sideband order to be used for heterodyne phase locking as the beat frequency is smaller than the sideband interval f_m .

the signal waves, respectively, including absorption, scattering of both cavity mirrors and the crystal, and the output transmission. Hence the finesses of the OPO resonator should be $F_i \sim F_s \geq \pi g^{-1} \sim 150$ for 200 mW of pump power. Because of the relatively large walk-off in the crystal in the 1.5- μm wavelength region, it is crucial that the above relation be satisfied in order to obtain an OPO cavity with high finesses for both idler and signal waves whose polarizations are orthogonal, especially when only a low pump power is available.

To realize precision frequency tuning, a frequency link to a reference frequency, such as an atomic absorption line, is necessary. We propose here a scheme for continuous precision tuning of the frequency, as shown in Fig. 3, by using an optical frequency comb generator (OFCG) and the phase-locking technique.³ The system is constructed basically by the OPA arrangement used above [see Fig. 3(a)]. A high-power 0.78- μm AlGaAs diode laser is used to pump the first KTP crystal (KTP1). This frequency can be locked to the atomic resonance frequency ν_1 of rubidium to be used as a precision frequency reference. Compared with the method of frequency locking through the second-harmonic wave of the 1.5- μm laser, because sufficiently high power is available, the saturation absorption resonance of rubidium can be employed to improve the performance. The frequency accuracy and stability can be as high as 1 part in 10^{11} .⁹ The amplified output of the 1.5- μm diode laser (ν_2) is incident upon the second KTP crystal (KTP2) to generate the second-harmonic wave.² A portion of the 0.78- μm laser power passes through an OFCG in which the light wave is modulated by an electro-optic modulator to generate sidebands with frequencies $\nu_1 \pm kf_m$, where k is the sideband order and f_m is the modulation frequency of the OFCG. The beat signal between the doubled frequency $2\nu_2$ of the 1.5- μm laser and one of the sidebands $\nu_1 \pm kf_m$ from the OFCG is used for heterodyne phase locking of the 1.5- μm laser. Thus the OPA output [output 1 in Fig. 3(a)] at the difference frequency $\nu_1 - \nu_2$ between the two lasers and the output 2 in Fig. 3(a) from the 1.5- μm laser itself of frequency ν_2 construct two outputs with precision frequency tunability. When ν_2 deviates from $\nu_1/2$ by d , i.e., $\nu_2 = \nu_1/2 + d$, the output 1 at the difference frequency will be $\nu_1/2 - d$. If the 1.5- μm laser is tuned with a range from 0 to d , the two outputs will cover a tuning range of $2d$, which is limited by the maximum difference frequency of the heterodyne phase locking with a beat frequency of $kf_m - 2d$ and the sideband order k . The continuous tuning of the outputs and the simultaneous heterodyne phase locking are accomplished by tuning the 1.5- μm laser through the injection current and the local oscillator frequency [see Fig. 3(b)]. It is necessary that the tuning range of the local oscillator be as

wide as $f_m/2$ to cover the span between the adjacent sideband modes of the OFCG. In comparison with the system that uses an OPO to construct an optical synthesizer,¹⁰ the advantage of the present scheme is that the continuous tuning range can be realized by employing a diode laser through OPA rather than the doubly resonant OPO to circumvent the discrete oscillation that is due to the cluster effect in doubly resonant OPO and the inherent low stability. Because the sidebands of the OFCG can span more than 4 THz,³ a precision frequency tuning range of 4 THz is reasonable, which is useful for the precision optical frequency measurements, e.g., in a multichannel coherent optical fiber communication system.

In summary, cw OPA has been performed by using a 1.5- μm diode laser and a Ti:sapphire laser in a KTP crystal to generate near-infrared light for our proposed OFSG. It is the first report, to our knowledge, of cw OPA by use of a diode laser. The highly coherent tunable output with microwatt power was obtained from 1.38 to 1.67 μm . The experiment demonstrated the feasibility of a diode-laser-based OPA and provided useful information for designing an OPO in this wavelength region. We have also proposed a scheme for a precision frequency-tunable light source based on OPA, using an OFCG and the phase-locking technique. A precision frequency-tunable range of 4 THz in the 1.5- μm wavelength region is expected.

The authors acknowledge useful discussions with K. Nakagawa of the Tokyo Institute of Technology and A. Akulshin of the P. N. Lebedev Physics Institute, Moscow, Russia.

References

1. M. Ohtsu, K. Nakagawa, C.-H. Shin, H. Kusuzawa, M. Kourogi, and H. Suzuki, in *Digest of Conference on Lasers and Electro-Optics* (Optical Society of America, Washington, D.C., 1990), paper CME5.
2. W. Wang, K. Nakagawa, Y. Toda, and M. Ohtsu, *Appl. Phys. Lett.* **61**, 1886 (1992).
3. M. Kourogi and M. Ohtsu, in *Digest of International Quantum Electronics Conference '92* (European Physical Society, Vienna, 1992), paper TuM5.
4. S. E. Harris, *Proc. IEEE* **57**, 2096 (1969).
5. G. D. Boyd and D. A. Kleinman, *J. Appl. Phys.* **39**, 3597 (1968).
6. H. Vanherzeele and J. D. Bierlein, *Opt. Lett.* **17**, 982 (1992).
7. T. Y. Fan, C. E. Huang, B. Q. Hu, R. C. Eckardt, Y. X. Fan, R. L. Byer, and R. S. Feigelson, *Appl. Opt.* **26**, 2390 (1987).
8. W. Wang, K. Nakagawa, S. Sayama, and M. Ohtsu, *Opt. Lett.* **17**, 1593 (1992).
9. H. Furuta and M. Ohtsu, *Appl. Opt.* **28**, 3737 (1989); H. Tsuchida, M. Ohtsu, T. Tako, N. Kuramochi, and N. Oura, *Jpn. J. Appl. Phys.* **21**, L561 (1982).
10. N. C. Wong, *Opt. Lett.* **15**, 1129 (1990).

Frequency control of semiconductor lasers

M. Ohtsu, K. Nakagawa, M. Kourogi, and W. Wang

Interdisciplinary Graduate School of Science and Engineering, Tokyo Institute of Technology, 4259 Nagatsuta, Midori-ku Yokohama 227, Japan

(Received 14 January 1993; accepted for publication 2 March 1993)

This article reviews our recent works on frequency control of semiconductor lasers. The magnitudes of quantum noise limited frequency modulation (FM) noise, realized by the negative electrical feedback, are given for four methods of using an external Fabry–Perot cavity as a frequency demodulator. It is shown that the theoretical expression for the quantum noise-limited FM noise of the feedback laser contains a factor of 1/8 as compared with that of the free running laser, which is due to the different ways of injecting the vacuum fluctuations to the laser cavity and to the external Fabry–Perot cavity for negative electrical feedback. The FM sideband technique is shown to be an effective method to reject the contribution of laser power fluctuations to the FM noise detection for the negative electrical feedback system. As a candidate for a high reflectivity and frequency selective external reflector for the optical feedback, characteristics of the semiconductor laser as a phase conjugate mirror, i.e., the characteristics of the nearly degenerate four-wave mixing and the nondegenerate four-wave mixing in a semiconductor laser, are shown. Optical feedback by using a velocity selective optical pumping and polarization spectroscopy of an atomic vapor is proposed as an effective method to realize simultaneously the center frequency stabilization and linewidth reduction of the field spectrum of the laser, and also the fine detuning of the stabilized center frequency. For the heterodyne frequency locking between two lasers, a spectroscopic method of using a Doppler-free spectrum of the three-level atomic vapor, obtained by using the phenomenon of coherent population trapping, is shown. In order to realize a highly efficient nonlinear optical frequency conversion for wideband frequency sweep of semiconductor lasers, a method of adding the output powers of several lasers, i.e., the coherent addition, is presented. After emphasizing that the wideband frequency sweep (covering from the near-infrared to the visible region) can be realized by using the techniques of nonlinear optical frequency conversions and the optical phase locking, relevant experimental results of nonlinear optical frequency conversions are presented which are the second harmonics generation, sum and difference frequency conversions. A highly accurate optical frequency measurement system is proposed using an optical frequency comb generator with a modulation sidebands up to several THz. Performances of the optical frequency comb generator used for this system are presented. As a candidate for an ultrafast and wavelength insensitive photodetector for optical frequency counting, nonbolometric optical response characteristics of a high transition temperature (T_c) oxide superconducting film are demonstrated.

TABLE OF CONTENTS

- I. Introduction
- II. Principle of frequency control
 - A. Negative electrical feedback
 - B. Optical feedback
- III. Experiments of reducing FM noise of a semiconductor laser
- IV. Frequency and/or phase locking and coherent addition
- V. Nonlinear frequency conversions for wideband frequency sweep
- VI. Accurate measurement of optical frequency
- VII. Summary

I. INTRODUCTION

In recent years, the techniques of molecular beam epitaxy, chemical beam epitaxy, and metalorganic chemical vapor deposition have been used to deposit homogeneous and reproducible thin films on a substrate for semiconductor laser devices, and the technique of large-scale laser fabrication and integration has been developed.¹ By these techniques, a structure of strained quantum wells has been employed to realize high-quality laser devices which cover a wide lasing wavelength region.² Although the semiconductor laser is inherently multilongitudinal mode lasers due to its wide gain spectral linewidth and strong coupling between longitudinal modes originated from fast intraband relaxation of carriers, an advanced laser device being considered approximately as a single mode laser³ has been

successfully fabricated by utilizing the quarter-wavelength shifted distributed feedback (DFB) structure to suppress the unwanted vestigial modes.⁴ In addition to these advanced devices, development of high-quality optical isolators enables laser devices to lase stably without suffering from the injection effects of external lightwaves. Furthermore, the frequency of a semiconductor laser can be swept by sweeping the injection current. The range of frequency sweep can be further extended if the technique of nonlinear optical frequency conversion is utilized by injecting the light of semiconductor lasers into the nonlinear optical crystals. With the progress of the performances of these active and passive devices, semiconductor lasers and the semiconductor laser-based coherent light sources have recently been widely used not only for the field of photonics but also for the study of basic physics such as atomic physics, verification of quantum mechanics, and quantum optics.

However, the magnitude of quantum frequency fluctuation [i.e., quantum frequency modulation (FM) noise] of the semiconductor laser device and its noise bandwidth are still large, which is due to a large cavity loss, and this FM noise must be reduced when the laser is used for the applications described above. For this purpose, it is advantageous to utilize a high efficiency and wide bandwidth of the direct FM characteristics, which is due to the modulation of refractive index of the active layer induced by plasma oscillation of carriers. That is, FM noise can be efficiently reduced by controlling the injection current of the laser. Moreover, control of carrier density by injecting the external light into the laser active waveguide has also been used as a convenient optical feedback technique to reduce the FM noise so as to control the laser frequency.

Studies on frequency control of semiconductor lasers have been actively carried out recently, and the resultant low noise semiconductor lasers have been used as the light sources for some advanced application systems. Based on this technical background, this review describes the recent progress on frequency control of semiconductor lasers. Since the related topics documented before 1991 have been reviewed in the monograph published by one of the authors (Ohtsu),⁵ this article is focused on reviewing the recent works since 1991.

As has been pointed out in Ref. 6, at least five requirements listed below should be met in order to realize a low noise and wideband tunable semiconductor laser system:

- (1) Center frequency stabilization of the field spectrum of the laser.
- (2) Linewidth reduction of the field spectrum.
- (3) Stable and wideband frequency sweep.

If the nonlinear optical frequency conversion technique is employed for meeting requirement (3), the following requirement should be met to increase the conversion efficiency:

- (4) Increase of the laser output power.

If the high-quality light source meeting these requirements is realized, the following requirement should also be met to utilize fully the low FM noise properties:

- (5) Accurate measurement of the optical frequency.

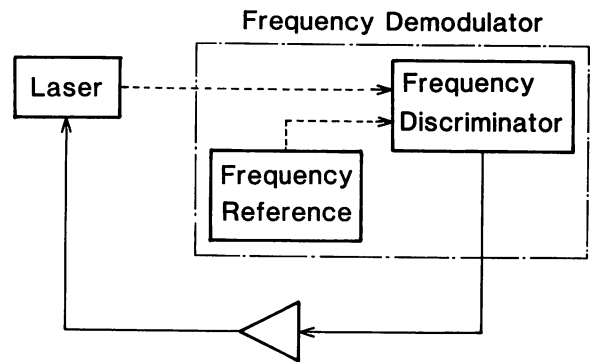


FIG. 1. Schematic explanation of the negative electrical feedback control of the semiconductor laser frequency.

We review recent progress in works for these five requirements by this article, in which authors' works will be mainly presented.

II. PRINCIPLE OF FREQUENCY CONTROL

This section briefly describes the principle of frequency control by negative electrical feedback, the quantum limit of the residual FM noise, and the principle of optical feedback.

A. Negative electrical feedback

For negative electrical feedback control of the semiconductor laser frequency, the injection current of the laser is controlled by the demodulated signal after the magnitude of FM noise is detected by an optical frequency demodulator composed of frequency discriminator and frequency reference, as shown by Fig. 1. The magnitude of FM noise $\delta\nu(t)$ is expressed as⁷

$$\delta\nu(t) = (1 + \alpha^2)\Gamma_s(t) + \Gamma_{ex}(t) - \int_{-\infty}^t h(\tau) [\delta\nu(t - \tau) + \Gamma_n(t - \tau)] d\tau. \quad (1)$$

In this equation, $\Gamma_s(t)$ is the magnitude of quantum FM noise generated in the laser cavity corresponding to the quantum frequency fluctuations of the coherent state, which is due to the spontaneous emission fluctuations (i.e., vacuum fluctuations) and has been called as the Schawlow-Townes' limit.⁸ $\Gamma_{ex}(t)$ and $\Gamma_n(t)$ are the fluctuations originating from the fluctuations of current or ambient temperature and from the feedback loop, respectively. The quantity α represents the linewidth enhancement factor.⁹ $h(t)$ is the impulse response function of the control loop. The Fourier transform of this equation gives

$$F(f) = \frac{1 + \alpha^2}{1 + H(f)} \Pi_s(f) + \frac{\Pi_{ex}(f)}{1 + H(f)} - \frac{H(f)}{1 + H(f)} \Pi_n(f), \quad (2)$$

TABLE I. The value of $|\Pi_n(f)|$ obtained by using several kinds of external Fabry–Perot cavities (EFP cavities) as frequency demodulators. Schematic explanations of the EFP cavities A–C, and D are given by Figs. 2 and 6, respectively. The quantity A is defined by Eq. (4). MZ/FP mode: An EFP cavity is installed in a Mach–Zehnder interferometer.

	$ \Pi_n(f) $
A: Transmission mode	$(64/9) A$
B: Reflection mode	$(64/27) A$
C: MZ/FP mode	A
D: FM sideband technique	2.1 A

where $F(f)$, $\Pi_s(f)$, $\Pi_{ex}(f)$, $\Pi_n(f)$, and $H(f)$ represent the Fourier transform of $\delta\nu(t)$, $\Gamma_s(t)$, $\Gamma_{ex}(t)$, $\Gamma_n(t)$, and $h(t)$, respectively. Here,

$$|\Pi_s(f)|^2 = \frac{h\nu}{(2\pi\tau_p)^2 P_o}, \quad (3)$$

where h is the Planck’s constant, ν is the laser frequency, τ_p is the photon lifetime of the laser cavity, and P_o is the output power from the laser cavity. This equation also shows that the value of $|F(f)|$ approaches the value of $|\Pi_n(f)|$ if the feedback gain $H(f)$ is sufficiently large. Furthermore, the magnitude of the residual FM noise under feedback can be smaller than that of the coherent state of the solitary laser if $|\Pi_n(f)| < |\Pi_s(f)|$. Thus, such a state of the light with very low FM noise below the Schawlow–Townes’ limit has been called as “hypercoherent” state.⁵

The fundamental fluctuations generated in the feedback loop is the shot noise from the photodetector which corresponds to the vacuum fluctuations injected into the feedback loop. Table I summarize the values of $|\Pi_n(f)|$, where it was assumed that several kinds of external Fabry–Perot (EFP) cavities are used as the frequency demodulators. Schematic explanations of the EFP cavities A–C and D in this table are given by Figs. 2 and 6(a), respectively. In this table, the quantity A is expressed as

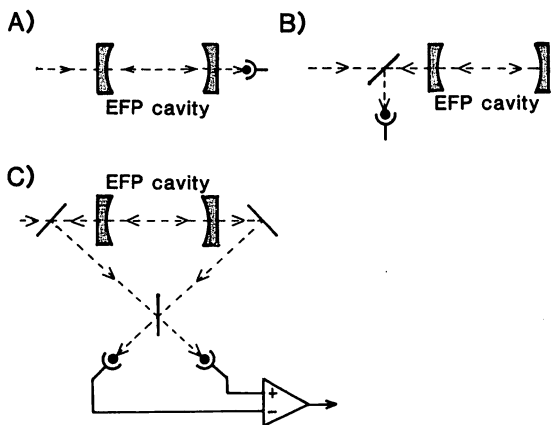


FIG. 2. Schematic explanations of external Fabry–Perot cavities A–C appeared in Table I. (A) Transmission mode of an external Fabry–Perot cavity. (B) reflection mode of an external Fabry–Perot cavity, (C) an external Fabry–Perot cavity is installed in a Mach–Zehnder interferometer.

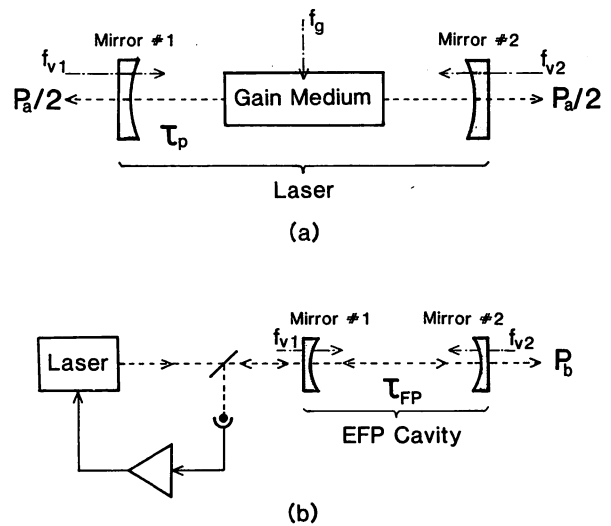


FIG. 3. Comparison of injecting the vacuum fluctuations into the free-running laser cavity (a) and the feedback laser system (b). f_{v1} , f_{v2} , f_g : magnitudes of vacuum fluctuations expressed as the Langevin forces in Langevin’s equation for the photon annihilation operator. They are injected to the laser cavity through the cavity mirrors and through the gain medium, respectively. P_a , P_b : output powers. τ_p , τ_{FP} : photon lifetimes of a laser cavity and an external Fabry–Perot cavity, respectively.

$$A = \frac{h\nu}{8(2\pi\tau_{FP})^2 P\eta}, \quad (4)$$

where τ_{FP} is the photon lifetime of the EFP cavity, P is the laser power incident into the EFP cavity, and η is the quantum efficiency of the photodetector used for detecting the FM noise. It is assumed here that the efficiency of the EFP cavity, i.e., the ratio between the laser power incident into the EFP cavity and the transmitted or reflected light power, is unity to simplify the analysis, which means that the P also corresponds to the output power from the negative electrical feedback laser system (see Fig. 3).

Comparison between Eqs. (3) and (4) shows that the mathematically expressed form of the value of quantity A given by Eq. (4) has the same mathematical form as the Schawlow–Townes’ limit given by Eq. (3) (i.e., the formula of vacuum fluctuations generated in the cavity of the solitary free-running laser), if τ_{FP} is replaced by τ_p . However, the difference between these expressions is that the factor of 1/8 appeared in Eq. (4), which is due to the difference in the way that the vacuum fluctuations, i.e., the spontaneous emission fluctuations, are injected into the laser cavity and into the EFP cavity. This difference can be explained as follows by referring to Figs. 3(a) and 3(b):¹⁰ These figures represent how the vacuum fluctuations are injected into the free-running laser cavity and the feedback laser system, where f_{v1} , f_{v2} , and f_g are the magnitudes of vacuum fluctuations expressed as the Langevin forces in Langevin’s equation for the photon annihilation operator. For both cases of Figs. 3(a) and 3(b), the vacuum fluctuations mixed into the light in the cavity could induce the FM noise. For the free-running laser cavity [Fig. 3(a)], the vacuum fluctuations f_g injected into the gain medium could also induce the FM noise in addition to those in-

duced by the f_{v1} and f_{v2} injected into the cavity through the two cavity mirrors. Here, $f_{v1}^2 = f_{v2}^2$ for the symmetric cavity configuration, and $f_{v1}^2 + f_{v2}^2 = f_g^2$ for the sufficiently highly biased laser. On the other hand, for the laser under negative electrical feedback [see Fig. 3(b)], the power fluctuations of the reflected light from the EFP cavity, i.e., the signal from the reflection-mode EFP cavity, is used as a frequency demodulation signal. Since the EFP cavity does not contain any gain medium (i.e., $f_g = 0$) and the feedback loop can eliminate the FM noise induced by the vacuum fluctuations f_{v1} , only the vacuum fluctuations f_{v2} , being injected from the EFP cavity mirror #2, gives the residual FM noise under feedback. Thus, the residual FM noise magnitude originated from the vacuum fluctuations is 1/4 times that of Fig. 3(a). Furthermore, since the half of output power P_a transmitted through the laser cavity mirror #2 in Fig. 3(a) corresponds to the output power P_b from the EFP cavity mirror #2 in Fig. 3(b), the intracavity laser power of Fig. 3(a) is 1/2 of the laser power in the EFP cavity of Fig. 3(b). The factor of 1/8 is thus given by the product of the two factors 1/4 and 1/2 derived above.

The factor of 64/27 can be seen in the value of $|\Pi_n(f)|$ for the reflection-mode EFP cavity given in Table I, which represents the result of the optimum tuning of the laser frequency in order to obtain the highest frequency demodulating gain of the EFP cavity. The values of this factor $|\Pi_n(f)|$ in Table I are different between each demodulation mode of the EFP cavity, which is due to the difference in the frequency demodulating gains for each demodulation mode of the EFP cavity. The main cause of this difference is that the laser power in the demodulator is different between each other even though the incident power P is equal. Among the different factors, the factor for a Mach-Zehnder/Fabry-Perot (MZ/FP) mode is the smallest, which is explained as follows: The MZ/FP mode in Table I demodulates the FM noise by interfering the transmitted and reflected lights from the EFP cavity.¹¹ Since the laser beam does not have to be divided to realize an interference in the MZ/FP mode, being different from other interferometers, the laser power in the EFP cavity is higher than those in other demodulation modes in Table I.

Absorption or emission spectral lines in atomic vapors can be used as the frequency demodulator as well as for the EFP cavity, for which the value of $|\Pi_n(f)|$ can be derived in similar ways for the EFP cavity because the response of the electrons in atoms can be approximated as a delay system of the first order. One of the main differences between the atoms and the EFP cavity is that the light absorbed by the atoms is incoherently dissipated by the atomic relaxation processes and cannot be utilized for frequency control.

The lasers with homogeneous frequency dependence of the direct FM efficiency are advantageous for increasing the control gain $|H(f)|$ and for extending the control bandwidth, for which the DFB lasers with segmented electrodes have been employed.^{12,13} For designing the high gain and wideband feedback control loop with the optimized phase-compensating circuit, the reliable and precise

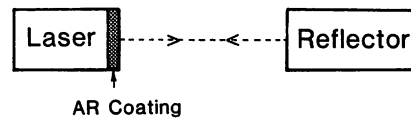


FIG. 4. Optical feedback scheme by utilizing an external reflector to induce the self-injection locking.

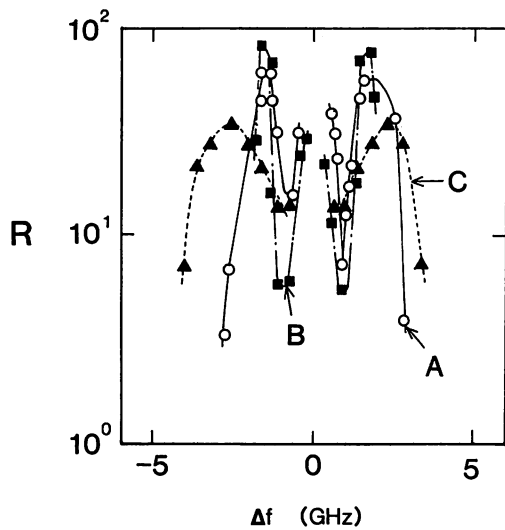
technique of the network analysis for analog electronic circuit design can be applied so as to realize a feedback laser with higher gain and lower drift,¹⁴ as compared with the optical feedback laser.

B. Optical feedback

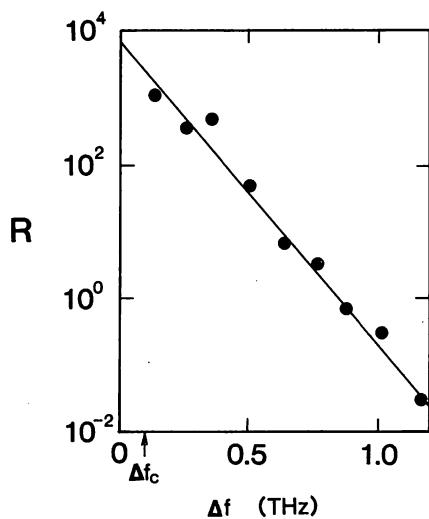
The carrier density in the laser active waveguide can be modulated by the injected light. The laser frequency is, thus, modulated through the refractive index modulation which is due to the change of plasma oscillation induced by the optically induced carrier density modulation. This phenomenon, called injection locking,¹⁵ has been popularly used to control the slave laser by injecting the light of the master laser. Modulation of the laser frequency by injection locking is also possible by self-injection of the laser light after reflected from an external surface. By utilizing this self-injection locking phenomenon, an external cavity type laser is constructed to control its frequency which is shown in Fig. 4. Since the photon lifetime is increased by this external cavity configuration, the value of the Schawlow-Townes' limit of Eq. (3) is decreased. The optical feedback has a wider bandwidth as compared with the bandwidth of negative electrical feedback because the photon lifetime of the external cavity is usually shorter than the response time of the negative electrical feedback loop. However, the control gain is usually lower than that of the negative electrical feedback. Furthermore, the oscillation instability, and even chaotic instabilities, can be induced depending on the value of the phase of the injected light, which means that precise control of the phase of the injected light is required to maintain the feedback stable. Thus, it could be advantageous to use optical feedback as an auxiliary feedback to extend the bandwidth of the feedback loop.¹⁶

It is more effective to use an EFP cavity as an external reflector for the optical feedback than to use a conventional mirror because the EFP cavity works simultaneously as a frequency reference.¹⁷ That is, the laser frequency is pulled into the reference frequency, i.e., the resonance frequency of the EFP cavity, because the injected light power is the highest when the laser frequency is tuned to the resonance frequency. Similar frequency selective optical feedback is also possible by injecting the transmitted light through an atomic vapor to the laser, which will be explained in the next section.

The injection of a phase conjugate wave can be also used to stabilize the phase of the reflected light. Since the response of conventional photorefractive materials is slow,¹⁸ it is more advantageous to use a semiconductor laser device as a phase conjugate mirror for its fast re-



(a)



(b)

FIG. 5. (a) The frequency characteristics of nearly degenerate four-wave mixing, i.e., the values of reflectivities R of semiconductor lasers used as the phase conjugate mirrors. The horizontal axis represents the detuning Δf between the pump and incident beams. Curves A, B, and C represent the results for a narrow stripe InGaAlP laser, a broad stripe InGaAsP laser, and a narrow stripe AlGaAs laser, respectively. Their stripe widths are 5, 30, and 5 μm , respectively. The lasing intracavity lights are used as the pump beams by biasing the laser above the threshold. For $|\Delta f| < 1$ GHz, data are unavailable because the pump beams are injection locked to the incident beam in this range. (from Ref. 20). (b) The detuning characteristics of nondegenerate four-wave mixing, i.e., the phase conjugate reflectivity R of an AlGaAs laser when the detuning Δf is larger than the relaxation oscillation frequency. The 3 dB high frequency cut-off Δf_c is 100 GHz (from Ref. 20).

response, in which the intracavity two counterpropagating traveling lasing lights in the device, biased slightly above the threshold, can work as high power density pump beams for four-wave mixing.¹⁹ Figure 5(a) shows the frequency characteristics of nearly degenerate four-wave mixing, i.e., the values of the reflectivities of the narrow and broad stripe InGaAlP lasers (0.67 μm wavelength) and the narrow stripe AlGaAs laser (0.83 μm wavelength) used as the

phase conjugate mirrors, where the horizontal axis represents detuning between the pump and incident beams.²⁰ This figure shows that the reflectivities are larger than 10 for the detuning frequency up to the relaxation oscillation frequency of the laser device. One of the experimental problems is the difficulty of separation between the pump beam and the phase conjugate light emitted from the narrow stripe laser cavity, which hinders the construction of a stable external cavity by using the semiconductor laser as the phase conjugate mirror. However, it was confirmed recently that the phase conjugate light and the pump beam were separated spatially and the phase conjugate light propagated counter-collinearly to the incident light when the incident light was injected to the broad stripe InGaAlP laser (30 μm stripe width) with the incidence angle of 5° while maintaining the phase conjugate reflectivity as high as 3.3. This spatial separation and high reflectivity could make the optical alignment easier to construct the external cavity laser.

Figure 5(b) shows the detuning characteristics of nondegenerate four-wave mixing, i.e., the phase conjugate reflectivity of an AlGaAs laser when the detuning was larger than the relaxation oscillation frequency. Although the reflectivity is lower than that of the nearly degenerate four-wave mixing, generation of the phase conjugate light was observed for the detuning frequency up to 1.2 THz. The 3 dB high frequency cutoff was as high as 100 GHz, which was determined by the phase mismatching for generating the phase conjugate light and was given by the reciprocal of the half round trip time of the light in the phase conjugate medium. It can be expected that the semiconductor laser can be used as a reliable external phase conjugate mirror with high efficiency and wide bandwidth phase conjugate mirror for reducing the FM noise of the other semiconductor laser.¹⁹

III. EXPERIMENTS OF REDUCING FM NOISE OF A SEMICONDUCTOR LASER

This section reviews recent works to meet requirements (1) and (2) of Sec. I. The center frequency of the laser field spectrum is stabilized by reducing the FM noise in the range of low Fourier frequency which can be realized by using a narrow band and high gain feedback loop. The linewidth can be narrowed by reducing this FM noise in the range of high Fourier frequency up to several tens of MHz.

To meet requirement (1), several atomic or molecular spectral lines have been used as reproducible and accurate frequency references.^{5,21} Although the reproducibility of the resonance frequency of an EFP cavity is lower than that of the atomic or molecular spectral lines, a simpler, accurate and low drift frequency reference can be realized by using extremely low expansion materials such as Zerodure (product of Schott Glasswork Co.) and ULE (product of Corning Glass Co.) as a spacer for the super cavity with the finesse of as high as 1×10^6 .²² By the negative electrical feedback, using the absorption spectral line of rubidium (Rb^{87}) atomic vapor (resonance wavelength at 780 nm) as a frequency reference, the theoretical limit of

the frequency stability determined by the value of $|\Pi_n(f)|$ of Eq. (2) was estimated to be 2×10^{-15} at the integration time of 100 s, and the experimentally realized stability was 2×10^{-12} .²³

Although the FM noise of the recently fabricated sub-MHz linewidth semiconductor laser²⁴ has been sufficiently low for a high bit rate coherent optical transmission, further reduction of this noise is still required for advanced and precise coherent optical systems. That is, requirement (2) of Sec. I should be met even for this advanced laser device. For this purpose an EFP cavity, especially its reflection mode, has been used as a wideband and high gain frequency demodulator of a negative electrical feedback system because of its high sensitivity of phase demodulation. By measuring the power fluctuations of the light reflected from the EFP cavity for the FM noise detection, the negative electrical feedback loop can be optimally designed for an AlGaAs laser and the gain bandwidth product of the feedback loop higher than 10 THz has been achieved.¹⁴ Similar frequency control for a 170 kHz linewidth segmented electrode multiquantum well distributed feedback (MQW DFB) laser at 1.5 μm wavelength has also succeeded in realizing a 250 Hz linewidth.²⁵ Furthermore as has been shown in Table I, the method of homodyne detection can be used in order to achieve higher sensitivity of FM noise detection by mixing the reflected and transmitted lights from the EFP cavity which is installed in a Mach-Zehnder interferometer (see also Table I).¹¹

Although the fundamental factor for limiting the sensitivity of FM noise detection is the quantum noise as was explained in Fig. 3(b), the laser power fluctuations usually limit the sensitivity in the practical feedback system. The FM sideband technique has been employed to achieve the quantum noise limited sensitivity by rejecting the contribution of the power fluctuations.²⁶ That is, since the contribution of the laser power fluctuations is the common mode noise in this system [see Fig. 6(a)], it can be rejected by taking the difference between the two heterodyne signals, i.e., the carrier-upper sideband heterodyne signal and the carrier-lower sideband heterodyne signal. Here, one should note that the upper and lower sidebands corresponds to the FM demodulation signals, i.e., their powers are proportional to that of the reflected light from the EFP cavity. Figures 6(b) and (c) show the results of rejecting the contribution from the laser power fluctuations, where a segmented-electrode MQW DFB laser of 1.5 μm wavelength was used.²⁷ By comparing with the experimental result using a conventional reflection mode of the EFP cavity,¹⁴ considerable FM noise reduction can be seen at the Fourier frequency region lower than 100 kHz, in which the main contribution has been the laser power fluctuations. The power spectral density at this low Fourier frequency region was reduced to a value lower than $25 \text{ Hz}^2/\text{Hz}$, by which it was estimated that the 3 dB linewidth of the field spectrum was reduced to narrower than 80 Hz.²⁸ Furthermore, the negative electrical feedback has realized the linewidth as narrow as 7 Hz by employing auxiliarily an optical feedback of the reflected light from an EFP cavity to expand the bandwidth of the feedback loop.¹⁶

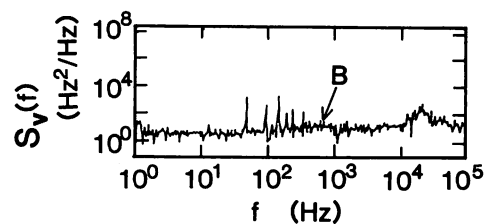
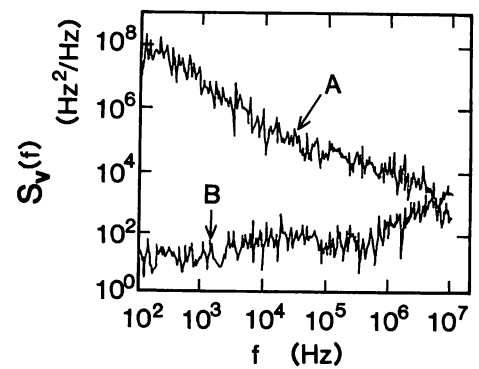
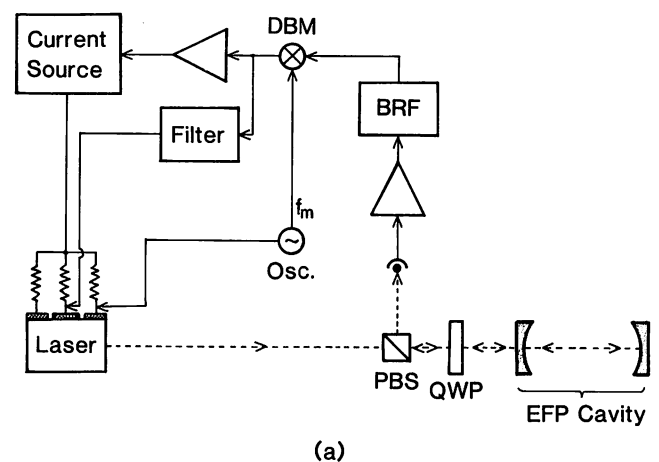


FIG. 6. (a) Experimental setup of the FM sideband technique. DBM: double balanced mixer, BRF: band rejection filter, PBS: polarizing beam splitter, QWP: quarter-wave plate. (b), (c) Power spectral densities $S_V(f)$ of frequency fluctuations of a segmented electrode MQW-DFB laser of 1.5 μm wavelength. Curves A and B are for the free-running and frequency-controlled lasers, respectively (from Ref. 28).

If a popularly used medium class EFP cavity, e.g. with 1 MHz resonance linewidth and 16 ns photon lifetime, a corresponding finesse of 150 (assuming the cavity length of 1 m) is used as a frequency demodulator for a 1.5 μm wavelength semiconductor laser; the field spectral linewidth limited by the quantum noise is estimated to be as narrow as 30 μHz by assuming that $P_b = 1 \text{ mW}$. Furthermore, if a recently developed super cavity with the finesse as high as 1×10^6 is used,²² corresponding quantum noise limited linewidth is expected to be 5 nHz by again assuming the cavity length of 1 m. Thus, it is possible in principle to realize such an ultralow noise semiconductor laser, which can be used as a coherent light source even for the long baseline interferometer for gravitational wave detec-

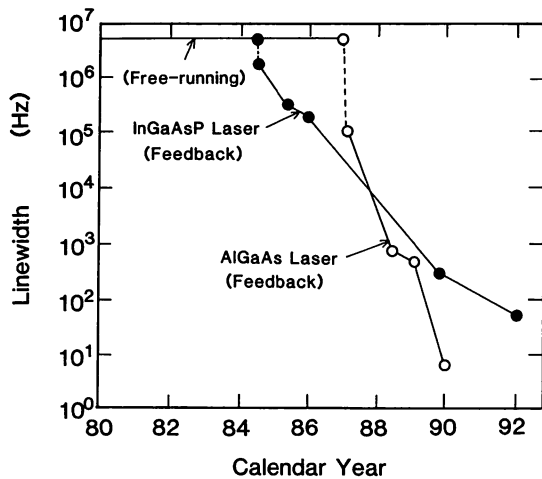
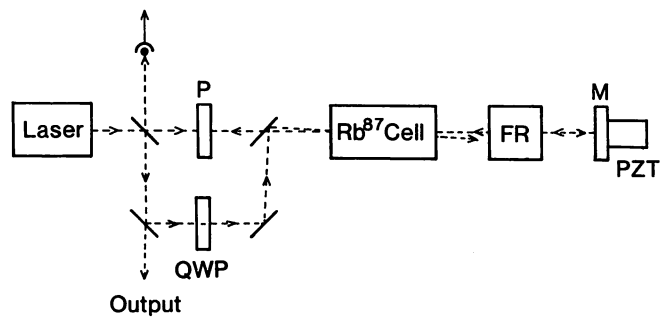


FIG. 7. Progress of the authors' linewidth reduction experiments on semiconductor lasers.

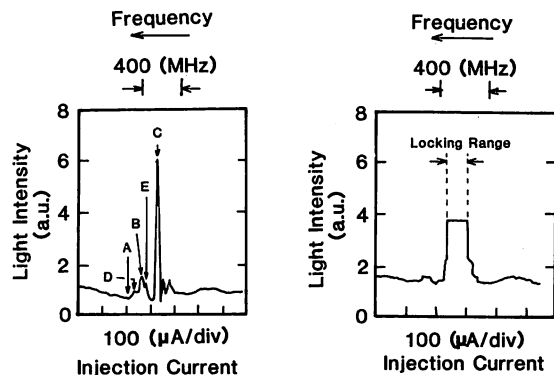
tion.²⁹ To summarize the discussions above, Fig. 7 shows the progress of authors' experiments of linewidth reduction, by which the realization of ultranarrow linewidth estimated above is expected in the near future.

Center frequency stabilization and linewidth reduction of the field spectrum can be simultaneously carried out by using an atomic spectral line as a frequency demodulator for optical feedback. Figure 8(a) explains schematically one of the examples of such an optical feedback method for an AlGaAs laser, which utilizes a velocity selective optical pumping (VSOP) and the polarization spectroscopy scheme of a Rb⁸⁷ atomic vapor.³⁰ In this method, the light possessing the information of Doppler-free atomic resonance spectral profile is injected into the laser. The VSOP and its detection are realized by the following process: The polarization of the probe beam was converted from linear to elliptic by passing through the Rb⁸⁷ cell due to the circular dichroism induced in the Rb⁸⁷ vapor by a nonlinear interaction with the strong pump beam. Furthermore, the circularly polarized strong pump beam produces velocity selective polarization in the Rb⁸⁷ vapor and induces velocity selective circular dichroism and birefringence in the probe beam reflected by a mirror. In order to inject the spectral selective probe beam to the laser, a Faraday rotator with a rotation angle of 45° is used. For the optical feedback, the polarizer also serves as an analyzer.

Figure 8(b) shows that the Doppler-free Rb⁸⁷-D₂ spectral line is due to hyperfine transition from the $F=2$ level in the ground state. It was measured under the free running condition by sweeping the laser injection current. Since this spectral profile exhibited a peak at the atomic resonant frequency ν_r , stable resonant optical feedback is achieved by injecting the reflected probe beam into the laser. As a result, the laser frequency ν is locked to ν_r . Figure 8(c) shows the deformed Doppler-free spectral profile measured as a result of this injection, i.e., the laser is under the optical feedback condition. The plateau at the center of the profile shows that the ν is locked to ν_r . The



(a)



(b)

(c)

FIG. 8. (a) Experimental setup of the optical feedback utilizing a velocity-selective optical pumping and the polarization spectroscopy scheme of a Rb⁸⁷ atomic vapor. P: polarizer, QWP: quarter-wave plate, FR: Faraday rotator, (M) mirror. (b) The Doppler-free Rb⁸⁷-D₂ spectral lines due to hyperfine transitions from the level $F=2$ in the ground state. Lines A, B, and C correspond to the transitions $F=2-1$, $2-2$, and $2-3$, respectively. Lines D and E correspond to the crossover resonances. These lineshapes were traced by sweeping the injection current of the free-running AlGaAs laser, which corresponds to sweeping the laser frequency (from Ref. 30). (c) The deformed spectral lineshape traced under the condition of the optical feedback. The center of this shape corresponds to the component C in (b).

locking range is as wide as 200 MHz which is estimated by the width of the plateau.

Since the bandwidth of this optical feedback is determined by the lifetime of the relevant atomic energy levels, the linewidth of the laser field spectrum can be reduced if this lifetime is sufficiently short. However, since the phase of the reflected light has to be controlled accurately to maintain a stable optical feedback, the negative electrical feedback is employed to control the position of the mirror by a piezoelectric transducer. The field spectral linewidth of this laser has been reduced more than 1/20 times by this method.

The advantage of the present optical feedback is that the stabilized laser frequency can be detuned continuously from ν_r with a magnitude of about $\pm\gamma/2$, i.e., $\nu_r - \gamma/2 < \nu < \nu_r + \gamma/2$, where γ represents the natural linewidth of the Rb⁸⁷ atomic resonance. By changing the Faraday rotation angle from 45°, the spectral profile of the reflected probe beam is deformed from absorptive to dispersive due to the circular birefringence of the Rb⁸⁷ vapor as is depicted by

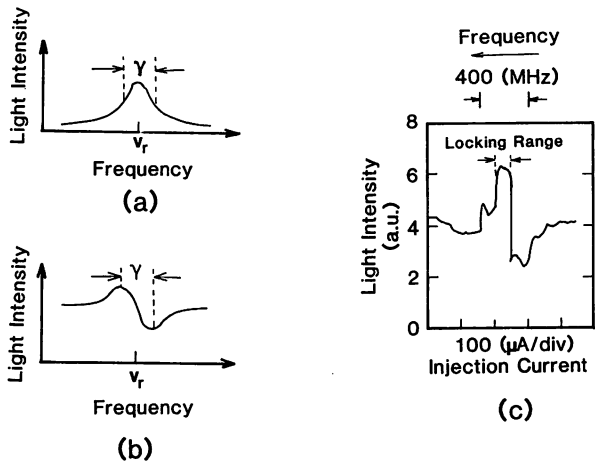


FIG. 9. (a), (b) Schematic explanation of the spectral shape of the light intensity obtained by the photodetector of Fig. 8(a) by fixing the Faraday rotation angle to 45° and 22.5° , respectively. These absorptive and dispersive shapes represent the induced Doppler-free circular dichroism and birefringence, respectively. The absorptive spectral shape of (a) corresponds to that of Fig. 8(b). (c) Spectral shapes, corresponding to that of (b) observed under the condition of optical feedback (from Ref. 30).

Figs. 9(a) and 9(b), and the peak of the dispersive profile appears approximately at $\nu_r \pm \gamma/2$, depending on the Faraday rotation angle. Figure 9(c) shows the spectral profile of the Rb⁸⁷ vapors, measured while injecting the reflected probe beam to the laser. The laser frequency ν was locked at the plateau of this profile, which suggests that the stabilized laser frequency ν was detuned from ν_r to $\nu_r + \gamma/2$ by changing the Faraday rotation angle from 45° to 22.5° .

This optical feedback laser is expected to be used for spectroscopy and atomic physics such as laser cooling of atoms because the frequency stabilization, linewidth reduction, and fine frequency tuning are carried out simultaneously. As one of the other examples of using the atomic spectral line, the optical feedback has been carried out by using a Doppler-free resonance spectral line, which was observed as a result of Faraday rotation in atoms induced by applying the dc magnetic field of several Gauss.³¹ The linewidth of the field spectrum has been reduced to 40 kHz with the locking range of 600 MHz. One of the problems to be solved for this system is that the reproducibility of this stabilized laser frequency becomes worse when the applied ambient magnetic field fluctuates.

IV. FREQUENCY AND/OR PHASE LOCKING AND COHERENT ADDITION

As the first step to meet requirement (3) of Sec. I, it is necessary to realize the accurate and fine sweep of the laser frequency. It can be realized by utilizing the heterodyne optical phase locked loop, i.e., the slave laser frequency is accurately fine tuned to the frequency stabilized master laser by sweeping the microwave frequency of the local oscillator used for the phase locked loop. A Fabry-Perot cavity-type AlGaAs laser frequency has been swept for 64 GHz by this technique,³² which was limited only by the mode hopping phenomenon of this conventional laser de-

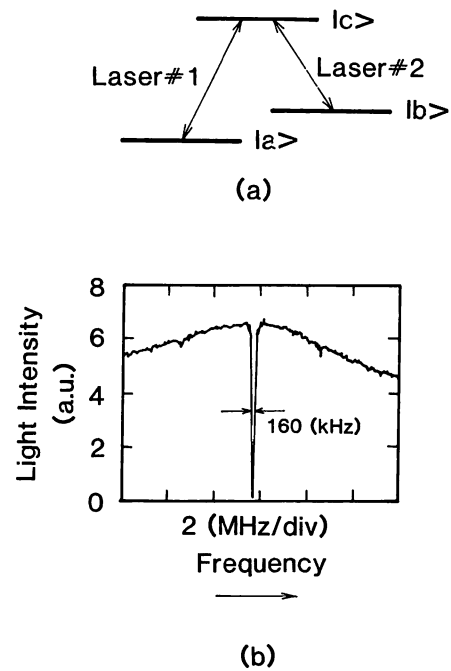


FIG. 10. (a) Three atomic energy levels relevant to the Λ shape transition induced by irradiating two laser beams. (b) The spectral profile of the Rb atomic vapor obtained by sweeping one AlGaAs, laser frequency while the other laser frequency was fixed. Due to the induced coherent population trapping phenomenon, the spectral profile is Doppler-free whose 3 dB linewidth is 160 kHz, being limited by the two laser linewidths (from Ref. 37).

vice. A wider range of accurate and fine frequency sweep is expected by using advanced laser devices such as a DFB laser. The authors have obtained the heterodyne signal frequency stability of 1×10^{-18} at the integration time of 70 s and the phase error variance of 0.02 rad^2 .³³ For the homodyne optical phase locking, the bandwidth as wide as 134 MHz³⁴ and the phase error variance of 0.02 rad^2 have been achieved.³⁵ Since the experimental details have been described in Ref. 5, the remainder of this section reviews an example of the recent progress on the experiments of frequency lockings.

Figure 10 explains schematically a method of heterodyne frequency locking based on spectroscopic method. A high-contrast Doppler-free spectral shape due to the Λ -shape transitions between three energy levels [see Fig. 10(a)] is obtained by using a phenomenon of coherent population trapping³⁶ which is induced when two AlGaAs lasers (master and slave laser) beams propagate parallel to the Rb atomic vapor. This phenomenon produces a special atomic state in which the atom is trapped to form a coherent superposition of the two energy levels $|a\rangle$ and $|b\rangle$ in Fig. 10(a) induced by the quantum interference effect under the two-photon resonance. As a result, the optical transition between this superposed state and the energy level $|c\rangle$ common to the Λ shape transition is inhibited.

Figure 10(b) shows the spectral profile (whose linewidth is as narrow as 160 kHz) which is determined by the very long lifetime of the lower energy levels $|b\rangle$ and $|c\rangle$. In the practical experimental setup, the main contribution to the linewidth is the sum of the field spectral linewidths of

the two lasers (80 kHz each). Thus, the heterodyne frequency between the two lasers can be accurately locked to the resonance frequency between the two hyperfine energy levels $|b\rangle$ and $|c\rangle$ in the ground state of the Rb atom (i.e., 6.8 GHz) if one of the laser frequencies is controlled by using this resonance frequency of Fig. 10(b) as a frequency reference.³⁷ This heterodyne frequency locking can be used as an optical method to generate a stable microwave frequency.

For wideband frequency sweep, highly efficient nonlinear optical frequency conversions are used as an essential technique, for which high power laser beams are required to ensure high conversion efficiency. Coherent addition, i.e., superposition of several frequency or phase locked laser beams, can be one of the promising techniques to realize high output power, which is schematically explained by Figs. 11(a) and 11(b). By this technique, requirement (4) of Sec. I can be met. The optical path lengths of beams from the frequency- or phase-locked slave lasers are controlled so that they are superposed in-phase at the output beam splitter. In Fig. 11(a), laser beam $\#k$ is used for the superposition $N-k$ times because the adjacent laser beams are superposed, where N represents the total number of laser beams. In Fig. 11(b) on the other hand, the beams from 2^n lasers are superposed by a method of, namely, binary-tree, which means that each laser beam is used for the superposition n times. Comparison between the two schemes shows that scheme (b) always has a higher addition efficiency than (a) because the number of superposition of each laser beam in (b) is always smaller than that in (a).

For a demonstration of the coherent addition, two slave lasers of $0.8 \mu\text{m}$ wavelength were phase locked to the master laser by using the technique of injection locking. The coherently added power, as high as 110 mW, was obtained when each slave laser power was 68 mW, i.e., efficiency of superposition as high as 85% was achieved.³⁸ This technique of coherent addition can be applied to arrayed laser devices.³⁹

V. NONLINEAR FREQUENCY CONVERSIONS FOR WIDEBAND FREQUENCY SWEEP

Performances of semiconductor lasers, e.g., characteristics of the output power, the single-mode oscillation, and the spatial beam profile, have not yet been sufficiently high as compared with conventional solid-state and gas lasers. However, they can be used as promising candidates of light sources for the practical optical frequency conversion systems because of the rapid progress of their performances and their inherent compatibility with electrical and optical feedback control to improve the performances.

Wideband frequency sweep can be realized by combining semiconductor lasers and nonlinear optical crystals because, as is shown by Fig. 12, variety of semiconductor lasers covering wide wavelength ranges have been developed. Thus, it is expected that the range of frequency sweep, from near infrared to near ultraviolet (i.e., approximately one PetaHz,) can be realized to meet requirement (3) of Sec. I. Although the method of Fig. 12 does not

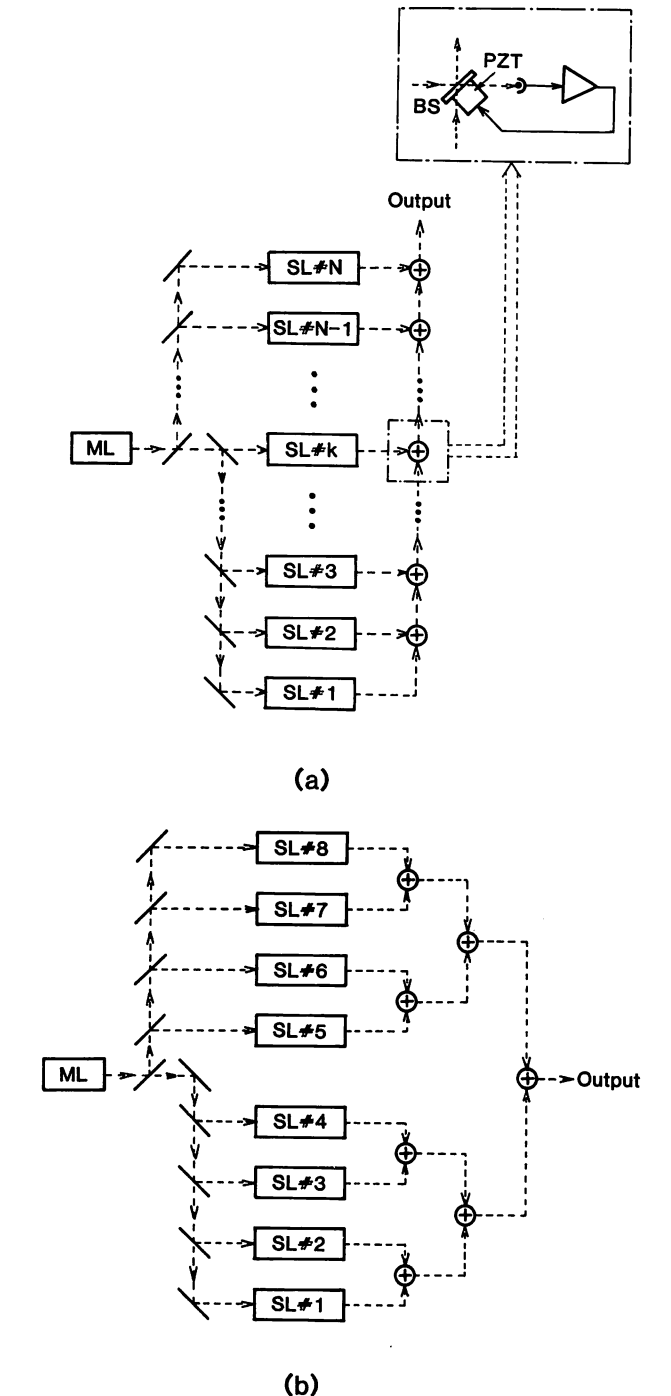


FIG. 11. Schematic explanation of two methods of coherent addition, for which the powers of the two laser beams are added by controlling their optical path difference. (ML): master laser, (SL $\#k$): slave laser $\#k$ ($k=1-N$), which is injection-locked to the master laser, (BS) beam splitter, (PZT): piezoelectric transducer. (a) The method of superposing adjacent laser beams. (b) The beams from 2^n lasers are superposed by a method of, namely, binary-tree ($n=3$ in this figure).

show that the frequency is swept continuously, a continuous frequency sweep can be expected if fine frequency tuning by heterodyne optical phase locking is auxiliary employed to fill the gap of the frequency region in which the coarse sweep is not possible. This section reviews authors' experiments on frequency conversion of semiconductor lasers by using nonlinear optical crystals which have been recently carried out to realize a PetaHz class coherent op-

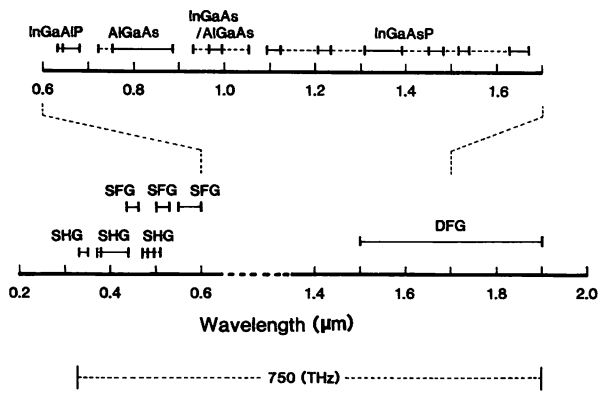


FIG. 12. Possible wavelength ranges of semiconductor lasers (upper part of this figure) and those of their nonlinearly up or down frequency converted lights (lower part). The solid lines in the upper part represent the wavelength ranges for commercially available semiconductor laser devices. The broken lines are for the ranges in which the lasings have been confirmed experimentally in the laboratories. (SHG): Second harmonics generation, (SFG): sum frequency generation, (DFG): difference-frequency generation. The total wavelength range covered by this figure corresponds to the frequency range of 750 THz, i.e., approximately one Peta-Hz.

tical frequency sweep generator. For realization of the wide range frequency sweep with accurate frequency reference, optical frequency link between different wavelength lasers can be achieved by using a phase locking technique between the second harmonic, sum frequency, and difference frequency lights of multiple lasers, e.g., the frequency of the 1.5 μm wavelength InGaAsP laser is linked to an AlGaAs laser by the phase locking of the SHG of the InGaAsP laser to the AlGaAs laser, and the AlGaAs laser can be further locked to an atomic resonance line, e.g., the Rb⁸⁷ resonance line at 780 nm wavelength.

Second harmonic generation of semiconductor lasers has been carried out by a number of research groups in order to obtain a short wavelength for an optical recording light source so as to increase the recording density.⁴⁰ However, experiments on sum frequency and difference frequency generations (SFG and DFG, respectively) and furthermore, frequency tunable light sources combining these nonlinear frequency conversions have not yet been fully documented. These systems should play essential roles for advanced optical systems, and they can be used even for the nonlinear saturation spectroscopy if the frequency-converted powers are sufficiently high by using the built-up cavity method.⁴¹ Figure 13 shows that a KNbO₃ crystal is installed in a built-up cavity for fundamental wave to increase the SHG efficiency. The FM noise of the fundamental wave is reduced by the optical feedback by the reflection from the front facet of the crystal,⁴² as have also been demonstrated by Refs. 41 and 43. The optical path length between the laser and the built-up cavity is controlled by negative electrical feedback to stabilize SHG power. The SHG power of 6.6 mW was obtained for the 100 mW fundamental wave power from a 0.86 μm wavelength AlGaAs laser. Furthermore, the SHG power was selectively modulated to realize the 100% modulation depth by

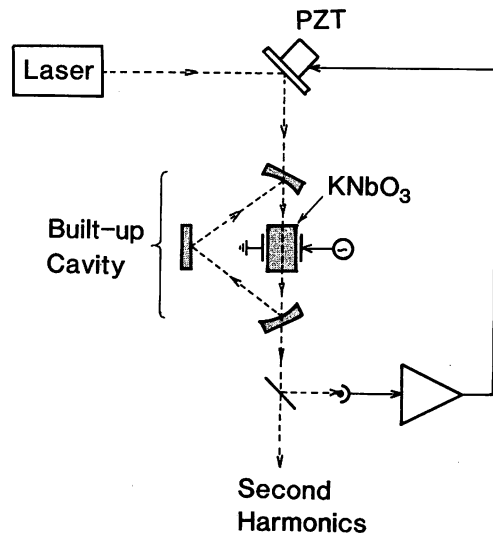


FIG. 13. Experimental setup of second harmonic generation of an AlGaAs laser by using a KNbO₃ crystal which is installed in a built-up cavity. The FM noise of the fundamental wave is reduced by the optical feedback by the reflection from the front facet of the crystal. The ac voltage is applied to the crystal to modulate the second harmonic power.

utilizing the different responses of the coefficients of the second harmonic and the fundamental waves to the electro-optical modulation in the KNbO₃ crystal. As an improved built-up cavity, a monolithic cavity has been fabricated by coating high-reflection films on a polished surface of the nonlinear crystal. The SHG powers as high as 24 mW⁴⁴ and 41 mW⁴⁵ have been achieved.

As another example of nonlinear frequency conversion, SHG of a strained quantum well InGaAs/AlGaAs laser of 0.98 μm wavelength has been generated by using a b-cut KNbO₃ crystal installed in a built-up cavity, where the crystal temperature was adjusted to be 22 °C for phase matching. The SHG power was 2 mW for the incident fundamental power of 70 mW. This 493 nm wavelength second harmonic wave can be used as a light source for the laser cooling of Ba⁺. A white light beam can be obtained if this blue second harmonic light is optically aligned with the green second harmonic light beam from a semiconductor laser-pumped YAG laser and red beam from an InGaAlP laser. The conventional He-Cd white color lasers can be replaced by this semiconductor laser-based white light source to improve the reliability and lifetime of the image processing systems.

The second harmonic wave of a 1.5 μm wavelength InGaAsP laser (i.e., an essential device for coherent optical transmission) can be tuned to a Rb⁸⁷ resonance frequency, which has been used as an accurate frequency reference for AlGaAs lasers.⁴⁶ Thus, frequency, accuracy, and stability of the InGaAsP laser can be improved by locking its second harmonic frequency to the Rb⁸⁷ resonance frequency. This frequency stabilization has been carried out by using the internal second harmonic wave generated in the active waveguide of the InGaAsP laser.⁴⁷ Recently, the second harmonic wave has been generated from a KTP crystal installed in a built-up cavity while the

FM noise of a fundamental wave is further reduced by the optical feedback from the built-up cavity.⁴⁸

To extend the range of frequency sweep, sum frequency generation by using an InGaAsP laser and a 0.83 μm wavelength AlGaAs laser has been carried out with a KTP crystal to obtain the sum-frequency power of 230 nW,⁴⁸ which is the first example of generating a green light by using semiconductor lasers. Although the green lights have been generated by nonlinear optical frequency conversions of solid-state lasers, e.g., a YAG laser, their frequency cannot be swept for a wide range. On the other hand, the range of frequency sweep of the sum frequency shown above can be as wide as about 30 THz (i.e., the wavelength range of 0.53–0.56 μm) because the oscillation wavelength of AlGaAs laser devices can cover the range from 810 to 890 nm.

Difference frequency generation has also been carried out for a 1.5 μm wavelength InGaAsP laser and a 0.77 μm wavelength Ti:Al₂O₃ laser. The same KTP crystal for the SFG experiment was used for its large nonlinear coefficient in the near infrared region and the large temperature tolerance. Under the phase matching condition by adjusting the crystal angle, the 1.6 μm wavelength difference frequency output power of about 2 μW was obtained when the incident powers of the two lasers were 5 and 200 mW, respectively. Since the Ti:Al₂O₃ laser can be replaced by an AlGaAs laser, the frequency sweep range of 42 THz, i.e., the wavelength range from 1.5 to 1.9 μm , can be expected.

One of the proposed systems employs the succeeding frequency division of the difference in two laser frequencies by using nonlinear optical crystals.^{49,50} This system can achieve a very wideband frequency sweep because there is no limitation of setting the maximum frequency difference for division as long as the phase matching of nonlinear optical crystal is ensured. Figure 14 shows one of the other systems proposed by the authors in order to measure the resonant frequency of the Ca spectral line (³P₁–¹S₀; 657.459 nm wavelength), which falls within the oscillation frequency range of InGaAlP lasers. It has been proposed that this spectral line can be used as a highly accurate frequency standard in the visible region because of its narrow natural linewidth, i.e., 400 Hz.⁵¹ For the measurement of Ca resonant frequency, the frequency of a InGaAlP laser (laser #2 in this figure) is locked to the Ca resonance frequency, and heterodyne-type optical phase locking is provided to other commercially available InGaAsP lasers, AlGaAs lasers, and the outputs from the nonlinear optical crystals for frequency conversions. The frequency ν_2 of laser #2, and thus, the resonant frequency of Ca, can be known accurately by using the following formula by measuring the output microwave frequencies f_k of the photo-diodes PD_k ($k=1-9$):

$$\begin{aligned} \nu_2 = & 2^8 M f_m - 2^0 f_1 - 2^1 f_2 + 2^2 f_3 + 2^3 f_4 + 2^4 f_5 + 2^5 f_6 \\ & + 2^6 f_7 + 2^7 f_8 - 2^8 f_9, \end{aligned} \quad (5)$$

where f_m and M represent the modulation frequency and the order of sideband in the optical frequency comb generator which can be used as a local oscillator for measuring

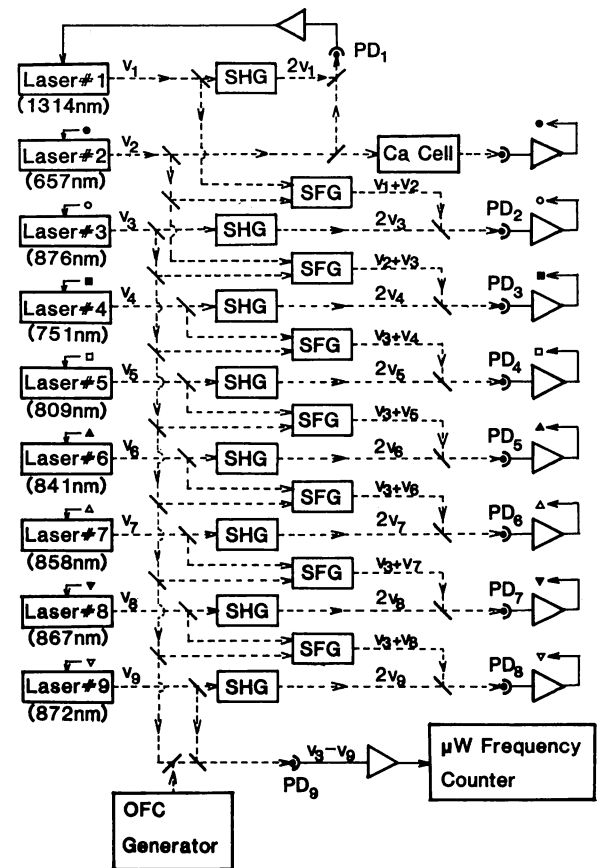


FIG. 14. Proposed system for measuring the resonant frequency of a Ca spectral line at 657 nm wavelength by using a frequency chain composed of nine semiconductor lasers: (SHG): second harmonic generator, (SFG): sum frequency generator, (PD_k) ($k=1-9$): photo-diode for measuring the heterodyne frequency and for heterodyne optical phase locking, OFC generator: optical frequency comb generator given by Fig. 16.

the 1.8 THz frequency difference between laser #3 (876 nm wavelength) and laser #9 (872 nm wavelength).

If a stable Rb atomic clock is used as a driver for the optical frequency comb generator, the order of sideband M has to be as high as 262 because the value of f_m is 6.8 GHz. However, this order of sideband can be generated and detected as will be described in Sec. 6. Since all the frequencies of lasers in Fig. 14 can be calibrated based on the Ca resonance frequency, this system realizes a highly accurate, multicolor coherent light source. Even by using bulky crystals of conventional nonlinear optical materials, frequency converted power can be sufficiently high for heterodyne optical phase locking, further increases in converted powers can be expected if devices such as domain-inverted nonlinear optical waveguides⁵² are used.

For realization of this system, several nonlinear frequency conversions have already been demonstrated, as described below:

(1) Second harmonic generation of the 1.3 μm wavelength light by a KTP: Optical feedback from an external grating was employed to realize a single longitudinal mode oscillation of a 1.3 μm wavelength high power InGaAsP laser. A side-mode suppression ratio larger than 40 dB was achieved at 50 mW output power. The 10 nW second har-

monic power of this laser was obtained from a KTP crystal. This power can be increased if a built-up cavity is used.

(2) Sum frequency generation of the two $0.8 \mu\text{m}$ wavelengths lights by a KNbO_3 : A KNbO_3 crystal was employed because of its large nonlinear optical coefficient (i.e., about 20 pm/V for the a-cut crystal used here). The noncritical type-I phase matching was realized by adjusting the crystal temperature within a range of between 0°C and 60°C . The sum frequency power of 100 nW was obtained while its wavelength was varied from 425 to 438 nm by sweeping one of the laser wavelengths from 825 to 876 nm and fixing the wavelength of another laser at 876 nm , where the two laser powers incident into the crystal were 100 mW . A tuning from 420 to 460 nm is expected if the temperature can be fully varied, i.e., from -30°C to 150°C , which is limited by the phase transition of the crystal.

(3) Sum frequency generation of the 1.3 and $0.74 \mu\text{m}$ wavelengths lights by a KNbO_3 : This experiment was carried out as a preliminary experiment on SFG between the 1.3 and $0.66 \mu\text{m}$ wavelengths lights. A b-cut KNbO_3 crystal with a phase matching temperature of 22°C , a $1.32 \mu\text{m}$ wavelength InGaAsP laser, and a $0.74 \mu\text{m}$ wavelength $\text{Ti:Al}_2\text{O}_3$ laser were used. The 100 nW sum-frequency power was obtained when the two laser powers incident into the crystal were 50 and 200 mW , respectively. It can be expected that the SFG of 1.3 and $0.66 \mu\text{m}$ wavelengths lights is realized by using an a-cut KNbO_3 crystal at 15°C , by which the main part of the system in Fig. 14, i.e., frequency tuning to Ca resonance frequency, is carried out.

Besides the well used inorganic nonlinear optical crystals, organic materials are also promising for nonlinear optical crystals because the figure of merit for nonlinear frequency conversion can be much larger than that of inorganic crystals. Moreover the versatility in design of the materials, such as compositions of the crystal and fabrication of the organic waveguide, is attractive in applications. Research on nonlinear frequency conversions using organic materials is in its primary stage and experimental results have not yet been fully documented. The authors have recently succeeded in generating the second harmonics from a DMNP organic crystal grown in a glass capillary of $1 \mu\text{m}$ inner diameter. Even under the phase mismatching condition, Cerenkov radiation has been obtained with 50 nW second harmonic power when the 50 mW power of an InGaAsP laser was incident into the capillary. This power has been sufficiently high to be used as optical phase locking with a conventional AlGaAs laser.

VI. ACCURATE MEASUREMENT OF OPTICAL FREQUENCY

Optical frequency of a highly stable laser has to be accurately measured when the laser is used for some optical systems, e.g., frequency division multiplex (FDM) coherent optical transmission and high resolution laser spectroscopy. The purpose of this section is to review the accurate measurement of optical frequency to meet requirement (5) of Sec. I. This measurement is possible by using an accurate frequency reference, a stable laser as a

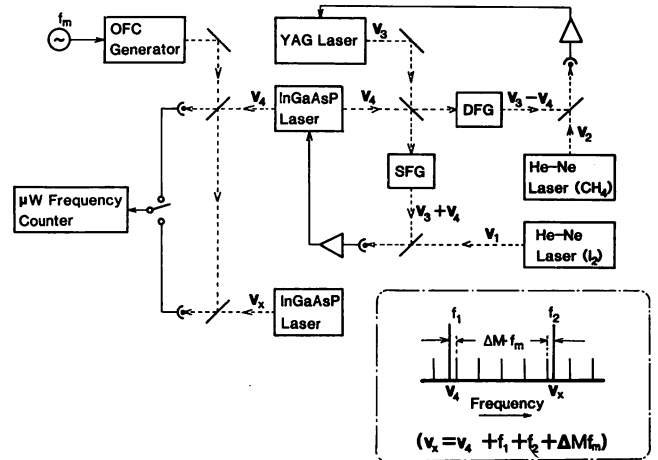


FIG. 15. Proposed system of accurate optical frequency counting of a $1.5 \mu\text{m}$ wavelength InGaAs laser (frequency: ν_x). A $0.63 \mu\text{m}$ wavelength I_2 stabilized He-Ne laser (ν_1) and a $3.39 \mu\text{m}$ wavelength CH_4 stabilized He-Ne laser (ν_2) are used as primary optical frequency standards. A YAG laser at $1.06 \mu\text{m}$ wavelength (ν_3) and an InGaAsP laser at $1.5 \mu\text{m}$ wavelength (ν_4) are used as the secondary optical frequency standards by phase locking their sum and difference frequency signals to the two primary standards. (SFG): sum frequency generator, (DFG): difference frequency generator, OFC generator: optical frequency comb generator given by Fig. 16. The inset of this figure represents the frequency spectra of the two InGaAsP lasers (ν_4 and ν_x) and the OFC generator. (f_m): modulation frequency of the OFC generator. (f_1, f_2): heterodyne frequency between the secondary optical frequency standard InGaAsP laser (ν_4) [between the InGaAsP laser under test (ν_x)] and the nearest modulation sideband frequency of the OFC generator, (ΔM): the difference of the orders of the two sidebands.

local oscillator, nonlinear optical conversions, and optical phase locking. The conventional measurement system employs an optical frequency chain from optical to microwave frequencies based on a stable microwave Cs atomic clock.⁵³ Although such a system is highly accurate, the problem of low reliability remains because it relies on a large oscillator system (composed of visible lasers, infrared lasers, far infrared lasers, and microwave oscillators) and short lifetime point contact diodes for harmonic mixers. This problem can be solved if a compact and long lifetime system is realized by combining several semiconductor lasers which cover a wide frequency range. As an example of such a system, a laser system combining $1.3 \mu\text{m}$ wavelength semiconductor lasers has been proposed in Ref. 49.

As another example, an optical frequency measurement system for $1.5 \mu\text{m}$ wavelength semiconductor lasers has been proposed by the authors for the FDM coherent optical transmission,⁵⁴ and is described here. In the FDM coherent optical transmission system, a great number of channels, e.g. hopefully as large as 1000 channels in the future, are prepared within the optical frequency range of about 10 THz (around $1.55 \mu\text{m}$ wavelength) at which an optical fiber shows the lowest transmission loss. In order to avoid channel switching errors, each channel frequency should be accurately measured. Figure 15 explains schematically the principle of measurement. A $0.63 \mu\text{m}$ wavelength I_2 -stabilized He-Ne laser and a $3.39 \mu\text{m}$ wavelength CH_4 -stabilized He-Ne laser are used as the primary optical frequency standards in this system, whose frequencies have

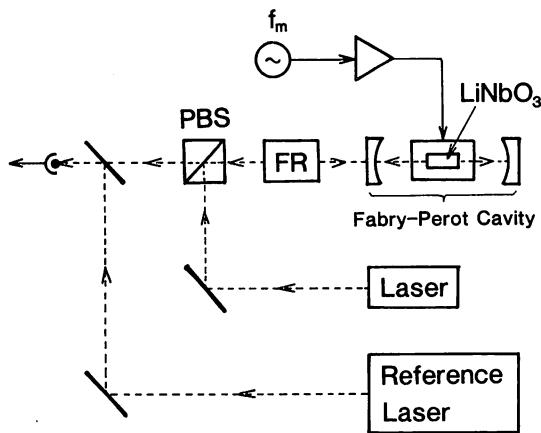


FIG. 16. Schematic explanation of an optical frequency comb (OFC) generator. A LiNbO₃ crystal is used as a phase modulator which is installed in a Fabry-Perot cavity to realize a high modulation efficiency. The crystal is also enclosed by a microwave waveguide to build up a microwave power for modulation. The modulation frequency f_m is fixed as a multiple of the free spectral range of the Fabry-Perot cavity for high modulation efficiency. The reference laser is used to measure the modulation sidebands spectra by a heterodyne technique.

been measured within the accuracy of 1×10^{-9} .⁵⁵ By using these standards, the expected accuracy of the measurement can be as high as 1×10^{-9} . Although such high accuracy may not be required to maintain the reliability of the FDM system described above, such a system can be used as a prototype for a highly accurate optical frequency measurement system for a variety of precise optical systems.

This system uses the fact that the frequencies ν_1 and ν_2 of the above-mentioned two He-Ne lasers have simple relations with those of a 1.06 μm wavelength YAG laser and a 1.5 μm wavelength InGaAsP laser ν_3 and ν_4 , which are approximately expressed as $\nu_3 = (\nu_1 + \nu_2)/2$ and $\nu_4 = (\nu_1 - \nu_2)/2$. Thus, the frequency of the InGaAsP laser is locked to the primary frequency standards by phase locking the sum frequency and difference frequency signals of the InGaAsP and YAG lasers to the two He-Ne lasers. By using this InGaAsP laser as the secondary frequency standard, the frequency ν_x of the other InGaAsP laser under test is known if the heterodyne frequency between these two InGaAsP lasers is measured by a conventional microwave frequency counter.

However, since this heterodyne frequency can be as high as 10 THz if the InGaAsP laser is used for the FDM coherent optical transmission system in the low transmission loss region of the optical fiber, an additional optical local oscillator is required to measure such a high heterodyne frequency. This can be realized by an optical frequency comb (OFC) generator shown by Fig. 16. The OFC generator is a system for generating modulation sidebands, i.e., an optical frequency comb, by transmitting the InGaAsP laser beam through a phase modulator which is composed of an electro-optical crystal driven by a microwave with the stable frequency of f_m . The heterodyne frequency f_1 between the secondary standard frequency ν_4 and the nearest modulation sideband frequency can be measured by a microwave frequency counter. Further-

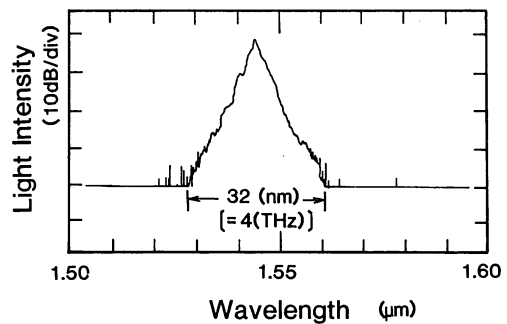


FIG. 17. The profile of the envelope of the modulation sidebands of the OFC generator observed by an optical spectrum analyzer. The observed width of this envelope is 32 nm (or 4 THz), which is limited by the sensitivity of the optical spectrum analyzer (from Ref. 56).

more, the heterodyne frequency f_2 between the frequency ν_x of the laser under test and the frequency of its nearest sideband can be also measured. Since the frequency difference between the two sidebands used above can be given by the product of f_m and the difference of the sideband orders ΔM , the value of ν_x can be given as $\nu_x = \nu_4 + f_1 + f_2 + \Delta M \cdot f_m$.

The main component of the highly efficient phase modulator in Fig. 16 is a LiNbO₃ crystal which is installed in a Fabry-Perot cavity to realize a high modulation efficiency. This crystal is also enclosed by a microwave waveguide to build up a microwave power for modulation, where the waveguide is designed to realize a spatial overlap between the lightwave and microwave fields and to match the optical group velocity and microwave phase velocity in the crystal. By this configuration, modulation efficiency θ as high as 0.2 rad has been achieved at the modulation frequency f_m of 5.8 GHz even by using a bulky LiNbO₃ crystal, where f_m was fixed to three times the free spectral range (FSR) of the Fabry-Perot cavity. The finesse of this crystal-installed Fabry-Perot cavity was obtained as high as 200.

The OFC was generated by inputting a 10 kHz linewidth DFB laser beam to the cavity, and the heterodyne signal between one of the modulation sidebands in the OFC and another 10 kHz linewidth reference laser was detected. The signal-to-noise (S/N) ratio of this detection was high, i.e., only 5 dB lower than that of the shot noise-limited theoretical value, which is expressed as S/N (in the unit of dB) = $75 - 0.11 \times |M|$, where M is the order of sideband in the OFC. Such a large value of the S/N was attributed to using the narrow linewidth lasers and an optical balanced receiver. The maximum of the shot noise-limited value of M , corresponding to $S/N = 0$ dB, is estimated to be 682, which gives the $M \times f_m = 4$ THz. Figure 17 shows the experimental results obtained to confirm this estimation. This figure represents the profile of the envelope of the OFC, i.e., a series of modulation sidebands, observed by an optical spectrum analyzer. It was confirmed by this profile that the modulation sidebands were generated within the frequency range of ± 2 THz around the carrier component and the profile of the envelope

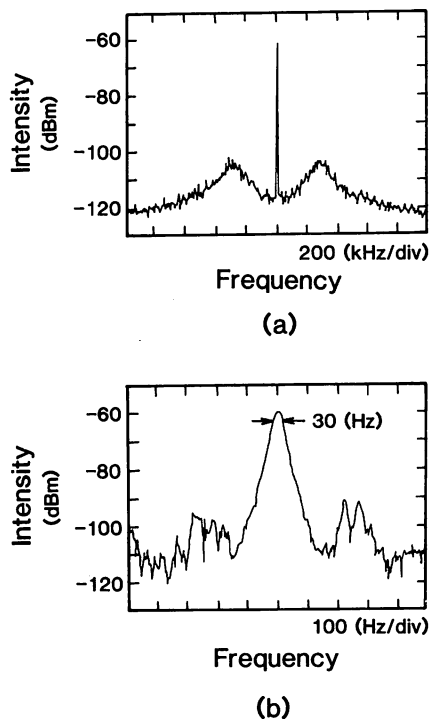


FIG. 18. The spectral profile of the heterodyne signal observed under the condition of the optical phase locking between the 84th sideband of the OFC generator and the reference laser. The horizontal axis of (a) is magnified and its central part is shown by (b). The 3 dB linewidth of the spectral profile of (b) is 30 Hz, limited by the resolution of the microwave spectrum analyzer (from Ref. 56).

agreed with the theoretical calculation. The width of the profile, i.e., 4 THz, corresponds to the wavelength span as large as 32 nm, which is larger than the tunable wavelength range of existing DFB lasers.

The width of the envelope can be increased to 10 THz if the modulation index is increased to $\pi/2$ rad by increasing the microwave power. It has been confirmed that an asymmetric profile of the envelope can be also realized by increasing the powers of lower or upper sidebands, for which the contribution of the dispersion of a Fabry-Perot cavity to the modulation efficiency is compensated for by detuning the value of f_m from $3 \times \text{FSR}$.⁵⁶ Based on these experimental results, it is expected that the frequency span of the OFC generator can be expanded to the value limited by the bandwidth of the mirror of the Fabry-Perot cavity, i.e., as wide as 20 THz, by using higher efficiency phase modulator and by fabricating a monolithic Fabry-Perot cavity to reduce the loss. Such a wide frequency span OFC generator can work as a local oscillator for optical frequency measurements of InGaAsP lasers in FDM coherent optical transmission at a 1.5 μm wavelength region.

Figure 18(a) represents the spectral profile of the heterodyne signal observed under the condition of the optical phase locking between the 84th sideband of the OFC generator and the reference laser.⁵⁶ Although the heterodyne frequency was 200 MHz, the separation between the carrier frequency of the modulated light and reference laser frequency was as large as 487 GHz, i.e., the carrier signal is optically phase locked to the reference signal with such a

large frequency separation. The control bandwidth of this phase locked loop was 250 kHz, and the phase error variance was estimated to be 0.01 rad^2 . Figure 18(b) shows a magnified profile of the central part of Fig. 18(a).⁵⁶ The 3 dB linewidth is 30 Hz, limited by the resolution of the microwave spectrum analyzer by which a high performance of the phase locking was confirmed.

The phase locking to the two He-Ne lasers can be realized by using a technique similar to the one demonstrated by Fig. 18. The sum and difference frequencies between the InGaAsP laser and a YAG laser have to be generated for this phase locking, which is possible by using the technique of nonlinear optical frequency conversion given in Sec. IV. Recent experiments have confirmed that the sum frequency signal of 0.2 μW power was generated from a LiNbO₃ crystal whose temperature was fixed at 323 $^\circ\text{C}$ for phase matching. This power is sufficiently high for the optical phase locking with the I₂ stabilized He-Ne laser of 1 mW power. It is also possible for the LiNbO₃ crystal to generate the difference frequency if its temperature is fixed at 570 $^\circ\text{C}$.⁵⁶

The OFC generator described above can be realized at a variety of wavelength regions by changing the high reflection or antireflection films coated on the surfaces of the relevant optical elements as long as the phase modulator crystal is transparent. If a series of the OFC generators with different wavelength regions is prepared and the sidebands of the adjacent OFC generators are phase locked with each other, a very wide span OFC is expected, which can be as wide as over 100 THz.

In addition to the optical frequency measurement at the 1.5 μm wavelength region, there can be at least three application systems for which the OFC generator is used: (1) The OFC generator is used as a highly accurate local oscillator in the system of Fig. 14, where the frequency difference between the two lasers is too large to measure directly by using a conventional photodiode. (2) The frequency of a Ca resonance spectral line at 657 nm wavelength can be measured by using a popular visible frequency standard of I₂ resonance line at 633 nm, if the two or three OFC generators are used for linking these two frequencies whose difference is as large as 17 THz. Based on these frequency measurements, the resonance atomic spectral line of Ca can become a promising candidate for a frequency standard in the visible region. This is because the accuracy of Ca frequency can be higher than that of I₂ since the hyperfine structure of Ca is simpler than that of I₂.⁵⁷ (3) Frequency division multiplex coherent optical transmission can be expected by using one laser as a primary light source, as is shown by Fig. 19, where modulation sidebands from an OFC generator are separated by an optical frequency filter after being amplified by an optical fiber amplifier.

At the end of this section, the possibility of realizing an ultrafast photodetector is proposed by using a high transition temperature (T_c) oxide superconducting film. One of the principal reasons of requiring an OFC generator for the optical frequency measurement system of Fig. 15(a) is the lack of a fast photodetector whose response bandwidth is

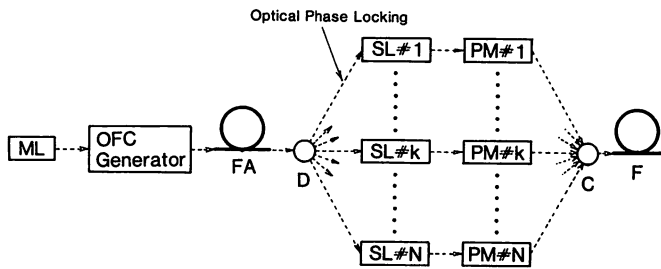
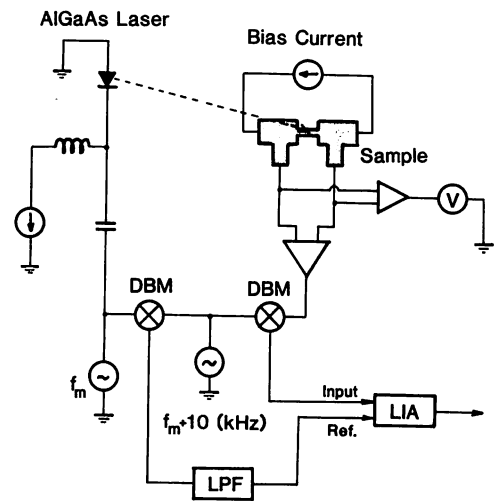


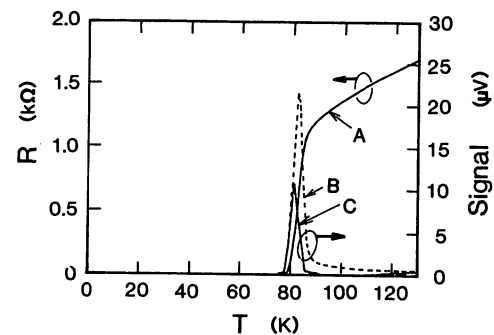
FIG. 19. Proposed system of frequency division multiplex coherent optical transmission by using an OFC generator: (ML): master laser, (FA): optical fiber amplifier, (D): optical frequency filter and divider, (SL#k): Slave laser which is phase locked to the k th modulation sideband of the OFC generator, (PM#k): phase modulator, (C): coupler, (F): optical fiber for transmission.

as wide as, e.g., 100 GHz. If this kind of photodetector is realized, the system becomes simpler because a wideband OFC generator will not be necessary. It has been proposed that a high T_c oxide superconducting film can be one of the candidates for such a photodetector.⁵⁸ Although details of the optical response mechanism have not yet been made clear, it has been understood that the Cooper pairs in the film are destroyed by the energy of the photon irradiated to the film slightly below the T_c . As a result the number of quasi-particles is increased so as to increase the film resistance. Since it is a quantum effect, the response time can be very short. According to the theory of nonequilibrium superconductivity, which is based on the Bardeen-Cooper-Schrieffer (BCS) theory, it has been calculated that nonbolometric response time is about several ten ps, which corresponds to several hundred GHz.⁵⁹ Although theoretical studies on this phenomenon have not been completed, it can be expected that the high T_c oxide superconducting film can be used as an ultrafast photodetector for a wide wavelength region because its absorption efficiency is high for visible and far-infrared regions.

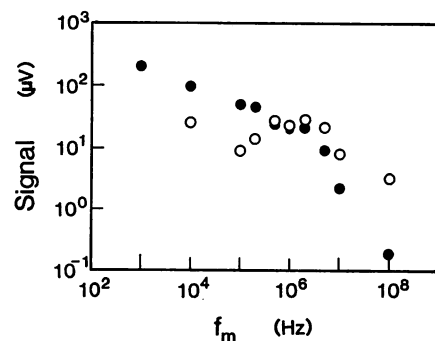
Figure 20(a) shows the experimental setup.^{60,61} A $\text{DyBa}_2\text{Cu}_3\text{O}_{7-x}$ superconducting film was deposited on a MgO (100) substrate by a molecular beam epitaxy technique. The samples with the $T_c=88$ K had constrictions with a size of $20 \mu\text{m}$ width, $400 \mu\text{m}$ length, and $0.1 \mu\text{m}$ thickness, which were fabricated by standard photolithography and Ar ion milling. This film was driven by a constant current of 0.5 mA, and the 100% power modulated $0.8 \mu\text{m}$ wavelength AlGaAs laser light of 3 mW power was irradiated. Figure 20(b) shows a relation between the temperature and the signal intensities. Curve A is the value of film resistance. Curve B is the derivative of curve A, representing the bolometric signal intensity originated from the temperature increase by the laser irradiation. Curve C, on the other hand, represents the difference between the value of the total signal and the value of curve B, which corresponds to the signal due to the nonbolometric quantum effect. Figure 20(c) shows the dependencies of the bolometric and nonbolometric signal intensities on the modulation frequency f_m of the laser power. Although the previous experiments have measured these dependencies only for $f_m < 1$ MHz,⁶² the present experiment expanded



(a)



(b)



(c)

FIG. 20. (a) Experimental setup for measuring the optical response of a $\text{DyBa}_2\text{Cu}_3\text{O}_{7-x}$ superconducting film. (DBM): double balanced mixer, (LPF): low pass filter, (LIA): lock-in amplifier. (b) Experimental results. A: temperature dependence of the film resistance, (B), (C): the bolometric and nonbolometric signal intensities obtained under the irradiation of an AlGaAs laser beam of 3 mW, respectively (from Refs. 60, 61). (c) Dependencies of the bolometric and nonbolometric signal intensities on the modulation frequency of the laser power, which are represented by closed and open circles, respectively (from Refs. 60, 61).

the range of measurements up to $f_m=100$ MHz by improving the performances of rf frequency driver and receiver circuits. In spite of the fact that this experimental work is still preliminary, it can be confirmed by this figure that the bandwidth of the nonbolometric signal is much

wider than that of the bolometric signal and that the signal voltage of about several μV was obtained.

Further expansion of the measurement range of f_m is expected by improving the performances of driver and receiver electronic circuits, by which detailed investigation on response characteristics and quantum mechanisms are carried out. By these investigations, it is expected that one can open a novel field of application to use a high T_c superconducting film as an ultrafast and wavelength insensitive photodetector.

VII. SUMMARY

This article reviewed the recent results of authors' studies on highly sensitive FM noise detection, wideband frequency control, and optical phase locking in order to suppress the laser FM noise originated from the quantum fluctuations. Possibilities of a wideband frequency tunable light source by using nonlinear optical frequency conversions were also presented. As an application of these frequency control methods, the possibility of highly accurate optical frequency measurement system was given. It is expected that realization of these systems can come true in the near future by selecting carefully nonlinear optical materials with higher efficiency, by using a higher finesse built-up cavity for nonlinear optical frequency conversions, and so on.

In addition to the frequency control methods of compensating for the effect of quantum FM noise described in this article, there can be other methods of realizing frequency stabilized lasers. One of these methods is to directly control the magnitude of quantum noise, i.e., probability of spontaneous emission, which can be a promising method even though it has not yet been applied to semiconductor lasers. There are at least two proposals for modifying the magnitudes of FM or phase noises:

(1) It has been pointed out that the laser oscillation without population inversion can be realized by using three-level atoms with Λ -shape transition due to the quantum interference between the levels. The FM noise magnitude of this lasing light can be lower than the value limited by conventional spontaneous emission fluctuations.⁶³

(2) The laser oscillation with correlated spontaneous emission is realized by using three-level atoms with V shape transition, which is also due to the quantum interference between the levels. The phase noise magnitude of this lasing light can be lower than the value limited by quantum fluctuations (more precisely, vacuum fluctuations). It means that the phase squeezing can be realized.⁶⁴

Experiments of these two proposals have not yet been carried out for semiconductor lasers except for preliminary experiments on correlated spontaneous emission.⁶⁵ However, since it has been experimentally proved that the negative electrical feedback to semiconductor laser can generate the squeezed light,⁶⁶ progress on these proposals can be expected in the near future. The future problems of using these quantum optical methods could be to find the application to frequency control and related experimental studies. By solving these problems, realization of novel light

sources with low FM noise are expected in which the quantum noise magnitude is directly controlled.

ACKNOWLEDGMENTS

The authors would like to thank Dr. Y. Higashino of Yokogawa Electric Corp. for his support of preparing high T_c superconducting films. A part of this work was supported by a Grant-in-Aid for Scientific Research (Grant Nos. 01850015, 03555006, and 04228102).

- ¹P. Vettiger, M. K. Benedict, G.-L. Bona, P. Buchmann, E. C. Cahoon, K. Datwyler, H.-P. Dietrich, A. Moser, H. K. Seitz, O. Voegeli, D. J. Webb, and P. Wolf, *IEEE J. Quantum Electron.* **QE-27**, 1319 (1991).
- ²P. J. A. Thijs, L. F. Tiemeijer, P. I. Kuindersma, J. J. M. Binsma, and T. V. Dongen, *IEEE J. Quantum Electron.* **QE-27**, 1426 (1991).
- ³M. Ohtsu and Y. Teramachi, *IEEE J. Quantum Electron.* **QE-25**, 31 (1989).
- ⁴M. Okai, S. Tsuji, and N. Chinone, *IEEE J. Quantum Electron.* **QE-25**, 1314 (1989).
- ⁵M. Ohtsu, *Highly Coherent Semiconductor Lasers* (Artech House, Inc., Norwood, 1992).
- ⁶M. Ohtsu, *J. Lightwave Technol.* **6**, 246 (1988).
- ⁷M. Ohtsu and N. Tabuchi, *J. Lightwave Technol.* **6**, 358 (1988).
- ⁸A. Blaquiere, *Comptes Rendus* **26**, 2929 (1962).
- ⁹C. H. Henry, *IEEE J. Quantum Electron.* **QE-18**, 259 (1982).
- ¹⁰K. Yoshida, M. Kourogi, K. Nakagawa, and M. Ohtsu, in *Proceedings of the International Conference on Noise in Physical Systems and 1/f Fluctuations*, Kyoto, 1991, edited by T. Musha, S. Sato, and M. Yamamoto (Ohm-sha Publishing, Tokyo, 1991), pp. 349-352.
- ¹¹M. Kourori and M. Ohtsu, *Opt. Commun.* **81**, 204 (1991).
- ¹²C. Y. Kuo and N. K. Dutta, *Electron. Lett.* **24**, 947 (1988).
- ¹³S. Ogita, Y. Kotaki, M. Matsuda, Y. Kuwahara, H. Onaka, H. Miyama, and H. Ishikawa, *IEEE Photon. Technol. Lett.* **2**, 165 (1990).
- ¹⁴M. Ohtsu, M. Murata, and M. Kourogi, *IEEE J. Quantum Electron.* **QE-26**, 231 (1990).
- ¹⁵S. Kobayashi and T. Kimura, *IEEE J. Quantum Electron.* **QE-17**, 681 (1981).
- ¹⁶C.-H. Shin and M. Ohtsu, *Opt. Lett.* **15**, 1455 (1990).
- ¹⁷B. Dahmani, L. Hollberg, and R. Drullinger, *Opt. Lett.* **12**, 876 (1987).
- ¹⁸J. Feinberg, *Optical Phase Conjugation*, edited by R. A. Fisher (Academic, New York, 1983), Chap. 11, pp. 434-435.
- ¹⁹M. Ohtsu, I. Koshiishi, and Y. Teramachi, *Jpn. J. Appl. Phys.* **29**, L2060 (1990).
- ²⁰Y. Awaji, S. Sayama, H. Suzuki, M. Ohtsu, and Y. Teramachi, *Jpn. J. Appl. Phys.* **32**, 1107 (1993).
- ²¹M. Ohtsu and K. Nakagawa, in *Coherence, Amplification, and Quantum Effects in Semiconductor Lasers*, edited by Y. Yamamoto (Wiley, New York, 1991), Chap. 5, pp. 137-190.
- ²²G. Rempe, R. J. Thompson, H. J. Kimble, and R. Lalezari, *Opt. Lett.* **17**, 363 (1992).
- ²³M. Ohtsu, H. Fukada, T. Tako, and H. Tsuchida, *Jpn. J. Appl. Phys.* **22**, 1157 (1983).
- ²⁴M. Okai, T. Tsuchiya, A. Takai, and N. Chinone, *IEEE Photon. Technol. Lett.* **4**, 526 (1992).
- ²⁵M. Kourogi, C.-H. Shin, and M. Ohtsu, *IEEE Photon. Technol. Lett.* **3**, 496 (1991).
- ²⁶R. W. Drever, J. L. Hall, F. V. Kowalski, J. Hough, G. M. Ford, A. J. Munley, and H. Ward, *Appl. Phys. B* **31**, 97 (1983).
- ²⁷M. Okai, T. Tsuchiya, K. Uomi, N. Chinone, and T. Harada, *IEEE Photon. Technol. Lett.* **3**, 427 (1991).
- ²⁸K. Nakagawa, M. Kourogi, and M. Ohtsu, *Opt. Lett.* **17**, 934 (1992).
- ²⁹K. S. Thorne, *Rev. Mod. Phys.* **52**, 285 (1980).
- ³⁰M. Kozuma, M. Kourogi, M. Ohtsu, and H. Hori, *Appl. Phys. Lett.* **61**, 1895 (1992).
- ³¹Y. Shevy, J. Iannelli, J. Kitching, and A. Yariv, *Opt. Lett.* **17**, 661 (1992).
- ³²K. Kuboki and M. Ohtsu, *IEEE J. Quantum Electron.* **QE-25**, 2084 (1989).
- ³³C.-H. Shin and M. Ohtsu, *IEEE Photon. Technol. Lett.* **2**, 297 (1990).
- ³⁴M. Kourogi, C.-H. Shin, and M. Ohtsu, *IEEE Photonics Technol. Lett.* **3**, 270 (1991).

- ³⁵C.-H. Shin and M. Ohtsu, *IEEE J. Quantum Electron.* **29**, 374 (1993).
- ³⁶A. M. Akulshin, A. A. Celikov, and V. L. Velichansky, *Opt. Commun.* **84**, 139 (1991).
- ³⁷A. M. Akulshin, A. A. Celikov, K. Nakagawa, M. Ohtsu, V. L. Velichansky, and V. V. Vashiljev, in *International Conference on Quantum Electronics Technical Digest*, Series 1992 (Institut für Nachrichtentechnik der TU, Wien, 1992), Vol. 9, pp. 24–25.
- ³⁸W. Wang, K. Nakagawa, S. Sayama, and M. Ohtsu, *Opt. Lett.* **17**, 1593 (1992).
- ³⁹L. J. Mawst, D. Botez, M. Jansen, T. J. Roth, C. Tu, and C. Zmudzinski, *Electron. Lett.* **27**, 1586 (1991).
- ⁴⁰K. Shinozaki, T. Fukunaga, K. Watanabe, and T. Kamijoh, *Appl. Phys. Lett.* **59**, 510 (1991).
- ⁴¹A. Hemmerich, D. H. McIntyre, C. Zimmermann, and T. Hansch, *Opt. Lett.* **15**, 372 (1990).
- ⁴²T. Senoh, Y. Fujino, Y. Tanabe, M. Hirano, M. Ohtsu, and K. Nakagawa, *Appl. Phys. Lett.* **60**, 1172 (1992).
- ⁴³G. J. Dixon, C. E. Tanner, and C. E. Wieman, *Opt. Lett.* **14**, 731 (1989).
- ⁴⁴L. Goldberg and M. K. Chun, *Appl. Phys. Lett.* **55**, 218 (1989).
- ⁴⁵W. J. Kozlovsky and W. Lenth, *Appl. Phys. Lett.* **56**, 2291 (1990).
- ⁴⁶H. Furuta and M. Ohtsu, *Appl. Opt.* **28**, 3737 (1989).
- ⁴⁷M. Ohtsu and E. Ikegami, *Electron. Lett.* **25**, 22 (1989).
- ⁴⁸W. Wang, K. Nakagawa, Y. Toda, and M. Ohtsu, *Appl. Phys. Lett.* **61**, 886 (1992).
- ⁴⁹T. Sato, S. Singh, W. Swarz, and J. L. Hall, in *International Conference on Quantum Electronics Technical Digest*, Series 1990 (Optical Society of America, Washington, DC, 1990), Vol. 8, pp. 216–217.
- ⁵⁰H. R. Telle, D. Meschede, and T. W. Hansch, *Opt. Lett.* **15**, 533 (1990).
- ⁵¹J. Helmcke, A. Morinaga, J. Ishikawa, and F. Riehle, *IEEE Trans. Instrum. Meas.* **IM-38**, 524 (1989).
- ⁵²K. Mizuuchi and K. Yamamoto, *Appl. Phys. Lett.* **60**, 1283 (1992).
- ⁵³C. R. Pollock, D. A. Jennings, F. R. Petersen; J. S. Wells, R. E. Drullinger, E. C. Beaty, and K. M. Evenson, *Opt. Lett.* **8**, 133 (1983).
- ⁵⁴M. Kourogi, K. Nakagawa, C.-H. Shin, M. Teshima, and M. Ohtsu, in *Technical Digest of Conference on Lasers and Electro-Optics*, 1991 (Optical Society of America, Washington, D.C., 1991), pp. 470–471.
- ⁵⁵D. A. Jennings, K. M. Evenson, and J. J. E. Knight, *Proc. IEEE* **74**, 168 (1986).
- ⁵⁶M. Kourogi, K. Nakagawa, and M. Ohtsu, in *International Conference on Quantum Electronics Technical Digest*, Series 1992 (Institut für Nachrichtentechnik der TU Wien, 1992), Vol. 9, pp. 100–102.
- ⁵⁷J. Helmcke, A. Morinaga, J. Ishikawa, and F. Riehle, *IEEE Trans. Instrum. Meas.* **IM-38**, 524 (1989).
- ⁵⁸Y. Enomoto and T. Murakami, *J. Appl. Phys.* **59**, 3808 (1986).
- ⁵⁹S. B. Kaplan, C. C. Chi, D. N. Langenberg, J. J. Chang, S. Jafarey, and D. J. Scalapino, *Phys. Rev. B* **14**, 4854 (1976).
- ⁶⁰Y. Harada, K. Narushima, M. Sano, M. Sekine, Y. Higashino, and M. Ohtsu, in *Proceedings of the 4th International Symposium on Superconductivity*, edited by H. Hayakawa and N. Koshizuka (Springer, Tokyo, 1992), pp. 763–766.
- ⁶¹Y. Harada, K. Narushima, M. Sano, M. Sekine, and M. Ohtsu, in *International Conference on Quantum Electronics Technical Digest*, Series 1992 (Institut für Nachrichtentechnik der TU Wien, 1992), Vol. 9, pp. 314–315.
- ⁶²K. Tanabe, Y. Enomoto, M. Suzuki, T. Iwata, and A. Yamaji, *Jpn. J. Appl. Phys.* **29**, L466 (1990).
- ⁶³M. O. Scully and S.-Y. Zhu, *Phys. Rev. Lett.* **62**, 2813 (1989).
- ⁶⁴M. Fleischauer, U. Rathe, and M. O. Scully, in *International Conference on Quantum Electronics Technical Digest*, Series 1992 (Institut für Nachrichtentechnik der TU Wien, 1992), Vol. 9, pp. 100–102.
- ⁶⁵M. Ohtsu and K.-Y. Liou, *Appl. Phys. Lett.* **52**, 10 (1988).
- ⁶⁶Y. Yamamoto, S. Machida, and O. Nilsson, in *Coherence, Amplification, and Quantum Effects in Semiconductor Lasers*, edited by Y. Yamamoto (Wiley, New York, 1991), Chap. 11, pp. 461–536.

Optical Response of $\text{YBa}_2\text{Cu}_3\text{O}_{7-x}$ Epitaxial Thin Films

Y. HARADA¹, K. NARUSHIMA¹, M. SANO¹, M. SEKINE¹, Y. HIGASHINO², and M. OHTSU¹

¹ The Graduate School at Nagatsuta, Tokyo Institute of Technology, Yokohama, 227 Japan

² Yokogawa Electronic Corporation, Musashino, Tokyo, 180 Japan

ABSTRACT

We have studied the optical response of epitaxial thin films of $\text{DyBa}_2\text{Cu}_3\text{O}_{7-x}$ by irradiation of semiconductor laser at the wavelength of 830 nm. $\text{DyBa}_2\text{Cu}_3\text{O}_{7-x}$ superconducting thin films are prepared on MgO (100) by molecular beam epitaxy (MBE). These are confirmed c-axis oriented epitaxial thin films using X-ray analysis and *in-situ* RHEED observation. We have investigated the output signals (i.e. optical response) under the irradiation of laser light, whose frequency can be modulated up to 100 MHz. We have obtained the evidence of nonbolometric response under irradiation of laser at the modulation frequency of 100 MHz.

KEY WORDS: optical detector, $\text{DyBa}_2\text{Cu}_3\text{O}_{7-x}$ thin film, nonbolometric response

INTRODUCTION

Since the discovery of high- T_C superconductors, the feasibility of optical and infrared detection using these materials has been much investigated as one of the promising electronic applications [1-5]. As they are used as optical detectors, they can be classified into two types; bolometric or nonbolometric devices due to the operation principle. Microbolometers are well known as the typical bolometric devices. Their theoretical and experimental investigations are advanced by P. L. Richards *et al.* [6,7]. They have shown that a high- T_C superconducting bolometer can be potentially two orders of magnitude more sensitive than any other infrared detector operating in the liquid nitrogen temperature at its wavelengths longer than 20 μm . This means that a high- T_C superconducting bolometric detector operate as the broadband detector. However its response time is generally late compared with other nonbolometric superconducting detectors. As regards a nonbolometric high- T_C superconducting detector, a lot of works were reported [3,4,5,8,9]. In general, it is considered that the response time of mostly nonbolometric superconducting devices is faster than that of bolometric ones. This is because their response time is decided by quantum mechanics. However its operating mechanism is still not clear, and it is doubtful whether nonbolometric response of high- T_C superconducting thin films exists.

In this paper, we have investigated optical response of epitaxial $\text{DyBa}_2\text{Cu}_3\text{O}_{7-x}$ superconducting thin films under the irradiation of laser light at the wavelength of 830 nm. $\text{DyBa}_2\text{Cu}_3\text{O}_{7-x}$ superconducting epitaxial thin films are grown by molecular beam epitaxy (MBE). We have investigated the optical response under the irradiation of laser light, whose frequency can be modulated up to 100 MHz. We have obtained the evidence of nonbolometric response.

EXPERIMENTAL

$\text{DyBa}_2\text{Cu}_3\text{O}_{7-x}$ superconducting thin films are deposited on MgO (100) substrate by MBE in an ultrahigh vacuum system [10]. We set the temperature of the effusion cells for Dy, Ba, and Cu to about 950 °C, 600 °C, and 1000 °C, respectively. The substrate is heated to 650 °C with a graphite carbon heater. Activated oxygen species by rf-discharge plasma are introduced to the substrate. The growth rate is 0.06 nm/sec. The critical temperature of these films with a thickness of 30 nm is 88 K measured by standard four-point probe method. From the X-ray diffraction pattern, these films are a high degree of c-axis orientation with a c-axis parameter of 11.71 Å. By means of *in-situ* RHEED observation, fine streak patterns appeared from the initial crystal growth, so it has been proved that an atomically smooth surface is epitaxially grown.

Fabrication process of samples is the following way. $\text{DyBa}_2\text{Cu}_3\text{O}_{7-x}$ superconducting thin films on MgO (100) with the thickness of 100 nm is prepared by MBE as mentioned above. Patterning of sample's configuration is used standard photolithography and Ar ion milling. Fabricated samples have constrictions with a size of 20 μm width and 400 μm length. The critical temperature of samples is 65 K. As samples are damaged during the fabrication process, its critical temperature is low compared with that of thin films.

The experimental arrangement for the study of the optical response is shown in Fig. 1. GaAlAs laser diode whose wavelength is 830 nm is used as the light source and its average power is 3.5 mW. A sample is mounted on the stage in the cryostat which can cool down to 20 K. A sample is biased by constant dc current from the current source. Laser

light is introduced perpendicularly to a sample through the window of the cryostat. Laser diode can be modulated by a dc-biased sinusoidal signal current and its modulation frequency can be varied from 1 kHz to 100 MHz. We have measured the output electrical signals through the lock-in amplifier under the irradiation of laser light. In this experimental arrangement, the output signals can't be detected even up to the laser modulation frequency of 200 kHz. The output signals at the modulation frequency from 200 kHz to 100 MHz is measured using the another experimental arrangement as shown in Fig.2. In this arrangement, a double balanced mixer (DBM) is used to beat down the output signals to 10 kHz.

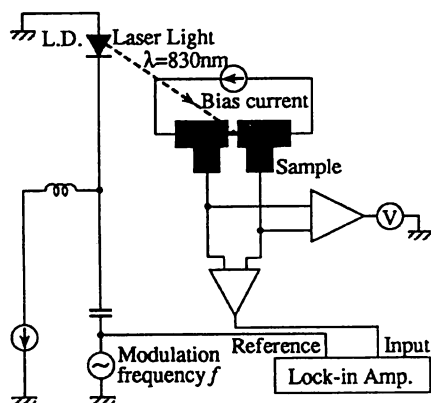


Fig. 1 Arrangement of optical response in $\text{DyBa}_2\text{Cu}_3\text{O}_{7-x}$ superconducting thin films by irradiation of laser light whose frequency can be modulated up to 200 kHz.

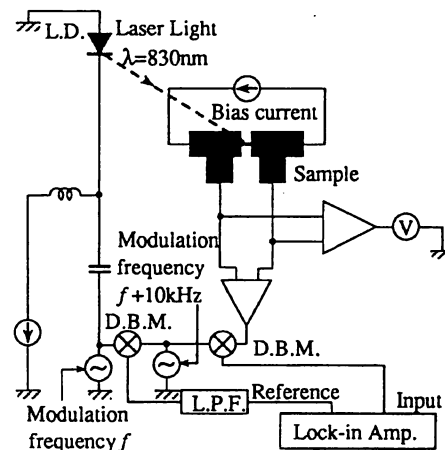


Fig. 2 Arrangement of optical response in $\text{DyBa}_2\text{Cu}_3\text{O}_{7-x}$ superconducting thin films by irradiation of laser light whose frequency can be modulated from 200 kHz to 100 MHz.

RESULTS AND DISCUSSIONS

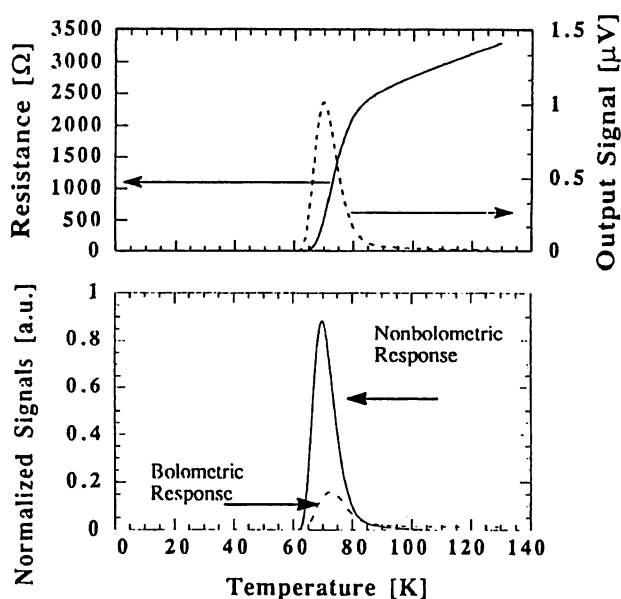
The upper part of Figs. 3 shows the temperature dependence of resistivity of a sample film (solid line) and output voltage (i.e. photo response) under the irradiation of laser light (break line). The modulation frequency of the laser is 1

MHz, and the biased current of the sample is 0.1 mA. The critical temperature of this sample is found 65 K from this figure. The maximum value of the optical response is obtained at the temperature of 70 K. This optical response includes both the bolometric and nonbolometric ones as mentioned in introduction. This relation is expressed as the following way,

$$\delta V = I_B \frac{\partial R}{\partial T} \Delta T + R \frac{\partial I}{\partial T} \Delta T, \quad (1)$$

where δV represents the output voltage produced from the laser irradiation, I_B and R are a bias current and the resistance of a sample, respectively. ΔT means the rising temperature by heating effect due to the laser irradiation. The first term of right hand in this equation indicates bolometric response which result from an increase of the sample's temperature by the laser irradiation. On the other hand, the second term of right hand in this equation means nonbolometric response. Recently some theories are suggested as the explanation of the mechanism on nonbolometric response [11-13].

The lower part of Fig. 3 shows the magnitude of both the bolometric and the nonbolometric signal under laser irradiation. Both signals are normalized by some factor. These values are calculated according to the expression (1). It is assumed that at the region of high temperature beyond T_C , the total signal equals the bolometric signal. From this figure, it is found that when the modulation frequency of the laser diode is 1



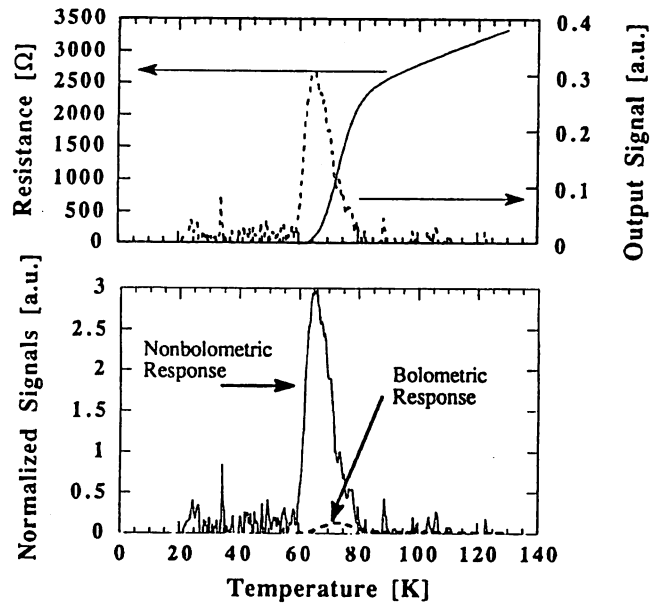
Figs. 3 The optical response of a sample under the irradiation of laser at the wavelength of 830 nm with the modulation frequency of 1 MHz.

MHz, the nonbolometric response is about 5.5 larger than the bolometric one. It is considered that the bolometric signal is so late that it can't follow the modulation of the laser source.

Figures 4 also show the optical response of the same sample under the irradiation of laser like Figs. 3. But the modulation frequency of laser is different from that of Figs.3, and its frequency is 100 MHz. Clearly, the ratio of a bolometric signal, S_B , to nonbolometric one, S_N , is smaller than that of Figs. 3. In other words, it is considered that the bolometric signal decreases at a higher modulation frequency of the laser.

To confirm this assumption, we have investigated the frequency dependence of the ratio, S_B / S_{TOTAL} ($S_{TOTAL} = S_B + S_N$), as shown in Fig. 5. At the region of low modulation frequency, this ratio is constant. This is because the bolometric signal dominates over the total signals and the nonbolometric signal doesn't contribute because of its rapid response. But it is found that the bolometric signal gradually decrease from the modulation frequency of about 100 kHz and in stead of bolometric signal, nonbolometric one dominates at the higher frequency. According to the theory of nonequilibrium superconductivity, which is based on the BCS theory, it can be calculated that nonbolometric response time is about several ten picosecond, which corresponds to several hundred GHz [14].

As additional facts, it is found that the peak temperature of the nonbolometric response is shifted toward a lower temperature compared with that of the



Figs. 4 The optical response of a sample under the irradiation of laser at the wavelength of 830 nm with the modulation frequency of 100 MHz. Bias current of this sample is 0.5 mA.

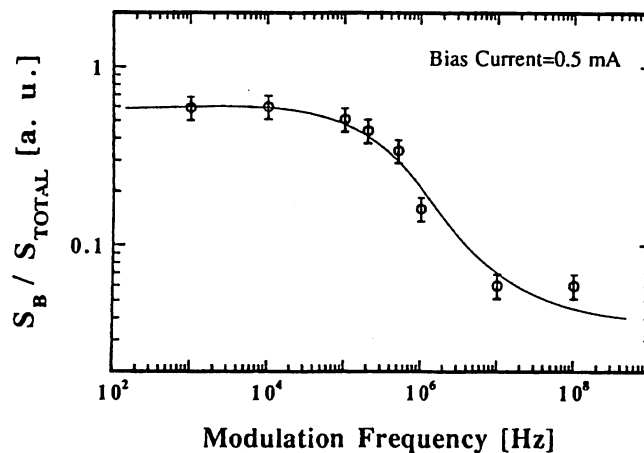


Fig. 5 Modulation frequency dependence of ratio of a bolometric signal to the total one, S_B / S_{TOTAL} .

bolometric response. This reason is not evident, but it may be related to the mechanism of the high- T_C superconductivity. We have also studied the bias current dependence of the optical response. Up to now, the evident relations between the bias current and optical response can't be observed.

CONCLUSIONS

We have investigated the optical response of $\text{DyBa}_2\text{Cu}_3\text{O}_{7-x}$ thin films under the irradiation of laser light ($\lambda=830$ nm), whose modulation frequency can be varied from 1 kHz to 100 MHz. $\text{DyBa}_2\text{Cu}_3\text{O}_{7-x}$ thin films are prepared by MBE and they are highly c-axis oriented epitaxial thin films. We have observed both bolometric and nonbolometric signal from $\text{DyBa}_2\text{Cu}_3\text{O}_{7-x}$ thin films under the laser irradiation. At the lower modulation frequency, the bolometric signal dominates the total optical response by the irradiation of laser light, but as the modulation frequency goes up, the bolometric signal decreases. At the modulation frequency of 100 MHz, the large part of total optical response is the

nonbolometric signal. To confirm this fact, we have also investigated the frequency dependence of the ratio S_B / S_{TOTAL} . It is found that this ratio becomes small as the modulation frequency becomes higher. As the result, we have obtained that the optical response includes the nonbolometric signal in evidence. However origin of the nonbolometric signals is not obvious. From our experiments, it can be stated that the nonbolometric response time is shorter than 10 ns and the bolometric response time of our sample size (constriction with the size of $20 \mu\text{m} \times 400 \mu\text{m}$) is within several nanoseconds.

REFERENCES

1. Forrester MG, Gottlieb M, Gavaler JR, Braginski AI (1988) *Appl. Phys. Lett.* 53: 1332-1334
2. Brocklesby WS, Monroe D, Levi AFJ, Hong M, Liou SH, Kwo J, Rice CE (1989) *Appl. Phys. Lett.* 54: 1175-1177
3. Frenkel A, Saifi MA, Venkatesan T, Lin C, Wu XD, Inam A (1989) *Appl. Phys. Lett.* 54: 1594-1596
4. Tanabe K, Enomoto Y, Suzuki M, Iwata T, Yamaji A (1990) *Jpn. J. Appl. Phys.* 29: L466-469
5. Han SG, Vardeny ZV, Wong KS, Symko OG, Koren G (1990) *Phys. Rev. Lett.* 65: 2708-2711
6. Richards PL, Clarke J, Leoni R, Lerch P, Verghese S, Beasley MR, Geballe TH, Hammond RH, Rosenthal P, Spielman SR (1989) *Appl. Phys. Lett.* 54: 283-285
7. Hu Q, Richards PL (1989) *Appl. Phys. Lett.* 55: 2444-2446
8. Chibane F, Bonnel de Longchamp N, Martin R, Perrière J, Hauchecorne G, Kerhervé F, Maneval JP (1989) *Solid State Commun.* 69: 907-909
9. Zeldov E, Amer NM, Koren G, Gupta A (1989) *Phys. Rev.* B39: 9712-9714
10. Higashino Y, Umezawa T, Mizobuchi K (1991) *Proceedings of the third International Superconducting Electronics Conference (ISEC '91), Glasgow*
11. Zeldov E, Amer NM, Gupta A, Gambino RJ, McElfresh MW (1989) *Phys. Rev. Lett.* 62: 3093-3098
12. Tanabe K, Enomoto Y, Suzuki M, Kubo S, Asano H, Iwata T, Tajima Y, Yamaji A (1990) *Proceedings of the third International Symposium on Superconductivity (ISS '90), Tokyo*
13. Kadin AM, Leung M, Smith AD, Murduck JM (1990) *Appl. Phys. Lett.* 57: 2847-2849
14. Kaplan SB, Chi CC, Langenberg DN, Chang JJ, Jafarey S, Scalapino DJ (1976) *Phys. Rev.* B14: 4854-4873

Nonbolometric Optical Response of $\text{YBa}_2\text{Cu}_3\text{O}_x$ Epitaxial Thin Films

ETSUO KAWATE¹, KEN-ICHI TANAKA², KATSUO MIZOBUCHI³,
YASHUSHI HIGASHINO³, MASAHIRO OKAJI¹, and MOTOICHI OHTSU²

¹National Research Laboratory of Metrology, Tsukuba, Ibaraki, 305 Japan

²Tokyo Institute of Technology, Yokohama, 227 Japan

³Yokogawa Electric Corp., Musashino, Tokyo, 180 Japan

Abstract

The optical response of high-quality epitaxial $\text{DyBa}_2\text{Cu}_3\text{O}_x$ thin films on MgO substrate is investigated using modulated light. To estimate the nonbolometric component of the optical response, we have observed the temperature dependence on light absorption by bulk high- T_c superconductors. All films show clear nonbolometric response as well as bolometric response below the onset of the superconducting transition. To clarify the mechanism of nonbolometric response in high- T_c superconductors, we have systematically studied the optical response at wavelengths in the visible to the microwave range. Irrespective of wavelength, nonbolometric response was observed.

KEY WORDS: epitaxial thin film, mechanism of nonbolometric response, wavelength dependence

Introduction

There have been a large number of studies¹⁻⁵⁾ on the optical response of high- T_c superconductor thin films. However, there has been much controversy regarding the existence¹⁻⁵⁾ of nonbolometric response. Investigations of nonbolometric response have been of two kinds. The first is the measurement of response time. A nonbolometric response can in principle be fast. The second type of investigation is the measurement of temperature dependence on optical response using relatively slow modulated light. The measured signal is the sum of the bolometric and nonbolometric components. In all literature¹⁻⁵⁾ the bolometric component was estimated by assuming that the amplitude of temperature oscillation (ΔT) derived above the transition temperature (T_c) due to the optical heating remained constant even below T_c . This assumption is not self-evident and it should be examined experimentally. Furthermore, the mechanism of nonbolometric response is still under debate. Three mechanisms have been claimed. A mechanism relating to vortex motions,³⁾ one relating to nonequilibrium gap suppression,⁴⁾ and an optically induced phase slip mechanism¹⁾ have been proposed in both epitaxial and granular thin films. The wavelength dependence is often sensitive to the response mechanism.

In this paper, we report direct measurements (using the far-infrared-laser calorimetric method: FILC method) of the temperature dependence of the light absorption by sintered $\text{YBa}_2\text{Cu}_3\text{O}_x$ and systematic investigations on the optical response of high-quality epitaxial $\text{DyBa}_2\text{Cu}_3\text{O}_x$ thin films covering an extremely wide spectral range from the visible (0.633 μm) to the microwave (3000 μm).

Table 1. Five types of light sources and temperatures relating to superconducting gap.

Wavelength [μm]	Light Source	Power [mW]	Optical system		$\frac{h\nu}{2\Delta(0)}$	T_g [K]
			Lens	Window		
0.633	He-Ne laser	5	BK-7	Quartz	71.2	0
10	CO_2 laser	15	ZnSe	KRS-5	4.51	0
119	CH_3OH laser	15	TPX	Quartz	0.38	85.5
513	HCOOH laser	5	TPX	Quartz	0.089	89.54
3000	Gunn Oscillator	5	TPX	Quartz	0.015	89.92

Experimental

A microbridge 25 μm wide, 400 μm long and 0.2 μm thick was made of $\text{DyBa}_2\text{Cu}_3\text{O}_x$ superconducting thin film.⁶⁾ To vary the excitation wavelengths in the visible to the microwave range, we used five types of light sources and varied the optical system depending on the wavelength. These are summarized in Table 1. The details of an optically pumped far-infrared laser have been described elsewhere.⁷⁾ The four-probe technique was used to measure the dc voltage (V_{dc}) and the optical response signal (V_{or}) simultaneously as a function of temperature at various bias current values. We have

developed a far-infrared-laser calorimetric method (FILC).⁷⁾ Use of a high-power laser (output > 5mW) enabled us to directly measure the light absorption by bulk high- T_c superconductors at any temperature below 300 K. In this method a sample was fully oxygenated single-phase sintered $\text{YBa}_2\text{Cu}_3\text{O}_x$ ($2 \times 2 \times 0.1 \text{ mm}^3$) and a temperature sensor was a thermocouple. The amplitude of temperature oscillation (ΔT_{ac}) induced by the chopped beam was measured by a phase-sensitive lock-in amplifier.

Results

The resistively measured transition temperature (T_c) for high-quality epitaxial $\text{DyBa}_2\text{Cu}_3\text{O}_x$ thin film was 85 K for a bias current of 0.01 mA, while the onset temperature (T_{co}) was approximately 90 K. With increasing current, the transition curve broadened towards lower temperatures as typically observed in high- T_c superconductors. Above 2.5 mA the gradient of the dc voltage curve became steep near T_c , so that the temperature derivative of the V_{dc} became unstable. We measured the temperature dependence on both the optical response and the dc voltage for a bias current below 2 mA and at a chopped frequency of 1.6 Hz because of the comparison of the absorption data with the data of the optical response. The data in Fig.1(a) was acquired simultaneously as the optical response (V_{or} : solid line) and the dc voltage (V_{dc} : dotted line) for a bias current of 2 mA and at a wavelength of 119 μm . The optical response shows a sharp maximum in the transition region. The induced voltage change ΔV due to small temperature variation ΔT will then be given by

$$\Delta V = (dV_{dc}/dT)\Delta T, \quad (1)$$

where dV_{dc}/dT is the temperature derivative of the V_{dc} . We can now estimate the nonbolometric component of the V_{or} . The V_{dc} in Fig.1(a) shows a finite slope above the onset temperature. Thus, in this region the bolometric signal will be present according to Eq.(1) and there will be no superconductivity-related component (i.e., nonbolometric effect). The temperature dependence on the measured optical response normalized by the dc voltage derivative ($\Delta T = V_{or}/(dV_{dc}/dT)$) is plotted in Fig.1(b). This ΔT is due to the optical heating (i.e., bolometric effect) above T_c , and we derive the value of 3 mK. As we mentioned in the introduction, we assume that the ΔT does not vary with temperature and remains constant even below T_c . (We will demonstrate that the assumption is correct in Fig.3.) In this figure the increase of the ΔT is due to nonbolometric effect with decreasing temperature below T_c . Thus, knowing ΔT and making use of Eq.(1), we can estimate the bolometric component at first. Figure 1(c) shows the measured optical response (solid line) and the estimated bolometric component (V_{bo} : dotted line). The difference between two signals in Fig.1(c) is due to nonbolometric response. Figure 1(d) shows the measured optical response (solid line) and the estimated nonbolometric component (V_{nb} : dotted line).

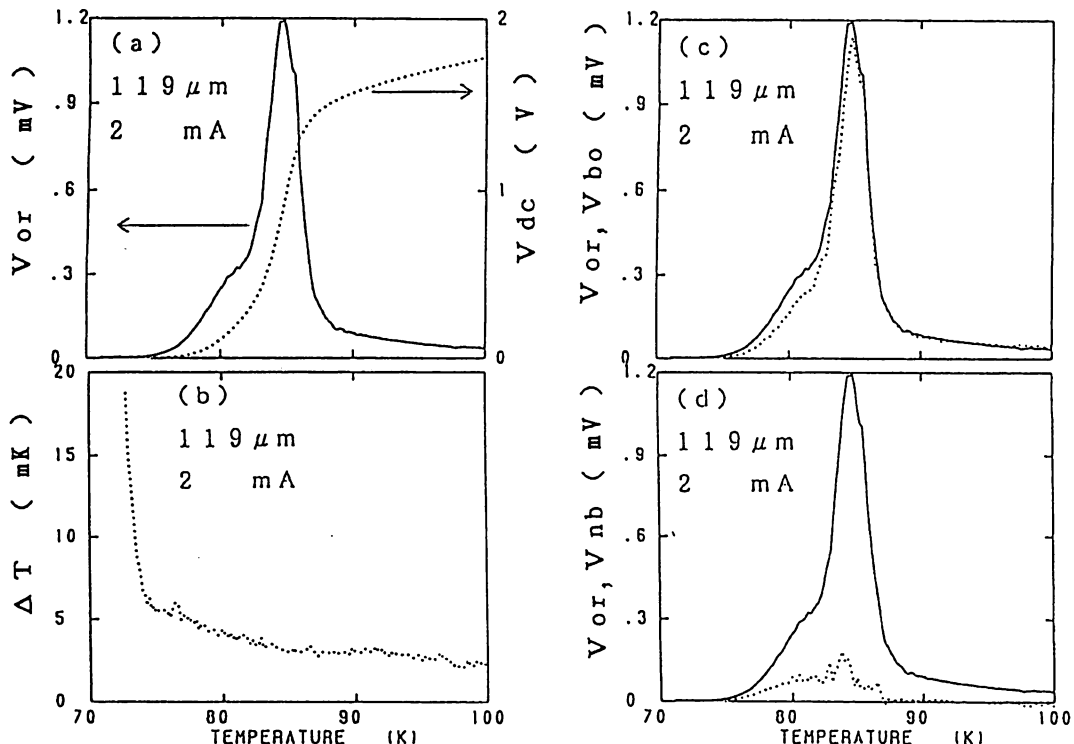


Fig.1 Temperature dependence of (a) dc voltage and optical response; (b) optical response normalized by dc voltage derivative; (c) optical response and estimated bolometric component; (d) optical response and estimated nonbolometric component.

A careful analysis of our results shows that, in addition to the bolometric effect, a non-bolometric response, albeit small, exists clearly below the onset temperature. The peak of the nonbolometric response is about one sixth as large as that of the optical response. Figures 2(a)-(e) show the measured optical response (solid line) and the estimated nonbolometric component (dotted line) at five different wavelengths for a bias current of 0.5 mA. These are qualitatively similar to each other at the same bias current in the region from the visible to the microwave.

Next, we measured the temperature dependence of the light absorption by bulk high- T_c superconductors, using the FILC method. The amplitude of temperature oscillation (ΔT_{ac}) induced by the chopped beam is plotted in Fig.3 as a function of the temperature at wavelengths in the visible ($0.633 \mu\text{m}$) to the far-infrared ($169 \mu\text{m}$) range. In Fig.3(b) all data were normalized by the intensity of laser (1 mW) but in Fig.3(a) data were not normalized.

Discussion

The amplitude of temperature oscillation (ΔT_{ac}) due to the light absorption by bulk high- T_c superconductors is almost constant or slowly decreases with decreasing temperature in the relevant temperature range (from $(T_c - 10)$ K to $(T_c + 10)$ K) in Fig.3. Measurements of the thermal diffusivity of MgO substrate do not show any significant variation in the above temperature range. These results support the assumption that in the microbridge the ΔT derived at temperature above T_c does not vary with temperature and remains constant even below T_c . The estimated bolometric response in Fig.1(c) was the largest because ΔT is assumed to be constant; hence, the estimated non-bolometric response in Fig.1(d) was the smallest. We demonstrated that the non-bolometric response is small but clearly exists.

We consider the three models of the non-bolometric response mentioned in the introduction. First, the mechanism relating to nonequilibrium gap suppression⁴⁾ is that the nonbolometric response is caused by nonequilibrium Cooper-pair-breaking and gap suppression. In this mechanism the relationship between superconducting energy gap and photon energy is essential. The superconducting energy gap emerges at the transition temperature. With decreasing temperature, the energy gap increases and reaches the constant value ($2\Delta(0)$). The value of $2\Delta(0)$ derived from the BCS relation is

$$2\Delta(0) = 3.52k_B T_c = 27.3 \text{ meV}$$

when T_c is 90 K. The ratios of the photon energy, $E=h\nu$, at each wavelength to the $2\Delta(0)$ are listed in Table 1. A photon ($E=h\nu$) can be absorbed by the microbridge due to breaking Cooper pairs below T_{co} , until the photon energy becomes equal to the gap energy with decreasing temperature. We define T_g as the temperature at which a photon ($E=h\nu$) becomes

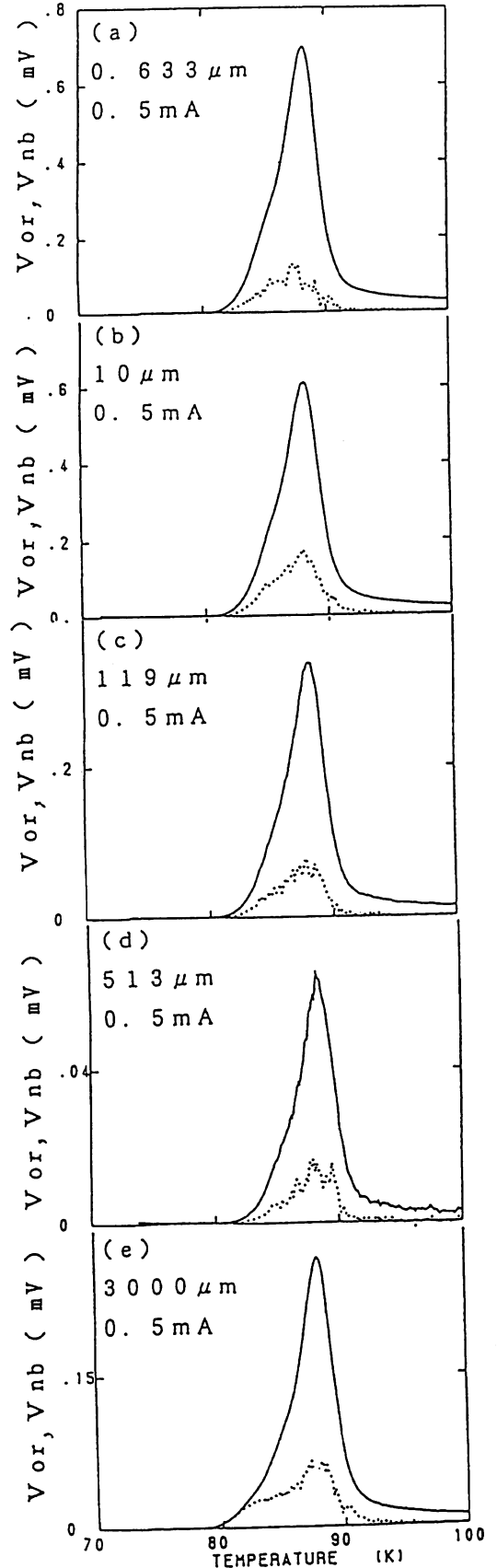
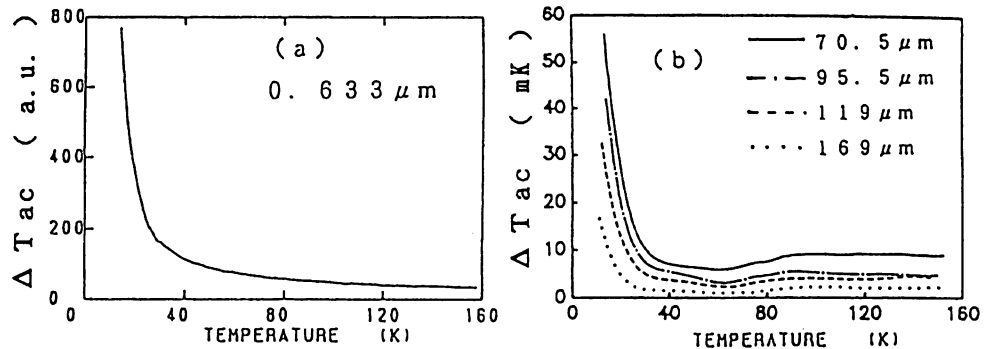


Fig.2 Temperature dependence of optical response and estimated nonbolometric component at five different wavelengths for a bias current of 0.5 mA.

Fig.3 Temperature dependence of amplitude of temperature oscillation induced by light absorption at wavelengths in the visible (0.633 μm) to the far-infrared (169 μm) range.



unabsorbed, $2\Delta(T_g) > h\nu$, with decreasing temperature. The T_g 's at each wavelength are also listed in Table 1. In this table a photon energy at the wavelengths of 0.633 μm and 10 μm is larger than $2\Delta(0)$, so a photon can excite a Cooper pair down to 0 K. Thus we expect that the nonbolometric response should abruptly decrease at the temperatures of 89.92 K, 89.5 K and 85.5 K at the wavelengths of 3000 μm , 513 μm and 119 μm , respectively. However, the data for 3000 μm , 513 μm and 119 μm exhibit qualitatively equivalent behavior to those for 0.633 μm and 10 μm in Fig.2. The nonbolometric response is not due to the nonequilibrium gap suppression.¹⁾ Second, we consider the optically induced phase slip mechanism.¹⁾ In the superconducting regime, absorption of photons destroys the phase coherence between the grains, causing a phase slip process to occur. Phase slips represent a resistive loss in the superconductor, which is measured as a voltage change at a constant current. However, we consider that reduction of the granularity strengthens the intergrain coupling and that thereby makes it more difficult to create a phase slip. In our high-quality epitaxial $\text{DyBa}_2\text{Cu}_3\text{O}_x$ films, no optical response is not due to the phase slip process.

Third, we carefully consider the mechanism relating to vortex motions.^{3),8)} There are two distinct regimes for vortex-pair creation. For photon energy below the energy gap, direct quantum absorption to produce a vortex pair is possible. For photon energy above the energy gap, however, direct Cooper-pair breaking is likely to dominate. This mechanism claims that a vortex-pair can be created independent of wavelength. A vortex-antivortex pair can be separated and moved to opposite sides of the film by the Lorentz force due to a bias current. The direction of movement is perpendicular to the bias current, so that voltage induced by movement (i.e., nonbolometric effect) is parallel to the bias current. With further decreasing temperature, more vortex pairs freeze out and nonbolometric response can not be observed. Our experimental results are that the ratios of the nonbolometric response to optical response are qualitatively similar to each other at the same bias current in the region from the visible to the microwave in Fig.2. These results can be explained well by the mechanism relating to vortex motions.

Conclusion

The temperature and wavelength dependences on the optical response of high-quality epitaxial $\text{DyBa}_2\text{Cu}_3\text{O}_x$ thin films were observed using modulated light. On the basis of the temperature dependence of the light absorption by bulk high- T_c superconductors obtained by means of the laser calorimetric method, we were able to estimate the nonbolometric component of the optical response. All films showed clear nonbolometric responses as well as bolometric responses below the onset of the superconducting transition. Irrespective of wavelength, the nonbolometric response was observable. Our experimental results can be explained well by the mechanism relating to vortex motions.

References

- 1) M. Leung, P.R. Broussard et al.: Appl. Phys. Lett. 51, 2046 (1987)
- 2) M.G. Forrester, M. Gottlieb et al.: Appl. Phys. Lett. 53, 1332 (1988)
- 3) E. Zeldov, N.M. Amer, G. Koren, and A. Gupta: Phys. Rev. B39, 9712, (1989)
- 4) K. Tanabe, Y. Enomoto et al.: Jpn. J. Appl. Phys. 29 L466 (1990)
- 5) G.L. Carr, M. Quijada et al.: Appl. Phys. Lett. 57, 2725, (1990)
- 6) Y. Higashino, T. Umezawa et al.: Proceedings of the third International Superconducting Electronics Conference (ISEC'91), Glasgow (1991)
- 7) E. Kawate, A. Onae et al.: Phys. Rev. B43, 12976, (1991)
- 8) A.M. Kadin, M. Leung, and A.D. Smith: Phys. Rev. Lett. 65, 3193, (1990)

HIGHLY STABLE AND HIGH POWER Nd:YAG LASERS

Ken'ichi Nakagawa, Yukitaka Shimizu, Takeshi Katsuda, and Motoichi Ohtsu

Graduate School at Nagatsuta, Tokyo Institute of Technology,
4259, Nagatsuta-cho, Midori-ku, Yokohama 227, Japan
Phone: +81-45-922-1111 ex. 2526, Fax: +81-45-921-1156

Abstract

We describe the design and performance of highly stable and high power Nd:YAG laser system for the interferometric gravitational wave detectors. The frequency of a diode-pumped Nd:YAG laser is stabilized by using a high finesse optical cavity, and its frequency noise is reduced to as low as $1.5 \text{ mHz}/\sqrt{\text{Hz}}$. Using a high power lamp-pumped ring Nd:YAG laser, single frequency output power of 4W is obtained, and the injection locking is realized by using a diode-pumped laser as a master laser. We also show the design of high power single frequency diode-pumped Nd:YAG lasers.

1. Introduction

Recent developments of frequency stabilized lasers have enabled to realize highly precise and sensitive measurements in many fields. One of the most exciting applications of frequency stabilized lasers is a gravitational wave detector based on a long baseline laser interferometer. It requires ultra low frequency noise ($\delta\nu/\nu \leq 10^{-21}/\sqrt{\text{Hz}}$) and high cw output power ($P \geq 100\text{W}$) to the laser. A promising candidate for such a highly stable and high power laser is a diode-pumped solid state laser. Recent progress of diode-pumped Nd:YAG lasers is remarkable for their frequency stability, high efficiency and high output power.

We have investigated the frequency stabilization of diode-pumped Nd:YAG lasers and high power single frequency Nd:YAG lasers for the gravitational wave detectors. The first goal of the technical requirements for the laser is;

$$\begin{aligned} \text{frequency noise:} & \quad \delta\nu \sim 3 \times 10^{-5} \text{ Hz}/\sqrt{\text{Hz}} \text{ at } 1\text{kHz} \\ \text{single frequency output power:} & \quad P \sim 20\text{W} \\ \text{amplitude noise:} & \quad \delta P/P \sim 10^{-9}/\sqrt{\text{Hz}}. \end{aligned}$$

Our strategy to realize above requirements is as follows;

First, a diode-pumped Nd:YAG laser with moderate output power is used as the master laser, which is locked to a high-finesse reference Fabry-Perot cavity to reduce frequency noise. Next, the output of this master laser is injected into one or several high power slave Nd:YAG lasers (injection locking). Finally, the outputs of these slave lasers are coherently added with beam splitters (coherent addition).

In this paper we report the preliminary results of the frequency stabilization of the master laser, and injection locking of the high power slave laser. We also show the design of a diode-pumped high power slave laser.

2. Frequency Stabilization

The frequency noise of lasers is fundamentally limited by the spontaneous emission (Schawlow-Townes limit) and is given by [1] $\delta\nu = \Delta\nu_c \sqrt{2h\nu/P}$, where $\Delta\nu_c$ is the laser cavity linewidth and P is the laser output power. Active frequency stabilization of lasers makes it possible to realize lower frequency noise than the Schawlow-Townes limit. In this case, the frequency noise is limited by the shot noise (quantum noise) on a photodetector and is given by the nearly same equation as the Schawlow-Townes limit except that $\Delta\nu_c$ and P are replaced by reference cavity linewidth and the laser power used for frequency stabilization. To obtain ultra low frequency noise as required, we have to use stable and narrow linewidth optical cavity as a frequency reference and also to achieve ultra high shot-noise-limited sensitivity in frequency noise measurement. If we use a high frequency FM sideband technique or so-called Pound-Drever method [2], it is not so difficult to obtain the shot-noise-limited sensitivity. Recent experiment of frequency stabilization of a diode-pumped Nd:YAG laser showed this shot-noise-limited low frequency noise by using the Pound-Drever method [3]. The intrinsic frequency noise of diode-pumped lasers is relatively lower than other lasers, so we do not need a high gain and wide bandwidth for the frequency feedback.

We have examined the performance of frequency stabilization of a diode-pumped Nd:YAG laser (Fig.1). We used a diode-pumped monolithic ring Nd:YAG laser (Lightwave Electronics Model 122-300) with 300mW of output power. The laser frequency can be tuned with a piezoelectric transducer (PZT). The PZT tuning coefficient is about 5.8 MHz/V and its bandwidth is about 100 kHz. About 5 % of the laser output is splitted by a wedge glass plate and introduced into an Acousto-Optic (A/O) modulator to prevent instability induced by the optical feedback. The laser frequency is modulated at a modulation frequency of 20MHz by a LiNbO₃ Electro-Optic (E/O) modulator.

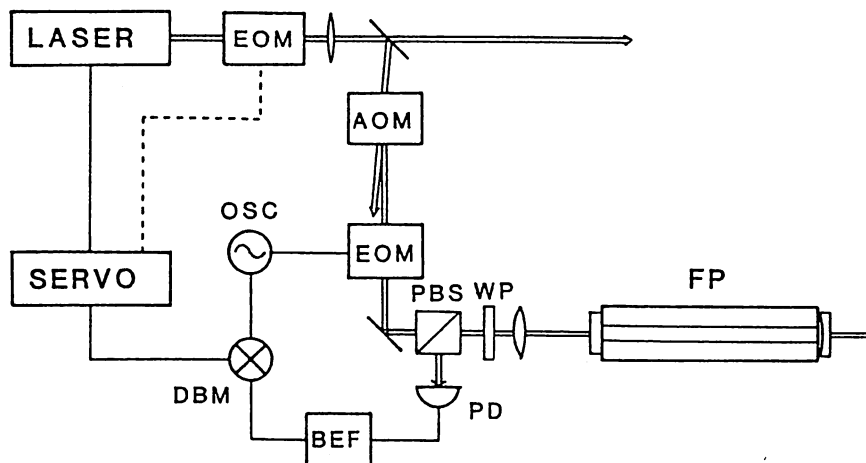


Fig.1 Schematic diagram of the frequency stabilization.

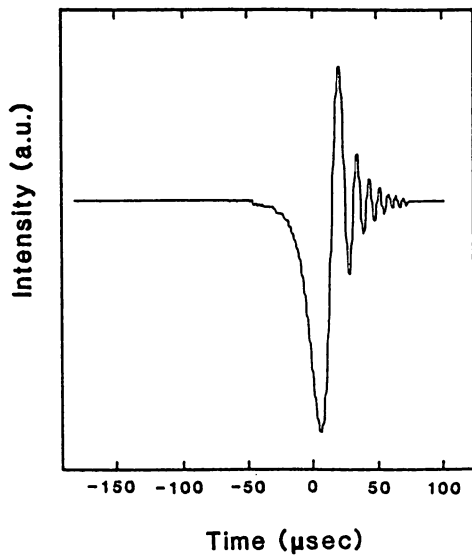


Fig.2 Fast response of the reference cavity.

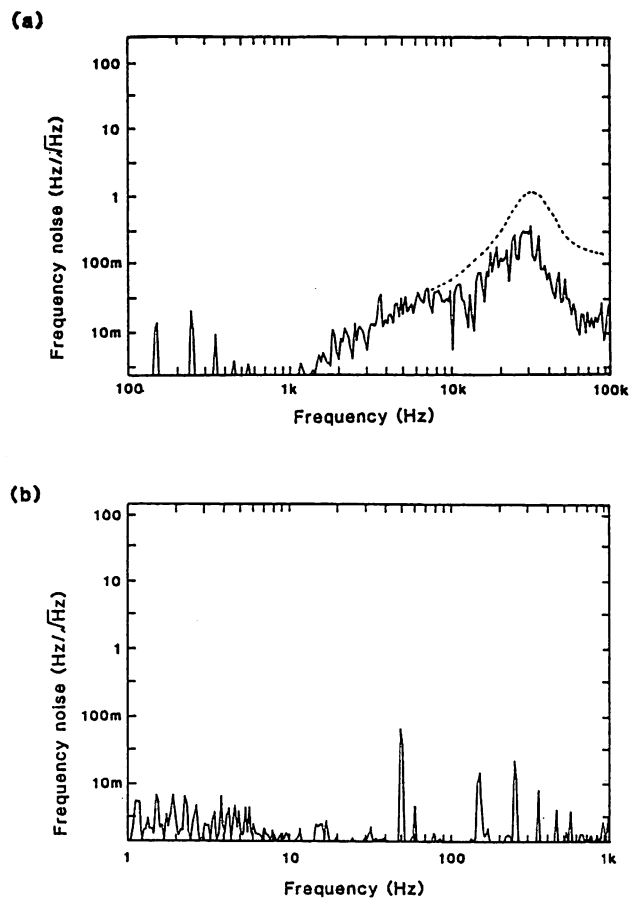


Fig.3 Frequency noise spectrum of the stabilized laser.

The reference Fabry-Perot(F-P) cavity is made of a Zerodur spacer($L=0.46\text{m}$), a flat mirror and a concave($R=1\text{m}$) mirror. The mirrors are super-polished fused silica substrates with high reflective($R\sim 0.9999$) coating and glued onto the spacer with epoxy.

First we measured the resonance linewidth of this reference cavity by slowly scanning the laser frequency and the linewidth was roughly estimated to be 23 kHz. However, this measurement was not so accurate because of the frequency drift and the short-term linewidth($\sim 5\text{kHz}$) of the laser. Next, we measured the fast response of the reflected light from the cavity by rapidly scanning the laser frequency around the resonance(Fig. 2). The beat between the input laser field and the cavity stored field showed the damping oscillation[5]. We have estimated the cavity linewidth of about $18\pm 2\text{kHz}$ by the damping rate of about $18\mu\text{sec}$. The free spectral range of this F-P cavity is 326 MHz and the finesse is determined to be about 18000 which is slightly less than the expected finesse of about 30000. The transmission efficiency on resonance is more than 25%. The reflected light power on resonance is about 25% which corresponds to the reflection fringe contrast of 75%.

The frequency error signal at the output of the mixer is given by

$$I_{err} = 4I_0J_0(M)J_1(M)\frac{1-\alpha}{\sqrt{1+(2f/\Delta\nu_c)^2}}\frac{2}{\Delta\nu_c}\delta\nu \quad (1)$$

where M is modulation index, I_0 is the off resonance DC photo current, $\Delta\nu_c$ is the reference cavity linewidth, f is Fourier frequency of the frequency noise $\delta\nu$. The parameter α is given by $\alpha = (r_1 - r_2(1 - a_1^2))/(1 - r_1r_2)$, where r_1 and r_2 are amplitude.refractivities of front and rear cavity mirrors, and a_1^2 is absorption and scattering loss of the front mirror. The reflection fringe contrast is given by $1 - \alpha^2$.

On the other hand, the shot noise current is given by

$$I_{qn}^2 = 2eI_0((J_0(M)\alpha)^2 + 2J_1(M)^2) \times 2. \quad (2)$$

The shot noise limited frequency noise is given by

$$\delta\nu = \frac{\Delta\nu_c}{2} \sqrt{\frac{h\nu}{\eta P_0} \frac{\sqrt{(J_0\alpha)^2 + 2J_1^2}}{2(1-\alpha)J_0J_1}} \quad (3)$$

where η is the quantum efficiency of the photodetector and P_0 is the laser power incident on the reference cavity.

Figure 3 shows the frequency noise spectrum evaluated by the frequency error signal. The feedback bandwidth was about 30 kHz and the frequency noise was reduced about $1.5 \times 10^{-3} Hz/\sqrt{Hz}$ at the Furier frequency of lower than 1 kHz. Several noise peaks at lower frequency are the harmonics of the 50 Hz line noise. The frequency error signal shows a 6dB/oct cut off above $\Delta\nu_c/2$ (~ 9 kHz)(eq.(1)). The dotted line in Fig.3(a) is the calibrated frequency noise.

Calculating the shot-noise-limited frequency noise of the present system from eq.(3), where M is 0.8 and I_0 is 1.8mA and α is about 0.5, the frequency noise limit is about $3.7 \times 10^{-4} Hz/\sqrt{Hz}$. The obtained frequency noise is about 4 times larger than this theoretical limit. This discrepancy is mainly due to the insufficient feedback gain and also pre-amplifier noise which is slightly higher than the shot noise. The feedback circuit is 3-stage lead-lag filter and the transfer function of this filter is 18 dB/oct for frequency lower than 7kHz and the DC gain is order of 160 dB. To obtain higher feedback gain, we should improve not only the filter transfer function but also the feedback bandwidth. We will employ the external E/O phase modulator for high frequency phase correction(Fig.1)[6]. In this case, we can effectively reduce the frequency noise at frequencies from 10 kHz and to 1 MHz, and the gain of more than 140 dB is possible at 1 kHz.

The first goal of the frequency noise is about $3 \times 10^{-5} Hz/\sqrt{Hz}$, which can be achieved with the present reference cavity and the laser power of 300mW for the stabilization.

There are two problems to be solved when we increase the laser power for the stabilization. One is that the sarutaion power of the present photo diode(InGaAs PIN) is about 15 mW. The other is the trerance of the high reflection mirror coating. The optical field inside the cavity is approximately six thousand times higher than the input laser field.The reflection contrast of 75 % is mainly determined by the mirror loss a_1^2 of 85ppm. If a_1^2 is reduced to 30ppm, the contrast will increase 97%.

In the present experiment, we only measured the frequency error signal and estimated the frequency noise relative to the reference cavity. For evaluating the real frequency noise, it is better to measure beat signal between two lasers which are independently locked to same cavity[4], or individually locked to independent cavities.

3. Injection locking

Injection locking is an effective method to obtain a single frequency operation with high power lasers as Nd:YAG laser. Recently, single frequency output power of more than 10W was reported by using a lamp-pumped Nd:YAG laser[7][8].

We have examined the performance of injection locking of a lamp-pumped Nd:YAG laser. A schematic diagram is shown in Fig. 4. The master laser is a diode-pumped ring Nd:YAG laser with single frequency output power of about 200mW. The output of the master laser is mode-matched into the slave laser with two lens. A Faraday isolator(30dB) is used to protect the master laser from the high slave laser power. The slave laser is a lamp-pumped ring Nd:YAG laser which consists of two flat mirrors, a dielectric polarizer, and the flat output coupling mirror[8]. Unidirectional operation is obtained by using a fused silica Faraday rotator and a half-wave plate. The cavity length can be varied by the PZT mounted mirror. Figure 5 shows the spectrum of the slave laser measured by using the confocal FP cavity(FSR=300MHz). Up to 4W this slave laser shows nearly single frequency operation.

When we inject the master laser power of about 100mW into the slave laser and vary the slave laser cavity length, we can get the injection locking of the slave laser. We used the FM sideband technique to measure the locking range[8]. Figure 6 shows the measured locking range versus the root power ratio between the master and slave lasers. The locking range is order of 1 MHz which is much narrower than the drift and fluctuation of the slave laser cavity.

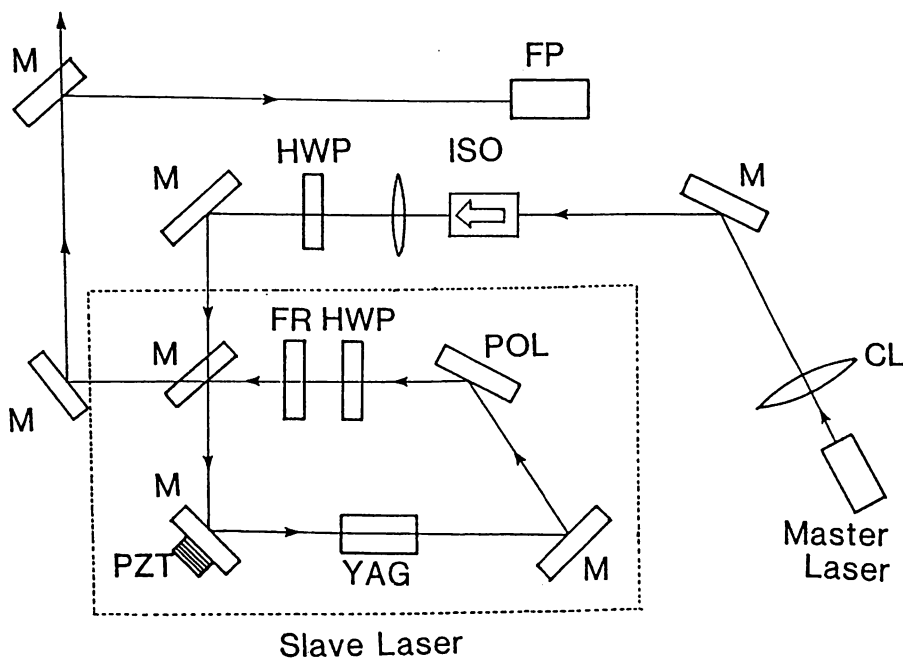


Fig.4 Schematic diagram of the injection locking experiment.

We tried to stabilize the slave laser cavity length by using a FM sideband technique[8], however, we could hardly maintain the injection locking condition. This is mainly due to the rather low feedback bandwidth of several kHz which is limited by the slow PZT.

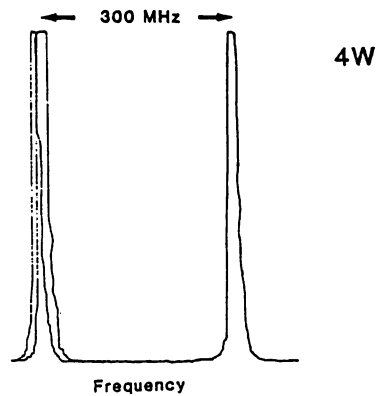


Fig.5 Spectrum of the lamp-pumped Nd:YAG laser..

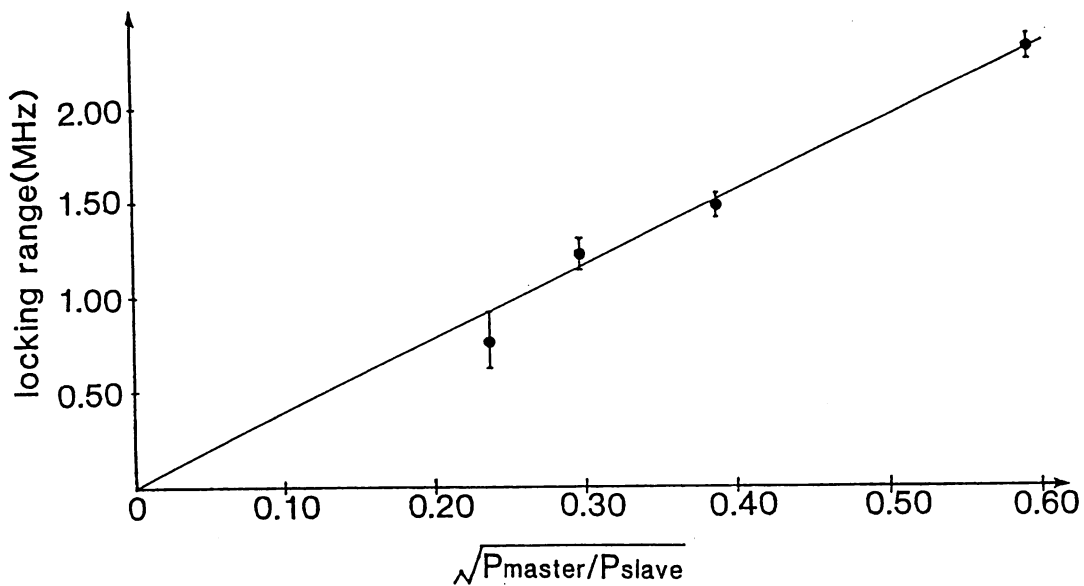


Fig.6 Locking range versus the root squar of ratio between the master and slave laser power.

4. High power diode-pumped Nd:YAG laser

In our preliminary experiment, we used a lamp-pumped Nd:YAG laser as the high power slave laser. However, it requires water cooling which cause large fluctuation to the laser cavity. In next stage, we will replace this noisy lamp-pumped laser by diode-pumped ones. We are planning to develop 2-3 W single or nearly single frequency Nd:YAG lasers pumped by multipule high power

diode lasers for the first stage. There are two ways to obtain single frequency high output power. One is to use ring cavity [10], and the other is to use twisted-mode cavity[9].

At first, we have examined a folded ring cavity laser which consists of Nd:YAG rod, two flat mirrors, and a concave output coupling mirror[10]. To obtain an unidirectional operation, the Nd:YAG rod is in a ring-shaped Nd high-field magnet. We have obtained 420 mW of unidirectional output power with two 1W diode lasers, whereas the effective pumping power was 1.5 W. However, we can hardly obtain single frequency operation with this configuration. Using a thin glass plate as an etalon, single frequency output power was about 200 mW.

Next, we have examined a twisted-mode cavity laser which consists of two quarter waveplates and Nd:YAG rod between them. With this configuration, we can easily obtain single frequency operation. The single mode output power was 160 mW with a pumping power of 0.8W.

Figure 7 shows our prototype design of high power diode-pumped slave laser. We choose the twisted-mode cavity because the alignment is not so critical. The pumping configuration is the combination of two ways , polarization coupling, and combined focusing of multipul lasers[11]. We expect 2W nearly single frequency output power with four 2W diode lasers.

Further output power can be obtained by using a coherent addition method[12][13]. Two or several individual laser outputs can be coherently added by using injection locking and optical phase locking[12][14]. In case of diode lasers, we have achieved the addition efficiency of more than 85%. Assuming that this efficiency is 90%, the output power of 20 W is expected with sixteen 2W high power slave diode-pumped Nd:YAG lasers.

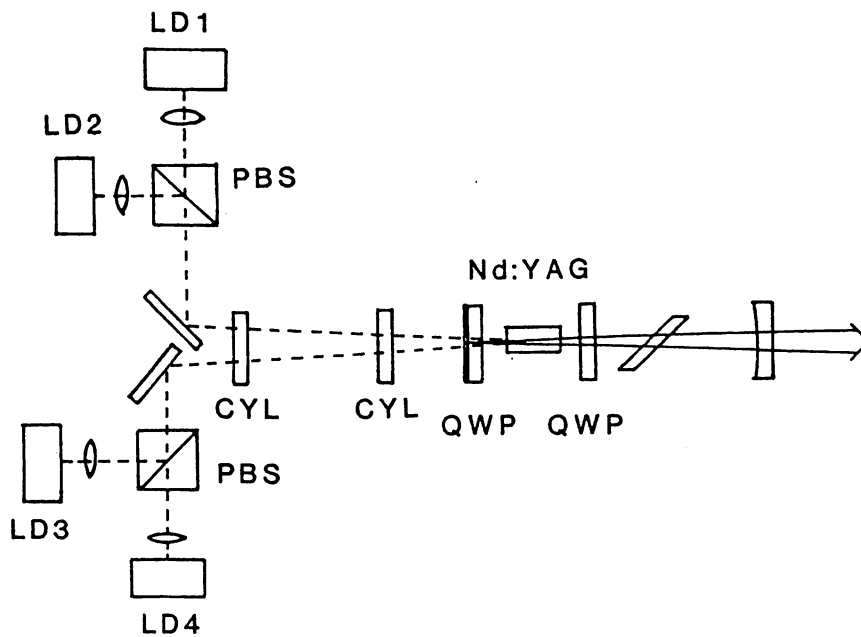


Fig.7 Design of high power diode-end-pumped Nd:YAG laser

5. Summary

We have demonstrated the frequency stabilization of a diode-pumped Nd:YAG laser and have realized the frequency noise of about $1.5 \times 10^{-3} Hz/\sqrt{Hz}$. We have verified the performance of single frequency lamp-pumped Nd:YAG laser. Single frequency output power of 4 W was obtained and injection locking was realized with a diode-pumped Nd:YAG laser as master laser. We have showed the design concept and preliminary results of high power single frequency diode-pumped Nd:YAG laser.

6. Acknowledgments

The authors thank K. Ueda and N. Uehara for their helpful discussions. This research was supported by a Grant-in-Aid for Scientific Research(No.03250205, No. 04234204) from the Ministry of Education, Science, and Culture of Japan.

References

- [1] A. Schawlow and C. Townes, "Theory of infrared and optical masers", *Phys. Rev.* **112**, 1940(1958).
- [2] R. W. P. Drever, et.al. "Laser phase and frequency stabilization using an optical resonator", *Appl. Phys.* **B31**, 97(1983).
- [3] D. Shoemaker, A. Brillet, C. N. Man, O. Cregut, and G. Kerr, "Frequency-stabilized laser-diode-pumped Nd:YAG laser", *Opt. Lett.* **14**, 609(1989).
- [4] Timothy Day, Eric. K. Gustafson, and Robert. L. Byer, "Sub-Hertz Relative Frequency Stabilization of Two-Diode Laser-Pumped Nd:YAG Lasers Locked to a Fabry-Perot Interferometer", *IEEE J. Quantum. Electron.* **28**, 1106(1992).
- [5] Ziyuan Li, R. G. T. Bennet and G. E. Stedman, "Swept-frequency induced optical cavity ringing", *Opt. Commun.* **86**, 51(1991).
- [6] J. L. Hall, T. W. Hänsch, "External dye-laser frequency stabilizer", *Opt. Lett.* **9**, 502(1984).
- [7] O.Cregut, C. N. Man, D. Shoemaker, A. Brillet, A. Menhert, P. Peuser, N. P. Schmitt, P. Zeller, K. Wallmeroth, "18 W SINGLE-FREQUENCY OPERATION OF AN INJECTION-LOCKED CW, Nd:YAG LASER", *Phys. Lett. A* **140**, 294(1989).
- [8] C. D. Nabors, A. D. Farinas, T. Day, S. T. Yang, E. K. Gustafson, and R. L. Byer, "Injection locking of a 13-W cw Nd:YAG ring laser", *Opt. Lett.* **14**, 1189(1989).
- [9] K. Wallmeroth, P. Peuser, "HIGH POWER, CW SINGLE-FREQUENCY, TEM₀₀, DIODE-LASER-PUMPED Nd:YAG LASER", *Electron. Lett.* **24**, 1086(1988).
- [10] Richard Scheps, and Joseph Myers, "A Single Frequency Nd:YAG Ring Laser Pumped by Laser Diodes", *IEEE J. Quantum. Electron.* **26**, 413(1990).

- [11] T. Y. Fan, A. Sanchez, and W. E. DeFeo, "Scalable, end-pumped, diode-laser-pumped laser", *Opt. Lett.* **14**, 1057(1989).
- [12] G. A. Kerr, J. Hough, "Coherent Addition of Laser Oscillators for use in Gravitational Wave Antennas", *Appl. Phys. B* **49**, 491(1989).
- [13] E. A. P. Cheng and T. J. Kane, "High-power single-mode diode-pumped Nd:YAG laser using a monolithic nonplanar ring resonator", *Opt. Lett.* **16**, 478(1991).
- [14] W. Wang, K. Nakagawa, S. Sayama, and M. Ohtsu, "Coherent addition of injection-locked high-power AlGaAs diode lasers", *Opt. Lett.* **17**, to be appeared.

A Highly accurate frequency counting system for $1.5\mu\text{m}$ wavelength semiconductor lasers.

M. Kouroggi, K. Nakagawa and M. Ohtsu

Interdisciplinary Graduate School of Science and Engineering,
Tokyo Institute of Technology, 4259 Nagatsuta,
Midori-ku, Yokohama, Kanagawa 227, Japan.

ABSTRACT

For highly accurate optical frequency measurement in $1.5\mu\text{m}$ wavelength region, an optical frequency comb (OFC) generator was realized by using a high frequency LiNbO_3 electro-optic phase modulator which was installed in a Fabry-Perot cavity. By using the OFC generator, we demonstrated the frequency difference measurement up to $0.5[\text{THz}]$ with a signal-to-noise ratio higher than $61[\text{dB}]$, and the heterodyne optical phase locking with a heterodyne frequency of $0.5[\text{THz}]$ in which the residual phase error variance was less than $0.01 [\text{radian}^2]$. The maximum measurable frequency difference, which was defined as a sideband frequency with the signal-to-noise ratio of $0[\text{dB}]$, was estimated to be $4[\text{THz}]$.

1. INTRODUCTION

Highly accurate laser frequency measurement is an essential technique for the industrial application such as coherent optical communication systems, and for the precision physical measurement, such as the standard of length and measurement of Rydberg constant¹. However, highly accurate laser frequency measurement systems^{2,3}, which directly measure the absolute optical frequency, need many big gas lasers and short-lifetime point contact diodes such as the metal-insulator-metal diodes⁴. Furthermore, the coherent optical communication systems require the frequency difference measurement to determine the arbitrary frequencies of lasers which are spaced in the span as wide as several tera hertz. However it is difficult to measure such a high frequency difference.

We have proposed a compact, highly accurate, and wide span optical frequency measurement system at $1.5\mu\text{m}$ wavelength⁵. This system covers a wide window region of optical fiber around $1.5\mu\text{m}$ wavelength for optical fiber communication systems, such as a channel selector for frequency division multiplexed communication systems over 1,000 channels. This system consists of two parts. One is a convenient and highly accurate standard laser at $1.55\mu\text{m}$. The other one is an OFC generator for accurate measurement of the frequency difference between the standard laser and lasers under test, and the frequency difference can be as large as several tera hertz. We have also reported the preliminary experimental result⁶ of the proposed frequency difference measurement system which used modulation sideband of the OFC, and have shown that $0.85[\text{THz}]$ frequency difference can be measured by using a modulator installed in an optical cavity.

In this paper, we show the principle of the proposed high accurate laser frequency measurement system at $1.5\mu\text{m}$ wavelength, and report the experimental results of the improved OFC generator.

We developed an OFC generator by using an improved electro-optic phase modulator, which is similar to the scheme proposed by Lee et al.⁷, and installed it in a Fabry-Perot cavity⁸. By using semiconductor lasers whose spectral linewidths were narrowed to 1[kHz] and a sensitive optical balanced-mixer-receiver for measuring beat signal between the OFC and laser, we demonstrated the frequency difference measurement up to 0.5[THz], and a heterodyne optical phase locking with the heterodyne frequency of 0.5[THz]. We show that the maximum measurable frequency difference using the OFC generator was 4[THz], which was defined as a sideband frequency with a signal-to-noise ratio of 0[dB].

2. OPTICAL FREQUENCY MEASUREMENT SYSTEM

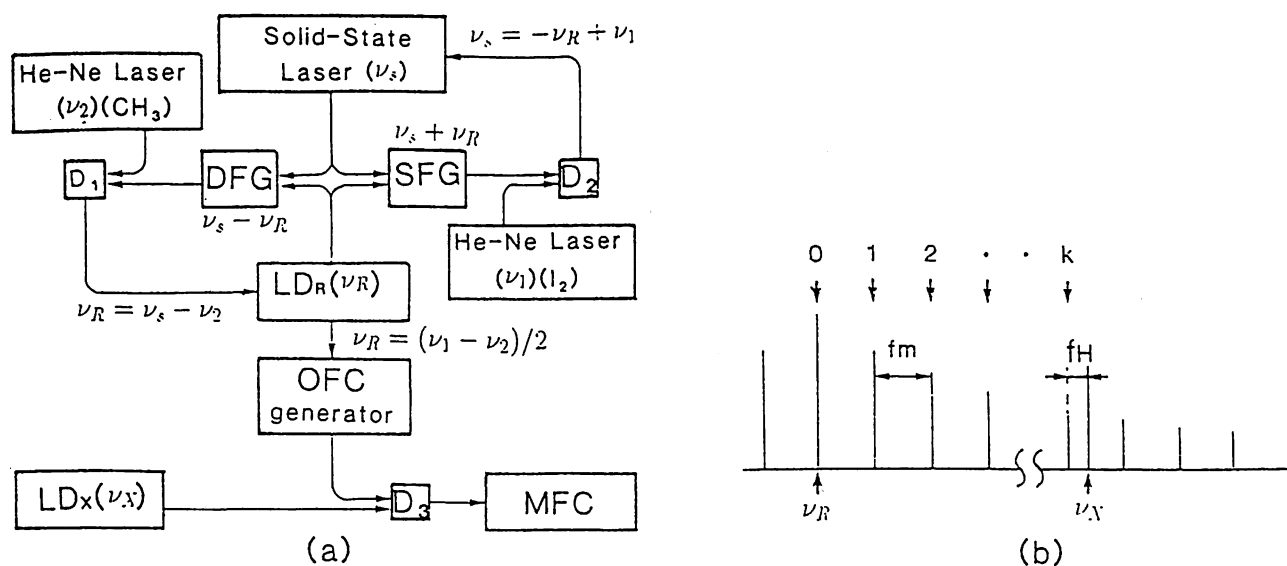


Figure 1: (a) Proposed optical frequency measurement system for 1.5 μm wavelength semiconductor lasers. SFG, sum frequency generator; DFG, difference frequency generator; MFC, microwave frequency counter; D's, photodiodes. (b) Schematic explanation of the relative frequency locations of the lasers.

Figure 1 (a) shows the proposed highly accurate optical frequency measurement system at 1.5 μm wavelength. The frequency ν_R of the LD_R (1.55 μm semiconductor laser for frequency standard) is fixed to $(\nu_1 - \nu_2)/2$ by generating the lightwave of the sum and difference frequencies of LD_R and a solid-state laser at 1.06 μm (ν_s), and by locking the sum and difference frequencies to the frequencies (ν_1 and ν_2) of two He-Ne lasers, where ν_1 and ν_2 are the absolute frequencies of two stabilized He-Ne lasers locked to $^{127}\text{I}_2$ (0.633 μm), and CH_4 (3.39 μm), respectively. LiNbO₃ can be used for sum and difference frequency generations. The accuracy of the ν_R is determined by those of two stabilized He-Ne lasers. The uncertainty of ν_R is estimated to be 37[kHz], or 1.9 part in 10^{10} , from the values of the uncertainty for I₂ and CH₄ which is documented in ³, i.e., 74[kHz] and 9[kHz], respectively. The frequency ν_X of laser under test LD_X is determined by measuring the frequency difference between the LD_X and the LD_R.

The OFC generator generates modulation sidebands from an incident laser beam, and the generated sidebands are used as local oscillators to measure the frequency difference between the LD_X and LD_R whose frequency difference is higher than the responsible frequency ($\cong 10GHz$) of photo diodes. As shown in Fig. 1 (b), the value of ν_X is determined by measuring the frequency difference f_H between k -th generated sideband of LD_R and the LD_X , i.e., $\nu_X = \nu_R + f_H + kf_m$, where f_m is the modulation frequency of the OFC generator.

3. EXPERIMENT

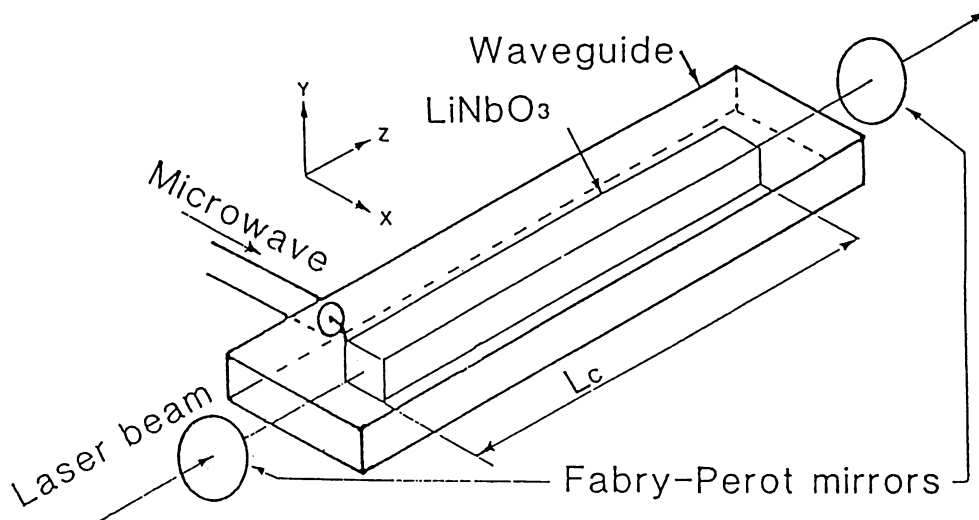


Figure 2: The construction of the present Optical Frequency Comb generator.

Figure 2 shows the improved OFC generator which consists of an improved bulk-type electro-optic (EO) phase modulator installed in a Fabry-Perot cavity. The EO phase modulator was composed of an anti-reflection coated $LiNbO_3$ crystal ($1.25 \times 1.0 \times 20.0$ [mm³]) inserted in a microwave guide. In order to realize a highly efficient EO phase modulator which is operated at a high frequency, the width of the microwave guide was designed to be microwave-resonant to concentrate the microwave power on the crystal and to make the optical group velocity and microwave phase velocity in the crystal be matched. By installing the modulator in the Fabry-Perot cavity⁸, it is possible to increase the span of an OFC when the modulation frequency is nearly equal to $n \times FSR$, where n is an integer and FSR is the free spectral range of the Fabry-Perot cavity.

Specifications of the OFC generator were:

Modulation frequency: $f_m \cong f_{mo} \cong 3FSR = 5.8$ [GHz] (TE₁₀₂ mode.)

Microwave power: $P_\mu = 10$ [W],

Modulation index: $m = 0.2 \pi$ [radian],

Crystal-loaded finesse of the Fabry-Perot cavity: $F = 200$,

Efficiency of the Fabry-Perot cavity: $\eta_{FP} = 5\%$

Figure 3 shows an experimental set up. LD_R and LD_X were both optically fed-back⁹ MQW DFB lasers at $1.5\mu m$ wavelength. Their 3dB-linewidths $\Delta\nu_X$ and $\Delta\nu_R$ were estimated to be about 1[kHz]. The laser power P_i of the LD_R incident into the OFC generator was about 7[mW]. The

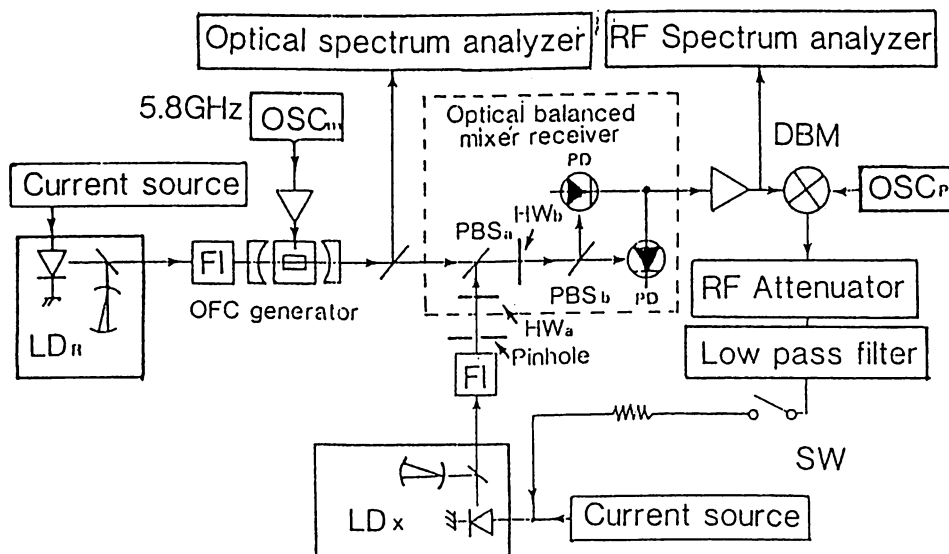


Figure 3: Experimental setup. LD's, optically fed-back multi-quantum-well distributed feedback lasers at $1.5\mu\text{m}$ wavelength; FI, Faraday isolator; PD's, photodiodes; PBS's, polarized beam splitters; HW's, half wave plates; DBM, RF double balanced mixer; OSC's, RF oscillators.

value of $\nu_R - \nu_X$ was controlled within $0.5[\text{THz}]$ by controlling the temperatures of the lasers. An optical balanced-mixer-receiver was used in order to realize the shot-noise-limited detection of the beat signal between LD_X and a sideband of LD_R . The optical balanced-mixer-receiver consisted of two photo-diodes with the quantum efficiency η_{PD} of 0.9, two polarization beam splitters and two half wave plates. Additional circuits, composed of a radio frequency (RF) double balanced mixer, a low pass filter, an RF attenuator, and an RF oscillator (OSC_P), inserted between the optical balanced-mixer-receiver and LD_X , were used for the optical phase locking.

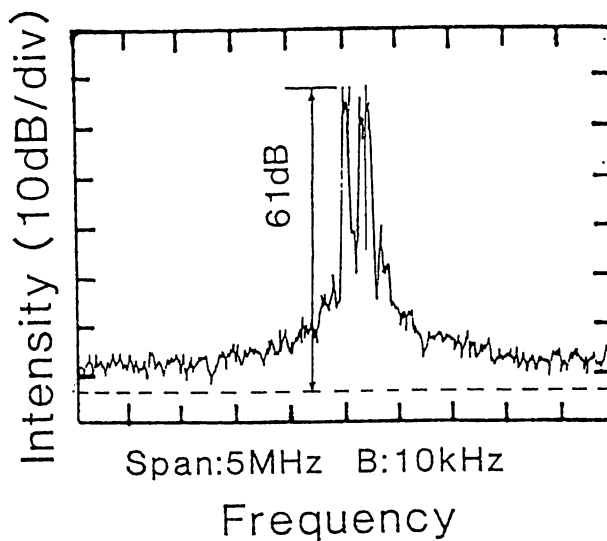


Figure 4: Spectral profile of a beat signal. Broken line is the shot noise level

Figure 4 shows a typical spectral profile of the beat signal between the LD_X and the sideband of the LD_R . The resolution bandwidth B of the RF spectrum analyzer was $10[\text{kHz}]$. The broken line

was the shot noise level. It is seen that the signal-to-noise ratio was 61[dB]. In this measurement, the detuning of the modulation frequency $\Delta f_m (\equiv f_m - f_{m0})$ and phase of the Fabry-Perot cavity φ ($\varphi \equiv \pi(\nu_R - \nu_{FP})/FSR$, where ν_{FP} is a closest resonant frequency of the Fabry-Perot cavity.) were set to 0[Hz] and 0[rad] by adjusting the modulation frequency and voltage of a PZT attached on the Fabry-Perot cavity mirror. In order to know the order of sideband, k , we measured the frequency shift of the f_H by changing slightly the modulation frequency. The shift of the f_H must be equal to the value of k times a shift of modulation frequency. As a result, k of the Fig. 4 was measured to be 84, i.e., $\nu_R - \nu_X \cong 84f_m = 0.487[\text{THz}]$. Uncertainty of the measured frequency difference is dependent on the accuracy of f_m and the RF spectrum analyzer. If the f_m is calibrated by an atomic clock, such as a rubidium clock or a Cesium clock, the value of frequency difference can be measured with a uncertainty of 1 part in $10^{12} \sim 10^{14}$.

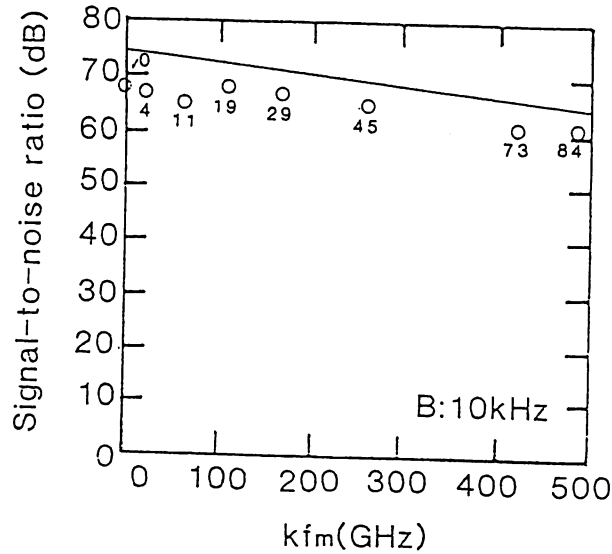


Figure 5: Signal to noise ratio of the beat signals. Solid line is the calculated result. Open circles are experimental results.

Figure 5 shows the relation between the signal-to-noise ratio and the $k f_m$. Open circles are the experimental results. The resolution bandwidth B was 10[kHz]. The numbers attached to the open circles indicate the orders of sidebands. The solid line shows the value calculated by eqs.(1) and (4) in section 4. It can be seen from this figure that the experimental results were in good agreement with the calculated results, and that the slope of the signal-to-noise ratio as a function of the $k f_m$ is 19[dB/THz]. The maximum measurable frequency difference is roughly estimated from this result to be 4[THz], which is defined as a $k f_m$ at a signal-to-noise ratio of 0[dB]. In section 4, we calculate it by taking account of a crystal dispersion.

Figures 6(a),(b),(c) show the envelope of the OFC spectrum observed by an optical spectrum analyzer, where (a) $\varphi = 0, \Delta f_m = 0$, (b) $\varphi = 0, \Delta f_m = 5.5[\text{MHz}]$, and (c) $\varphi = 0.15\pi, \Delta f_m = 5.5[\text{MHz}]$. The broken lines in these figures show the limit of the sensitivity of the optical spectrum analyzer. The center wavelength in these figures is the wavelength of the LD_R. From these figures, the shape of the envelope of the OFC was controlled by changing the values of φ and Δf_m . In section 4, we will discuss about the optimization of φ and Δf_m to increase a maximum measurable frequency difference. It is seen from Fig. 6(a) that the envelope extends to the width as wide as 32nm (or 4[THz]). To our knowledge, this value is the widest span of an OFC which is generated

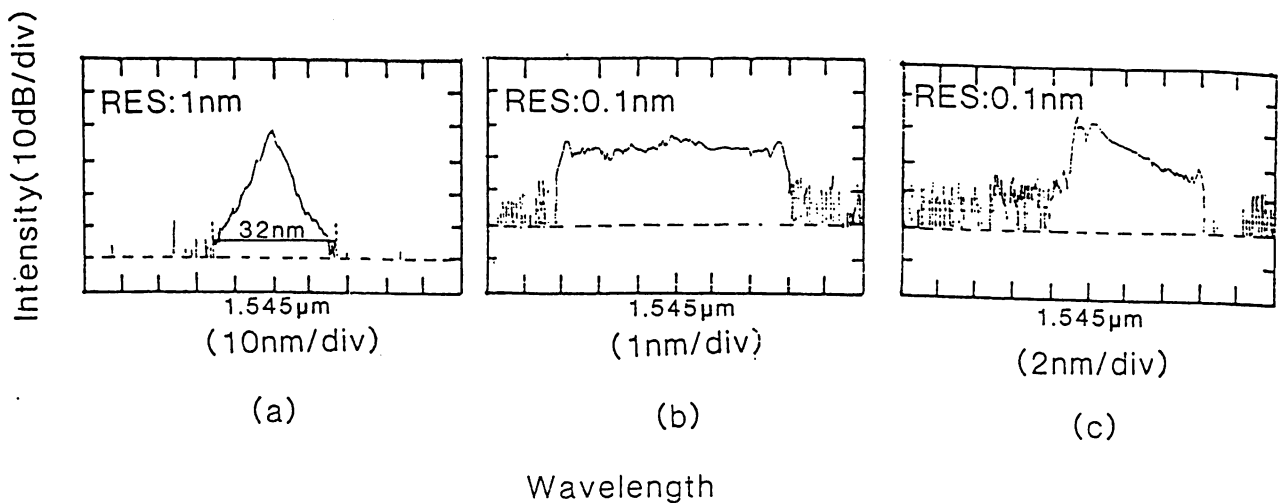


Figure 6: Experimental results of the spectral envelope of the OFC. Broken lines are the limits of the sensitivity of the optical spectrum analyzer. (a) $\varphi = 0, \Delta f_m = 0$. (b) $\varphi = 0, \Delta f_m = 5.5[\text{MHz}]$. (c) $\varphi = 0.15\pi, \Delta f_m = 5.5[\text{MHz}]$.

by EO modulation. Because the measurement of the optical beat signal is more sensitive than the measurement by the optical spectrum analyzer, it is possible to use higher order of sideband which have not been observed by the optical spectrum analyzer. Compared with the result in Fig. 5, it is expected that the signal-to-noise ratio of the beat signal detection between sideband of $k f_m \cong 2[\text{THz}]$ and LD_X will be higher than 30[dB].

Optical phase locking loop is an essential technique for synthesizing and measuring the optical frequency. By using the optical phase lock loop technique⁹ and the OFC generators, frequency interval of the lasers can be locked each other, and the span of the OFC can be expanded. Thus, we tried to demonstrate the optical phase locking. Figures 7 (a) and (b) show the spectral profile of the beat signal under phase locked condition for which LD_X was locked to 84th sideband of the OFC, i.e., $\nu_R - \nu_X = 0.487[\text{THz}]$. The resolution bandwidths of Figs. 7 (a) and (b) were 1[kHz] and 30 [Hz], respectively. This is the first report of the optical phase locking with the frequency difference as high as 0.5[THz]. From the wing of residual phase noise seen in these figures, short-term residual phase error variance was estimated to be less than 0.01 [radian²]. From the Fig. 7(b), the linewidth of the beat signal was estimated to be narrower than 30[Hz] since the resolution bandwidth is 30[Hz]. Therefore the present phase locking does not limit the accuracy of the frequency measurement, and the measurable range can be increased by applying optical phase locking to the higher order of sidebands. Residual phase noise in low Fourier frequency shown in Fig. 7(b) resulted from the low gain of the feedback circuit. If an active loop filter is used, further reduction of the residual phase noise can be expected.

4. THEORETICAL ANALYSIS of AN OFC GENERATOR

From the experimental results, the maximum measurable frequency difference have been roughly

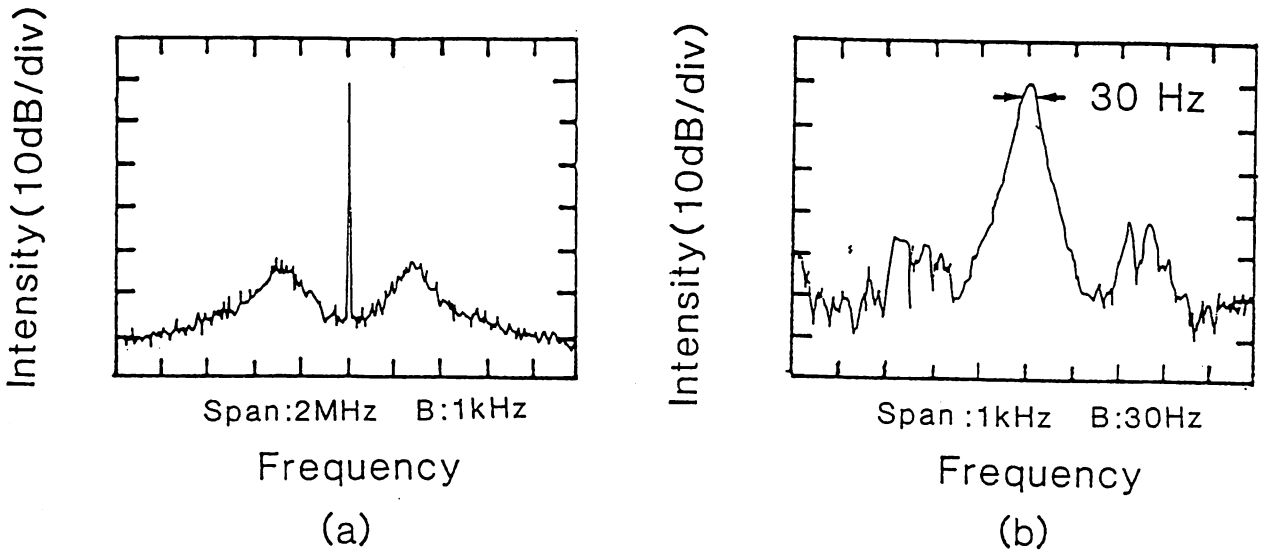


Figure 7: Spectral profile of a beat signal under optical phase-locked condition.

estimated to be 4[THz]. In this section, we calculate the spectrum of OFC by taking account of a crystal dispersion, and then show the maximum measurable frequency difference.

By using a linear approximation of the refraction index n_e of the extraordinary ray in a LiNbO₃ crystal, the optical power P_{ok} of the k -th order of the sideband generated by OFC generator is

$$P_{ok} = \eta_{FP} \left| \frac{E_{ok}}{E_i} \right|^2 P_i \quad (1-a)$$

where

$$E_{ok} = t \times E_i \delta(k) + r \exp\left(-\frac{j4\pi L_c (k f_m)^2}{c} \frac{dn_e}{d\nu} - \frac{j2\pi k \Delta f_m}{FSR} - j2\varphi\right) \sum_{q=-\infty}^{\infty} J_{k-q}(2m) E_{oq} \quad (1-b)$$

where E_i and E_{ok} are amplitudes of the electric fields of the incident laser beam and that of a k -th sideband of output beam of OFC generator, respectively. $J_{k-q}()$ is the $(k-q)$ -th Bessel function. $\delta()$ is the delta function. r and t are reflectivity and transmittance, i.e., $r \cong 1 - \pi/F$, $t = 1 - r$, respectively. c is the speed of light in vacuum. The value of $\frac{dn_e}{d\nu}$ is $2.3 \times 10^{-16} [\text{Hz}^{-1}] (1.5 \mu\text{m})$. L_c is the crystal length. A dispersion in reflectivity of the Fabry-Perot mirror is ignored because it is very small in comparison with the effect of the crystal dispersion.

The calculated results of the envelope of the OFC spectrum from the eq. (1), are shown by solid lines in Figs. 8 (a),(b), and (c), where (a) $\varphi = 0$, $\Delta f_m = 0$, (b) $\varphi = 0$, $\Delta f_m = 5.5 [\text{MHz}]$, and (c) $\varphi = 0.15\pi$, $\Delta f_m = 5.5 [\text{MHz}]$. For comparing them with the experimental results in Figs. 6 (a),(b), and (c) directly, we replace the k by the wavelength of the k -th sideband λ_k in the relation between P_{ok} and k considering $\lambda_k \cong \lambda_R - \frac{c}{\nu_R^2} k f_m$ (where $\lambda_R \equiv c/\nu_R$ is the wavelength of the LD_R), it is found that they are in good agreement with each other.

Though, eq.(1) can represent the results which are in good agreement with experimental results, this calculation is too complicated to estimate the maximum measurable frequency difference. Then we derived the approximated expression of eq. (1). That is

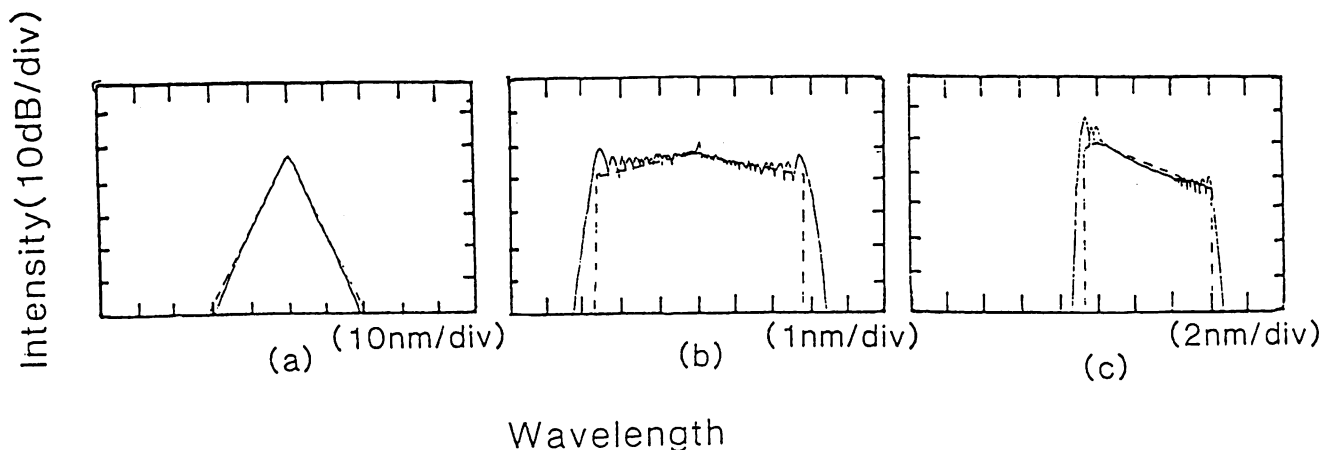


Figure 8: Calculated results of the spectral envelope of the OFC. Solid and broken lines are calculated results by eqs.(1) and (5), respectively.(a) $\varphi = 0, \Delta f_m = 0$. (b) $\varphi = 0, \Delta f_m = 5.5[\text{MHz}]$. (c) $\varphi = 0.15\pi, \Delta f_m = 5.5[\text{MHz}]$. The center wavelength is λ_R .

$$P_{ok} = \begin{cases} \eta_{FP} \left(\frac{\pi}{2mF}\right)^2 \exp\left(-\frac{|k|\pi}{mF}\right) P_i & , g(k') \leq m; \\ 0 & , \text{otherwise.} \end{cases} \quad (2-a)$$

$$g(k') = \left| \frac{2\pi L_c (k' f m)^2}{c} \frac{dn_e}{d\nu} + \frac{\pi k' \Delta f_m}{FSR} + \varphi + M\pi \right| \quad (2-b)$$

where M is an integer which satisfies $|\varphi + M\pi| \leq m$, and the condition should be valid when k' involves all integers from 0 to k . Relation $P_{ok} = \eta_{FP} \left(\frac{\pi}{2mF}\right)^2 \exp\left(-\frac{|k|\pi}{mF}\right) P_i$ in eq.(2-a) represents an analytical equation calculated from eq.(1) under the condition in which the crystal dispersion is ignored and $mF \gg 1$. The value of $g(k')$ is proportional to the frequency difference between the k' th sideband and the closest resonant frequency of the Fabry-Perot cavity. When a value of the k does not satisfy the relation of $g(k) \leq m$, the order of the sideband is higher than the value of k and such a sideband cannot exist. We show examples of the calculation using eq.(2) by broken lines in Figs. 8(a),(b), and (c) to compare the solid lines exactly calculated result by using eqs.(1). By comparing the calculations, it is known that they are in good agreement with each other. We use eq.(2) in the following discussion.

The signal-to-noise ratio S/N_k of the beat signal detection between the k th sideband of LD_R and LD_X is

$$S/N_k = \frac{\eta_{PD} P_{ok} P_X}{\left(\sum_{k=-\infty}^{\infty} P_{ok} + P_X\right) (B + \Delta\nu_X + \Delta\nu_R) h\nu_X} \quad (3)$$

where h is a Planck's constant. By using the relation $\sum_{k=-\infty}^{\infty} P_{ok} \cong \frac{\eta_{FP}\pi}{mF} P_i \ll P_X, \Delta\nu_X, \Delta\nu_R \ll B$, eq. (3) can be reduced to

$$S/N_k \cong \frac{\eta_{PD} P_k}{h\nu_X B} \quad (4)$$

One should remember that the experimental results are in good agreement with the calculated result of eq.(4) in Fig. 5.

The maximum measurable frequency difference f_{d-max} , which is defined as a $k f_m$ at a signal-to-noise of 0[dB], estimated from eqs. (2-a),(2-b) and (4), is the smaller one between $f_{d-max-a}$ and $f_{d-max-b}$.

$$f_{d-max-a} = f_m \frac{\ln\left(\frac{\pi}{2mF}\right) + 0.5 \ln(Z)}{\frac{\pi}{2mF}} \quad (5-a)$$

$$f_{d-max-b} = 2 \sqrt{\frac{mc}{\pi L_c \frac{dn}{dv}}} \quad (5-b)$$

where $Z = \frac{\eta_{FP} \eta_{PD} P_i}{h \nu_X B}$, is a signal-to-noise ratio of the beat signal detection between the LD_R through the Fabry-Perot cavity and LD_X . $f_{d-max-a}$ is calculated results by assuming $\frac{dn_i}{dv} = 0$. $f_{d-max-b}$ is calculated results by assuming $Z = \infty$ and optimizing the values of φ and Δf_m .

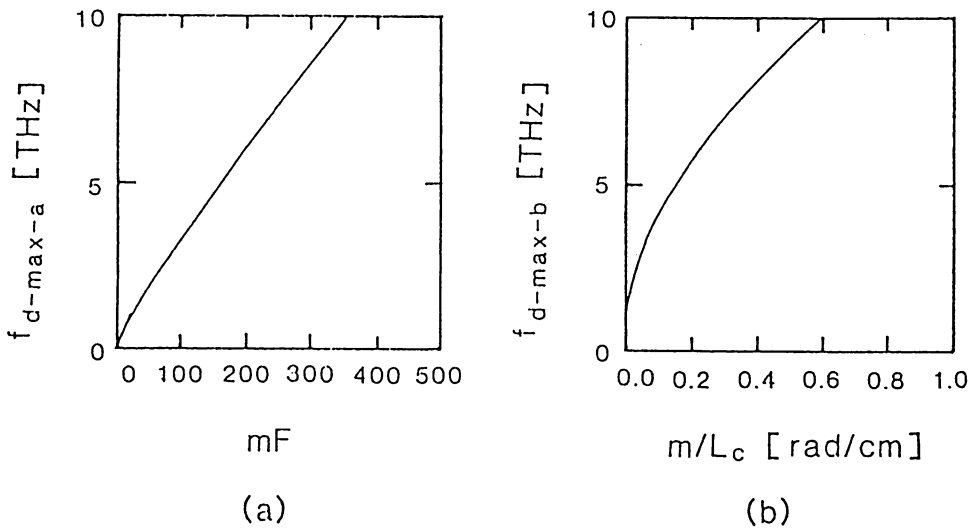


Figure 9: The maximum measurable frequency difference. (a) $f_{d-max-a}$. (b) $f_{d-max-b}$.

In Figs. 9(a) and (b), $f_{d-max-a}$ and $f_{d-max-b}$ are shown as functions of mF and m/L_c , respectively. Fig. 9(a) is calculated result by using values of experimental condition such as $Z = 2 \times 10^{11}$ ($\eta_{FP}=0.05$, $\eta_{PD}=0.9$, $P_i=7$ [mW], and $B = 10$ [kHz]). From curve A in Fig. 9(a), and Fig. 9(b), the value of f_{d-max} can be estimated to be 4[THz] by the experimental conditions $mF \cong 125$, and $m/L_c = 0.31$ [radian/cm].

It is interesting and important to consider how the OFC generator works in the other wavelength region. By assuming that all incident microwave power is feeded to the crystal, the modulation index m is expressed as

$$m \cong \frac{1}{\sqrt{2}} \frac{n_e^3 \gamma_{33}}{\lambda_R} \sqrt{\frac{P_\mu L_c \pi}{A f_m \epsilon \tan \delta}} \quad (6)$$

where A , γ_{33} , and ϵ are the cross-sectional area of the crystal, EO coefficient, and dielectric constant, respectively. By substituting the experimental values into eq. (6), dielectric loss tangent $\tan \delta$ is

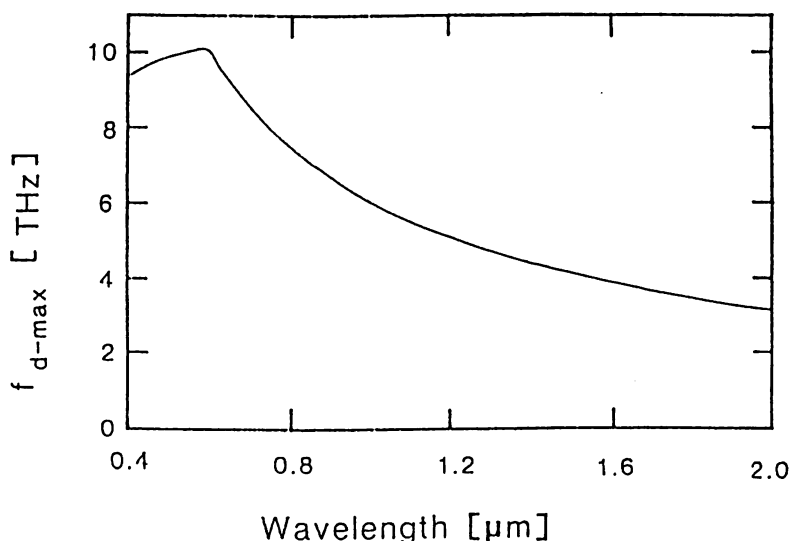


Figure 10: The maximum measurable frequency difference as a function of wavelength.

estimated to be 0.0017. The value of $\frac{dn_e}{d\nu}$ is calculated from a Sellmeir equation given in ¹⁰. In Fig. 10, $f_{d-\text{max}}$ is shown as a function of λ_R , in which it can be seen that $f_{d-\text{max}}$ reaches to 10[THz] at $\lambda_R \cong 0.6\mu\text{m}$. This wavelength is important for the precision spectroscopy, such as for I_2 and Ca. In the range of wavelength shorter than $0.6\mu\text{m}$, the decrease of $f_{d-\text{max}}$ can be seen owing to the increase of dispersion effect of the LiNbO_3 crystal near the absorption.

5.SUMMARY

A wide-span optical frequency comb (OFC) generator was realized for accurate optical frequency measurement of $1.5\mu\text{m}$ wavelength semiconductor lasers by using a high frequency electro-optic phase modulator (LiNbO_3) which is installed in a Fabry-Perot cavity. It was confirmed that the span of the OFC is wider than 4[THz]. By using such an OFC generator, semiconductor lasers whose spectrum linewidths are narrowed to 1[kHz], and a sensitive optical balanced-mixer-receiver, we demonstrated the frequency difference measurement up to 0.5[THz] with signal-to-noise ratio higher than 61[dB]. We also demonstrated the heterodyne optical phase locking with the heterodyne frequency of 0.5[THz] and achieved the residual phase error variance less than 0.01 [radian²]. The maximum measurable frequency difference, which is defined by a signal-to-noise ratio of 0[dB], was estimated to be 4[THz].

6.ACKNOWLEDGEMENTS

The authors would like to thank Professor Kobayashi and Dr. Morimoto of the Osaka university for helpful comments on an electro-optic modulator. They also thank Drs. Okai and Kuboki of the Hitachi corporation for discussions on the semiconductor lasers. This works was partly supported by a Grant-in-Aid for Scientific Research (No. 03555006) from the Ministry of Education, Science, and Culture of Japan.

7. REFERENCES

1. M. Weitz, F. Schmidt-Kaler, and T. W. Hänsch, "Precise Optical Lamb Shift Measurements in Atomic Hydrogen," *Phys. Rev. Lett.*, vol. 68, pp. 1120-1123, 1992.
2. C. R. Pollock, D. A. Jennings, F. R. Petersen, J. S. Wells, R. E. Drullinger, E. C. Beaty, and K. M. Evenson "Direct frequency measurements of transitions at 520 THz [576 nm] in iodine and 260 THz [1.15 μm] in neon," *Opt. Lett.*, vol. 8, pp. 133-135, 1983.
3. D. A. Jennings, C. R. Pollock, F. R. Petersen, R. E. Drullinger, K. M. Evenson, and J. S. Wells, "Direct frequency measurement of the I₂-stabilized He-Ne 473-THz (633-nm) laser," *Opt. Lett.*, vol. 8, pp. 136-138, 1983.
4. R. E. Drullinger, K. M. Evenson, D. A. Jennings, F. R. Petersen, J. C. Bergquist, and Lee Burkins, "2.5-THz frequency difference measurement in the visible using metal insulator-metal diodes," *Appl. Phys. Lett.*, vol. 42, pp. 137-138, 1983.
5. M. Kourogi, K. Nakagawa, C. H. Shin, M. Teshima, and M. Ohtsu, "Accurate frequency measurement system for 1.5- μm wavelength laser diodes," in *Proc. Conf. on Lasers and Electro-Opt.*, Baltimore, May 1991, paper number CThR57.
6. Kourogi, K. Nakagawa, and M. Ohtsu, "A Wideband Optical Frequency Comb Generator for a Highly Accurate Laser Frequency Measurement," in *Proc. International Quantum Electronics Conf.*, Vienna, June 1992, paper number TuM5
7. B. Y. Lee, T. Kobayashi, A. Morimoto, and T. Sueta, "Picosecond electro-optic modulator/deflector with velocity matching," in *Proc. Conf. on Lasers and Electro-Opt.*, Baltimore, May 1991, paper number CTuR4.
8. T. Kobayashi, T. Sueta, Y. Cho and Y. Matsuo, "High-repetition-rate optical pulse generator using a Fabry-Perot electro-optic modulator," *Appl. Phys. Lett.*, vol. 21 pp. 341-343, 1972.
9. C. H. Shin, and M. Ohtsu, "Optical phase-locking of resonant cavity coupled semiconductor lasers," *IEEE J. Quantum Electron.*, to be submitted.
10. R. C. Eckardt, C. D. Nabors, William J. Kozlovsky, and Robert L. Byer, "Optical parametric oscillator frequency tuning and control," *J. Opt. Soc. Am. B*, vol. 8 pp. 646-667, 1991.

CThS24 Continuous-wave optical parametric amplifier by using diode laser for wideband coherent optical frequency sweep generator

Weizhi Wang, Motoichi Ohtsu
Interdisciplinary Graduate School of Science and Engineering, Tokyo Institute of Technology, 4259, Nagatsuta-cho, Midori-ku, Yokohama 227, Japan

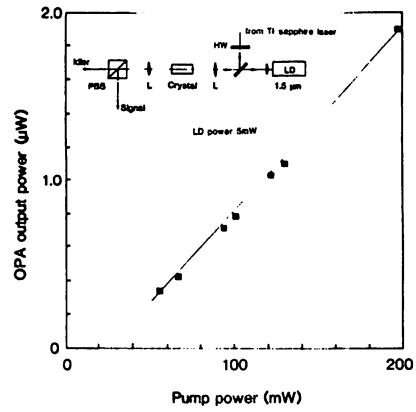
Highly coherent tunable light source is an essential tool in applications from basic physical investigation to precision measurement. For this purpose, we have proposed an all diode-laser-based optical frequency sweep generator (OFSG) by using nonlinear frequency conversions to cover the tunable frequency range about 1 PHz from UR to near IR region,¹ and reported some experimental results towards realization of OFSG.^{1,2} Among various frequency conversions, optical parametric amplification (OPA) is an important part for generating tunable output in the near IR region for OFSG. In this paper, we present, for the first time to our knowledge, the experimental result of the cw OPA by using a 15- μm MQW-DFB diode laser and a Ti:sapphire laser in a potassium titanyl phosphate (KTP) crystal, and we propose a scheme for precision frequency tunable source based on our previous experiments.

Although in the conventional case of OPA, the wavelength of the pump source is fixed while the signal is tuned to obtain a tunable output, we used the tunability of the pump laser to extend the wavelength range of the output while the fine tuning was performed by the diode laser. Figures 1 and 2 show the relationship of the input-output powers and the angle dependence for phase matching. The wavelength tuning of the output was carried out by tuning the wavelength of the input lasers and the angle of the crystal simultaneously. The obtained tunable range was from 1.35 to 1.67 μm . The maximum available tuning range can be as wide as 600

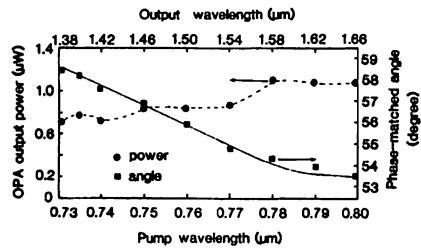
nm (i.e., 65 THz) around 1.54 μm which is limited only by the used crystal size ($3 \times 3 \times 10\text{mm}^3$). Since both lasers used in this frequency conversion are highly coherent whose linewidths were measured to be less than 500 kHz, the linewidth of the output at the difference frequency was estimated to be less than 1 MHz. From the experimental result, we can conclude that all diode laser-based OPA with output power higher than 1 μW is also feasible when the Ti:sapphire laser is replaced by an AlGaAs laser diode with high power and high coherence, which has been realized by using a coherent addition technique.³ Further improvement of the output power can be realized by using an external built-up cavity for OPA.

For precision tuning of the output frequency we propose a scheme, as shown in Fig. 3, by using an optical frequency comb generator (OFCG) and the phase-locking technique.⁴ The system is constructed basically by the OPA arrangement used above. The 0.78- μm diode laser is locked to the Rb absorption line to work as a frequency standard. One of the sidebands from OFCG is used to generate a beat signal with the 1.5- μm diode laser through the second harmonic wave for phase locking. Because the sidebands of the comb can span over 4 THz, the precision frequency tuning range of 4 THz around 1.5 μm is reasonable, which is important for the frequency measurement, e.g., in multichannel optical fiber communication.

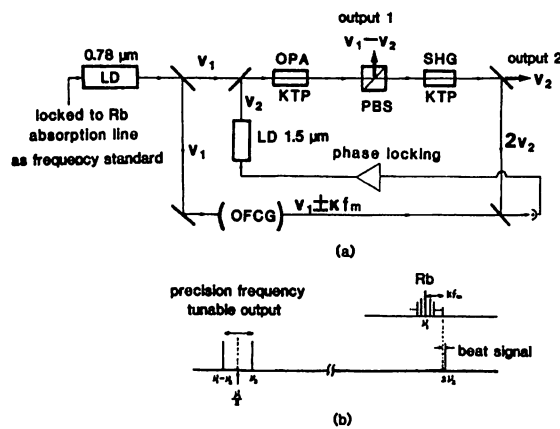
1. M. Ohtsu, K. Nakagawa, C.-H. Shin, H. Kusuzawa, M. Kourogi, H. Suzuki, *Conference on Lasers and Electro-Optics*, Vol. 7, 1990 OSA Technical Digest Series (Optical Society of America, Washington, DC, 1990), paper CME5.
2. W. Wang, K. Nakagawa, Y. Toda, M. Ohtsu, *Appl. Phys. Lett.* 61, 1886 (1992).
3. W. Wang, K. Nakagawa, S. Sayama, M. Ohtsu, *Opt. Lett.* 17 (1992).
4. M. Kourogi, M. Ohtsu, IQEC'92 (American Physical Society and European Physical Society, June 1992, Vienna, Austria) paper TuM5.



CThS24 Fig. 1. Measured relation between the output power of OPA and the pump power at $\lambda_{LD} = 2\lambda_{pump}$ while the signal power was fixed. The inset is the experimental setup for the optical parametric amplification. The polarizations of the two lasers were orthogonal to satisfy the type II phase matching. HW: half-wave plate; PBS: polarized beam splitter.



CThS24 Fig. 2. Measured dependence of the phase-matched crystal angle on the wavelength and relation between output power and the wavelength. Pump power = 100 mW, diode laser power = 5 mW.



CThS24 Fig. 3. (a) Proposed scheme of a OPA-based precision frequency tunable source in 1.5 μm wavelength region by using a OFCG and the phase locking technique. OPA: optical parametric amplifier; SHG: second harmonic generation; OFCG: optical frequency comb generator; PBS: polarized beam splitter; f_m : modulation frequency of OFCG; k : order of the sideband. (b) Explanation of the frequency relation in the system.

Thursday Poster

QThE7

12:15 pm

Nonlinear optical frequency conversion of a 1.5- μ m-wavelength diode laser for frequency linking to the 0.6- μ m optical frequency standard

Y. Awaji, M. Kourogi, K. Nakagawa, T. Enami, M. Ohtsu, *Interdisciplinary Graduate School of Science and Engineering, Tokyo Institute of Technology, 4259 Nagatsuta, Midori-ku, Yokohama, Kanagawa, 227, Japan*

We have proposed a highly accurate frequency-measurement system that uses 1.5- μ m-wavelength semiconductor lasers, which are important for spectroscopy and optical-communication systems, and we have carried out some preliminary experiments.^{1,2} We present here a frequency link for making highly accurate secondary frequency standards at 1.5 μ m, which is a basic part of the frequency-measurement system.

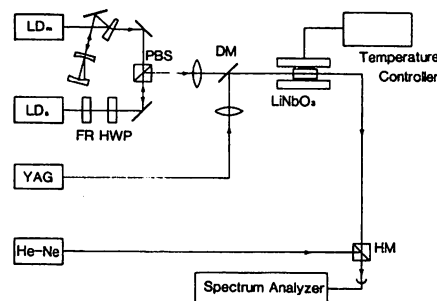
Figure 1 shows our experimental setup. A high-power multimode semiconductor laser was injection locked to a low-power single-mode semiconductor laser. A non-doped LiNbO₃ bulk crystal whose size was 5 mm \times 5 mm \times 20 mm was used for nonlinear optical frequency conversion.

We installed the crystal in a temperature-stabilized heat sink and realized the sum-frequency generation (SFG) of the 1.5- μ m laser diode and the 1.06- μ m Nd:YAG laser at 331°C by noncritical phase matching. This is, to our knowledge, the first report on this type of frequency conversion in the 1.5- μ m region. The relation between the incident power of 1.5- μ m-laser ($P_{1.5}$) and the output of the SFG (P_{SFG}) can be expressed as

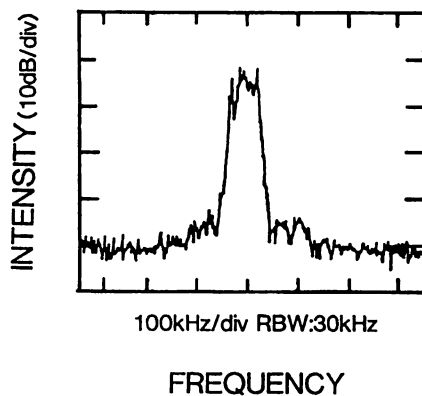
$P_{SFG} [\mu W] = 9.72 \times 10^{-2} \times P_{1.5} [mW]$, where the YAG laser power was 220 mW and maximum of P_{SFG} was 0.7 μ W. Higher conversion efficiency can be expected by improving the accuracy of the optical alignment and so on. As the next step, we observed the beat frequency between SFG and a He-Ne laser for optical phase locking (Fig. 3). For this experiment the SFG power was 0.2 μ W when the 1.5- μ m laser-diode power was 6.25 mW, the 1.06- μ m Nd:YAG laser power was 160 mW, and the He-Ne laser power was 1.4 mW. The master semiconductor laser of the injection-locking system was optically fed back by using a Fabry-Perot cavity, and its linewidth was reduced to narrower than 1 MHz. The linewidth of the Nd:YAG laser was below 5 kHz. The signal-to-noise ratio of the beat signal was 37 dB, and the jitter was 600 kHz. The short-term linewidth of the beat signal was estimated to be lower than 100 kHz.

In summary, we present the possibility of a frequency link between the 1.5- μ m and 0.63- μ m frequency standards with an experimental scheme that uses two types of laser diodes, a Nd:YAG laser, and a He-Ne laser.

1. M. Kourogi, K. Nakagawa, C. H. Shin, M. Teshima, and M. Ohtsu, in *Digest of Conference on Lasers and Electro-Optics*, Vol. 10 of the 1991 OSA Technical Digest Series (Optical Society of America, Washington, D.C., 1991), paper C:ThR57.
2. M. Kourogi, K. Nakagawa, and M. Ohtsu, in *Digest of Conference on Quantum Electronics and Laser Science*, Vol. 13 of the 1992 OSA Technical Digest Series (Optical Society of America, Washington, D.C., 1992), paper TuM5.



QThE7 Fig. 1. Experimental setup: LDm, 1.5- μ m-wavelength multiple-quantum-well distributed-feedback laser diode; LDs, 1.5- μ m multimode high-power semiconductor laser; FR, Faraday rotator; HWP, half wave plate; PBS, polarized beam splitter; DM, dichroic mirror; HM, cube half-mirror.



QThE7 Fig. 2. Beat signal between SFG and the He-Ne laser.

THURSDAY

Reproducible Fabrication Technique of Nanometric Tip Diameter Fiber Probe for Photon Scanning Tunneling Microscope

Togaru PANGARIBUAN, Kazunobu YAMADA, Shudong JIANG,
Hisao OHSAWA¹ and Motoichi OHTSU

*Graduate School at Nagatsuta, Tokyo Institute of Technology,
4259 Nagatsuta, Midori-ku, Yokohama, Kanagawa 227*

¹*Nikon Corporation, Nishi-Ohi 1-Chome, Shinagawa-ku, Tokyo 140*

(Received June 3, 1992; accepted for publication June 30, 1992)

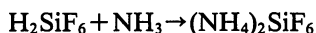
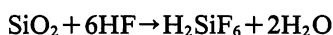
Nanometric tip diameter fiber probes for photon scanning tunneling microscopes (PSTM) were fabricated by selective chemical etching of GeO₂-doped optical fibers. The cone angle θ of the fiber probe tip was controlled by varying the doping ratio of the fiber core and the composition of the etching solution, and the standard deviation of the cone angle $\Delta\theta$ was within 0.5°. A fiber probe with $\theta=20^\circ$ and tip diameter of less than 10 nm was fabricated. This is, to the authors' knowledge, the sharpest PSTM probe which has ever been reported.

KEYWORDS: photon, scanning tunneling microscope, optical fiber, chemical etching

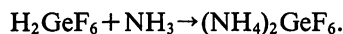
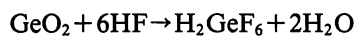
The photon scanning tunneling microscope (PSTM) has recently been developed¹⁻⁴⁾ for surpassing the diffraction limit of the resolution in an optical microscope. In the PSTM, the spatially distributed evanescent field which is generated under the total internal reflection and modulated by the sample is picked up by a probe. Because the lateral resolution of such a system is determined by the probe tip diameter,⁵⁾ the fabrication of the probe becomes very important for PSTM. Although methods such as pulling heated glass capillaries past the breaking point³⁾ and sharpening quartz rods or optical fibers by chemical etching^{1,2)} have been applied to PSTM probe fabrication, sufficiently high reproducibility and transmission efficiency have not yet been achieved. Moreover, the tip diameter of the fabricated probe has not been small enough for resolving the nanometric-scale structure of the sample.

For solving these problems, we have reported a reproducible fabrication technique for the fiber probe with a tip diameter of 160 nm by selectively etching a single-mode fiber in buffered hydrofluoric acid (HF) solution.⁴⁾ In this letter, the fabrication of the fiber probe with the smallest cone angle θ of 20° and a tip diameter of less than 10 nm is reported. The tip diameter of such a fiber probe has been improved to be more than one order smaller than that of the previously reported fiber probes.¹⁻⁴⁾

In the selective chemical etching method, the difference in etching rates of the GeO₂-doped silica core and the pure silica cladding has been employed to form the sharpened fiber probe. The etching solution used in our experiment was composed of 50% (weight %) hydrofluoric acid (HF), 40% ammonium fluoride (NH₄F), and water (H₂O). The chemical reactions of SiO₂ and GeO₂ with HF and NH₄F can be expressed as



and



The difference in the solubility of the generated (NH₄)₂SiF₆ and (NH₄)₂GeF₆, which adsorbed on the fiber end surface, in the etching solution leads to the difference in the etching rates between core and cladding. Various fiber probes have been fabricated by adjusting the composition of the etching solution, the doping ratio of GeO₂, and the etching time.

Three kinds of fibers with the GeO₂-doping ratios of 3.6 mol%, 8.5 mol%, and 23 mol%, (which correspond to the relative refractive-index differences of 0.36%, 0.85%, and 2.3%, respectively) were used. For adjusting the composition of etching solution, the volume ratio X of NH₄F was varied while the volume ratio of HF to H₂O was maintained at 1:1. Thus, the composition of the etching solution can be expressed as $X:1:1$. To avoid the high-temperature operation of HF and to save etching time, all the experiments were carried out at the etching solution temperature of 22°C.

Figure 1(a) shows the scanning electron microscopic (SEM) (Hitachi, S-800) images of the various etched fiber tips at different etching times. An Au-Pd thin film with the thickness of 6 nm was coated for SEM observation. The fiber with the doping ratio of 23 mol% was etched by the etching solution with composition of $X=5$, and the etching times were 10, 40, and 90 minutes, respectively. With increasing etching time, the upper diameter of the mesa at the fiber end became smaller until it could not be resolved by the SEM with a magnification of 1.5×10^4 . Figure 1(b) shows the relationship between the etching time and the upper diameter d_0 of the mesa at the fiber end. Curves A, B, and C correspond to the compositions of etching solutions with $X=4, 5$, and 6, respectively. From this figure, it can be seen that d_0 decreased linearly with increasing etching time, and for a larger value of X , longer etching time is necessary in order to obtain the same d_0 .

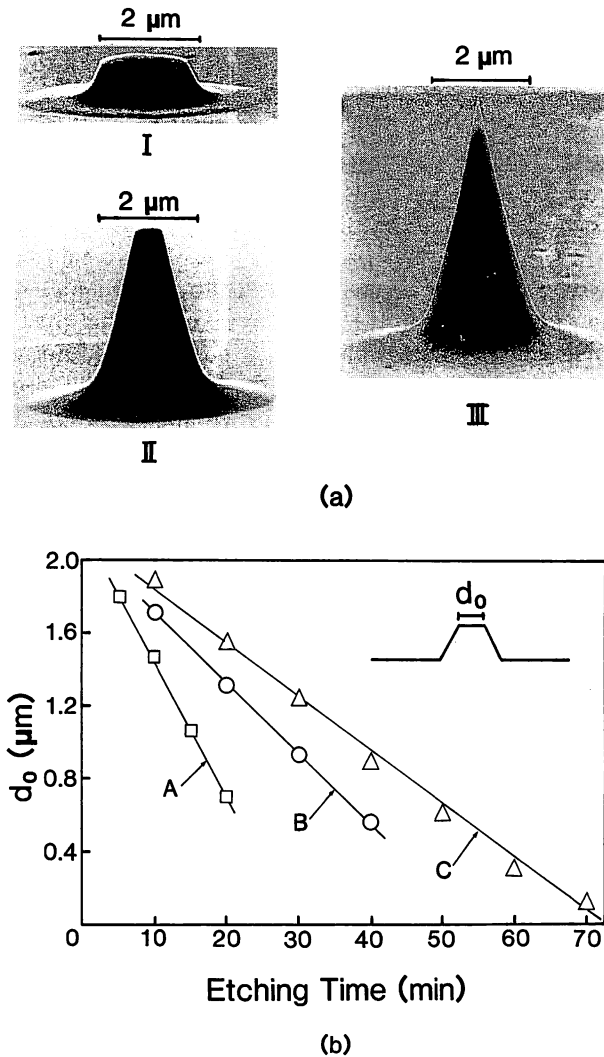


Fig. 1. Dependence of the shape of the etched fiber end on etching time. The fiber with the doping ratio of 23 mol% was used. (a) SEM images of the fiber probe tips. The composition of etching solution is $X=5$. Pictures I, II, and III correspond to the etching times of 10, 40, and 90 minutes, respectively. (b) Relationship between the etching time and the diameter d_0 of the mesa at the fiber end. Curves A, B, and C correspond to $X=4, 5,$ and 6 , respectively.

The sharpest fiber probe among all the fiber probes obtained so far is shown in Fig. 2. Figures 2(a), 2(b), and 2(c) are the SEM images with different magnifications and Fig. 2(d) gives the definition of the tip diameter d and cone angle θ of the fiber probe. Etching time was 180 minutes and the value of X was 7. The fiber used has the doping ratio of 23 mol% and a core diameter of 3.1 μm. It can be claimed that the base of the cone is nearly equal to the core diameter (see Fig. 2(a)), a cone angle of 20° (see Fig. 2(b)), and a tip diameter smaller than 10 nm (see Fig. 2(c)) were achieved. These values are more than one order smaller than that of the previously reported fiber probes¹⁻⁴⁾ and the same order as that of the AFM probe.⁶⁾

The dependence of θ on X is shown in Fig. 3(a). Curves A, B, and C are the results for which the fibers with the doping ratios of 3.6 mol%, 8.5 mol%, and 23 mol%, were used, respectively. It can be seen that the cone angle θ and the value of $d\theta/dX$ became smaller

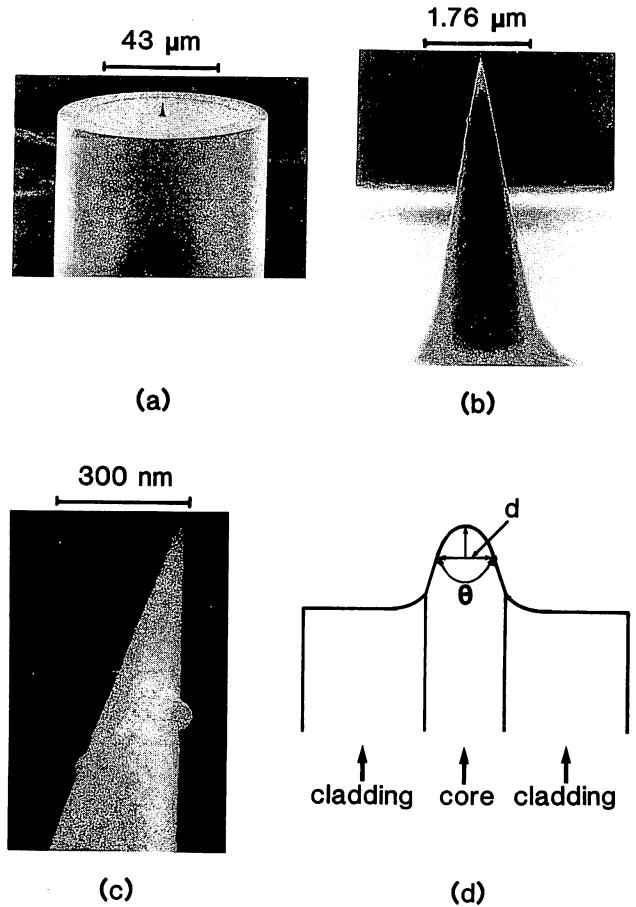


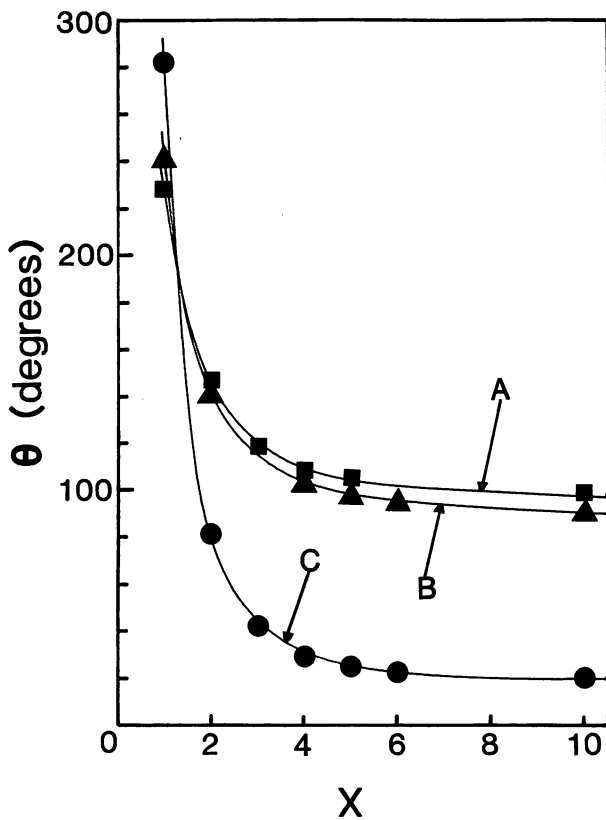
Fig. 2. SEM images of the sharpest fiber probe. Etching time and the value of X were 180 minutes and 7, respectively. From pictures (a) to (c), the magnification of the SEM was increased. Figure (d) gives the definition of the tip diameter d and cone angle θ of the fiber probe.

with increasing values of X . The asymptotic value of θ was smaller for the higher doping ratio.

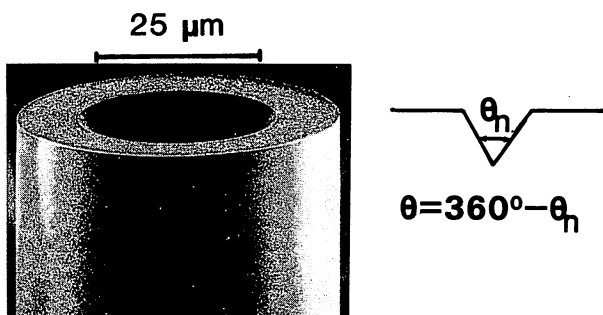
Although it has been reported that the etching rate of the core is different from that of cladding and θ is dependent only on the doping ratio,⁷⁾ we found, for the first time, that θ is dependent also on X , especially in the case of the fiber with the high GeO_2 doping ratio. This means that we can obtain the fiber probes with various cone angles by controlling X , which can be convenient to vary the magnification of the PSTM for the needs of measurement of the different-sized samples.⁵⁾ In Fig. 3, the etched fiber probe with cone angle θ larger than 180° corresponds to the case in which the etching rate of the core was larger than that of the cladding and the θ shown in this figure was defined by $\theta=360^\circ-\theta_n$, where θ_n is the "negative cone angle" (see Fig. 3(b)).

On the other hand, it was confirmed by numerous experimental results that the standard deviation of the cone angle $\Delta\theta$ of the fabricated fiber probes was smaller than 0.5° under the conditions where the etching solution temperature fluctuation was less than $\pm 1^\circ\text{C}$.

The reason for the fiber probe sharpening was attributed only to the difference in etching rates between the GeO_2 -doped silica core and the pure silica cladding. However, it is still uncertain why the uniformly GeO_2 -doped fiber was sharpened and the tip diameter of less



(a)



(b)

Fig. 3. (a) The dependence of cone angle θ of the fiber probes on X . Curves A, B, and C are the results for the fibers with the doping ratios of 3.6 mol%, 8.5 mol%, and 23 mol%, respectively. (b) SEM image of the fiber probe with the "negative cone angle" θ_n .

than 10 nm was realized. One of the other reasons may be the existence of a binding energy distribution of the Si-O-Ge network along the core radius resulting from the residual stress which is generated by the rapid cooling during the fiber fabrication process.⁸⁾ During the etching process, polar materials such as H₂O could change the dissolution rate along the core radius.*

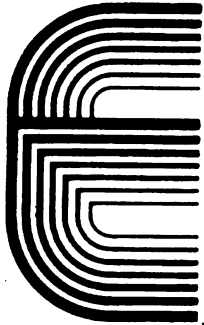
In summary, fiber probes for PSTM were fabricated by selective chemical etching of the fiber with a high doping ratio of GeO₂ in the core. It was found that the cone angle θ of the fiber probe tip can be controlled not only by varying the doping ratio of the fiber core, but also by varying the composition of the etching solution. The smallest cone angle of 20° and a tip diameter less than 10 nm were obtained with the standard deviation of the cone angle $\Delta\theta$ smaller than 0.5°. The fabricated fiber probes have been successfully applied to observation of the bacteriophage T4.⁵⁾

The authors would like to thank Dr. S. Kodato (Anritsu), Dr. S. Miyamoto (Fujikura), and Professor H. Kawazoe (Tokyo Inst. Tech.) for discussions on optical fiber, and Ms. F. Sugimoto for taking SEM photographs.

References

- 1) D. W. Pohl, W. Denk and M. Lanz: Appl. Phys. Lett. **44** (1984) 651.
- 2) H. Pagnia, J. Radojewski and N. Sotnik: Optik **86** (1990) 87.
- 3) K. Lieberman, S. Harush, A. Lewis and R. Kopelman: Science **247** (1990) 59.
- 4) S. Jiang, N. Tomita, H. Ohsawa and M. Ohtsu: Jpn. J. Appl. Phys. **30** (1991) 2107.
- 5) S. Jiang, H. Ohsawa, K. Yamada, T. Pangaribuan, M. Ohtsu, K. Imai and A. Ikai: Jpn. J. Appl. Phys. **31** (1992) 2282.
- 6) T. Fujii, M. Suzuki and M. Miyashita: J. Vac. Sci. & Technol. **B9** (1991) 666.
- 7) M. Kawachi and T. Edahiro: Electron. Lett. **21** (1982) 71.
- 8) F. L. Galeener: J. Non-Cryst. Solids **49** (1982) 53.

*Private communication with Prof. H. Kawazoe (Tokyo Inst. Tech.).



光と原子をどこまで制御できるか?

教養のページ

大津元一

大津元一：正員 東京工業大学大学院総合理工学研究科

What are the Limits of Controlling Lights and Atoms? By Motoichi OHTSU, Member (Graduate School at Nagatsuta, Tokyo Institute of Technology, Yokohama-shi 227 Japan).

1. まえがき

はじめに光ありき。すなわち、宇宙の誕生の瞬間に光は宇宙に満ち満ちていた。時は過ぎて現在、光を発するのは物質であり、デモクリトスの主張以来、その物質の基本構成要素の探求の結果として原子が研究された。更に、原子からの光の発生、およびその制御が行われ、レーザなどの装置が実現している。つまり、エレクトロニクス、光エレクトロニクス、に代表される先端技術分野は主に理学的興味に基づいて行われていた「光と原子との相互作用」の研究を工学へ応用した成果である。

最近では、高性能の光を使って原子1個ずつの運動を制御すること、更には原子から従来のレーザ光などの形態と異なる光を発生させること、が試みられている。以上の話題は今世紀初頭から議論されており、その歴史は長い。しかし最近のレーザ技術、超高真空技術、などの急速な進歩によりようやくそれらの実験を行うことが可能な時期を迎えている。但し、それは今のところ主に理学的興味に基づいて行われているので、ここでは工学的応用への可能性を探るヒントを提供させて頂くためにそれらの内容について略説する。

2. 光の制御

光は波動として、あるいは光子（フォトン）として考えることができる。ここではまず波動とみなすと、レーザ光は周波数揺らぎの少ない

波と考えられている。しかし、コヒーレント状態とよばれる揺らぎの最小状態でも周波数はわずかに揺らいでいる。この揺らぎの値は小さいが、高精度光応用システムには無視できない。

コヒーレント状態での揺らぎの値は次の二つの量の積により決まる：

- (i) レーザ共振器の損失の大きさ。
- (ii) レーザ発振モードに混入する自然放出光揺らぎ成分の大きさ。

半導体レーザを例にとると、揺らぎの大きさを表す尺度である「発振スペクトル線幅」の値はコヒーレント状態では数十 kHz である。この値を更に小さくするために、まず (i) の問題を解決する。つまり、共振器の損失を小さくしたり、更にこれと類似であるが揺らぎ抑圧の量子力学的限界が更に 1/8 小さくなる方法として⁽¹⁾、光学素子や電子回路素子を外付けしてレーザに自動制御を施すことが試みられている。これにより発振スペクトル線幅は 7 Hz まで減少されている⁽²⁾。図 1 にはこの自動制御の性能の向上の結果、発振スペクトル線幅が近年急速に小さくなっている様子を示す。レーザに外付け素子を付加して自動制御を行った場合、揺らぎの値はレーザ単体の場合の揺らぎの限界値、すなわちコヒーレント状態での値よりもはるかに小さく、この光の状態は「ハイパーコヒーレント状態」とよばれている⁽³⁾。このような外付け素子の一つとして、最近性能が急速に向上している「スーパー共振器」とよばれるファブリペロー共振器（鏡面反射率が 99.99997 % に

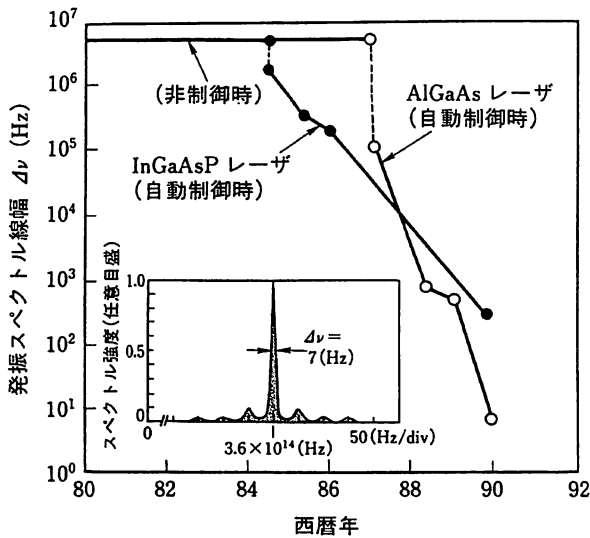


図1 自動制御による半導体レーザーの発振スペクトル線幅の狭化の進歩 内挿図は線幅7 Hz⁽²⁾をもつ発振スペクトル形状を表す。内挿図の横軸は一目盛り当り50 Hz。

達するもの)を使うと、発振スペクトル幅は近い将来約10 mHzに達すると見積もられている^{(4), (5)}。

(ii) の自然放出光の揺らぎは真空場の揺らぎであり、従来はその大きさは制御不可能と考えられていたが、適当な条件下では制御できる。例えば、レーザー共振器の一辺の長さが光の波長と同程度になると共振器の共振モードが少数になるので自然放出光発生確率の値が自由空間で

の値と異なってくる。自然放出光の周波数が共振器の共振周波数と一致するときはその確率は増加し、一致しないときは減少する。従って、これをレーザーに応用すると、微小レーザー共振器の形状を適当に設計することにより周波数揺らぎの値や発振しきい値を素子設計段階で所望する値に調節させることができ、新しい発光素子が誕生する可能性がある。

さて、以上の議論では光は遠くへ伝搬し、干渉、回折などを起す波動とみなされていた。従って、光波長以下の寸法の開口にこれらの光を照射すると、開口からはこのような通常の伝搬光は出射せず、開口付近に非伝搬光のみが発生する。これは光波長よりも小さな寸法をもつ極微空間に局在する光であり、従来はエバネッセント光とよばれている。このエバネッセント光によって試料の形状を測定する顕微鏡を作ると、その分解能は光の波長ではなく、開口径によって決まる⁽⁶⁾。従来の顕微鏡の分解能は波動としての光の回折現象によって制限されていたが、この新しい顕微鏡はその限界を打破しており、数nmの寸法の生体試料が非破壊・非接触で測定されている⁽⁷⁾。これはフォトン走査トンネル顕微鏡とよばれており、実際には開口の代りに図2に示すように光ファイバの先端を尖らせた

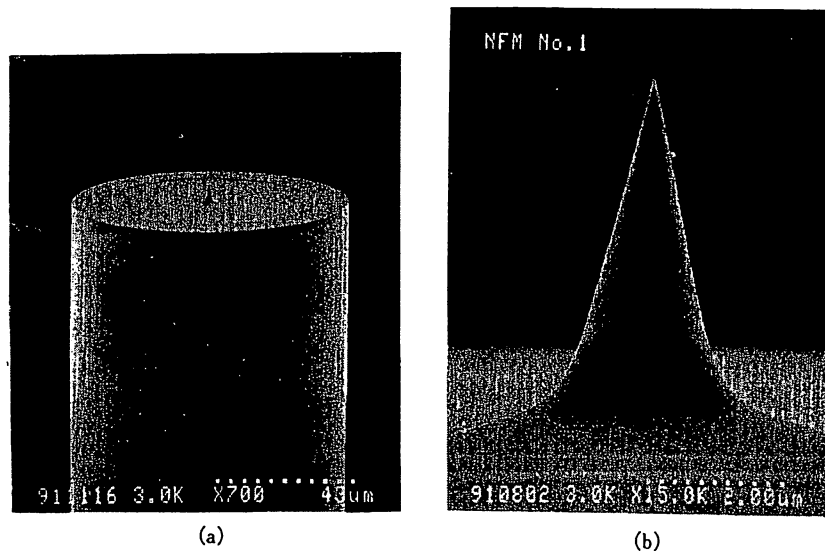


図2 コア先端を尖らせた光ファイバの電子顕微鏡写真⁽⁷⁾

(a) 全体図。ファイバ直径は約90 μm。

(b) 尖らせたコア先端の拡大図。写真の幅は5.6 μmに相当。

ものが使われている。この顕微鏡の動作原理を検討する際にはもはや光を波動としてではなく、極微空間に局在した光子（フォトン）とみなす方が有利であることが指摘されている⁽⁷⁾。すなわち、これは光子の性質を利用した装置であり、その動作原理は原子間力（ファンデルワールス力）を利用した原子間力顕微鏡と等価であることから、原子の寸法と同程度の測定分解能が得られることがわかっている⁽⁷⁾。

3. 原子の制御

光の持つ圧力は小さいが、これを利用すると真空中を飛び回る中性原子集団の熱運動を制御できる。これらの原子は室温では速度数百 m/s で飛んでいるが、これに左右、上下、前後から 6 本のレーザー光を照射し、光の圧力で原子集団を 6 本のレーザー光の交差位置に閉じ込め、その運動エネルギーを減ずることができる。平均速度は数 cm/s になる⁽⁸⁾。中性原子の代わりにイオンを対象とする場合、光のほかにマイクロ波電磁場を補助的に援用することができ、閉じ込めイオン数を調節できる⁽⁹⁾。例えば図 3 にも示すように 1 個のイオンを閉じ込めることができる。



図3 レーザ光により閉じ込められ、静止した1個の水銀イオンからの蛍光 矢印の先の青い点。他の青い色の部分は実験装置からのレーザーの散乱光である（この写真は1990年12月、米国国立標準局、Itano W.博士の御好意による）。

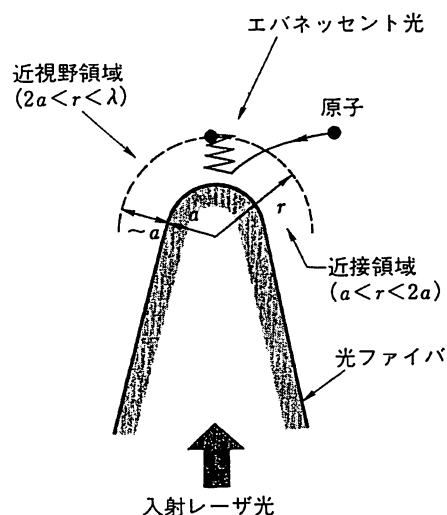


図4 図2のような光ファイバ先端に発生するエバネッセント光の場の中に飛び込む1個の中性原子を捕獲する概念図⁽⁷⁾ a はファイバ先端の曲率半径、 r は曲率中心からの動径方向座標。エバネッセント光の特性を議論するために $a < r < 2a$ の範囲を近接領域とよび、 $2a < r < \lambda$ (λ は光の波長) の範囲を近視野領域とよぶが、原子は両領域の境目付近に捕獲される。

上記のように中性原子の集団や1個のイオンを光の中に閉じ込めることは既に行われているが、今までのところ1個の中性原子の熱運動を制御し、閉じ込めることは行われていない。しかし、最近それを可能にする提案が成されている^{(10),(11)}。すなわち、フォトン走査トンネル顕微鏡に使われた極微空間局在光を使う。この極

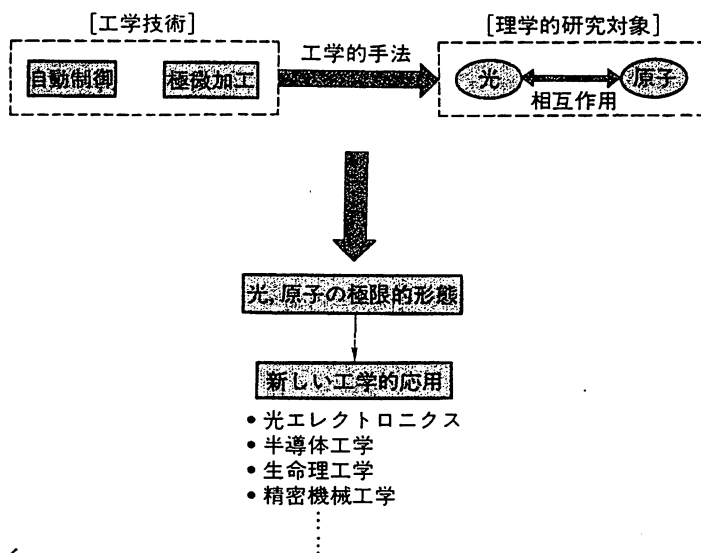


図5 理学的研究対象であった光と原子とに工学的手法を用いてその性能を極限状態まで向上させ、新しい工学的応用を開く試みの説明図。

微空間局在光のエネルギー密度、波数の値、更にそれらの空間的变化率、は通常の伝搬光よりもはるかに大きい。この特徴を利用して図4のように先鋭化された光ファイバ先端のエバネッセント光中に1個の原子のみが安定に捕獲できることがわかってきた。このような原子捕獲技術は単一原子レベルでの結晶成長（つまり、基板の上に基石を一つずつ置いて行くような結晶成長法）、単原子メモリ、原子サイズの光リソグラフィ、などへの応用可能性を秘めている。

4. ま と め

光と原子とを制御することにより多くの新しい応用可能性が開ける。例えば半導体工学における新形発光素子、極微メモリ素子、更に生命工学、精密機械工学、などの分野である。これらを実現するには光の制御と原子の制御とを図5に示すように平行して行い、両者の成果が互いの進歩を促進させる必要がある。従来の理学的常識ではコヒーレント状態よりも揺らぎの小さな光を発生させたり、光の自然放出確率や1個の原子の運動を制御することは不可能と信じられていた。しかし、工学の常套手段、すなわち、高精度な「自動制御」と「極微加工」、を駆使するとこれらの常識を打破することができる。いわば、「理学的な常識により推定されていた限界を打破する量子工学」(Quantum Technology Beyond the Scientific Limit)が可能となる。現在、この量子工学を可能とする周辺技術が整備されつつあるので、近い将来このような極限的な工学分野の実現をめざし努力したい。

なお、これらの議論のうち紙数の制限上記述しきれなかった詳細については文献(12)、(13)を御参照されたい。

文 献

- (1) Yoshida K., Kourogi M., Nakagawa K. and Ohtsu M. : "1/8 Correction Factor of Schawlow-Townes Limit in FM Noise of Negative Frequency Feedback Lasers", Proc. of International Conf. on Noise in Physical Systems and 1/f Fluctuations, Musha T., Sato S., and Yamamoto M., ed., Ohm-sha pp.349-352 (Nov. 1991).

- (2) Shin C.-H and Ohtsu M. : "Stable semiconductor laser with a 7-Hz linewidth by an optical-electrical double-feedback technique", Opt. Lett., 15, 24, pp.1455-1457 (Dec. 1990).
- (3) 大津元一 : "ハイパー・コヒーレント光の実現", 日経サイエンス, pp.64-73, 日経サイエンス社 (1989-03).
- (4) Ohtsu M. and Tabuchi N. : "Electrical Feedback and its Network Analysis for Linewidth Reduction of Semiconductor Laser", J. Lightwave Technol., 6, 3, pp.357-369 (March 1988).
- (5) 大津元一 : "あなたの時計はいま何時?", パリティ, 6, 10, pp.28-34, 丸善 (1991-10).
- (6) Jiang S., Tomita N., Ohsawa H. and Ohtsu M. : "A Photon Scanning Tunneling Microscope Using an AlGaAs Laser", Jpn. J. Appl. Phys., 30, 9A, pp.2107-2111 (Sept. 1991).
- (7) Jiang S., Ohsawa H., Tomita N. and Ohtsu M. : "Photon scanning tunneling microscope using diode lasers", Tech. Digest of Annual Meeting of Opt. Soc. Am., Opt. Soc. Am., San Jose, p.65 (Nov. 1991).
- (8) 清水富士夫 : "原子のレーザー冷却とその周辺技術", 応用物理, 60, 9, pp.864-874 (1991-09).
- (9) Itano W., Bergquist J.C. and Wineland D.J. : "Laser Spectroscopy of Trapped Atomic Ions", Science, 237, pp.612-617 (Aug. 1987).
- (10) 大津元一, 蔭曙東, 富田直幸, 中川賢一, 藤江嘉彦 : "フォトンSTM (V) — 単一原子レベル結晶成長 —", 第51回応用物理学会講演会予稿集, 27 a-L-9/III (1990-09).
- (11) Ohtsu M. : "Frequency control of semiconductor lasers and its applications", Conf. Digest of Jpn.—US Seminar on Quantum Electronic Manipulation of Atoms and Fields, Shimizu F., Phillips W.D., and Westbrook C.I., ed., Jpn. Soc. Prom. Sci., pp.452-472 (Sept. 1990).
- (12) 大津元一 : "コヒーレント光量子工学", 朝倉書店 (1990).
- (13) Ohtsu M. : "Highly Coherent Semiconductor Lasers", Artech House Inc., Boston (1991).



おおつ もといち
大津 元一 (正員)

昭48東工大・工・電子卒。昭53同大学院博士課程了。同年東工大助手。以来、レーザー制御と応用の研究に従事。昭57同助教授、平3教授、現在に至る。工博。

昭59 I. KOGA 金賞, 昭63日本IBM科学賞, 昭57, 平2応用物理学会賞など受賞。著書「コヒーレント光量子工学」など。

光による原子レベルの計測と制御

おお っ もと いち* ほり ひろ かず**
大 津 元 一* 堀 裕 和**

1. はじめに

従来よりひろく知られている光の代表的な性質は「自由空間を伝搬し、波長より小さい寸法の領域には局在しない」ことである。このような「通常」の光による物体の計測と制御について考えよう。まず計測のための代表的装置である光学顕微鏡の場合、微小物体観測の測定限界、すなわち分解能、は光の回折の特性によって決まり、この回折限界のために波長より小さい物体の像は観測できない。これは上記の光の空間的非局在の性質に起因する。より高い分解能を得るために、光の代わりに電子線を用いた顕微鏡が使われ、さらに最近ではトンネル電子を用いた走査トンネル顕微鏡 (STM) により原子レベルの分解能が実現しているのは周知のとおりである。

つぎに、物体の制御のうち、特にその運動を制御する場合について考える。光が力をもつことは太陽の近くを通り抜ける彗星の尾が太陽から遠ざかる方向になびいていることから確認されている。この力を利用して、最近ではレーザー光による微粒子、原子、イオンの減速、捕獲、などが試みられている^{1),2)}。

ところで上記の通常の光ではなく、微小空間に閉じ込められた別形態の光を使うと新奇な計測と制御が可能になることが最近になってわかってきた³⁾⁻⁷⁾。この光は従来の光学の用語を使うとエバネッセント光と呼ばれ、これを用いた計測方法のアイデアは20世紀初頭にアインシュタインが友人にあてた手紙の中に記してあるといわれているが、現在に至るまでこの光の実体を記述する精密な理論は完備していない。筆者らはこれらの未開発分野に挑戦しているので、その研究を中心にご紹介する。ここで扱う内容はいくつかの新

* 東京工業大学大学院 横浜市緑区長津田町 4259

** 山梨大学工学部 甲府市武田 4-3-11

キーワード: エバネッセント光 (evanescent light), 光ファイバ (optical fiber), 走査トンネル顕微鏡 (scanning tunneling microscope), 原子操作 (atom manipulation).

しい原理を含むので、本特集の企画趣旨に従い、「計測技術のフロンティア」を模索するために原理に関する説明も含めて記述させていただく。

2. エバネッセント光による計測

物体表面から放射する光には前節冒頭に示した通常の光の他に物体表面に局在するエバネッセント光が含まれる。この光は後述のように「自由空間を伝搬せず、波長より小さい寸法の領域に局在する」性質をもっている。そこで図1に示すように光プローブを走査しながら微小物体表面に局在するエバネッセント光を散乱し、散乱光パワーの地図を作れば物体形状が測定できる。測定の分解能は光プローブ先端の寸法により決まるのでこの値が光波長より小さければ通常の光の回折限界をはるかに超える超高分解能光学顕微鏡ができる。これがフォトン走査トンネル顕微鏡 (フォトン STM と略記する) の原理である。

実際の光プローブとしては先端先鋭化加工の再現性

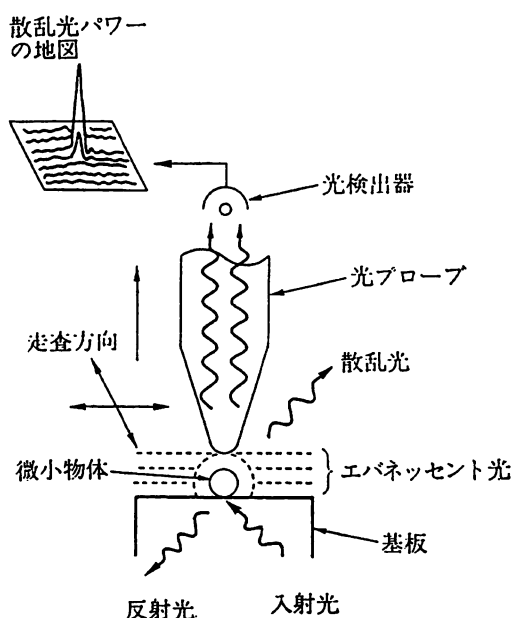
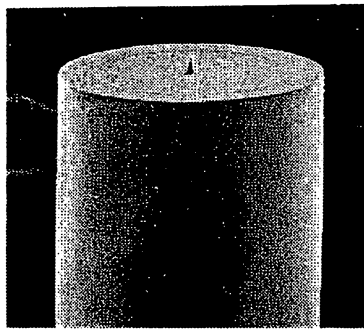
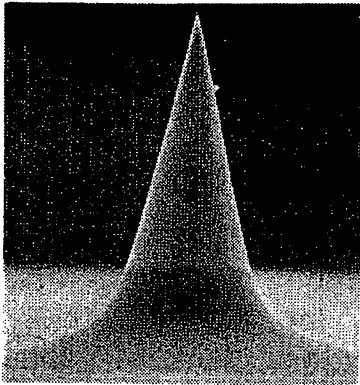


図1 フォトン走査トンネル顕微鏡 (フォトン STM) の原理



(a)



(b)

図2 コア先端を先鋭化した光ファイバの電子顕微鏡写真⁹⁾ (a)光ファイバ端全体図. 外径は90 μm (b)先端部の拡大図. 写真の横幅は5.6 μm に相当

が高いこと、および散乱したエバネッセント光を効率よく導波・集光できること、が重要である。これを實現するために筆者らは光通信などで用いられている光ファイバを用いている。ふっ酸系溶液を用いた化学エッチングにより加工された光ファイバ先端の電子顕微鏡写真の例を図2に示す。光ファイバ・コア円錐

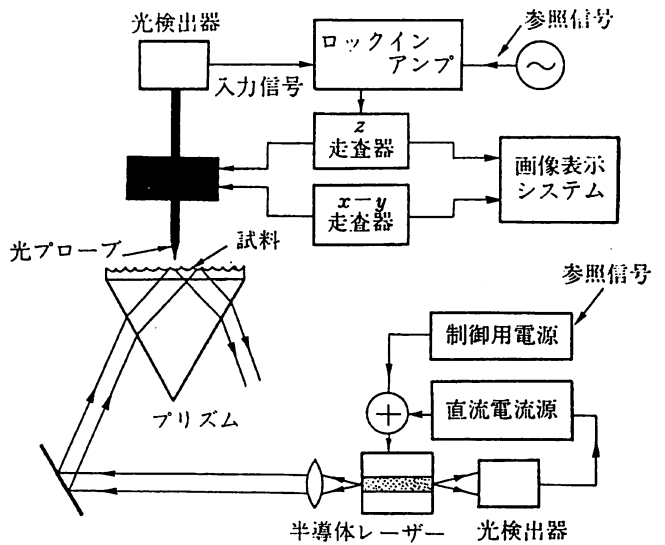


図3 フォトンSTMの装置¹⁰⁾

角、先端曲率半径の最小値として20度、5nm以内が得られている⁸⁾。従来のピペットなどを用いる方法⁹⁾よりもこの光ファイバを用いる方がつぎに示すように約1桁優れた分解能を實現している。

図3は筆者らの測定装置である¹⁰⁾。装置の小型化、高信頼性のために光源として波長0.8 μm の半導体レーザーを用いている。図4は周期1.5 μm および0.22 μm の格子が網の目状に直交し、網の目の位置に直径300nm、深さ80nmのピットを有する蛾の目形光ディスクの表面測定結果である⁸⁾。また、図5には頭部直径100nm、尾部の幅9nm、長さ100nmのバクテリオファージT4が2体、空気中で観測されている像を示す⁸⁾。両図とも空気中で非接触・非破壊測定されたものである。これら一連の実験により試料厚み方向分解能2nm以内、面内方向分解能5nm以

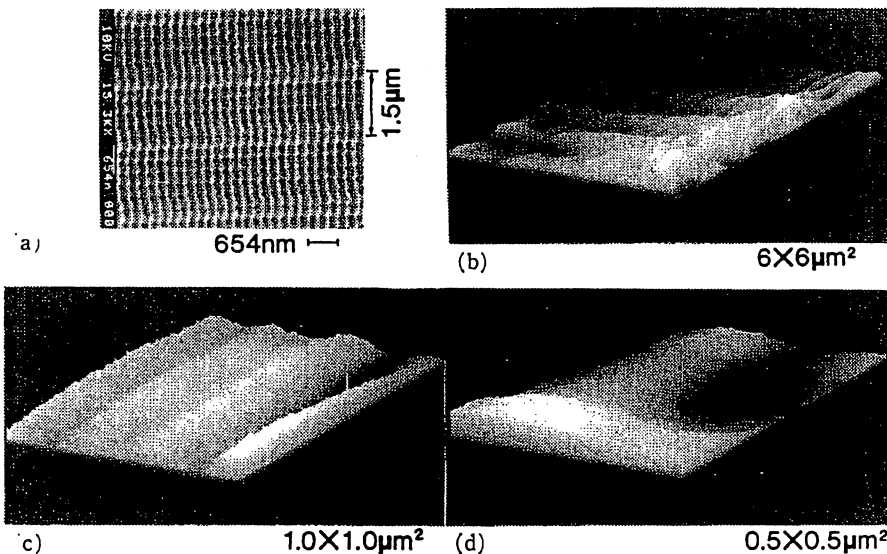


図4 蛾の目形光ディスクの表面形状測定結果⁸⁾ (a)電子顕微鏡による測定結果 (b)~(d)フォトンSTMによる測定結果. 右下の数値は像の縦横の寸法

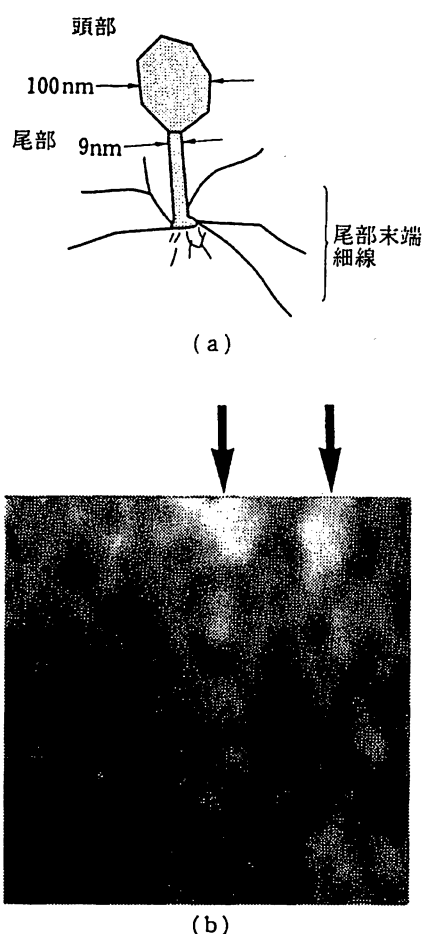


図5 バクテリオファージT4の測定結果 (a)形状説明図 (b)測定結果. 2本の矢印の先の位置に像が見られる. 写真の一辺の幅は $0.6\mu\text{m}$ に相当

内、と推定されている。これらの分解能は光プローブの音響振動、温度ドリフト、により制限されているが、今後システム改良によりこれらの影響を低減し、光検出雑音から決まる分解能が達成されれば、その値は 0.1nm となると推定される。すなわち原子寸法レベルの値が期待される。この根拠について次節で述べる。

3. フォトン STM の分解能

半径 a が光波長よりずっと小さい被測定微小物体が平面基板上に置かれた場合を考える。ハイゼンベルグの不確定性原理 $\Delta x \cdot \Delta p \sim h$ (h はプランク定数) から、この微小物体近傍に発生したエバネッセント光の場は $\Delta x \sim a$ なる広がり、 $\Delta p \sim h/a$ なる運動量をもつ。この運動量成分は微小物体表面に平行で通常の光の運動量より大きいため、分散関係によると法線方向運動量は虚数となる。すなわち、エバネッセント光は自由空間を伝搬できず、 $a \ll \lambda$ なる寸法の微小物体近傍に局在する。このように複素数の運動量をもつエバネッセント光の場を、微小物体の寸法 a に対応するコ

ンプトン波長をもつ仮想光子 (重い光子) とみなし、その伝達を湯川ポテンシャルで表わすと、現象の理解を容易にするのみならず、多体相互作用に関わる摂動計算を省略してエバネッセント光の場を見積ることが可能になる。

エバネッセント光の分布を、複素数の運動量をもつ「エバネッセント場の波動関数」と呼ぶ。微小物体近傍のエバネッセント光を散乱して検出し、フォトン STM の画像を得るためにはつぎの条件が必要である。

(1) 微小物体のエバネッセント場の波動関数および光プローブのそれに互いに一致する成分が存在すること。

(2) 微小物体のエバネッセント場の波動関数よりも広がった成分は散乱されないこと。

これらの条件を満たすために、フォトン STM に用いられる光プローブの形状にはつぎの条件が課せられる。

(A) 光プローブ先端の曲率半径が、微小物体の半径 a 程度に小さいこと。

(B) 光プローブ先端の円錐角が十分に小さいこと。

(A) は上記 (1) に対応し、微小物体のエバネッセント光が光プローブ先端で効率よく散乱され通常光成分に変換されることを示す。(B) は (2) に対応し、基板表面の粗さに対応して広がったエバネッセント光が、これと一致する光プローブの太い部分のエバネッセント場の波動関数と重なりをもたず散乱されないことを示す。このことは、光プローブを半径の異なる微小球の集合と考えれば容易に理解される (図6)。すなわちエバネッセント場の波動関数の一致は微小物体と光プローブ先端との間でエバネッセント光子のトンネル過程での運動量保存則に対応する。

以上の条件により、高い分解能を得るためには先端曲率半径が小さいのみでなく円錐角の小さい光プローブが必要であることがわかる。条件 (A)、(B) を満たすためには光ファイバを化学エッチング法により先端鋭化する方法が今のところ最も優れている。条件 (A)、(B) を満たす光プローブを、微小物体から先端半径程度の距離を保って掃引すれば、微小物体表面の、さらに細かい構造によって生じる減衰距離の短いエバネッセント光成分も散乱されない。このようにフォトン STM は、被測定物体表面の微細な凹凸の空間周波数の中から、帯域通過フィルタのように、光プローブ先端の曲率半径に対応する細かさをもつ成分を選択的に抽出する装置であり、その分解能は光プローブ先端の曲率半径と円錐角で決定される。光プローブ先端を拡大して観察できたとすれば、その最小の凹凸の寸法を

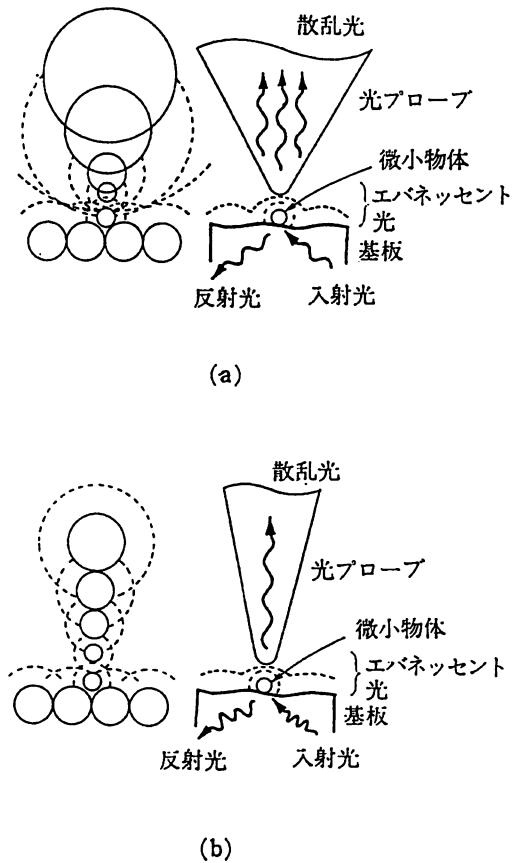


図6 フォトンSTMの分解能の説明。(a),(b)はそれぞれ円錐角の大きい,小さい光プローブを用いる場合。両図の左側は被測定微小物体,基板,光プローブを微小球の集合と見なした場合の説明図

決めるのは原子である。したがって、光プローブ先端と微小物体表面との距離を原子寸法程度まで近づけることができれば、原子レベルの分解能が実現する。

ここで述べた測定装置は近視野顕微鏡などとも呼ばれるが¹¹⁾、以上の議論によりわかるようにこの装置は物体表面に束縛され局在した光を利用し、分解能がハイゼンベルグの不確定性原理によって決まること、さらにトンネル電子を使ったSTMと類似であることから、著者らは「フォトンSTM」という名称を用いている⁷⁾。

4. 単一中性原子の運動制御

前節までに示したような計測からさらに考えを進め、微小物体の運動を制御し新しい物質を加工することを試みる。1節に記したように通常の光を使う微小物体の捕獲はすでに実現しているが、これは中性原子集団、イオン、または寸法が光波長程度以上の微粒子に対するのみであり、単一中性原子の捕獲は実現していない。本節では図2のような光プローブを用いるとそれが可能であることを示す。

図7に示すように真空中に設置した光プローブ先端

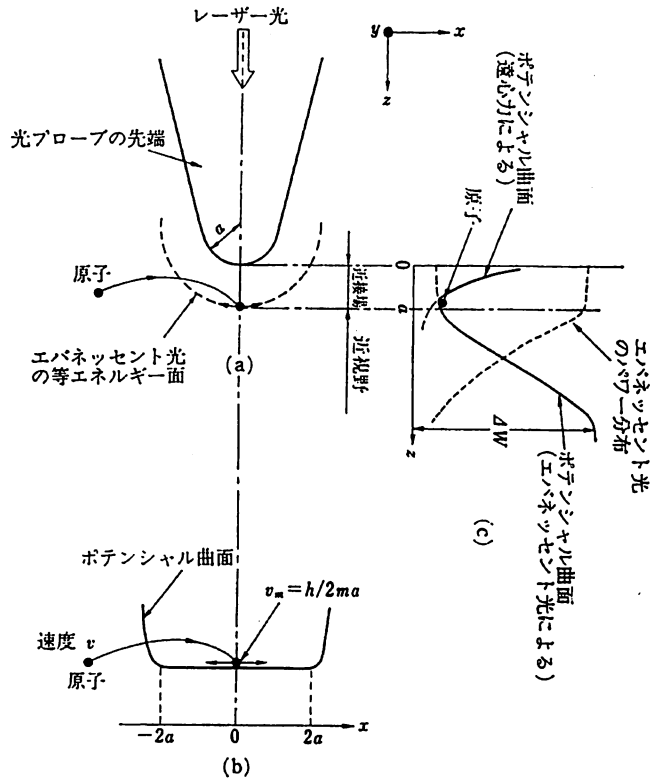


図7 光プローブ先端のエバネッセント光による単一中性原子捕獲の説明図 (a)実体図 (b)光プローブ軸と直角方向の捕獲ポテンシャル形状 (c)光プローブ軸方向の捕獲ポテンシャル形状 ΔW は捕獲ポテンシャルの深さ

からエバネッセント光をしみ出させておく。このとき、速度 v にて先端接線方向から飛来してきた中性原子はエバネッセント光子のもつ大きな運動量接線成分のために、光子との衝突の際の反跳効果により運動量を失い、減速される。減速後の速度 $v_m (=h/2ma)$ 、 h はプランクの定数、 m は原子の質量) は数 10 cm/s と試算される。この速度をもって原子は光プローブ先端表面に沿ってゆっくりブラウン運動する。一方、この原子は光プローブ軸方向に急激に減少するエバネッセント光パワーによる双極子力を受ける。光周波数が原子共鳴周波数以下の場合には原子はこれにより光プローブ表面方向への引力を受ける。一方、上記のブラウン運動による遠心力により原子は同時に斥力も受ける。この2つの力の釣り合いにより原子は光プローブ先端に浮上した状態で捕獲される。捕獲位置は光パワー変化率の最大地点、すなわち $x=a$ である。また、エバネッセント光の波動関数の広がり数は数 10 nm 以内なので、このような微小領域には原子間の反発力のために複数の原子が捕獲されることはない¹²⁾。

光プローブへの入射光が 10 mW の低パワーでもエバネッセント光パワーの単位断面積当りの密度は 100 W/cm² 以上となり、深い捕獲ポテンシャルが形

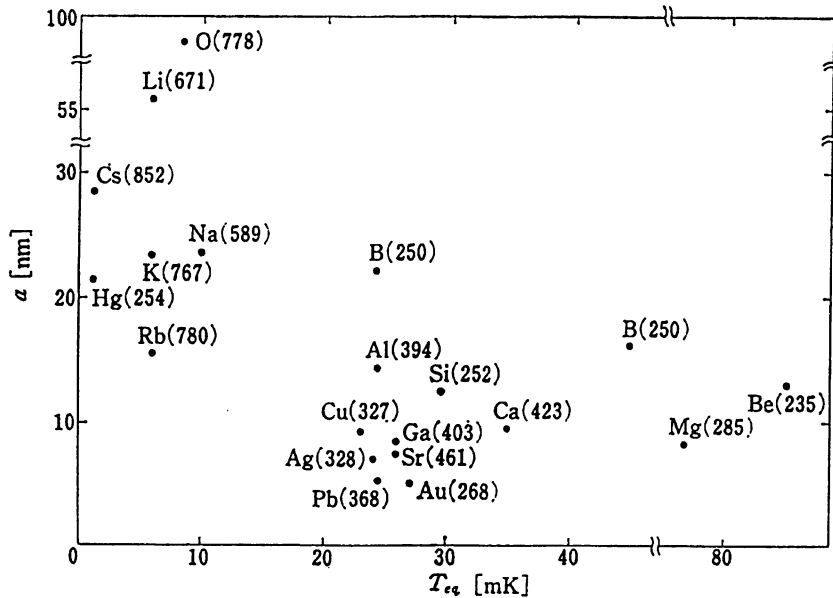


図8 各種原子の捕獲のためのポテンシャル深さを表わす等価温度 T_{eq} と光プローブ先端曲率半径 a の最適値の計算結果¹²⁾。かっこ内の数字は使用する光波長を単位 nm にて表わす

成される。図8はこの場合について前節の理論モデルを用い、各種の原子捕獲のためのファイバ先端曲率半径の最適値、捕獲ポテンシャルの深さ ΔW を表わす等価温度 $T_{eq} (= \Delta W/k_B, k_B$ はボルツマン定数) との関係を実算した結果である¹²⁾。これらの等価温度は数 10 mK であるが、通常の光を用いた「光糖蜜法」^{1),2)} により原子集団を数 μ K まで予備冷却しておく、この原子集団のうちの1つの原子を捕獲する方法が採用できるのでこのポテンシャルは十分深いことがわかる。すなわち、このように予備冷却された原子集団から自由落下してくる原子を光プローブによって待ちうければ約1秒に1回ずつ捕獲が可能と試算されている。たとえば波長 252 nm のエバネッセント光を用いればシリコン原子が捕獲できるが、このような各種波長を備えたコヒーレント・レーザー光源はわれわれのレーザー光周波数掃引システムによりまかなえる¹³⁾。

原子を捕獲後、光周波数を原子共鳴周波数以上の値へとシフトさせれば双極子力は原子に対して斥力を与えるので原子は押し出され、加熱される。こうしてこの原子をファンデルワールス力またはその他の化学結合力によって冷却基板の上に吹き付ければ単一原子レベルでの結合成長が可能である。

以上の他にも、エバネッセント光のもつ大きなエネルギー密度、力を利用して、光子モードでの超高密度光記録、生体微粒子の操作、マイクロマシンの駆動、などが可能である。

5. おわりに

わが国の誇る光ファイバ技術、レーザー技術をもと

にフォトン STM による計測と制御の研究が発展している。これにより空間的に局在した新しい形態の光子、さらにこれを用いた原子レベルでの計測と制御による新しい形態の極微物質の創造、ひいては極微結晶工学の誕生、が期待される。ただし、この研究を遂行するには従来の光学理論から脱却し、場の理論、素粒子論、などに立脚した基本的な問題に取り組み、新しい「極微空間局在光学」の学問体系を構築する必要がある。

(1992年6月22日受付)

参考文献

- 1) 清水：原子のレーザー冷却とその周辺技術，応用物理，60-9，864/874 (1991)
- 2) 大津：コヒーレント光量子工学，朝倉書店 (1990)
- 3) 大津：フォトン走査トンネル顕微鏡，触媒，32-8，548/550 (1990)
- 4) 蔭，富田，大津：フォトン走査トンネル顕微鏡，光学，20-3，134/141 (1991)
- 5) 大津，蔭，大澤：フォトン走査トンネル顕微鏡，レーザー研究，19-8，839/848 (1991)
- 6) 大津：光による単一原子の運動制御，精密工学会誌，58-3，410/414 (1992)
- 7) 堀：フォトン走査トンネル顕微鏡とその理論的解釈，応用物理，61-6，612/616 (1992)
- 8) S. Jiang, H. Ohsawa, K. Yamada, T. Pangaribuan, M. Ohtsu, K. Imai and A. Ikai: Nanometric Scale Biosample Observation Using a Photon Scanning Tunneling Microscope, Jpn. J. Appl. Phys., 31-7A, 2282/2287 (1992)
- 9) R. C. Redick, R. J. Warmack and T. L. Ferrel: New Form of Scanning Optical Microscopy, Phys. Rev. B., 39, 767/770 (1989)
- 10) S. Jiang, N. Tomita, H. Ohsawa and M. Ohtsu: A Photon Scanning Tunneling Microscope Using an

AlGaAs Laser, Jpn. J. Appl. Phys., 30-9A, 2107/2111 (1991)

- 11) U. Ch. Fischer, U. T. Durig and D. W. Pohl: Scanning Near Field Optical Microscopy in Reflection or Scanning Optical Tunneling Microscopy, Scanning Microscopy, 3, 1/7 (1989)
- 12) H. Hori, S. Jiang, M. Ohtsu and H. Ohsawa: A Nanometer-Resolution Photon Scanning Tunneling Microscope and Proposal of Single Atom Manipulation, Technical Digest of the 28th International Quantum Electronics Conference, Vienna, Austria, June 14-19, 1992, American Phys. Soc./European Phys. Soc., 論文番号 MoM7
- 13) 大津, 申, 楠澤, 興梠, 鈴木: 半導体レーザの周波数・位相制御, 電子情報通信学会誌, J73-C-I-5, 277/285 (1990)

.....

[著者紹介]

おお っ もと いち
大 津 元 一 君



昭和25年10月5日生。昭和48年東京工業大学工学部, 53年同大学院理工学研究科博士課程修了。工学博士。東京工業大学助手, 助教授を経て, 現在教授。61~62年, 米国 AT&T ベル研究所研究員。専門は光量子エレクトロニクス(レーザー制御, 極限光子と原子の生成)。電波科学国際連合・KOGA ゴールドメダル, 日本 IBM 科学賞, 応用物理学会賞など受賞。応用物理学会, 米国光学会, などの会員。IEEE シニア会員。

ほり ひろ かず
堀 裕 和 君



昭和30年6月14日生。昭和53年京都大学工学部電子工学科卒業。58年同大学大学院博士課程修了。工学博士。山梨大学工学部講師, 同助教授を経て現在に至る。63年~平成1年アメリカ合衆国ワシントン大学客員准教授。専門は, 量子エレクトロニクス(量子光学, 光ポンピング, レーザー分光を応用した計測, レーザーの制御など)。日本物理学会, 応用物理学会会員。

.....

解説

フォトン STM の実験と理論

大津 元一*・堀 裕和**

* 東京工業大学大学院総合理工学研究科 〒227 横浜市緑区長津田 4259

** 山梨大学工学部電子情報工学科 〒400 甲府市武田 4-3-11

(1992年7月21日受理)

Experiment and Theory of Photon STM

Motoichi OHTSU* and Hirokazu HORI**

* Interdisciplinary Graduate School of Science and Engineering, Tokyo Institute of Technology, 4259, Nagatsuta, Midori-ku, Yokohama 227

** Faculty of Engineering, Yamanashi University, 4-3-11, Takeda, Kofu 400

1. はじめに

近視野顕微鏡(本稿では「フォトン STM」と呼んでいる)の歴史, 波動光学の手法に基づく理論解析については本号の総合報告欄に取り上げられており, また著者らもすでに複数の解説を書いているので¹⁻⁹⁾, ここでは著者らの行っている実験と理論解析を中心に述べる. 近視野顕微鏡では可視光の波長よりもはるかに小さいナノメートル程度の寸法を取り扱うので, その理論解析には光と物質との相互作用をあらわに取り扱うことが必要となる(従来の光学理論では主として伝搬光を取り扱うので, それらの相互作用は境界条件や媒質の誘電定数などの中に隠されていた). また, 光子の局在の問題などと同様¹⁰⁾, 光子と電子の類似性が近視野顕微鏡においても顕著に現れている. この顕微鏡では物体表面に束縛された光を利用し, 分解能がハイゼンベルグの不確定性によること, 電子 STM や原子間力顕微鏡 (AFM) との同等性などの点から, 著者らは「フォトン STM」という名称を用いている.

特に理論解析においては著者らはエバネッセント光を仮想光子(重い光子)とみなして, STM, AFM, フォトン STM などのトンネル形の顕微鏡を統一的に表現する相互作用モデルの確立を試みているので, これらについて紹介する. このモデルは光学の分野ではなじみが薄いかも知れないが, 素粒子, 場の量子論, などの分野で

はよく知られた概念を使う. したがって, 決して異端の議論ではないが, 光学分野の読者諸氏には若干難解な部分もあるかもしれない. しかし, 光学の新しい方向を提示するためにも, 僭越ではあるがここでは厳密性を失わぬよう議論したい. なお, 本解説の内容は他誌でも記述しており¹⁻⁹⁾, 一部分重複があることを了承いただきたい.

2. 原理と分解能

物体によって散乱された光の場は通常の伝搬光の他に物体表面に局在するエバネッセント光が含まれる. そこで, 図1に示すように光プローブを走査しながら微小物体近傍に局在するエバネッセント光を伝搬光に散乱し, 散乱光強度の地図を作ると物体形状が測定できる. 測定の分解能は光プローブ先端の寸法により決まるのでこの値が光波長より小さければ通常の光の回折限界をはるかに越える超解像光学顕微鏡ができる. これがフォトン走査トンネル顕微鏡(「フォトン STM」と略記する)の原理である.

フォトン STM の分解能は, 物体照射光の波長によらず, プローブの形状のみに依存する. これを明らかにするために物体裏面から全反射角で平行光(波長 λ)を照射した比較的滑らかな誘電体基板上に置かれた, 半径 $a(\ll \lambda)$ の微小誘電体球を被測定微小物体と考える. ハイゼンベルグの不確定性 $\Delta x \cdot \Delta p \sim h$ (h はプランク定数)

から、微小物体近傍に発生したエバネッセント光の場は、 $\Delta x \sim a$ に対する $\Delta p \sim h/a$ の運動量を持つ。この運動量成分は、微小物体表面に平行で真空中の光の運動量よりも大きい ($\Delta p \gg h/\lambda$) ため、分散関係から物体表面の法線方向の運動量成分は虚数となり ($\sim ih/a$) 伝搬することができず、エバネッセント光は微小物体近傍に局在する。

エバネッセント光の強度分布は、散乱体内部との連続性から、散乱体の寸法 (a) と同程度の近傍ではほぼ一様であり、この領域は近接場 (proximity) と呼ばれる。この外側のエバネッセント光強度が指数関数的 ($\exp(-r/a)$) に減少する領域は近視野 (near-field) と呼ばれる¹¹⁾。さらに外側では、伝搬光成分のみとなり、この領域が遠視野 (far-field) である。近接場と近視野におけるエバネッセント光の分布を、電子 STM における電子のエバネッセント波動関数との類似性から、複素数の運動量をもつ「エバネッセント場の波動関数」と呼ぶことにする。エバネッセント場は、光照射により微小物体に誘起された分極がつくる多重極電磁場で、遠視野では消滅する。

エバネッセント光と遠視野における伝搬光の相対的な強度の比のおよその値は、不確定性原理と伝搬光の遮断についての考察から容易に与えられる。図 2 に示すように半径 $a (\ll \lambda)$ の微小誘電体球近傍に局在させられた光の場の運動量の一次元成分 p は、 $\Delta p = h/a$ の半値幅をもつガウス分布をしていると考えられる。これに対して、伝搬光の周波数 ν と波数 k とは分散関係、 $(2\pi\nu/c)^2 = |k|^2$ (c は光速) を満たさなくてはならないので、伝搬光の波数の一成分の取り得る最大値、すなわち遮断波数は $2\pi\nu/c$ となる。このことから半径 a の微小誘電

体球近傍の光の場は、運動量が $h\nu/c$ よりも小さい成分は遠視野まで存在する伝搬光、 $h\nu/c$ よりも大きい成分はエバネッセント光である。以上により、伝搬光の波長に比べてきわめて小さい物体に散乱された光の場がほとんどすべてエバネッセント光成分であることがわかる。したがって、エバネッセント光のパワーが大きく、それが散乱されて伝搬光に変換されれば十分検出可能であることが確認される。

微小物体近傍のエバネッセント光を散乱して検出し、微小物体の像を描くためには次の条件が必要である。

- (1) 微小物体と光プローブの両者のエバネッセント場の波動関数の重なり部分が十分に大きく、微小物体のエバネッセント光が光プローブで効率よく散乱され伝搬光となること。
- (2) 基板などの大きな凹凸による背景光を除去するために、微小物体のエバネッセント場の波動関数よりも広がった成分が光プローブで大きく散乱されないこと。

これらの条件を満たすために、フォトン STM に用いられる光プローブの形状には次の条件が課せられる。

- (A) 光プローブ先端の曲率半径が、微小物体の半径 a 程度に小さいこと。
- (B) 光プローブ先端の円錐角が十分に小さいこと。

(A) は (1) に、(B) は (2) に対応することは、図 3 に示すように光プローブを半径の異なる誘電体球の集合と考えることによって理解することができる。すなわちいま、フォトン STM とは逆に、光プローブ内部からの伝搬光によって光プローブ先端を照射した場合を考えると、伝搬光によってそれぞれの微小誘電体球の表面に作られた波長以下の微小な構造を持つ分極の分布は、それ

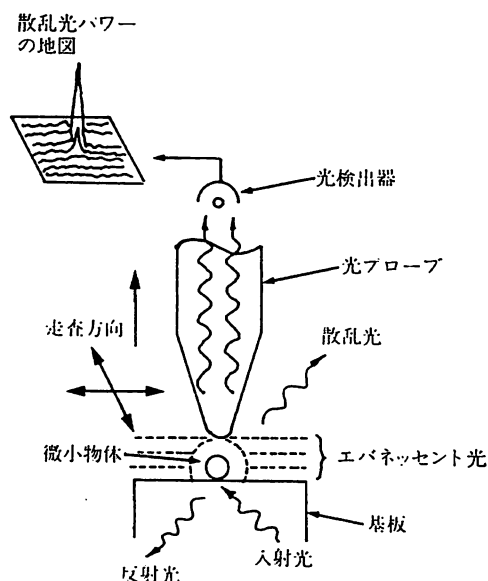


図 1 フォトン STM の原理

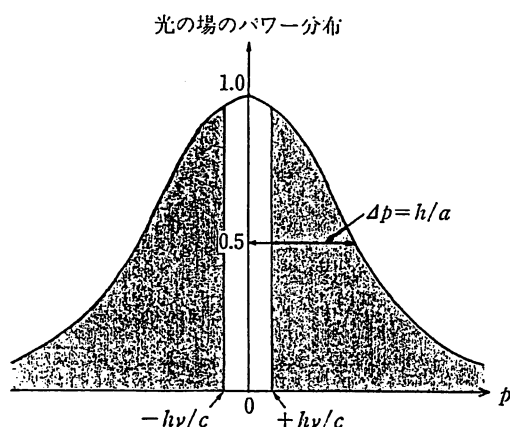


図 2 微小物体のまわりに局在した光の場の強度と運動量との関係。曲線の半値幅は $\Delta p = h/a$ 。運動量 $|h\nu/c|$ より大きい部分 (図の網かけの部分) がエバネッセント光である。

それぞれの微小誘電体球の大きさと同程度に局在したエバネッセント場をつくる。このエバネッセント場の分布を光プローブのエバネッセント場の波動関数と考える。この過程を時間反転して考えると、光プローブ先端の微小誘電体球は、その大きさと同程度に局在したエバネッセント場の中に置かれたとき、光プローブ内に伝搬光を効率よく発生することができる^{*1}。このことから、条件(1)および(A)のように、微小物体と光プローブ先端両者のエバネッセント場の波動関数が同程度に局在しており、しかも互いに重なりが大きいとき、微小物体のエバネッセント光は効率よく散乱され伝搬光となる。また、条件(2)および(B)のように、基板表面の荒い凹凸に対応す

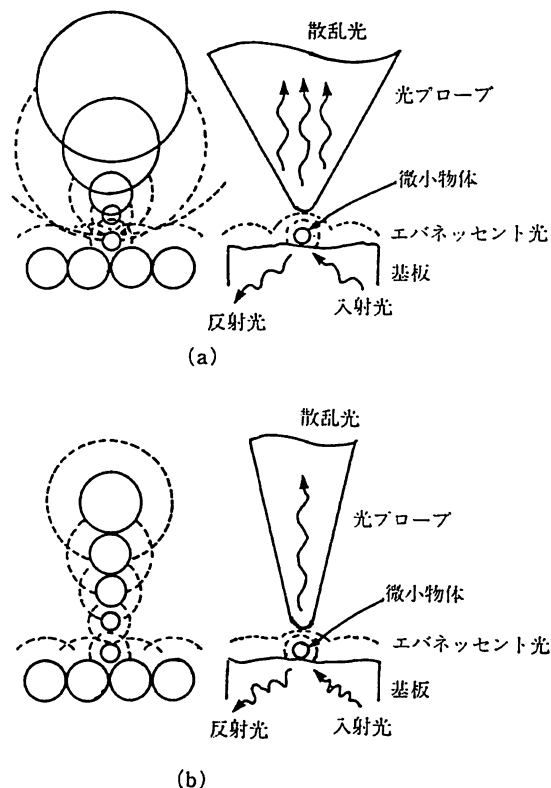


図3 フォトンSTMの分解能の説明。(a),(b)は各々円錐角の大きい、小さい光プローブを用いる場合。両図の左側は被測定微小物体、基板、光プローブを微小誘電体球の集合と見なした場合の説明図。

^{*1} このように、実際に電磁場がない場合でも光プローブ先端のエバネッセント場の波動関数を励起し得る電磁場の状態として考えるのは、電子STMの理論的取扱(本論文末の参考文献のうち30)を参照されたい)にあるように、微小物体とプローブの電子波動関数の重なり積分によるトンネル電流の表現を、フォトンSTMの場合にも適用できるものと考えていることによる。また、ナノメータ領域の分解能を持つフォトンSTMにおいては、光プローブ先端に励起される電磁場のエネルギーは一光子のエネルギーに近いものと考えられ、この点からも場の量子論的取扱が必要ではないかと考えられる。

る広がったエバネッセント光成分は光プローブの太い部分と一致するエバネッセント場の波動関数を持つが、光プローブ先端の円錐角が小さいとき、太い部分は基板から離れてしまい、両者の重なりが少ないので伝搬光への散乱効率は低くなる。

条件(1),(A)を微小物体と光プローブとの電磁相互作用という観点から見ると、次のように説明できる。微小物体の表面に光照射で作られた分極は、光プローブ先端に分極の分布を誘起する。このとき、微小物体と光プローブ先端の曲率半径が一致しないとき、光プローブ先端の分極分布が光プローブ内に誘起する伝搬光は干渉して消えてしまうが、両者の曲率半径が一致し、また両者の距離が曲率半径程度であるときには位相のそろった伝搬光を光プローブ内に発生する。また後で示すように、エバネッセント場の波動関数が一致するということは、フォトンSTMを仮想光子(エバネッセント光子)のトンネル過程として捉えた場合に、仮想光子交換の際の運動量保存則として表すことができる。

以上の条件により、高い分解能を得るためには先端曲率半径が小さいのみでなく円錐角の小さい光プローブが必要である。条件(A),(B)を満たす光プローブを微小物体から先端半径程度の距離を保って掃引すれば、これより細かい構造が微小物体表面にあってもそのようなエバネッセント光成分は伝達距離が短いため光プローブ先端で散乱されない。

このようにフォトンSTMは、被測定物体表面の微細な凹凸の空間周波数の中から帯域通過フィルタのように光プローブ先端の曲率半径に対応する細かさをもつ成分を選択的に抽出する装置であり、その分解能は光プローブ先端の曲率半径と円錐角で決定される。光プローブ先端の最小の凹凸の寸法を決めるのは当然のことながら原子である。したがって、原子寸法まで尖らせた光プローブを用意し、先端と微小物体表面との距離を原子寸法程度まで近づけて掃引することができれば原子レベルの分解能を実現し得る。このような原子レベルの分解能が実現したとき、フォトンSTMはその原理から「光誘起原子間力顕微鏡」と呼ぶこともできよう。これは原子間に働くファンデルワールス力を、仮想的な二個の光子の交換によって表したものと比較すると、フォトンSTMはそのうちの一光子を伝搬光によって外部から与えているものと見なすことができることによる。言い換えると、揺らぎによって自発的に発生した分極によるファンデルワールス力に対して、フォトンSTMでは光照射によって微小物体の表面に作られた分極による光プローブとの

電磁的相互作用を用いている。

3. 光プローブ作成と実験結果

光プローブとしては先端を鋭利に加工した誘電体や金属の針、または微小開口を用いることができるが、散乱光を高効率で収集できる導波路構造をもち、さらに2節の条件(A), (B)を満たすために化学エッチング法により先鋭化する方法が適用できる光伝送用の光ファイバを使用することが今のところ最も優れている。

単一モードファイバのコア部には GeO₂ がドーピングされていることを利用し、緩衝フッ酸により選択エッチングを行う。図4(a)は緩衝フッ酸溶液中の NH₄F の体積

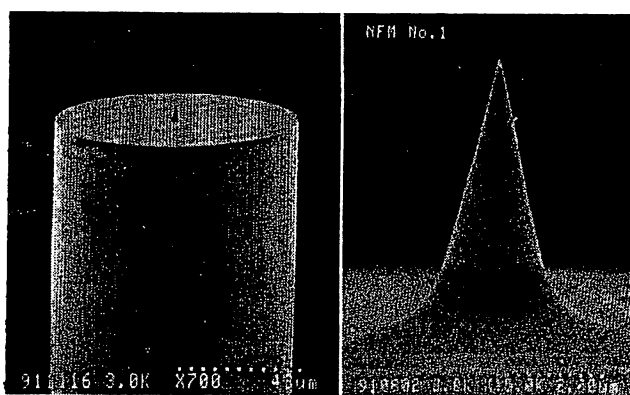
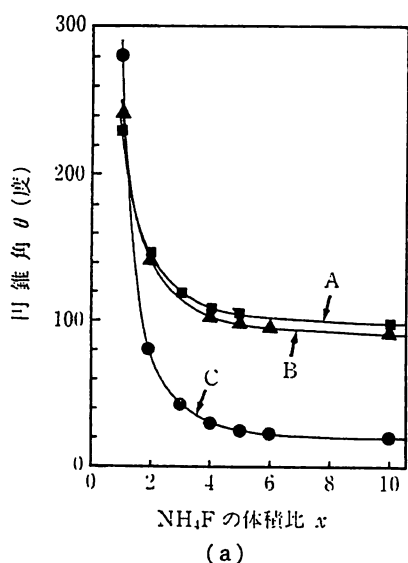


図4 (a)光ファイバ・コア先端の円錐角 θ の x 依存性¹²⁾。ここで x はエッチング溶液中の NH₄F の体積比であり、NH₄F : HF : H₂O = x : 1 : 1 と定義される。曲線 A, B, C は各々 GeO₂ のドーピング比が 3.6, 8.5, 23 モル % の光ファイバを使った場合。(b)コア先端を先鋭化した光ファイバの電子顕微鏡写真¹²⁾。左：光ファイバ端全体図。外径は 90 μ m。右：先端部の拡大図。写真の横幅は 5.6 μ m に相当。

比 x に対し、エッチングにより得られたコア先端の円錐角 θ の値をプロットしたものである¹²⁾。GeO₂ のドーピング量が多いほど小さい θ の値が実現している。現在までのところわれわれが得た θ の最小値は 20 度である。図中、 $\theta > 180$ 度の領域はコア先端が尖るのではなく、クラッド中にへこむことを表している。すなわち、このエッチング法はクラッドに対し、コアを凸状にも凹状にもできる。ちなみに、複数本のファイバを同時に同じ条件でエッチングした時に得られた θ の値の再現性を表す標準偏差値は 0.5 度であり、このことは本方法が高い再現性を有することを意味している。図4(b)は先鋭化されたコアを持つ光ファイバの先端形状を表す走査電子顕微鏡写真である¹²⁾。先端が鋭いために明瞭な像を得ることが困難であるが、この写真より先端曲率半径は 5 nm 以内と推定されており、現在までで国内外を通じ、最も鋭い光プローブとなっている。

このように選択エッチングにより先鋭化できる理由として、ファイバ線引きの段階で生じたファイバ断面内の残留応力分布、などが考えられているが、現在のところ先鋭化の素過程は明らかにされておらず、今後、光プローブの性能向上のためにはその解明が必要である。

なお、著者らは二段階エッチングにより、クラッド端部を切り欠くこと、また、マルチコアファイバ中の複数コアを同時先鋭化すること、などにも成功している¹³⁾。これらはフォトン STM の機能を拡大するための素子作成技術として有用である。

図5は筆者らのフォトン STM 装置である¹⁴⁾。装置の小型化、高信頼性のために光源として波長 0.8 μ m の光ディスク用半導体レーザーを用いている。光プローブ走査、画像処理、などの装置は STM, AFM などの技術

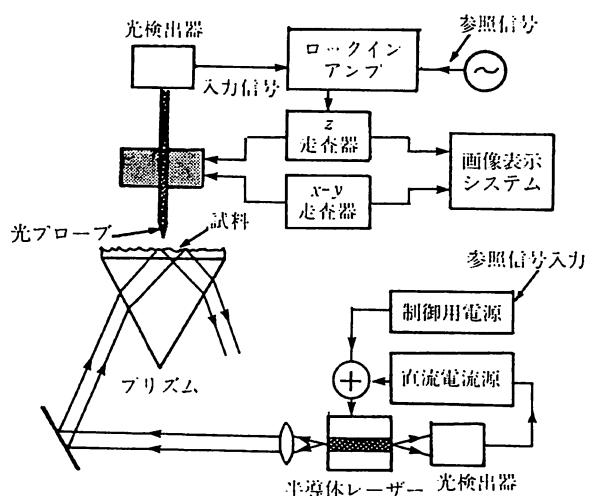


図5 フォトン STM の装置¹⁴⁾

が共通に使用できる. この装置により頭部直径 100 nm, 尾部の幅 9 nm, 長さ 100 nm のバクテリオファージ T4 を 2 本観測した結果を図 6 に示す¹⁵⁾. この他, ガラス基板の上に凝集した直径 80 nm のラテックス球集団¹⁴⁾, 周期 1.5 μm および 0.22 μm の格子が網の目状に直交し, 網の目の位置に直径 300 nm, 深さ 80 nm のピットを有する蛾の目形光ディスクの表面¹⁵⁾, など種々の試料形状が測定されている. これらはすべて空气中で非接触・非破壊測定されたものであり, 一連の実験により試料厚み方向分解能 2 nm 以内, 面内方向分解能 5 nm 以内, と推定されている. これらの分解能は光プローブの音響振動, 温度ドリフト, により制限されているが, 今後システム改良によりこれらの影響を低減し, 光検出雑音から決まる信号雑音比が得られれば, 分解能は 0.1 nm となると推定されている. すなわち 2 節で述べたように原子寸法レベルの値が期待される.

図 5 の装置では試料を透過したエバネッセント光パワーを検出しているのので, 透過形フォトン STM と呼ぶことができる. したがって分解能は数 pW の微弱な光パワー測定感度に依存する. これに対し, 波長より小さい直径の開口を持った短ファブリ・ペロー共振器を光プローブとして用い, これを試料面上を走査する際に試料形状によって生ずる共振器の共振周波数シフトを光位同期技術により検出する方法も提案されている¹⁶⁻²⁰⁾. これは

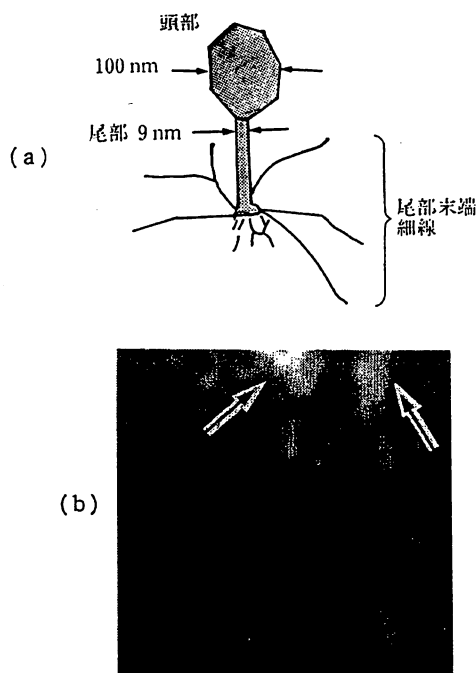


図 6 バクテリオファージ T4 の測定結果. (a) 形状説明図. (b) 測定結果¹⁵⁾. 二本の矢印の先の位置の一つずつ像が見られる. 写真の一边の幅は 0.6 μm に相当.

反射共振形フォトン STM と呼ばれているが, 光位同期ループの残留周波数揺らぎが 1×10^{-13} まで抑圧されているので²¹⁾, 測定感度は透過形に比べ 10 倍以上優れていることが数値解析により示されている¹⁶⁻²⁰⁾. 今後, 微小開口つきの高フィネス短ファブリ・ペロー共振器の製作を実現することが課題である.

4. フォトン STM の理論モデル

エバネッセント光とは波長以下の狭い領域で屈折率が急激に変化するように境界において (すなわち電磁波が伝搬する空間の一様性が破れたときに), あらわになった分極が作る電磁場である. したがってこれは微視的な領域での電磁波と物質との相互作用のあらわれであると言える. また, 遅延効果が無視できるほど狭い領域に局在する, 言い換えるとこの領域を光速で横切る時間に比べて電磁場の振動の一周期がはるかに長い, という意味で, エバネッセント光はクーロン相互作用に類似した準静的な相互作用を媒介する電磁場である. フォトン STM はこのようなエバネッセント光を媒介とした準静的相互作用を利用しているため, 通常の光学顕微鏡のような光の波としての性質を利用した場合に生じる回折限界をはるかに越える分解能を実現することができる.

従来の光学理論は電磁波の波長に比べて巨視的な系または遠視野に関わる問題を取り扱っているのので, 電磁波と物質との相互作用を媒質中では誘電率, 境界面では境界条件に繰り込んで扱っている. この理論を用いると, 波長に比べて平坦な誘電体と真空との境界の場合には, 全反射角で入射した平行光線によって生じるエバネッセント光を, 境界条件を表すフレネルの公式から導出することができる²²⁾. しかし, 電磁波の波長よりも小さい境界面に対してこのような波動光学的境界条件に基づく理論を適用しようとする種々の困難が生じ²³⁾, 相互作用の直接的取扱いが必要となる^{*2)}. 実際, 電磁波の一つの形態のように取り扱われる平坦な境界におけるエバネッセント光も, 実は境界条件によって入射波と反射波に結びつけられており, 物質表面に誘起された分極の間の相互作用を媒介する電磁場を表している.

このような相互作用を媒介している電磁場, すなわち

*2) もちろん, ナノメートル領域のフォトン STM においても境界は原子寸法に比べれば巨視的であり, 電磁気学的な境界条件を設定することは原理的に可能であると考えられるが, どのような境界条件が成立するのかは物質の電磁気的応答の直接的な取扱いから導く必要がある. 実際, そのような取扱いと複雑な多体相互作用を考慮した自己無撞着の方法による近視野光学顕微鏡の理論的検討も存在する (参考文献 26) を参照されたい).

エバネッセント光, を観測するためには, 光プローブとなる物質を場の中に置き, 物質表面の相互作用に攪乱を与え, エバネッセント光を外部に取り出せる伝搬光に変換することが必要である. このとき, 光プローブの存在によってエバネッセント光の分布が変化すること, すなわち, 測定が破壊的に行われることを考慮しなくてはならない. 特にナノメータ領域を取り扱うフォトン STM の場合, 相互作用に関与する光子数が少ないと考えられるので, このような変化は重大である. このような効果は摂動論的取扱いにおいては, 多重散乱やその干渉などの多体効果として表される. このような現象を正しく取扱い, フォトン STM の理論解析を行うためには, 場の理論などの量子力学的手法を利用することが有効であると考えられる.

フォトン STM の素過程解析に用いる微小物体と光プローブのモデルとして, 図 7 に示す, (a) 近接して置かれた二つの微小開口, (b) 近接して置かれた二つの微小誘電体球を考える⁹⁾. いずれの場合にも, 微小物体と光プローブとを同時に置いて, その相互作用を取り扱うことが重要である. モデル(a)に関しては, 単一微小開口における境界条件からのエバネッセント光分布の計算法が提案されているが²³⁻²⁵⁾, 光プローブをも含め多重散乱

を考慮した場合の正しい境界条件は明らかにされていない. また, 微小物体と光プローブの間の力の伝達などの機構も明らかにならない. モデル(b)に対しては多体相互作用の摂動計算による取扱いが試みられているが²⁶⁾, 自己無撞着な計算はきわめて複雑であり, 得られた結果は見通しのよいフォトン STM の描像を与えない.

以上の背景をもとに筆者らは, フォトン STM の理論的取扱いにおいて, その素過程が局在したエバネッセント光を媒介とする準静的な近距離相互作用であることと, 大きな運動量をもつエバネッセント光の交換にともしない力学的作用があること, の二点に注目すれば, トンネル電子による STM の取扱いに用いられる仮想粒子の交換, 共鳴エネルギー, トンネル効果, などの理論と類似した直感的に理解しやすいモデルを作ることができる. と考え, このような素過程を統一して図 7 (c) に示すようなダイアグラムで表現することを提案している²⁷⁾. ダイアグラムは横軸を空間, 縦軸を時間とし, 微小物体と光プローブ先端をそれぞれ縦の太線で描き, これらの間の準静的な近距離を仮想粒子の交換によって表す. ここで微小物体を太線と網かけにより表したのはこれらが多くの原子からなる多体系であることを示すためである. 入射波のように描いた部分は物質内部の伝搬波をまとめて表している. 仮想粒子は入射波によって微小物体それ自身と光プローブ先端との間に生じた原子レベルの複雑な相互作用, すなわち多体効果を繰り込んだものであると考える.

電子による STM の場合, 入射波, 散乱波は電子のプロホ波に, 仮想粒子はトンネル電子に対応する. フォトン STM では入射波と散乱波は伝搬光であり, また仮想粒子は仮想光子 (virtual photon) としてのエバネッセント光である (なおここで, トンネル電子を電子のエバネッセント波として表現している量子力学の教科書²⁸⁾もあることを記しておく). ダイアグラム各頂点には微小誘電体としての微小物体および光プローブ先端の電磁相互作用の強さを表す定数と, エネルギー, 運動量の保存則が与えられる. このように描けば, 伝搬光からエバネッセント光への変換はラマン散乱と類似の過程であるとみなせることがわかる²⁵⁾.

微小物体近傍に局在したエバネッセント光は二つの運動量成分を持つ. すなわち, 空間的な指数関数的減衰を表す虚数の運動量成分と, これに直交する自由光子の運動量よりも大きな運動量成分である. このような電磁場の持つ過剰な運動量は, 相互作用によって生じた物質の機械的歪みなどに対応する力学的運動量であることが,

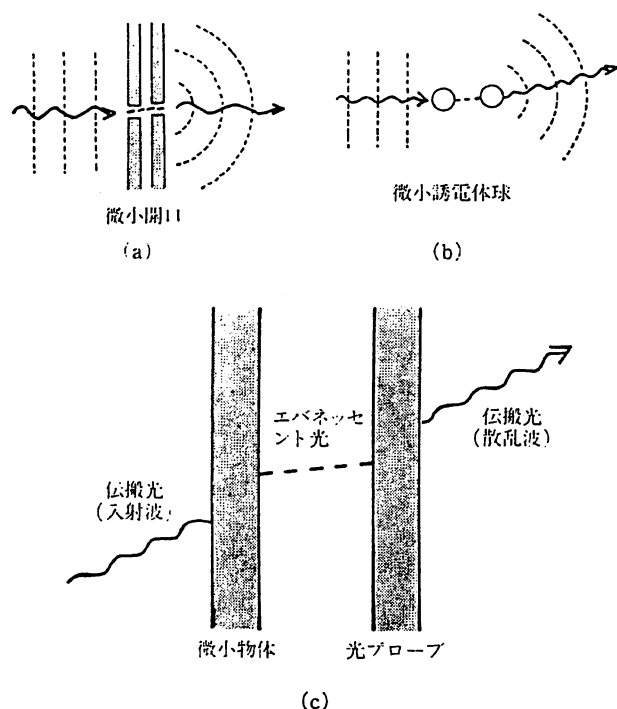


図 7 フォトン STM における微小物体と光プローブの間の相互作用を取り扱うためのモデルとして, (a) 近接して置かれた二つの微小開口, (b) 近接して置かれた微小誘電体球, を考え, (c) 微小物体-光プローブ間の相互作用を統一的にダイアグラムによって表す.

Gordon によって示されている²⁹⁾. このような大きな運動量を持つエバネッセント光を媒介として起こる相互作用は, 物体間に力学的相互作用を生じる. 図7(c)のダイアグラム各頂点での運動量保存則が, このような仮想光子のトンネリングと同様に被測定物体とプローブとの間に働く力を表している. ここでエバネッセント光の運動量が場の空間的広がり, すなわちエバネッセント場の波動関数を決定することに注意すると, 微小物体と光プローブ先端の間の運動量保存の条件は, 両者のエバネッセント場の波動関数が一致するという条件に対応する.

このような力学的作用の存在は各種のトンネル顕微鏡に共通の重要な性質であると考えられる. 実際, 原子レベルの分解能を持つ電子STMにおいて, トンネル電流に伴って引力が働き分解能を高めることが知られており, この力は物体とプローブの電子の波動関数の重なり積分によっても, トンネル電流の積分によっても与えられることが Chen によって示されている³⁰⁾. AFM では, ピックアップの変位によって直接測定される原子間力を, 二つの仮想光子の交換に伴う運動量のやり取りによって表すことができる.

以上のような観点から, 複素数の運動量を持つエバネッセント光の場を, 微小物体の寸法に対応するコンプトン波長をもつ仮想光子(重い光子)とみなし, その伝達を湯川ポテンシャルで表すものとする. このことは, 現象の理解を容易にするのみならず, 多体相互作用に関わる摂動計算を省略してエバネッセント光の場の分布を見積ることを可能にする. 図8は円形微小開口の中心軸上のエバネッセント光の強度分布を, 開口の半径に等しいコンプトン波長を持つ仮想光子の寄与として湯川ポテンシャルの単純な足し合わせから計算し, これに遠視野の強度を足し合わせた結果である. この結果は Leviatan による境界条件を用いた数値計算の結果²⁵⁾をよく再現し

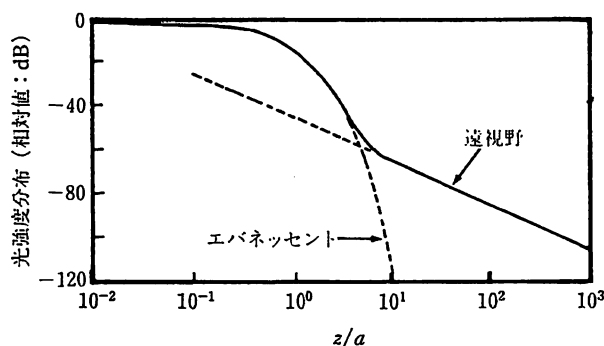


図8 半径 $a(= \lambda/50)$ の微小開口の中心軸上の光強度分布を, コンプトン波長 a に対する湯川ポテンシャルの重ね合わせから計算した結果²⁷⁾

ている. 同様の方法を用いれば, 任意の形状をもつ散乱体について, エバネッセント光の分布を良い近似で推定できると考えられる. 2節に述べたフォトンSTMの分解能の考え方によれば, 重要なのはエバネッセント光の全強度分布ではなく, 空間周波数で区別されるエバネッセント場の波動関数の各成分の大きさである. このことから, コンプトン波長を変数として, 微小物体と光プローブ先端の間の相互作用を計算することは有用である.

5. 可能な応用と今後の課題

従来の STM, AFM などと比較すると現在のフォトンSTMの分解能はまだ低いが, 原理的には2節に示したとおり, これらと同等の分解能が可能である. 従来の超高分解能顕微鏡に対しフォトンSTMは次の利点を有すると考えられる.

- (1) 試料表面に金属膜をコーティングする必要がないので非接触・非破壊測定ができる.
- (2) 光源波長掃引により試料の分光特性測定ができる.
- (3) 溶液中での測定が可能である.
- (4) 特に半導体レーザーを光源として使う場合, そのパワー変調周波数帯域が広く, 100 MHz 程度の高速変調可能なので, 同期検波による信号増幅の増幅数を $1 \mu\text{s}$ 以下まで短くし, 短時間で測定可能である.

以上の利点により, 次の応用が可能と考えられる.

- (1) 固体表面に吸着した単原子層の分光.
- (2) 量子井戸層など, サブミクロン寸法素子の形状評価.
- (3) 光ファイバ後端からレーザー光を入射した時に先端にしみ出すエバネッセント光による有機薄膜への超高密度光記録.
- (4) 前項(3)と同様に光ファイバ先端にしみ出すエバネッセント光を用い, その光の中に単一中性原子を捕獲し運動制御すること. さらにそれによる単原子レベルの極微結晶成長^{5-9, 20, 27)}. 同様に生体微粒子の運動制御.

これらのうち, (3), (4)はフォトンSTMを顕微鏡としてではなく, 微粒子の操作装置(manipulator)として使うことに対応する(したがって, 装置の略名は依然としてフォトンSTMであるが, 末尾のMの意味が異なる).

フォトンSTMの性能をさらに向上させ, これらの

応用に用いるためには光プローブ先端の一層の先鋭化、フォトン STM の試料基板上への試料固定法の確立、さらには試料に適した波長を持つコヒーレント光源の開発^{31,32)}、などの実験技術上のいくつかの問題を解決する必要がある。また、三次元的に局在したエバネッセント光の理論解析を行い、より進んだ装置設計指針を得るためには従来の波動光学理論から脱却し、場の理論、素粒子論、などに立脚した基本的な問題に取り組み、新しい「極微空間局在光学」の学問体系を構築する必要があることを付記したい。

6. おわりに

フォトン STM に関するアイデアは古いが、その実験と理論的研究の歴史は浅い。さらに、この装置は単に超高倍率顕微鏡としてのみに留まらず原子運動の制御にも使えることがわかってきた。ここ数年、研究が活発化しており、今年はこの分野に関する国際的なワークショップが開かれるまでに至った (Workshop on Near Field Optics, 1992 年 10 月, フランス・ブザンソン市において)。わが国の誇る光ファイバ技術、レーザー技術をもとにフォトン STM の著しい技術的進歩が見られるが、今後は理論的研究が進み、新しい光学が拓かれることを期待したい。

理論的なことからに関して有益なご助言をいただいた京都大学藪崎努教授、北野正雄助教授に感謝いたします。光ファイバに関し有益なご議論をいただいたアンリツ(株)古田土節夫博士、藤倉電線(株)宮本末広氏、また、生体試料に関して指導いただいた東京工業大学猪飼篤教授、さらに研究を推進した著者の研究室所属の学生諸氏、特に原稿作成段階で討論と援助をいただいた蔣曙東博士に感謝します。なお、この研究の一部は文部省科学研究費補助金一般研究 (B) (課題番号 02452084, 03452089) およびマツダ財団からの研究費補助を受けて行われた。

文 献

- 1) 大津元一：“フォトン走査トンネル顕微鏡”，*触媒*, **32** (1990) 548-550.
- 2) 蔣 曙東, 富田直幸, 大津元一：“フォトン走査トンネル顕微鏡”，*光学*, **20** (1991) 134-141.
- 3) 大津元一, 蔣 曙東, 大澤日佐雄：“フォトン走査トンネル顕微鏡”，*レーザー研究*, **19** (1991) 839-848.
- 4) 大津元一：“フォトン走査トンネル顕微鏡とその展開”，*O plus E*, **138** (1991) 90-97.
- 5) 大津元一：“光による単一原子の運動制御”，*精密工学会誌*, **58** (1992) 410-414.
- 6) 大津元一：“光 STM による極微細加工技術”，*金属*, 1992 年 3 月号, 39-44.
- 7) 大津元一：“「フォトン STM」で何が可能か？”，*エレクトロニクス*, 1992 年 4 月号, 68-72.
- 8) 大津元一：“フォトン STM”，*バウンダリー*, 1992 年 5 月号, 10-13.
- 9) 堀 裕和：“フォトン走査トンネル顕微鏡とその理論的解釈”，*応用物理*, **61** (1992) 612-616.
- 10) S. John：“Localization of light,” *Phys. Today*, May (1991) 32-40.
- 11) U. Durig, D.W. Pohl and F. Rohner：“Near field optical scanning microscopy,” *J. Appl. Phys.*, **59** (1986) 3318-3327.
- 12) T. Pangaribuan, K. Yamada, S. Jiang, H. Ohsawa and M. Ohtsu：“Reproducible fabrication technique of nanometric tip diameter fiber probe for photon scanning tunneling microscope,” *Jpn. J. Appl. Phys.*, **31** (1992) 印刷中.
- 13) P. トガル, 山田和延, 蔣 曙東, 大澤日佐雄, 大津元一：“フォトン STM 用ファイバプローブの高再現性製作法”，第 53 回応用物理学会学術講演会, 平成 4 年 9 月, 発表予定.
- 14) S. Jiang, N. Tomita, H. Ohsawa and M. Ohtsu：“A photon scanning tunneling microscope using an Al-GaAs laser,” *Jpn. J. Appl. Phys.*, **30** (1991) 2107-2111.
- 15) S. Jiang, H. Ohsawa, K. Yamada, T. Panagaribuan, M. Ohtsu, K. Imai and A. Ikai：“Nanometric scale biosample observation using a photon scanning tunneling microscope,” *Jpn. J. Appl. Phys.*, **31** (1992) 2282-2287.
- 16) M. Ohtsu, K. Nakagawa, S. Jiang and N. Tomita：“Super-resolution photon scanning tunneling microscope,” *Third Optoelectronics Conference* (電子情報通信学会, 東京, 1990) pp. 166-167.
- 17) S. Jiang, N. Tomita, K. Nakagawa and M. Ohtsu：“Proposal of super-sensitive reflection-mode phase-locked photon scanning tunneling microscope by diode lasers,” *Third Optoelectronic Conference* (電子情報通信学会, 東京, 1990) pp. 170-171.
- 18) S. Jiang, N. Tomita, K. Nakagawa and M. Ohtsu：“Super-resolution photon scanning tunneling microscope using diode lasers,” *Conference on Lasers and Electro-Optics* (Opt. Soc. Am., Washington, D.C., 1991) pp. 420-421.
- 19) S. Jiang, H. Ohsawa, N. Tomita and M. Ohtsu：“Photon scanning tunneling microscope using diode lasers,” *OSA Annual Meeting* (Opt. Soc. Am., Washington, D.C., 1991) p. 65.
- 20) M. Ohtsu：“Photon STM, application to biotechnology and single atom crystal growth,” *New Trends on Scanning Optical Microscopy* (光産業技術振興協会, 東京, 1992) pp. 67-71.
- 21) C.-H. Shin and M. Ohtsu：“Heterodyne optical phase-locked loop by confocal Fabry-Perot cavity coupled AlGaAs lasers,” *IEEE Photon. Technol. Lett.*, **2** (1990) 297-300.
- 22) C.K. Carniglia and L. Mandel：“Quantization of evanescent electromagnetic waves,” *Phys. Rev.*, **D 3** (1971) 280-296.
- 23) C. J. Bouwkamp：“Diffraction theory,” *Rep. Progr. Phys. (Lond. Phys. Soc.)*, **17** (1954) 35-100.
- 24) H. A. Bethe：“Theory of diffraction by small holes,” *Phys. Rev.*, **66** (1944) 163-183.
- 25) Y. Leviatan：“Study on near-zone fields of a small aperture,” *J. Appl. Phys.*, **60** (1986) 1577-1583.

- 26) C. Girard and D. Courjon: "Model for scanning tunneling optical microscopy: A microscopic self-consistent approach," *Phys. Rev.*, **B42** (1990) 9340-9349.
- 27) H. Hori, S. Jiang, M. Ohtsu and H. Ohsawa: "A nanometer-resolution photon scanning tunneling microscope and proposal of single atom manipulation," *The 18th International Quantum Electronics Conference* (Institut für Nachrichtentechnik der TU Wien, Vienna, 1992) pp. 48-49.
- 28) C. Cohen-Tannoudji, B. Diu and F. Laloe: *Quantum Mechanics* (Wiley-Interscience, New York, 1978).
- 29) J.P. Gordon: "Radiation forces and momenta in dielectric media," *Phys. Rev.*, **A8** (1973) 14-21.
- 30) C.J. Chen: "Attractive interatomic force as a tunnelling phenomenon," *J. Phys. Condens. Mater.*, **3** (1991) 1227-1245.
- 31) M. Ohtsu, K. Nakagawa, C.-H. Shin, H. Kusuzawa, M. Kouroggi and H. Suzuki: "Progress toward a 1-PHz hyper-coherent optical sweep generator by semiconductor lasers," *Conference on Lasers and Electro-Optics* (Opt. Soc. Am., Washington, D.C., 1990) paper number CME5.
- 32) H. Kusuzawa, E. Ikegami, H. Furuta, K. Nakagawa and M. Ohtsu: "Proposal of a semiconductor laser diode based Peta Hertz class coherent optical sweep generator," *Third Optoelectronics Conference* (電子情報通信学会, 東京, 1990) pp. 174-175.

大津 元一 (東京工業大学総合理工学研究科 227 横浜市緑区長津田 4259)

1. はじめに

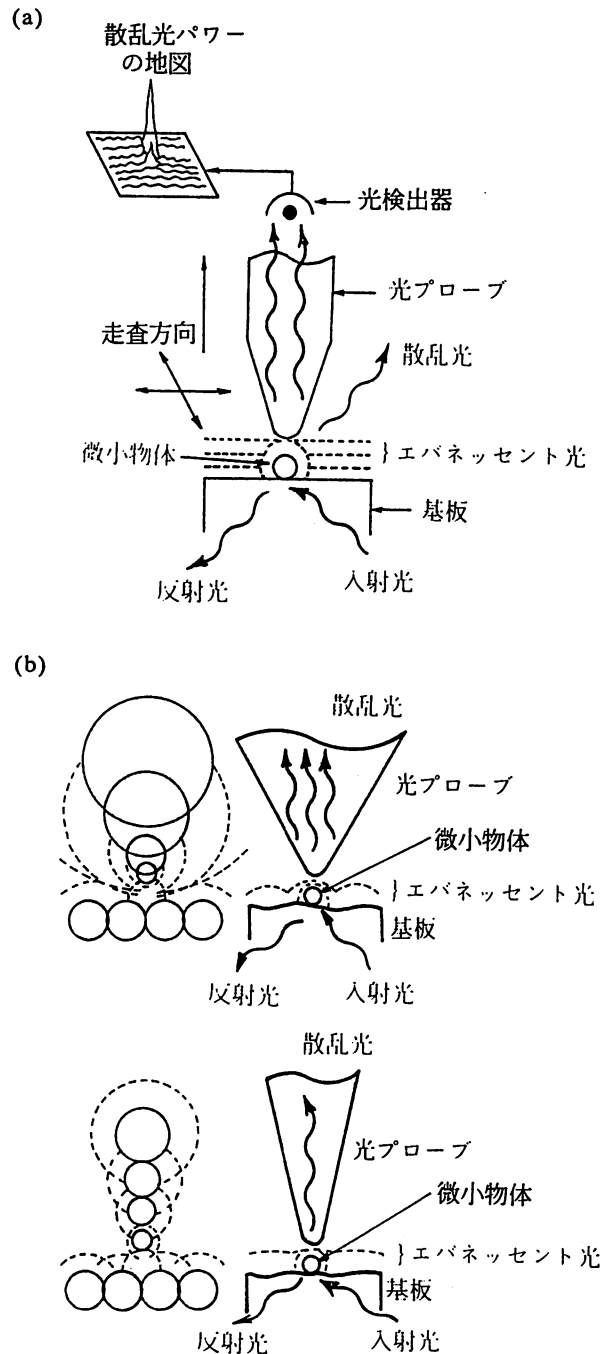
光学顕微鏡の分解能は光の回折の特性によって決まる。この回折限界のために波長より小さい物体の像は観測できない。これは従来の教科書に記述されている通りの事実であるが、それは光が波長より小さい寸法の領域に局在しない性質に起因する。より高い分解能を得るために、光の代わりに電子線を用いた顕微鏡が使われ、さらに最近ではトンネル電子を用いた走査トンネル顕微鏡 (STM) により原子レベルの分解能が実現しているのは周知の通りである。

しかし上記のような光ではなく、微小空間に局在した別形態の光を使うと、回折限界を越える分解能が得られる。^{1,2)} この光は、従来の光学の用語ではエバネッセント光と呼ばれる。これを用いた計測方法のアイデアは、20世紀初頭にアインシュタインが友人に宛てた手紙の中に記してあると言われている。しかし、本格的な実験が試みられるようになったのは1980年代後半以降で、現在に至るまでこの光の実体を記述する精密な理論はまだ完備していない。この装置は近視野顕微鏡 (near field microscope) などとも呼ばれているが、³⁾ 以下の議論により分かるように、物体表面に局在した光を利用し、分解能がハイゼンベルグの不確定性原理によって決まること、さらにトンネル電子を使った STM と類似であることから、著者らは「フォトン走査トンネル顕微鏡 (フォトン STM)」という名称を用いている。^{1,2)} この装置は物理計測・分析、さらに極微小物体の運動制御・操作などに広い応用可能性を示す。本稿では筆者らの研究を中心に、その動作原理、性能等を紹介したい。

2. 原理と分解能

物体表面から放射する光には、前節冒頭に示したような

図1 (a) フォトン走査トンネル顕微鏡 (フォトン STM) の原理。 (b) フォトン STM の分解能。図の上、下は各々大、小の円錐角の光プローブを用いる場合。両図の左側には被測定微小物体、基板、光プローブを微小球の集合と見なした場合の概念図を示した。基板表面の粗さに対応する球と同じ大きさの球が光プローブ側にもあるが、その位置は、円錐角の小さい光プローブの方が、光プローブ先端から遠い。従って、基板表面の粗さの影響を受けず、微小物体のみを選択的に検出するには、後者の光プローブの方が高い分解能が得られる。(大津元一、堀裕和：計測と制御 31 (1992) No. 9 より転載。)



「通常の光」の他に、物体表面に局在するエバネッセント光が含まれる。この光は後述のように「波長より小さい寸法の領域に局在し、自由空間を伝搬しない」性質を持っている。そこで、図1(a)に示すように光プローブを走査しながら微小物体表面に局在するエバネッセント光を散乱し、散乱光パワーの地図を作れば、物体形状が測定できる。測定の分解能は光プローブ先端の寸法により決まる。この寸法が光波長より小さければ、通常の光の回折限界をはるかに越える超高分解能光学顕微鏡が実現できる。

半径 a が光波長 λ よりずっと小さい微小な測定対象物体が、平面基板上に置かれている場合を考える。ハイゼンベルグの不確定性原理 $\Delta x \cdot \Delta p \sim h$ (h はプランク定数) から、この微小物体近傍に発生したエバネッセント光の場合は、 $\Delta x \sim a$ に対応して $\Delta p \sim h/a$ なる運動量を持つ。この運動量成分は微小物体表面に平行で、通常の光の運動量より大きいため、分散関係によると法線方向運動量が虚数となる。すなわち、エバネッセント光は自由空間を伝搬できず、 $a \ll \lambda$ なる寸法の微小物体の近傍に局在している。このような複素の運動量をもつエバネッセント光の場を、微小物体の寸法 a に等しいコンプトン波長をもった仮想光子(重い光子)とみなし、その伝達を湯川ポテンシャルで表すと、現象の理解・解析が容易になる。²⁾ エバネッセント光の分布を、複素の運動量をもつ「エバネッセント場の波動関数」と呼ぶことにすると、微小物体近傍のエバネッセント光を散乱して検出し、微小物体の像を描くためには、次の条件が必要となる。

- (1) 微小物体と光プローブの両者のエバネッセント場の波動関数に、互いに一致する成分が存在すること。
- (2) 微小物体のエバネッセント場の波動関数よりも広がった成分は散乱されないこと。

フォトン STM に用いられる光プローブの形状には、これらの条件を満たすために、次の条件が課せられる。

- (A) 光プローブ先端の曲率半径が、微小物体の半径 a 程度に小さいこと。
- (B) 光プローブ先端の円錐角が十分に小さいこと。

(A) は上記 (1) に対応し、微小物体のエバネッセント光が光プローブ先端で効率よく散乱され通常光に変換されることを示す。これに対して、(B) は (2) に対応する。エバネッセント光は基板表面の粗さによって広がった分布となる。これが光プローブの太い部分のエバネッセント場の波動関数と重なると散乱される。

(B) は、このような散乱が生じないための条件である。このことは、図1(b)に示すように、光プローブが半径の異なる微小球の集合体であると考えれば、容易に理解される。微小物体と光プローブのエバネッセント場の波動関数が一致することは、微小物体と光プローブ先端のエバネッセント光子の間に運動量保存則が成立し、トンネル過程が生じることに対応する。

以上の条件より、高い分解能を得るためには、先端曲率半径が小さいのみでなく、円錐角の小さい光プローブが必要であることがわかる。条件 (A), (B) を満たすような光プローブを作るためには、光ファイバを化学エッチング法により尖鋭化する方法が今のところ最も優れている。条件 (A), (B) を満たす光プローブを、微小物体から先端半径程度の距離を保って掃引する。微小物体表面には a よりもさらに細かい構造が存在しているが、それによって生じる減衰距離の短いエバネッセント光成分は散乱されない。このように、フォトン STM は、被測定物体表面の微細な凹凸の空間周波数の中から、光プローブ先端の曲率半径に対応する細かさを持つ成分を、帯域通過フィルタのように、選択的に抽出する装置である。その分解能は光プローブ先端の曲率半径と円錐角で決定される。光プローブ先端の凹凸の最小寸法を決めているのは、当然のことながら原子である。従って、光プローブ先端と微小物体表面との距離を原子寸法程度まで近づけることができれば、原子レベルの

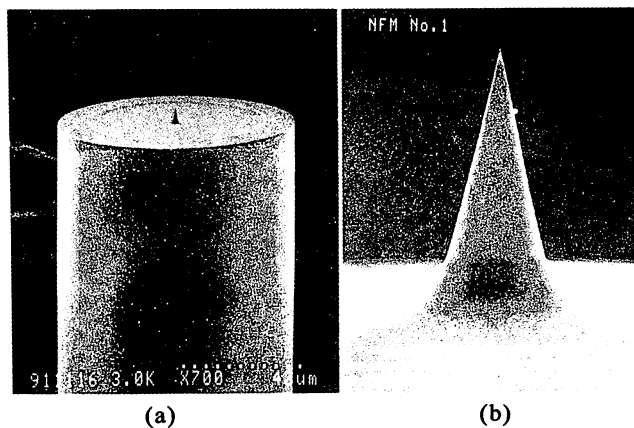


図2 コア先端を先鋭化した光ファイバの電子顕微鏡写真。(a) 光ファイバ先端全体図。外径は $90 \mu\text{m}$ 。(大津元一: 金属 (1992) 3月号, 39より転載。)(b) 先端部の拡大図。写真の横幅は $5.6 \mu\text{m}$ に相当。(S. Jiang, H. Ohsawa, K. Nakagawa, M. Ohtsu, K. Imai and A. Ikai: Jpn. J. Appl. Phys. 31 (1992) 2282より転載。)

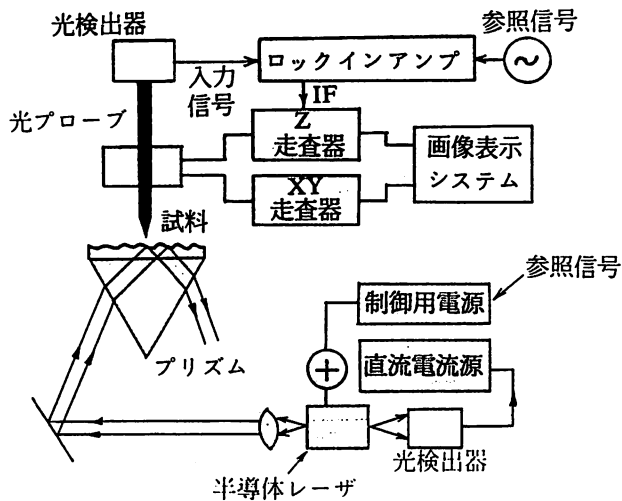


図3 フォトンSTMの装置。⁶⁾(大津元一, 他: レーザー研究 19 (1991) No. 8, 839より転載)

3. 装置と測定例

実際の光プローブとしては、先端鋭化のための加工再現性が高いこと、および散乱したエバネッセント光を効率よく導波・集光できること、が重要である。これを実現するために、筆者らは光通信などで用いられている光ファイバを用いている。弗酸系溶液を用いた化学エッチングにより加工された光ファイバ先端の電子顕微鏡写真を図2に示す。光ファイバ・コア円錐角と先端曲率半径の最小値としては、各々20度、5 nm以内が得られている。⁴⁾ この光ファイバを用いることにより、従来のピペットなどを用いる方法⁵⁾よりも約1桁以上高い分解能が実現でき、さらに、光ファイバ走査中に測定試料面と外周部とが接触することを

防ぐため、2段階エッチングにより光ファイバ・クラッド外周部の角を落すことも可能である。また、クラッド中に複数のコアがあるマルチコア・ファイバの加工も可能となっている。これは測定感度を向上させるための作動光プローブ、測定物体の動的振舞を調べるマルチ・プローブとして有望である。

図3は筆者らの用いている測定装置である。¹⁾ 装置の小型化、高信頼性のために光源としては波長0.8 μm の半導体レーザーを用いている。図4には、頭部直径100 nm、尾部幅9 nm、長さ100 nmのバクテリオファージT4が2体、空気中で観測されている像を示す。⁴⁾ この他、直径300 nm、深さ80 nmのピットを有する蛾の目形光ディスクの表面、⁴⁾ 直径80 nmのラテックス球群、⁶⁾ などの像が観測されている。以上の結果は、いずれも空気中で非接触・非破壊測定されたものである。これらの一連の実験により、試料の厚み方向の分解能2 nm以内、面内方向の分解能5 nm以内、と推定されている。これらの分解能は光プローブの音響振動、温度ドリフト、などにより制限されているが、システム改良によりこれらの影響を低減し、光検出雑音から決まる分解能が達成されれば、その値は0.1 nmとなると推定される。⁴⁾ すなわち2節で記したように原子寸法レベルの値が期待される。

なお、図3の装置では、試料を透過したエバネッセントの光パワーを検出しているので、透過形フォトンSTMと呼ぶことができる。その分解能は数pWの微弱な光パワー測定感度に依存する。これに対して、波長より小さい直径の開口を持った短ファブリ・ペロー共振器を光プローブとし、これを試料面上で走査する際に、試料形状によって生じる共振器の共振周波数シフトを光位同期技術により検出する方法も提案されている。⁷⁾ これは反射共振形フォトンSTMと呼ばれている。光位同期ループの精度は 1×10^{-18} に達しているので、⁸⁾ 数値解析によると測定感度は透過形に比べて10倍以上優れていることがわかっている。⁷⁾ 今後、フィネスが高い短光路ファブリ・ペロー共振器の製作を実現することが課題である。

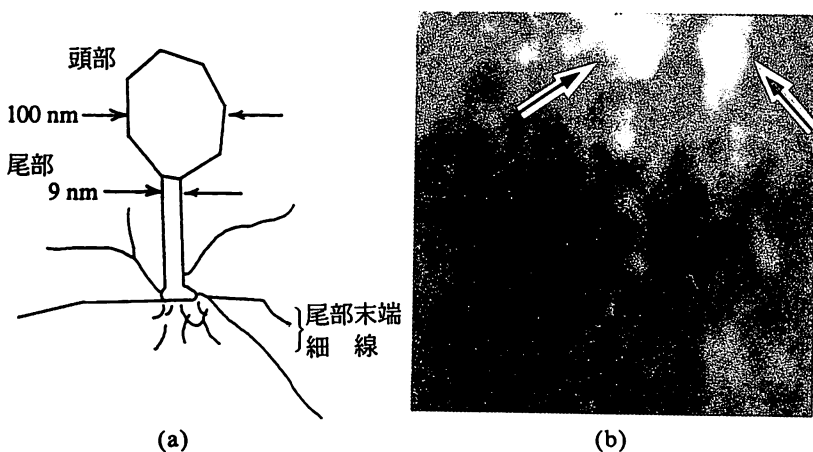


図4 バクテリオファージT4の測定結果。⁴⁾(a) 形状説明図。(b) 測定結果。二本の矢印の先の位置に一つずつ像が見られる。写真の一边の幅は0.6 μm に相当。(H. Ohsawa, K. Yamada, T. Pangaribuan, M. Ohtsu, K. Imai and A. Ikai: Jpn. J. Appl. Phys. 31 (1992) Pt. 1, No. 7より転載)

4. 応用と今後の課題

従来の走査トンネル顕微鏡、原子間力

顕微鏡などと比較すると、現在のフォトン STM の分解能はまだ低い。しかし原理的には、2 節に示したとおり、これらと同等の分解能が可能である。従来の超高分解能顕微鏡に対して、フォトン STM は次の利点を有する。

- (1) 試料表面に金属膜をコーティングする必要などがないので、非接触・非破壊測定ができる。
- (2) 光源波長掃引により試料の分光特性が測定できる。
- (3) 溶液中での測定が可能である。
- (4) 半導体レーザーを光源として使うと、そのパワー変調周波数帯域が広く、100 MHz 程度の高速変調が可能であるため、同期検波による信号増幅の時定数を $1 \mu\text{s}$ 以下まで短くできる。これによって、短時間での測定が可能となる。

以上の利点を利用して、次のような応用の可能性が考えられる。

- (1) 固体表面に吸着した単原子層の分光。
- (2) 光ファイバ後端からレーザー光を入射し、先端にしみ出すエバネッセント光により有機薄膜に光記録を行うこと。
- (3) 前項と同様なエバネッセント光による中性単原子や生体微粒子の捕獲・運動制御、それによる極微結晶成長。^{2,9)}

これらのうち (2), (3) は本装置を顕微鏡 (microscope) としてではなく、操作器 (manipulator) として使うことに対応する (従って、装置の略名は依然としてフォトン STM であるが、末尾の M の意味が異なる)。しかしいずれの意味で利用するとしても、現在のフォトン STM の性能を向上させ、これらの応用を可能にするためには、光プローブ先端をさらに尖鋭化させること、フォトン STM の試料基板上に試料を固定する方法を確立するなど、実験技術上のいくつかの問題を解決する必要がある。さらに、三次元的に局在したエバネッセント光の理論解析を行い、より進んだ装置を設計する指針を得る必要がある。そのためには、従来の光学理論から脱却し、場の理論、素粒子論などに立脚した基本的な問題に取り組み、²⁾ 新しい「極微空

間局在光学」の学問体系を構築する必要がある。

5. おわりに

フォトン STM に関するアイデアは古いが、その実験と理論的研究の歴史はまだ浅い。さらに、この装置は、単に超高倍率顕微鏡としてのみに留まらず、原子運動の制御にも使える可能性を持つことがわかってきた。ここ数年、研究が活発化しており、今年はこの分野に関する国際的なワークショップが開かれるまでに至った (Workshop on Near Field Optics, 1992年10月, フランス, ブザンソン)。わが国の誇る光ファイバ技術、レーザー技術をもとに、工学的視野に立った研究が発展しているが、今後は理学的な視野からの研究が必要とされる段階に至っている。この機会に本誌読者の方々からの教示を得ることができれば幸いである。

理論面に関し、山梨大学助教授の堀裕和博士に多くのご討論を賜り、ここに感謝します。

参考文献

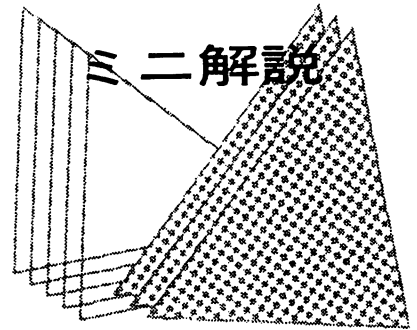
- 1) 大津元一, 蔭 曙東, 大澤日佐雄: レーザー研究 **19** (1991) 839.
- 2) 堀 裕和: 応用物理 **61** (1992) 612.
- 3) U. Ch. Fischer, U. T. Durig and D. W. Pohl: Scanning Microsc. **3** (1989) 1.
- 4) S. Jiang, H. Ohsawa, K. Yamada, T. Pangaribuan, M. Ohtsu, K. Imai and A. Ikai: Jpn. J. Appl. Phys. **31** (1992) 2282.
- 5) R. C. Redick, R. J. Warmack, T. L. Ferrel: Phys. Rev. B. **39** (1989) 767.
- 6) S. Jiang, N. Tomita, H. Ohsawa and M. Ohtsu: Jpn. J. Appl. Phys. **30** (1991) 2107.
- 7) S. Jiang, N. Tomita, K. Nakagawa and M. Ohtsu: *Technical Digest of the 3rd Optoelectronics Conf., Makuhari, 1991*, 論文番号 12D1-3.
- 8) C.-H. Shin and M. Ohtsu: IEEE Photonics Technol. Lett. **2** (1990) 297.
- 9) H. Hori, S. Jiang, M. Ohtsu and H. Ohsawa: *Technical Digest of the 28th Int. Quantum Electronics Conf., Vienna, 1992*, 論文番号 MoM7.

非会員著者の紹介: 大津元一氏は1950年神奈川県生まれ。1973年東工大工学部卒、1978年同大学院理工学研究科博士課程修了。東工大助手、助教授を経て、現在教授。1986~87年の間AT&Tベル研究所研究員。専門は光量子エレクトロニクス(レーザー制御、極限光子と原子の生成)。電波科学国際連合・KOGA ゴールドメダル、日本IBM科学費、等を受賞。

原子も見える光学顕微鏡

——フォトンSTMで極微計測・加工——

正員 ^{おお}大 ^つ津 ^{もと}元 ^{いち}一 東京工業大学総合理工学研究科



キーワード：フォトン，顕微鏡，光記録，原子捕獲

1. 回折限界を超える分解能

従来の光学顕微鏡の分解能は、光の波長程度である。光をレンズの焦点面に結像させようとしても、波長より小さい領域には集光できないという光の波の性質により、像がぼけるからである。このような分解能は光学の教科書などでは「回折限界」と呼ばれ、超えることができない基本的な限界のように記述されている。

しかし物質との相互作用によって、その近傍の小さな領域に局在させられた光を使えば、回折限界を超える分解能をもつ光学顕微鏡を実現することが可能である。これは「フォトン走査トンネル顕微鏡(フォトンSTM)」と呼ばれ、最近になって研究が急激に活発化している。本稿ではこの原理と実際について解説する。この装置は、単に微小物体形状の測定機としてのみではなく、極微加工機としても使用可能であるので、これについても触れる。

2. フォトンで原子が見えるわけ

物体に光を照射すると、その散乱光には図1に示すように二つの成分が含まれる。第一は、遠くまで伝搬する波としての光であり、これは従来の光学顕微鏡、さらには一般に光計測や光通信にも使われている。第二は、光照射によって物質に誘起された分極どうしの相互作用によって、その近傍のみに作られる電磁場、すなわち伝搬しない光である。この光は教科書には「エバネッセント光」として記述されているが、フォトンSTMではこの光を用いる。

すなわち図2に示すように、エバネッセント光パワーは物質表面から光の波長程度離れたとほぼ0となり、物質表面形状と同等の空間分布をもっている。そこで、先端の鋭いプローブの先でこの

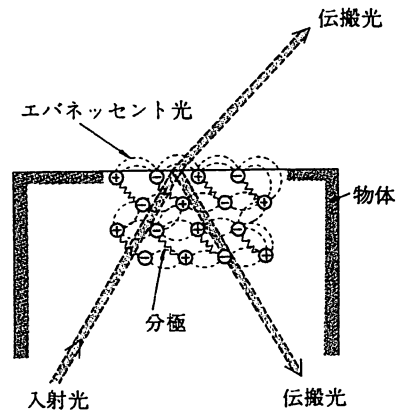


図1 伝搬光とエバネッセント光の説明

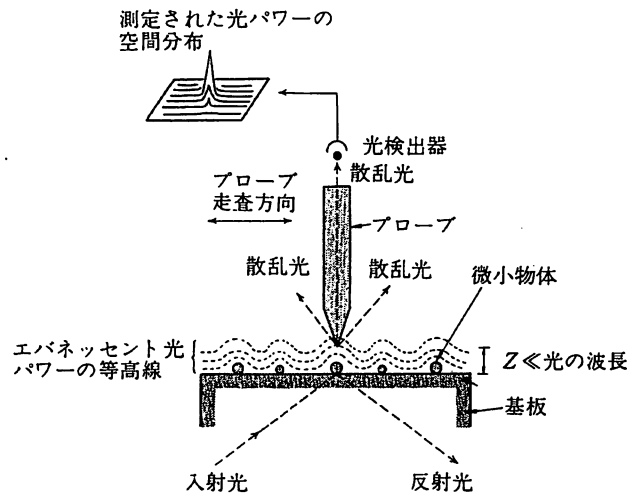


図2 フォトンSTMの原理

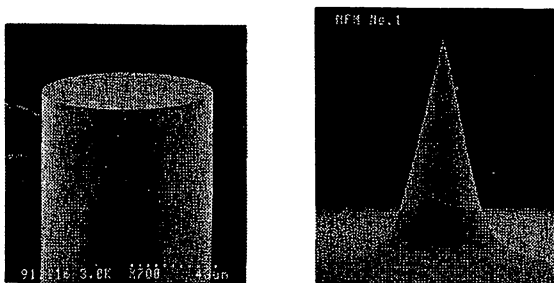
光を散乱させて、上記の第一の光に変換し、このパワーを測定する。そのとき、プローブを物体のわずか上空で物体表面に沿って走査し、プローブの位置の関数として測定パワー値を図示すれば物体の三次元形状が観測される。この場合、分解能はプローブ先端の形状によって決まるので、プローブ先端の曲率半径を原子のサイズまでとがらせば、原子を見ることのできる分解能が実現する。さて、上記の2種類の光を物質との相互作用の

見地から調べてみよう。図1に示すように物質を構成する原子には光照射により分極が誘起される。各原子に誘起された分極は、その近傍の原子に誘起された分極とさらに相互作用し、この結果、光の散乱体としての物体の形状に依存した複雑な分極の分布が作られる。したがってこのような分極が作る第二波の波数ベクトルは完全には平行、同位相ではなく、物質の形状によって変化している。それらのうち平行、同位相の成分は干渉せず重ね合わさって遠くまで伝搬する光となる。これが第一の光である。一方、非平行、異位相成分は互いに干渉するので、そのパワーは物質表面からの距離の増加とともに急激に減少する。これが第二の光、すなわちエバネッセント光である。

言い換えると、光照射のもとでは近接する原子どうしは光を介して相互作用しており、その相互作用を媒介する光が第二の光である。すなわち、原子はエバネッセント光を交換しながら相互作用しているので、この波数ベクトルは第一の光の伝搬方向とは非平行であり、原子の周りに局在している。この交換は、原子間のフォトン(光子)のトンネル効果にほかならない。類似の現象として、原子核中の陽子と中性子とを結び付ける中間子の交換など、多くの例がある。このようなトンネル効果を利用していることから、この顕微鏡はフォトンSTMと呼ばれている。

3. フォトンSTMの実際

基本となる素子は、先端のとがったプローブである。現在のところ、光ファイバをフッ酸などによりエッチングして作るのが加工の再現性の高さの点で最も優れている。また、散乱させたエバネッセント光を光検出器の位置まで効率よく導波するために光ファイバの使用が特に有利である。図3には光ファイバプローブの電子顕微鏡写真を示す⁽¹⁾。コア先端は先鋭角20度である。先端曲率



(a) 光ファイバ外径は90 μm (b) 先端部の拡大写真
写真の横幅は5.6 μmに相当
図3 光ファイバプローブの電子顕微鏡写真⁽¹⁾

半径は非常に小さく、高分解能の電子顕微鏡を用いても観測するのが容易ではないが、ほぼ5 nm以内と推定されている。最近では先鋭角15度、先端曲率半径約1 nmのものも再現性よく作られている。

実際の装置の構成例を図4に示す。光源には波長0.8 μmの半導体レーザを用いることで測定ヘッドが小型化されている。プリズム面に試料を固定し、試料裏側から全反射が起こるように光を入射すると、第一の光は反射されるのでプローブには到達しない。第二のエバネッセント光だけが試料表面に発生する。これを試料表面に接近させたプローブで測定する。プローブはピエゾアクチュエータにより掃引する。光検出器で検出した信号をコンピュータディスプレイ上に表示させる。なお、不透明物質を観測する場合、表面の斜め上から光を照射し、発生するエバネッセント光だけを検出してもよい。プローブ先端寸法が光の波長以下であれば、第一の光は光ファイバ中に入っていない。

図5は直径80 nmのポリスチレン製のラテックス球がプリズム上に密に並んでいる様子を測定した結果である⁽²⁾。視野の一辺は1 μmである。このほか、SiO₂薄膜⁽²⁾、蛾の目形光ディスク表面⁽²⁾⁽³⁾、さらには生体微粒子(バクテリオファ-

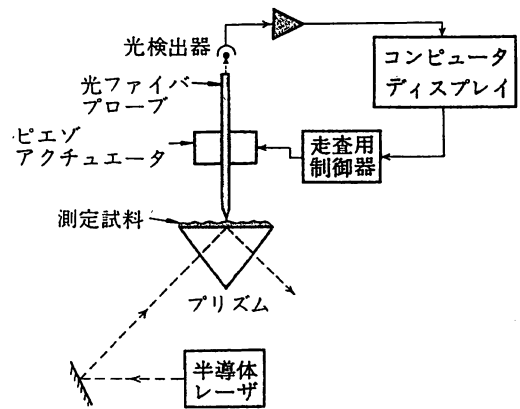


図4 フォトンSTMの装置の例

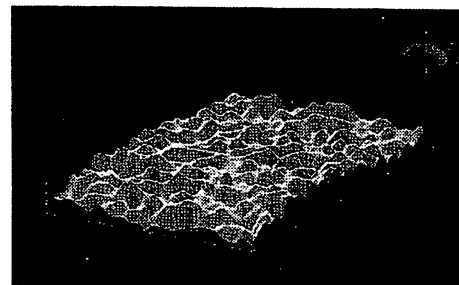


図5 直径80 nmのラテックス球の集団の形状測定結果(視野の一辺は1.0 μm)⁽²⁾

ジ T 4 など⁽³⁾，などの像が大気中で観測されている。

なお，この分解能は測定の際に混入する雑音（プローブの音響振動など）によって制限される。これを除去し，光検出器のショット雑音レベルまで低雑音化すれば測定感度は現在より約 30 dB 向上する。このときの分解能は 0.1 nm 以内，すなわち原子レベルの分解能が得られると予測されている。

4. 極微計測から極微加工へ

エバネッセント光が原子間相互作用を媒介していることに注意すると，エバネッセント光によって原子間の相互作用を誘起し制御することが可能になる。すなわち，エバネッセント光のもつエネルギー，力（運動量）によって極微加工ができる。ここではそのような例を二つ示す。

第一の例は，超高密度光記録である。フォトン STR のプローブとして用いる光ファイバの後端からレーザー光を入射し，先端からしみ出したエバネッセント光により，光記録材料に書き込みを行う。従来の光メモリではレーザー光をレンズで集光して記録していたが，この場合は光学顕微鏡と同様，記録の最小寸法は，光の回折限界により決まる。それに対し本方法では，プローブ先端寸法によって微小な記録寸法が決まる。

アメリカの AT & T ベル研究所では，磁気光学材料に直径 100 nm の記録を行い，従来の光メモリより数 10 倍高密度の光記録を実現した⁽⁴⁾。これは光のエネルギーにより材料を局所的加熱することによる記録であり，サーマルモード記録と呼ばれる。

一方，光により材料の構造を変化させる記録方法，すなわちフォトンモード記録もある。図 6 にその結果の例を示す。ガラス板上に固定したジアゾベンゼン誘導体高分子からなる有機超薄膜（ラングミュア・プロジェクト膜）にエバネッセント光を照射すると，高分子がトランス型からシス型へ遷移することにより膜の吸光度が変化する。このような光化学反応はフォトクロミック反応と呼ばれているが，この反応を起こさせることが記録に相当する。吸光度変化量を測定することにより読み出しができる。さらに，他の光を照射したり，温度を変化させると消去も可能であるという特長をもつ。

図 6 の記録寸法は直径約 270 nm である。この

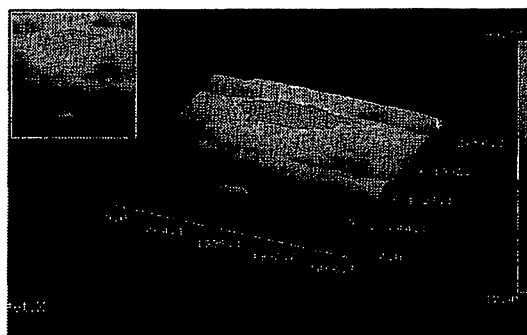
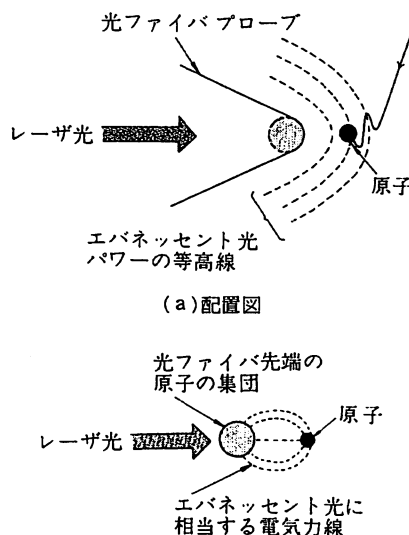


図 6 有機超薄膜への光記録の結果。視野の一边は約 2.6 μm。図中の真中のやや黒い部分の吸光度が変化している。左上の内挿図は中央の鳥かん図を真上から見たもの。



(b) ファンデルワールス分子としての説明図

図 7 単原子捕獲の原理⁽⁵⁾

値の下限は，微弱なパワーのエバネッセント光による数分間にわたる記録中のプローブの位置変動により制限されている。プローブ位置制御の精度を向上させれば，記録寸法をプローブ曲率半径によって決まる値まで小さくすることが可能である。

第二の例は，単原子捕獲の可能性である⁽⁵⁾。これは，結晶成長技術の極限ともいえる。図 7 に示すように，真空中に置いたプローブ先端らエバネッセント光をしみ出させておく。そこに真空中を浮遊する原子が飛び込むと，プローブ先端とその原子との間でエバネッセント光を媒介として相互作用が発生し，ファンデルワールス分子のように 2 原子分子を形成する。図 7 の場合，プローブ先端から光を絶えず照射していることを除いては，ファンデルワールス力による 2 原子分子の構成と

同等である。

原子を捕獲する場合、エバネッセント光の空間的広がりが小さいため、二つ以上の原子が同時に飛び込むことはまれであり、このようなことが起きたとしても原子間の相互作用により単原子捕獲のみが安定に起こる。一方、原子が捕獲されれば、原子から発する蛍光を検出することにより、捕獲原子の有無を知ることができる。また、捕獲位置はプローブ先端からプローブ先端曲率半径ほど離れた位置であるが、これは通常の原子間力であるファンデルワールス力のポテンシャルが最小となる位置に比べて10倍以上離れているので、このファンデルワールス力により、原子がプローブ表面に吸着することはない。

なお図7では、原子がエバネッセント光によって捕獲される場合を説明しているが、これは原子の共鳴周波数に対して光の周波数が10 MHz程度低周波側にある時である。高周波側にある時は原子はエバネッセント光によって、プローブ先端から遠ざかる方向へ押し出されてしまう。このことを利用し、光周波数を調節して、まず真空中に浮遊する原子を捕獲し、その後押し出し、冷えた結晶基板に吹き付け吸着させることが可能である。これにより単一原子レベルでの結晶成長が期待される。

多種類の原子に対して、捕獲のためのパラメータが設計されている。例えばシリコン原子では波長252 nmの光が必要で、プローブ先端曲率半径の最適値は13 nmである。これらの光源やプローブは、入手または作成可能であり、単原子レベルの結晶成長の実現が待たれる。真空中を浮遊する原子とエバネッセント光との相互作用についての予備実験がすでに行われている。

5. 動作原理の解明はこれから

フォトンSTMの提案は60年前にさかのぼるといわれるが、良好なプローブが実現したのはこの数年のことである。電気工学用の極微材料の評価、バイオエレクトロニクス、光記録、極微結晶成長などへの広い応用可能性のためにごく最近に

なって研究が急激に活発化し、昨年末にはフランスで国際集会在初めて開催され盛会であった。今回は本年10月、アメリカのノースカロライナ州で開催される。しかし、この顕微鏡の動作原理については、まだ解明されていない問題が多い。また光を古典的に扱うべきか量子論的に扱うべきかの問題についても十分理解されていない。このような光の本質に迫る問題も含め、フォトンSTMの研究は新しく、重要で、かつ魅力に富む。この分野の研究人口の増加を祈念したい。なお、本記事の内容より詳しい解説があるので、それをご参考にされたい⁽⁶⁾。本稿の内容に関し有益な助言をいただいた山梨大学の堀 裕和助教授に感謝致します。(平成5年3月19日受付)

文 献

- (1) T. Pangaribuan, K. Yamada, S. Jiang, H. Ohsawa, & M. Ohtsu: "Reproducible Fabrication Technique of Nanometric Tip Diameter Fiber Probe for Photon Scanning Tunneling Microscope", *Jpn. J. Appl. Phys.*, 31, L 1302(1992)
- (2) S. Jiang, N. Tomita, H. Ohsawa, & M. Ohtsu: "A Photon Scanning Tunneling Microscope Using an AlGaAs Laser", *Jpn. J. Appl. Phys.*, 30, 2107(1991)
- (3) S. Jiang, H. Ohsawa, K. Yamada, T. Pangaribuan, M. Ohtsu, K. Imai, & A. Ikai: "Nanometric Scale Biosample Observation Using a Photon Scanning Tunneling Microscope", *Jpn. J. Appl. Phys.*, 31, 2282(1992)
- (4) E. Betzig, J. K. Trautman, R. Wolfe, E. M. Gyorgy, & P. L. Finn: "Near-field magneto-optics and high density data storage", *Appl. Phys. Lett.*, 61, 142(1992)
- (5) 大津元一・堀 裕和:「フォトンSTMの実験と理論」, 光学, 21, 780(平4)
- (6) 大津元一:「フォトン走査トンネル顕微鏡: 光の回折限界を越えて」, 日本物理学会誌, 48, 25(平5)



大津元一(正員)

昭和48年東京工業大学電子工学科卒業。53年同大学院博士課程修了。工学博士。同大学助手、助教授を経て平成3年同大学教授。平成5年4月より神奈川科学技術アカデミー・「フォトン制御」プロジェクトリーダーを兼任。量子操作工学、特に極限光子と極限物質の創造に関する研究に従事。

0 (ゼロ) を制御する工学

——— 光による新しい「真空」の工学 ———

大 津 元 一*

(受付1993年2月4日, 掲載決定1993年4月3日)

Controlling Zero

——— New “Vacuum” Technology by Light ———

Motoichi OHTSU

(Interdisciplinary Graduate School of Science and Engineering, Tokyo Institute of Technology, 4259 Nafatsuta, Midori-ku, Yokohama-shi, Kanagawa 227)

(Received February 4, 1993, Accepted April 3, 1993)

1. ま え が き

本誌で従来より扱われている「真空」の概念は, ある容器内の気体を排気した後に残された, 原子や分子などがきわめて少ない空間を表していると考えてよいだろう。宇宙空間はこのような「真空」の代表であり, 現在の超高真空技術はこのようからっぽな空間を実験室に実現することをめざしているといえる。ところが, からっぽなはずの宇宙も, 背景放射とよばれ, 約3ケルビンの等価温度に相当するエネルギーをもつ光子(ただしこの場合はマイクロ波領域の電磁波)によって満たされていることが, 宇宙の起源を説明しようとする「ビッグバン」理論と関連して, よく知られている。

このように, からっぽな空間にも, さらにいろいろな「場」を考えることができる。すなわち, 空間の各点には, 各々の「場」に対応する「空間」があり, 普通に「真空」といってもこのような「場」の「空間」までからっぽというわけではない。反対に本誌で従来より扱われている意味での「真空」ではなくとも, 「場」の空間はからっぽである場合, すなわち気体はあるが光子がない場合, もありえる。そこで, 「場」の空間までからっぽな

真の「真空」状態を, たとえば $|0\rangle$ と書き表すことにしよう**。そうすると, $|0\rangle$ の意味はどのような「場」を考えるかによって異なってくるので, 真の「真空」 $|0\rangle$ にも多様性がでてくる。また, 考えている空間の大きさや時間の間隔などによっても, いろいろな「真空」のもつ意味の重要性が異なってくる。第2節では, このような「真空」の多様性について述べる。

一方, 「場」は量子力学的な見方をすると, 電磁波に対する光子のような, 各々の「場」に対応する粒子を生成・消滅させる空間の各点の能力を表しているといえることができる。このような理由により, 真の「真空」 $|0\rangle$ といっても, そこにはいろいろな「場」の揺らぎがあり, いろいろな粒子が絶えず生成・消滅している。第3節では, 広く用いられている光源装置であるレーザーから出て来る光の周波数揺らぎを例にとり, 共振器という「空間」における電磁「場」とその「真空」の揺らぎを紹介する。

さらに, いろいろな「場」あるいはこれに対応する「粒子」の間に相互作用がある場合には, 真の「真空」 $|0\rangle$ の意味もまた複雑になってくる。すなわち, 空間の各点

* 東京工業大学大学院総合理工学研究科 (〒227 横浜市緑区長津田 4259)

** $| \rangle$ は系の量子力学的な状態を表すのに使われている記号でケット (Ket) と呼ばれている。次節以降では真空に対して量子力学的考察を加えることが必要であることを読者諸氏に訴えたいので, ここでは真の真空状態をケット記号を用いて $|0\rangle$ と表した。

における、いろいろ異なった「場」に対応する粒子の生成・消滅が、互いに関連しあって起こることになる。このような相互作用を積極的に利用することにより「真空」を制御し、「場」の揺らぎを抑制することも可能である。第4節ではこのような制御された「真空」を利用して、レーザーの次にくるべき新しい光源を実現する試みについて紹介する。

第5節では相互作用を利用して「空間」の寸法を極端に小さく制限したときには、そこで重要となる「場」の性質が大きく変化し、さまざまな新しい現象が起こることを、フォトン走査トンネル顕微鏡という新しい装置を例にとって説明する。

このように、「真空」や「場」についての広い視点からの考察は、単に理学的研究に留まらず、新しい状態の光や極微物質を創造する工学的応用を可能にする。実際、ごく最近この様な工学的研究の萌芽が見られる。このことから、本稿ではタイトルを「0を制御する工学」とし、 $|0\rangle$ を扱い応用する工学的研究の概説を試みる。

なお、本稿の議論の中には、従来より扱われている「真空」技術としては馴染みの薄い概念や用語が用いられるかもしれないが、現在の真空技術はこれらの量子光学、場の理論、素粒子論などの基礎研究を支えていることや、他の文献でしばしば取り上げられている話題も多いと思われるので、本誌の読者諸氏のご理解を頂ければ幸いである。

2. 真空の種類

冒頭に示したような従来より扱われている「真空」の概念では、排除されるべき気体状物質の内部にはもはや真空は存在しないと考えている。しかし、これらの気体状物質を構成する原子は原子核と電子からなり、その電子核と電子との間の空間、すなわち原子の中の空間には電氣的な力を伝える真空がある。原子核の内部にはパイ中間子を交換しながら引き合う陽子と中性子があり、真空はない。しかし、陽子や中性子の中には真空があって、この真空とクォークとが陽子や中性子の運動量を担

表1 考えている領域の寸法 Δx により考えられる空間と場の分類、それに関連する現象。

	空間	場	現象
宇宙の寸法	宇宙全体	光子	3 K背景放射
可視光の波長 {	レーザー共振器	光子	[1] 周波数揺らぎのS-T限界 (注1)
		光子	[2] 共振器内量子電気力学
原子の大きさ {	メゾスコピック物質	結晶場(物質内光子)	[3] フォトン STM
電子のコンプトン波長 {	原子内部	電子・陽電子の海	γ 線による電子・陽電子対生成・消滅
	原子核内部	パイ中間子, グルーオン, など	素粒子の物理現象

(注1) S-T限界とは本文中の(1)式で与えられる周波数揺らぎを表す。

っている。以上の事実は素粒子論では既知であり、物質が階層構造をもつと同様に「真空」にもいろいろな種類があることを意味している。たとえば、宇宙の中の真空は重力を伝え、グラビトンによって星と星とを結び付けている。原子中の真空は電氣的な力を伝え光子により原子核と電子とを結び付けている。さらに陽子の中の真空は色の力を伝え、グルーオンによってクォーク同士を結び付けている。

さらにまた真空が粒子と反粒子とを生成することはよく知られている通りである。このことは真空はエネルギーを生み出す能力があることを意味する。なぜなら、生成される粒子は質量を持ち、その質量は相対論によればエネルギーと等価だからである。そこで、上記のいろいろな種類の真空のもつエネルギー、特にその揺らぎに注目すると、この値は今考えている真空の占める空間の寸法に依存する。そのような寸法の値により真空を類別した結果を表1にまとめる。これらの空間内にあり、各種粒子を結び付ける力を担う光子族（ゲージ粒子と呼ばれるもの、すなわちグラビトン、光子、グルーオン、ウィークボゾン）が、ここで議論する空間領域（その一辺の寸法を Δx とする）を横切るのに要する時間 $\Delta t = \Delta x/c$ 、ここで c は光速）の間に真空のエネルギーを測定すると、その測定誤差 ΔE はハイゼンベルグの不確定性原理により $\Delta E \approx hc/2\pi\Delta x$ となる（ h はプランクの定数）。これが真空のエネルギー揺らぎ量に相当するが、表1はこの揺らぎ量に対応する現象を記した。本稿ではこの表のうち[1]~[3]を扱う。

3. 真空の揺らぎによるレーザー周波数の揺らぎとその抑圧

レーザーは周波数揺らぎの少ない光の波を出す光源であり、それは図1(a)に示すように電源などからエネルギーを供給される発光物質とそれを取り囲む共振器とからなる。通常のレーザーの共振器寸法は光の波長よりずっと大きいので、表1の[1]に相当する。この共振器中には多数の定在波が共振して安定に存在する（図4(a)も参照されたい）。その定在波の半波長の整数倍が共振器長に等しい。ただしその整数は非常に大きい値をとるので、このように大きな共振器中には各々の整数値に対応する多種類の定在波が存在し得る。このような各々の定在波は共振器のモード（Mode）と呼ばれている。レーザー装置から発生する光の周波数はそのような多数のモードのうちの一つの周波数に等しい。ところで、図1(b)に示すように、発光物質を構成する原子は次の二つの過程により光を発生する：

(1) 誘導放出；原子がそれに入射する光に刺激され、入射光と同じ周波数の光を入射光と同じ方向に放出する過程である。これは原子による入射光の増幅作用を意味し、これがレーザー発振に利用される。すなわち、原子から出た誘導放出光のうち共振器の一つのモードの周波数に合致したものを共振させ、光の発振器を実現する。そしてその光の一部分を共振器の鏡を透過させて取り出し、各種応用に使う。

(2) 自然放出；入射光の有無とは無関係に、原子が任意の時刻、任意の方向に不規則に光を放出する過程である。これは原子が「電磁場に関する真空」の揺らぎに刺激されて誘導放出を起こしたとみなすことができる。

レーザー電源のスイッチを投入すると、まず不規則な自然放出光が発生し、それが他の原子に入射して誘導放出が起こりレーザー発振が始まる。すなわち、自然放出光はレーザー発振の種として働く。しかし、発振後の定常動作時にはこの不規則な自然放出光はレーザー周波数の揺らぎを与え、レーザー応用上障害となる。量子論によると光エネルギーは $h\nu$ なる関係により光周波数 ν に比例するので、自然放出による周波数揺らぎの大きさは原子のエネルギーの不確定性 ΔE の値より求めることができる。その揺らぎがレーザー発振スペクトルの幅 $\Delta\nu$ を与える。この値が0であればレーザー光は完全な正弦波であるが、実際には自然放出光の影響を受けている。より詳細な議論によると¹⁾、その値は

$$\Delta\nu = \pi h\nu^3 / PQ_L^2 \quad (1)$$

と表せる。ここで π は円周率、 P はレーザー光パワーである。 Q_L は共振器の損失を表す性能定数であり、 $\Delta\nu$ が

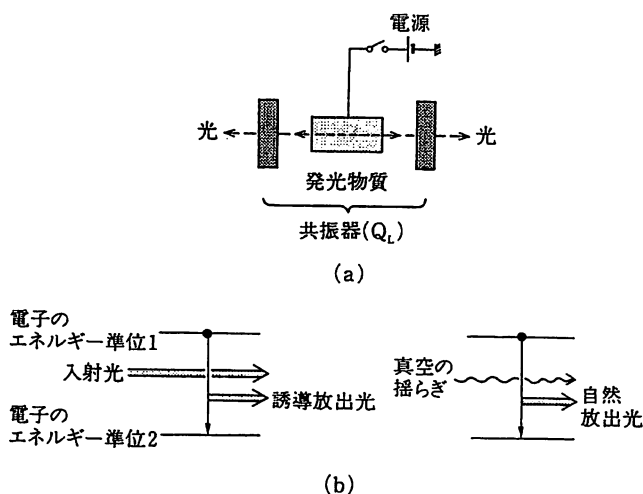


図1 (a) レーザーの構成。(b) 誘導放出(左図)と自然放出(右図)による光発生過程の説明。

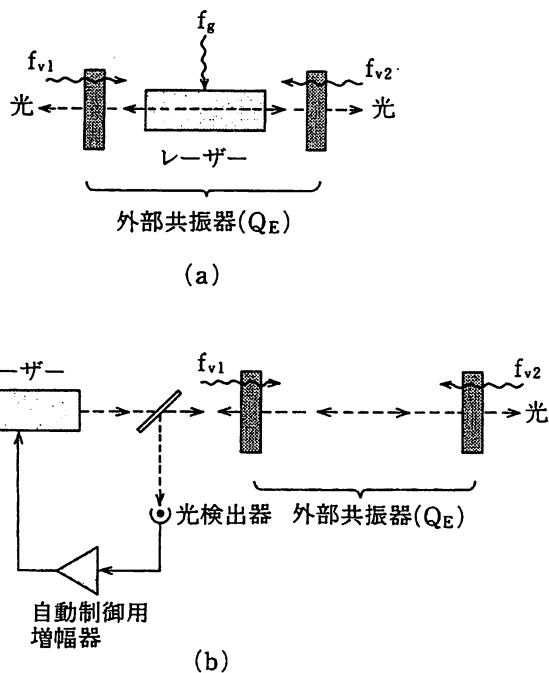


図2 外部共振器（性能定数 Q_E ）を用いたレーザー周波数揺らぎの抑圧法。(a) 外部共振器中にレーザーを設置する。(b) 外部共振器の一つのモードの共振周波数にレーザー周波数を安定化するように自動制御する。 f_{v1} , f_{v2} は共振器用の鏡を通して混入して来る真空の揺らぎ, f_g は発光物質に混入する真空の揺らぎを表す。

Q_L の値に依存することは、共振器が原因としての自然放出光揺らぎの大きさと結果としての周波数揺らぎの大きさとの間を橋渡しするフィルタとして働くことを意味している。すなわち、共振器壁面の反射率が100%であれば、性能定数は無限大となり、自然放出光揺らぎの影響を完全に除去できるので $\Delta\nu$ の値は0となる。しかし一般には共振器損失があるために、自然放出光揺らぎの影響を完全に除去することはできず、その結果(1)式の $\Delta\nu$ になる。(1)式は、それを導出した研究者の名前にちなみ、シャウロウ・タウンズ (Schawlow-Townes) の式²⁾と呼ばれている。

実用的な光応用システムに広く使われている半導体レーザーでは共振器損失が大きく、従って、性能係数の値が小さいので、 $\Delta\nu$ の値は大きい。これを小さくするためにこのレーザーを図2(a)に示すような性能定数の大きな外部共振器に納める。すると(1)式中の性能定数として外部共振器の値 Q_E を代入した値がレーザー発振スペクトル幅を与える。一方、図2(b)の様に、同じ外部共振器の外側にレーザーを置き、外部共振器の一つのモードの共振周波数とレーザー周波数との差を測定し、その差の値が0になるようにレーザー周波数を自動制御し

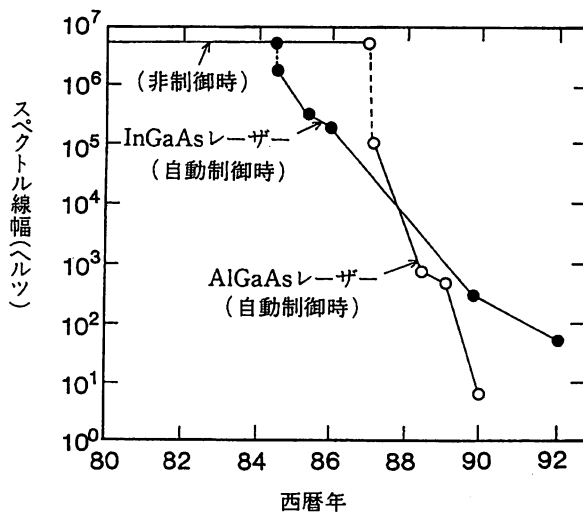


図3 自動制御による半導体レーザーの発振スペクトル線幅抑圧実験の進歩のようす。

てその共振周波数に安定化する方法も考えられる。これは図2(a)と同一の共振器を使って制御しているので、理想的な制御状態では図2(a)と等価であるように見える。しかし、この場合実現する $\Delta\nu$ の値は(1)式の $1/Q_E^2$ のかわりに $1/8Q_E^2$ を代入しなくてはならない。すなわち、新たに1/8の値を付加する必要がある。

真空の揺らぎがレーザー発振に与える影響の大きさの評価の仕方はいくつかあるが、その内の一つの方法は真空の揺らぎが共振器の鏡を通して外界から混入してくると考える方法である。それによると、この1/8の違いは図2を使って次のように説明できる³⁾: 図2(a)の場合には共振器の2枚の鏡から真空揺らぎ f_{v1} , f_{v2} が混入する。共振器構成が左右対称であるとすれば $f_{v1}=f_{v2}$ である。また、発光媒質には自然放出揺らぎ f_g も混入している。(ここで、 $f_{v1}^2+f_{v2}^2=f_g^2$ なる関係がなりたつこともわかっている³⁾。) さらに、共振器内のレーザー光は二分され共振器両端から出射する。これに対し、図2(b)の場合には次の3点が(a)とは異なる。すなわち、(1) 左側の鏡から共振器に混入した真空揺らぎ f_{v1} の大きさは制御用光検出器で測定され、それが0になるようにレーザー周波数が制御される。従って、制御時の真空揺らぎの寄与は f_{v2} からのみなる。(2) 共振器内には発光物質がないので f_g の寄与はない。(3) レーザー周波数が共振器の共振周波数に合致しているとき、レーザー光パワーはすべて共振器右側に出射する。

真空の揺らぎの寄与の仕方に関して上記の3つの差異点が見いだされ、これにより1/8の違いが説明された。通常の半導体レーザー(代表的な波長は $0.8\mu\text{m}$, $1.5\mu\text{m}$ など、すなわち ν は数100 THz(テラヘルツ))のもつスペクトル幅 $\Delta\nu$ ((1)式)の値は数 MHz(メガヘルツ)

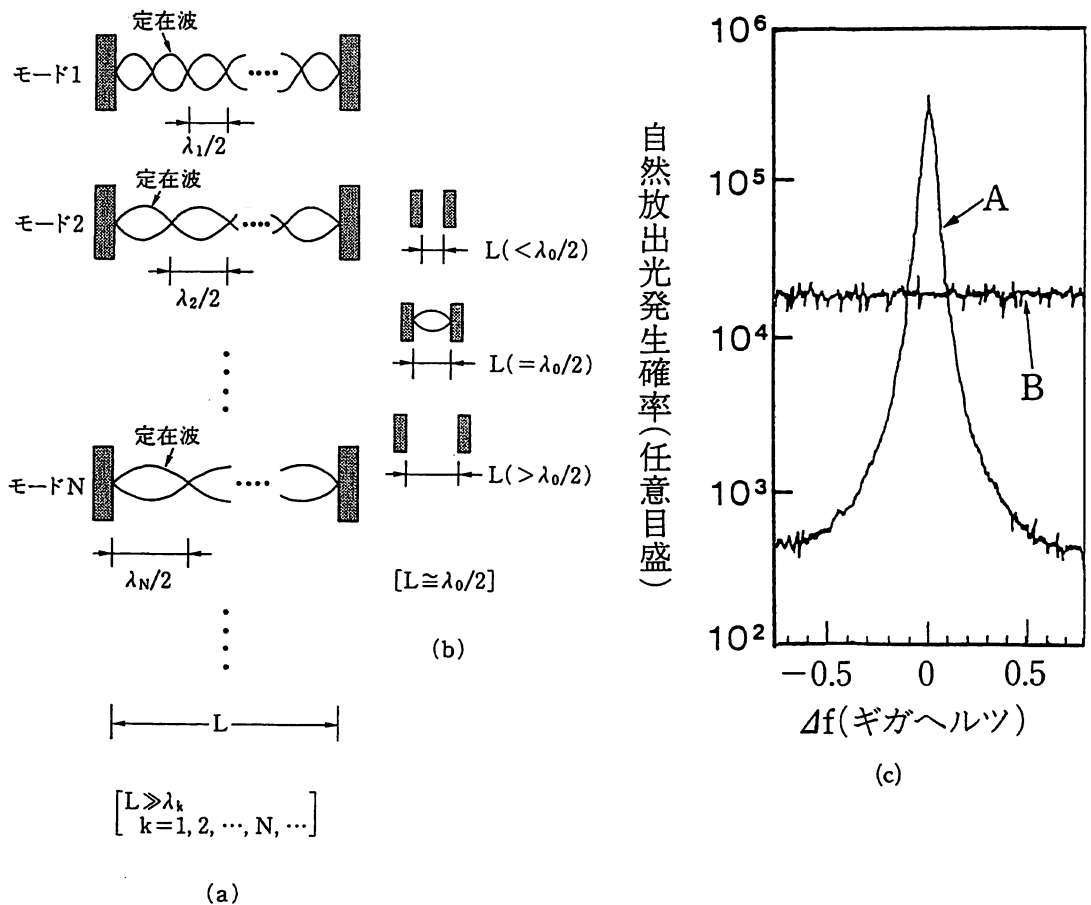


図4 共振器の各モードの定在波の形状，各モードへの自然放出光の混入の様子。(a) 共振器長 L が光の半波長に比べずっと長い場合。多数のモード (その波長は λ_k ($k=1, 2, \dots, N, \dots$)) が存在する。自然放出光はこれらのモードに等しく分散して混入する。(b) 共振器長 L が光の半波長 $\lambda_0/2$ にはほぼ等しい場合。 $L=\lambda_0/2$ の場合には一種類の定在波のみが存在するので、自然放出光はすべてこのモードと結合する。 L が $\lambda_0/2$ の値からずれると定在波は存在しないので自然放出光は共振器中に存在し得ない。(c) 微小共振器中の Yb 原子からの自然放出光発生確率の測定結果 (曲線 A)⁶⁾。横軸は原子の共鳴周波数と共振器の共鳴周波数との差 Δf 。 Δf の値は共振器の長さを掃引することにより変化させた。曲線 B は大きな共振器中の自然放出光の発生確率に相当する値。

であり、従って $\Delta\nu/\nu \sim 1 \times 10^{-8}$ である。この値を見るとレーザーは十分揺らぎの小さい光源といえるが、高精度光計測や周波数多重コヒーレント光通信などにはこれでも不十分であることが多く、その場合には図 2(b) のような制御を施して揺らぎをさらに抑圧する。このような半導体レーザーの周波数制御の実験結果の進歩のようすを図 3 に示す。現在までに制御により得られた $\Delta\nu$ の最小値は 7 Hz、すなわち $\Delta\nu/\nu \sim 1 \times 10^{-13}$ に達しているが⁴⁾、実際の制御系自身の利得不足などによりこの値もまだ (1) 式の $1/Q_L$ の代わりに $1/8Q_E^2$ を代入した理論値に達していない。その理論値は $\Delta\nu \sim 1 \mu\text{Hz}$ (マイクロヘルツ) と推定されており⁵⁾、これは真空の揺らぎの影響を自動制御によって補正すること、すなわち「0 を制御する工学」の今後の実験の進展によりきわめて揺らぎの少ない高性能レーザーが実現する可能性があることを意味している。

4. 共振器内量子電気力学

表 1 の [2] の話題は共振器内量子電気力学 (Cavity Quantum Electrodynamics: 以下 CQED と略記する) である。前節で述べたレーザーの共振器は図 4 (a) に示すように多数のモードを持つ。ところで最近、半導体デバイス加工技術の進歩により $1 \mu\text{m}$ 以下の寸法をもつ半導体共振器が実現している。このような微小共振器の寸法は図 4 (b) に示すように光の半波長以下になり得るので、表 1 において Δx の値は [2] の範ちゅうに入る。このような微小共振器のモードの数は 1 または 0 である。従ってその中に発光物質を置いたとき、その発光物質中の原子が真空の揺らぎにより刺激されて自然放出光を発生しようとしても、その発生確率は共振器長に依存するようになる。なぜなら、共振器長が光の半波長以下では発生した自然放出光は共振器内に定在波として存在し得な

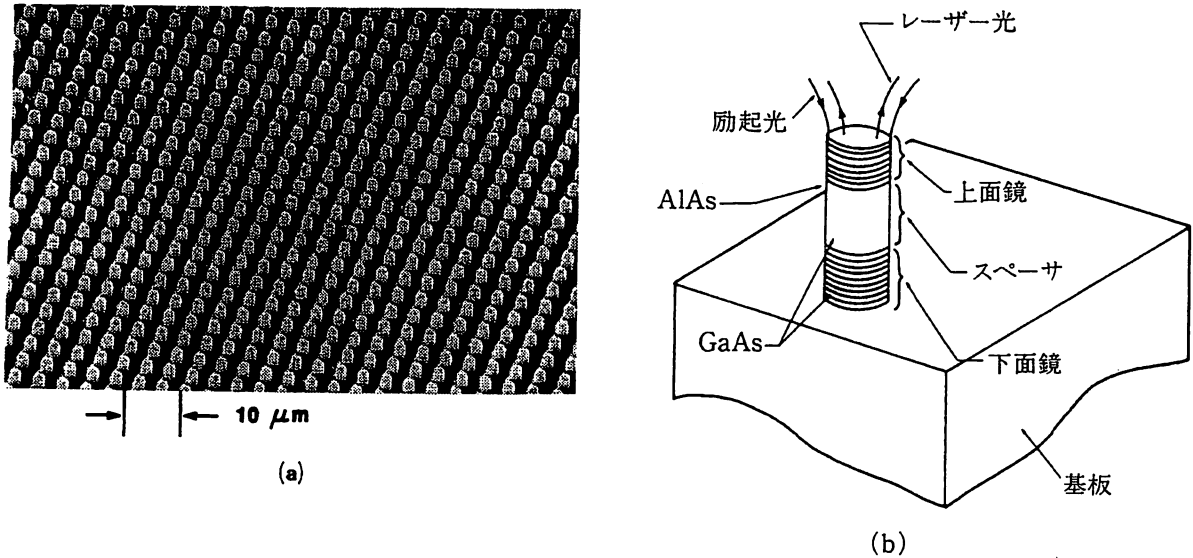


図5 半導体基板上に2次元アレイ状に加工された半導体微小共振器の写真⁸⁾。(b) 各微小共振器の構造。

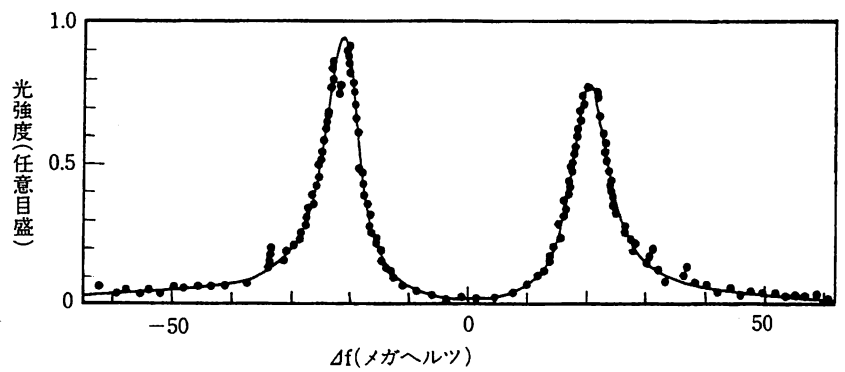


図6 微小共振器中の少数個のNa原子による真空のラビ共鳴スペクトル形状の測定結果⁹⁾。横軸の Δf は図4と同じ。

いからである(この状況は、大きな共振器中の自然放出光の発生とは大きく異なる。すなわち、そのような大きな共振器の中では発生した自然放出光は多数のモードとして分散して共振し得る)。つまり、微小共振器中ではその長さが光の半波長よりもわずかに短くまたは長くなるように調節すれば自然放出光の発生が抑圧される。一方、その長さを半波長に等しくすると発生した全ての自然放出光は共振器中で共振する。この場合、1つのモードしかないの、自然放射光はすべてそのモードに結合し、従ってその自然放出光発生確率は大形共振器の場合に比べずっと大きくなる。つまり、共振器という物質によって真空を制御し、その揺らぎを増加させたことになる。

以上の現象は微小共振器の長さを調節することにより自然放出光発生確率を制御することが可能になることを意味する。すなわち、真空の揺らぎを制御することができる。そのような実験の例として図4(c)に、微小共振

器中に置かれたイッテルビウム(Yb)原子からの自然放出光発生確率を、共振器長の関数として測定した結果を示す⁶⁾。このような微小共振器を使ったレーザーは、発振のしきい値が無かったり、揺らぎの特性が通常のレーザーとは異なったりするなど、特異な性質を持つ⁷⁾。レーザーが発明された30年以上経過した今日、このような新奇な発光素子はいわば次世代の光源とみなすことができ、その発展が期待されている。図5にはそのような微小共振器が半導体基板上に2次元アレイ状に加工された様子を示す⁸⁾。

CQEDのもう一つの例を図6に示す。これは微小共振器中に数個のナトリウム(Na)原子を置いたとき、原子は真空の揺らぎに相当する自然放出光に共鳴しその共鳴スペクトルが2つに分裂する現象(真空のラビ(Rabi)共鳴と呼ばれる)⁹⁾を表したものである。共振器の寸法が大きければこのようなラビ共鳴は外部から光を入射しないかぎり発生しないが、微小共振器中では自

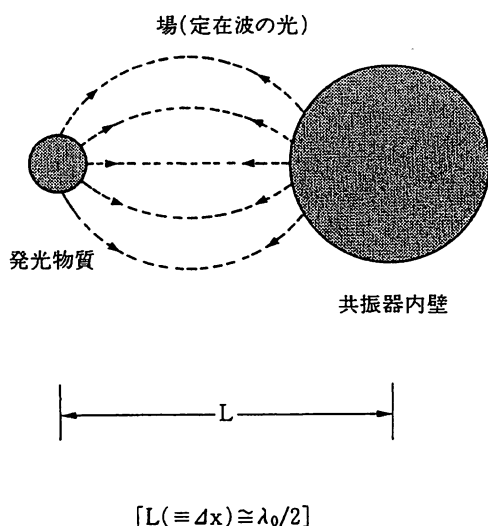


図7 CQEDの現象を光を介した2原子分子の形成と見なす概念図。

自然放出光が発生すれば、これは効率良く共振器内に存在し続け、従って原子との相互作用が強くなるので、外部光がなくてもラビ共鳴が生じる。つまり、微小共振器内に原子を置き、その共振器長を微調して自然放出光発生確率を調節すれば、原子の状態が操作できる。これは原子を真空により操作できることを意味し、3節と同様、この場合も「0を制御する工学」の萌芽的研究例と言えよう。

さて、以上の2例について別の見方をしよう。微小共振器の長さによって自然放出光発生確率が変化することは次のように説明できる。すなわち、原子のエネルギー揺らぎ ΔE が場の揺らぎ（自然放出光発生確率）の大きさへ寄与する割合は共振器内壁の原子共振器内の場との相互作用によって決まるが、共振器長を調節することによりこの相互作用を制御し、自然放出光発生確率を増加・減少させている。

以上の説明方法に従うと、図7に示すようにCQEDでは共振器内壁と発光物質との間で共振器内の場の揺らぎを介して2原子分子を形成すると考えることができる。これは2つの原子がファンデルワールス（Van der Waals）力を介して分子を形成すること、さらには電子と原子核とがクーロン力を介して原子を形成することにも類似している。

5. フォトン走査トンネル顕微鏡

フォトン走査トンネル顕微鏡（フォトンSTM）は光波長以下の寸法を持つ微小物体の形状を観測できる超高倍率の光学顕微鏡である。従来の光学顕微鏡の分解能は光波長程度であったが、これは光の波が広がろうとする

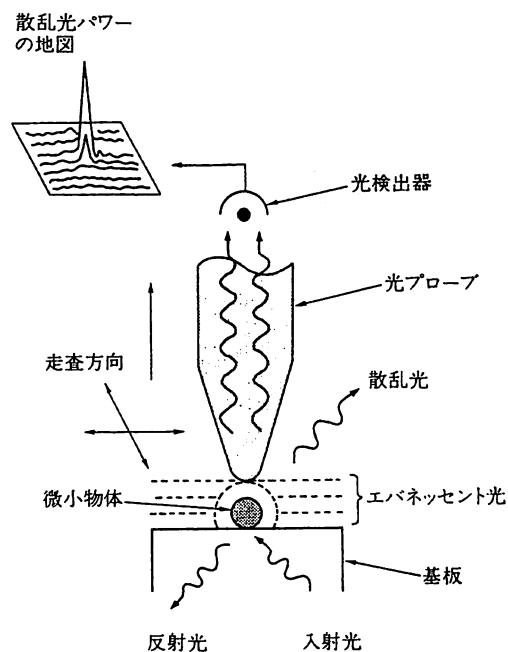


図8 フォトンSTMの原理図。

性質（これは回折と呼ばれる）に起因している。すなわち、物体に光を照射したとき発生する散乱光が有限直径をもつレンズまで自由空間を伝搬し、集光されるが、回折効果により像がぼける。これに対しフォトンSTMでは発生する散乱光のうち図8に示すように物体の周りに局在する光を使う。このような光、すなわち表面波、はエバネッセント（Evanescent）光と呼ばれ、その光パワーは物質との距離の増加とともに指数関数的に減少する。図8のように先鋭化された針を試料面上を走査させることによりエバネッセント光を散乱して伝搬光に変換し、そのパワーを測定する。そしてそのパワー値を針の位置の関数としてプロットすれば物体の3次元形状を高分解能で測定できる。つまりこの形状測定の分解能はプローブとして使う針の先端曲率半径の大きさによって決まるので、光波長よりずっと小さな寸法をもつ物体形状が測定できる。

フォトンSTMの提案は1930年頃にさかのぼるが、高性能な微小プローブの作成およびそれを用いた実験は1980年代になって行われ、現在その研究開発が活発化している。特に、プローブとして図9に示すように先鋭化された光ファイバ¹⁰⁾が実現して以来、実験が飛躍的に進歩した。この図の光ファイバ先端曲率半径は5ナノメートル以内と推定されており、これにより多数のナノメートルの微小物体が観測された。図10は生体試料の一つであるバクテリオファージT4の像を初めて空気中で観測した例である¹¹⁾。

さてこの顕微鏡は表1の[3]に対応するが、その原

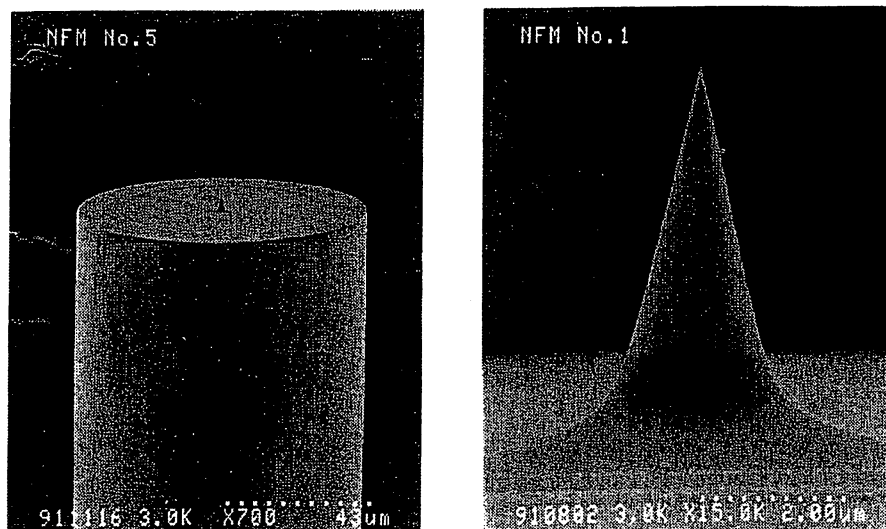
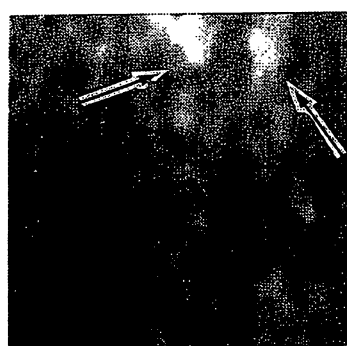
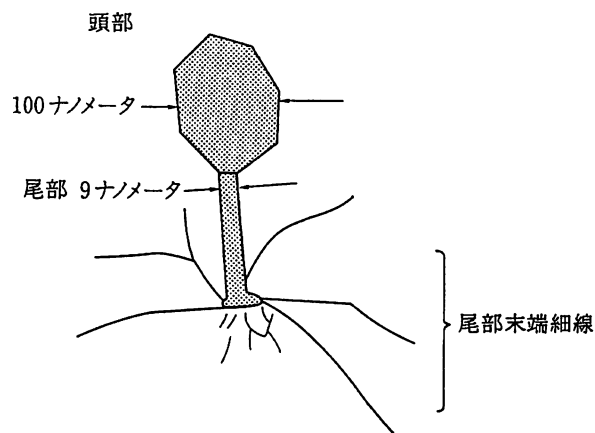


図9 フォトンSTMのプロープ用の先鋭化光ファイバの先端形状を観察した電子顕微鏡写真¹⁰⁾。左側の写真は光ファイバ端全体像。外形は90 μm 。右側は先端部の拡大像で、写真の横幅は5.6 μm に相当。



(a)



(b)

図10 (a) フォトンSTMにより空气中で観測されたバクテリオファージ T4 の像¹¹⁾。二つの矢印の先端に一つずつ像がある。写真の一辺の幅は0.6 μm に相当。(b) バクテリオファージ T4 の形状説明図。

理を説明すると次のようになる。図11に示すように、微小物体とプローブ先端とが互いに非常に近距離にあるので、その間の電磁場が物質と強く相互作用する。その結果、共振器が構成されていないにもかかわらず、CQEDと同様、場の性質、物質の性質が変化する。その変化量を測定することが微小物体表面のエバネッセント光パワー分布を測定することに他ならず、これにより物体形状が測定できる。このように非常に近距離なので、その相互作用はクーロン力に類似している。

微小物体とプローブとの間の距離、すなわち今考えている領域の寸法 Δx は数ナノメートルなので、通常の伝搬光が存在する領域（光波長と同程度またはそれ以上）と比べるとその力は大きい。このようにエバネッセント光が媒介して微小物体とプローブとが引き付けあっている

様子は陽子と中性子とを結び付けるパイ中間子と類似である。実際、フォトンSTMのエバネッセント光子はパイ中間子のように質量を持つ場の粒子と同様、微小物質とプローブとの間をトンネルして行き来している。このような考え方に基づいたトンネル光子理論が最近展開され¹²⁾、このような重い光子としてのエバネッセント光子の質量に相当するコンプトン (compton) 波長は微小物体の大きさに等しいこと、などが指摘されている。

さらに、このトンネル光子理論の応用として、フォトンSTMを顕微鏡としてではなく、加工機として使う方法が提案されてい添る¹³⁾。すなわち図12に示すように真空容器中にて光ファイバ後端からレーザー光を入射させ、先鋭化端からエバネッセント光を発生させる。そのエバネッセント光中に原子が飛び込むと、この原子と光

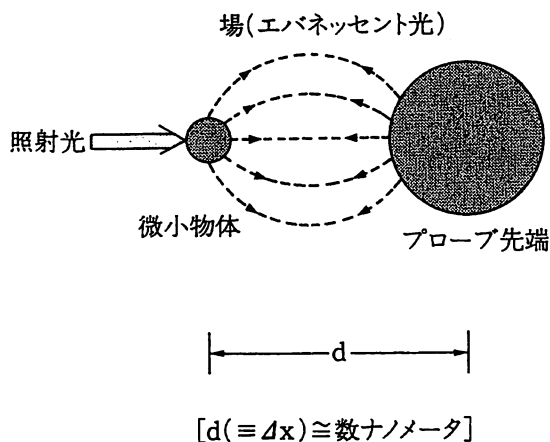


図11 光照射により形成される「擬似ファンデルワールス分子」の概念によるフォトンSTMの説明図。

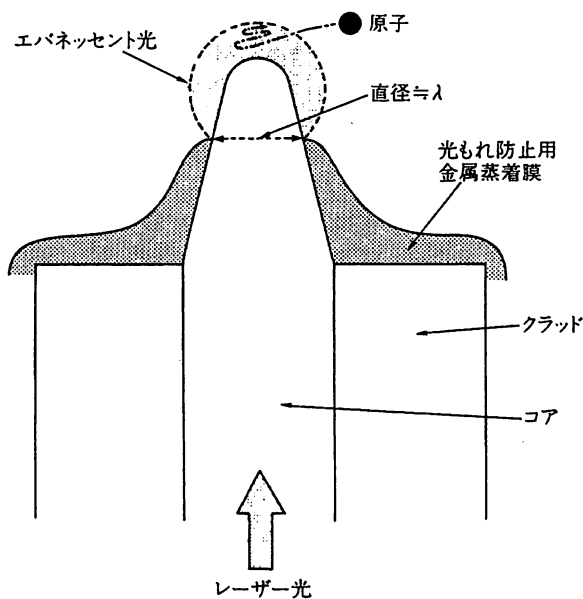


図12 フォトンSTMのプローブ用の先鋭化光ファイバの先端からエバネッセント光をしみ出させ、それによる「擬似ファンデルワールス力」により一つの原子を捕獲する方法の概念図。

ファイバ先端の原子とがエバネッセント光（すなわち大きな運動量をもつ重い光子）をトンネル効果によりやり取りして、二原子分子と類似の物質を形成する。これは光照射により作られる「擬似ファンデルワールス分子」とでも呼ぶべき物質状態である。この二原子分子形成のための光誘起「擬似ファンデルワールス力」のポテンシャルの最小値は、光ファイバ先端からちょうど先端曲率半径だけ離れた位置にある。この値は通常のファンデルワールス力のポテンシャルの最小値の位置に比べ光ファイバ先端からずっとはなれているので、安定な擬似ファ

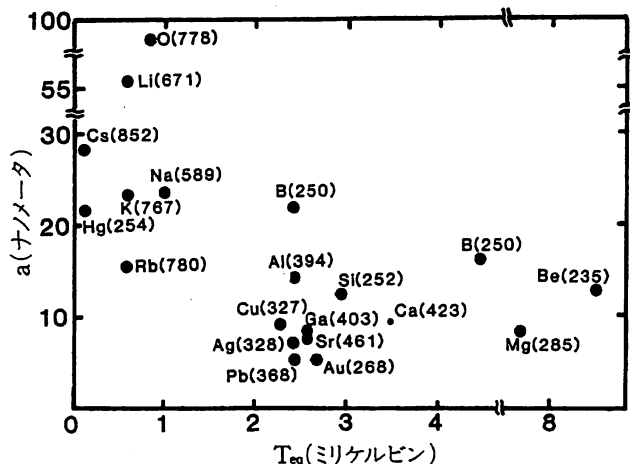


図13 一つの原子を捕獲する際のポテンシャル深さを表す等価温度 T_{eq} と光ファイバ先端曲率半径の最適値 a との関係の計算結果¹³⁾。図中の各原子の脇の () 内の数値は捕獲に必要な光波長 (単位; ナノメートル)。

ンデルワールス分子が形成される。すなわち、通常のファンデルワールス力により原子が光ファイバ先端に吸着されることのない。このことは光ファイバプローブが一つの原子を捕獲する「光ピンセット」をして働くことを意味する。」

図13にはそのための光ファイバ先端曲率半径の最適値、ポテンシャルの深さを表す等価温度、を各種原子について示してある¹³⁾。() 内の数値は原子に共鳴する光波長であり、実際にはこのような波長の光を各々の原子捕獲の際に使う。ポテンシャル深さを表す等価温度は数ミリケルビンであり、この値は小さい。しかし現在、通常の伝搬光を用いて真空容器中に浮遊する原子の熱運動を奪い、冷却した原子集団を作る技術（レーザ冷却と呼ばれる¹⁴⁾）が確立しており、等価温度は数マイクロケルビンに達している。そこでこのような予備冷却原子集団の内の1つの原子を上記光ファイバにより捕獲すればよい。

このようにして捕獲された原子を冷却結晶基板の上に光ファイバごと移動し、落下させれば原子は基板上に通常のファンデルワールス力またはその他の化学的相互作用によって吸着固定される。こうして単原子レベルの結晶成長、すなわち「1を扱う工学」が可能となると考えられるが、これも真空を扱う技術に他ならず、「0を制御する工学」の一種およびその応用といえる。

6. あとがき

物質に階層構造があると同様に真空にもいろいろな種類があることを指摘した。特に光に関連した真空の揺

らぎの場合、考えている領域の寸法によって、一見無関係の現象が統一的に議論できることを示した。これらの議論の最近の特徴は、単に理学的立場から現象の解析をするに留まらず、工学的な立場から新しい光や微小物質を創造する方向に向かっていることである。これらは半導体工学における新形発光素子、極微メモリ素子、さらには生命理工学、精密機械工学、などの分野の発展に大きく寄与すると考えられる。これらを実現するためにも光の制御（真空の制御）と原子の制御とを並行して行い、両者の成果が互いの進歩を促進させる必要がある。

従来の理学的常識では自然放出光発生確率の制御や一個の原子の運動状態の制御は不可能と信じられていた。しかし、工学の常套手段、すなわち高精度な「自動制御」と「極微加工」、を駆使するとこれらの常識を打破することができる。いわば「理学的な常識により推定されていた限界を打破する量子工学」(Quantum Technology Beyond the Scientific Limit)¹⁵⁾可能となる。それが標題にある「0を制御する工学」と言えよう。換言すれば「量子操作工学」(Quantum Manipulation Technology)となるが、真空はここで述べたような新しい光を創造する宝庫と考えられる。この光を使えば原子の新しい操作ができる。現在、このような工学を可能とする周辺技術が整備されつつある。我々も非力ながらこのような極限的な工学分野の実現をめざし努力したい。なお、本稿の内容に関し、より詳細な説明、参考文献などについては文献1), 16)などを参照されたい。

謝辞

貴重な御助言と御討論を賜った山梨大学工学部助教授堀裕和博士に感謝します。

〔文 献〕

1) 大津元一, コヒーレント光量子工学, 朝倉書店,

1990年, 第4章

- 2) A. Blaquiere: Comptes Rendus 26 (1962) 2929.
- 3) K. Yoshida, M. Kouogi, K. Nakagawa and M. Ohtsu: Proc. of the Int. Conf. on Noise in Physical Systems and 1/f Fluctuations, ed. by T. Musha, S. Sato and M. Yamamoto (Ohm-sha, Tokyo, 1991), (Nov. 24-27, 1991, Kyoto) 349
- 4) C. -H. Shin and M. Ohtsu: Opt. Lett. 15 (1990) 1455
- 5) M. Ohtsu, K. Nakagawa, M. Kouogi and W. Wang: Appl. Phys. Rev., to be published
- 6) D. J. Heinzen, J. J. Childs, J. F. Thomas and M. S. Feld: Phys. Rev. Lett. 58 (1987) 1320
- 7) Y. Yamamoto, S. Machida and G. Bjork: Phys. Rev. A, 44 (1991) 657
- 8) J. Jewell 博士 (AT & T ベル研究所, 1991) のご好意による
- 9) M. G. Raisen, R. J. Thompson, R. J. Brecha, H. J. Kimble and H. J. Carmichael: Phys. Rev. Lett. 64 (1989) 240
- 10) T. Pangaribuan, K. Yamada, S. Jiang, H. Ohsawa and M. Ohtsu: Jpn. J. Appl. Phys. 31 (1992) L1302
- 11) S. Jiang, H. Ohsawa, K. Yamada, T. Pangaribuan, M. Ohtsu, K. Imai and A. Ikai: Jpn. J. Appl. Phys. 31 (1992) 2282
- 12) H. Hori, S. Jiang, M. Ohtsu and H. Ohsawa: Proc. of the 18th Int. Quantum Electron. Conf., ed. by P. L. Knight, P. L. Kelley and Y. Yamamoto, (Institut fur Nachrichtentechnik der Tu Wien, Vienna, 1992) 48
- 13) M. Ohtsu: Proc. of OITDA Second International Forum on New Trends on Scanning Optical Microscopy, ed. by S. Minami (Optoelectronic Industry and Technology Development Association, Tokyo, 1992), (Jos. 8-10, 1992, Naha) 67
- 14) D. Sesko, C. F. Fan and C. E. Wieman: J. Opt. Soc. Am B 5 (1988) 1225
- 15) 大津元一: 電子情報通信学会, Vol. 75 (1992) 870
- 16) M. Ohtsu: Highly Coherent Semiconductor Lasers, (Artech House, Inc., Boston, 1992)

Quantum Optical Aspects on Single Atom Manipulation by a Photon STM Probe

Hirokazu Hori^a and Motoichi Ohtsu^b

^aFaculty of Engineering, Yamanashi University,
4-3-11 Takeda, Kofu 400, Japan

^bGraduate School at Nagatsuta, Tokyo Institute of Technology,
4259 Nagatsuta, Midori-ku, Yokohama 227, Japan

Abstract

We present a theoretical consideration on the nanometer-resolution photon scanning tunneling microscope (PSTM) from the view point of the quasi-static short-range electromagnetic interaction between microscopic objects. A similarity between particle tunneling and optical near-field problem is demonstrated by employing an intuitive Yukawa potential model describing localized evanescent field. We investigate the atomic interaction with localized evanescent field and propose a novel technique of single atom manipulation using a nanometric optical fiber-probe of PSTM.

1. INTRODUCTION

The photon scanning tunneling microscope (PSTM) is the optical analog of STM utilizing evanescent or tunneling photons [1-4]. The achievement of nanometer resolution, being far beyond the diffraction limit, was recently demonstrated on the PSTM image of bacteriophages T4, which was taken by using a sharpened optical fiber-probe [4-6]. This confirms that the PSTM technique opened a novel area of measurement and control of highly localized electromagnetic interaction between microscopic objects.

The fundamental process of the PSTM is described in terms of quasi-static short-range electromagnetic interaction between microscopic dielectric particles induced by laser irradiation. We present a simple quantum optical picture of the interaction by introducing virtual photons with nanometric Compton wavelength which corresponds to the size of the microscopic particles [6]. Although conventional treatments based on the boundary problem [7] or many-body electromagnetic interaction between small dielectric spheres [8] might be still valid in the nanometric region, the intuitive virtual photon model helps the understanding of the PSTM process in a generalized framework of the tunneling microscopes including the electron tunneling microscopes (STM), atomic force microscopes (AFM), and so on. It is emphasized that the tunneling process is, in general, associated with a mechanical action between microscopic sample and probe tip. Although it has not been observed yet in the case of PSTM, the tunneling of evanescent photons should exhibit mechanical force, due to the extraordinary large field momentum resulting from locality.

As the reversal process of the PSTM, a localized evanescent electromagnetic field will

be produced in the narrow vicinity of the PSTM probe-tip by the laser light propagating in the probe. This makes it possible to control the electromagnetic interaction in the nanometric scale. Among numbers of applications of this novel technique, it is especially interesting to study the atomic interaction with localized evanescent field because of several remarkable features which can not be achieved in the usual atomic interaction with propagating photons. We present a possibility of trapping a single atom from a very cold source by resonance tunneling of virtual photons from the probe-tip to atom [6].

2. PHOTON STM

The principle of operation of our PSTM system, employing a sharpened optical fiber-probe, is schematically shown in Fig. 1 (a). A microscopic sample is put on a cleaned surface of a prism which is irradiated by laser light with the incident angle of total internal

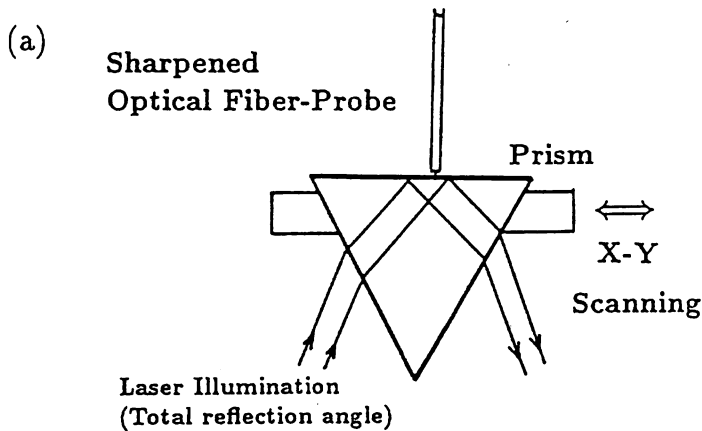
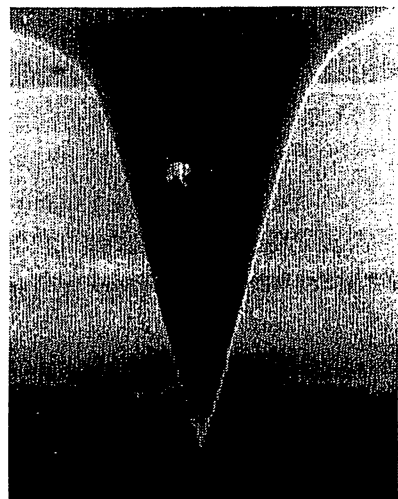
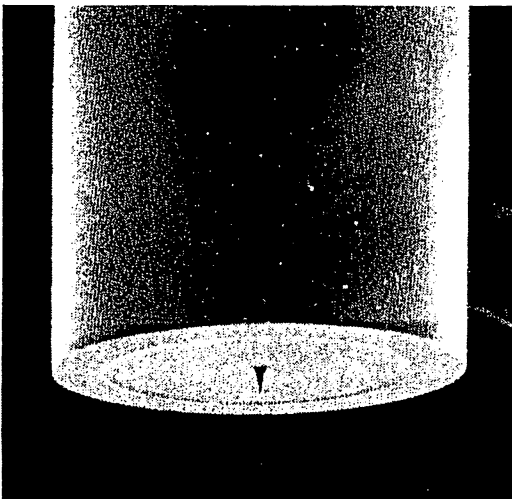


Fig. 1. The principle of PSTM operation (a), and the detailed profiles of the sharpened optical fiber-probes (b).

(b)



reflection. The sharpened optical fiber-probe picks up or scatters the evanescent photons localized in the vicinity of a microscopic sample into the propagating photons in the probe. The number of scattered photons are measured by a photo-detector on the other end of the optical fiber-probe, scanning the prism by using a piezoelectric transducer system. When the optical fiber-probe with its curvature radius of the extremity as small as the microscopic sample is employed, the efficiency of the scattering process depends strongly on the position of the probe-tip due to locality of the evanescent field. Mapping the number of scattered photons versus the relative position of the probe tip, with the aid of a micro-computer, one can obtain a topographical image of the microscopic sample as a PSTM picture.

The resolution, being far beyond the diffraction-limit, is determined only by the curvature radius of a sharpened fiber-probe tip. The merits of using the optical fiber-probe are the high efficiency of collecting scattered photons and the facility in reproducible production process. By the recent development of etching technique, we can easily produce the optical fiber-probes with tip curvature radius ~ 5 nm and conical angle of 20° [5]. Figure 1 (b) shows the detailed profile of a sharpened optical fiber-probe being made from a single-mode optical fiber with core diameter $3\mu\text{m}$. The curvature radius and conical angle of the tip are controlled by changing the condition for selective etching process, such as the concentration of impurities doped in the core of the optical fiber and the concentration of the etching chemical. By using one of these optical fiber-probes, we succeeded in obtaining a PSTM image of bacteriophages T4 with resolving power ~ 5 nm [4], by using 780 nm semiconductor laser.

3. INTERACTION PICTURE OF THE PSTM

It is confirmed from the PSTM experiment that the interaction between the microscopic sample and probe tip via evanescent electromagnetic field is localized in the narrow region determined by the scale of the probe tip. This meets the Heisenberg's uncertainty principle that, since the resolving power of the microscopes is determined by the shortest wavelength available in the measurement, the electromagnetic field with extraordinary large wave-vector, or momentum, is concerned with the PSTM measurement due to locality of the interaction. It is natural to describe the fundamental process of PSTM by a short-range quasi-static interaction via evanescent photons scattered from/to propagating photons in the material medium. Here the microscopic particles are the sample object and the probe tip, and the term "quasi-static" is used in the sense that the propagation or retardation effects can be neglected because of the short distance between the microscopic particles. A simple and intuitive picture of PSTM seems to be required for understanding the nature of the fundamental process in terms of the generalized framework of tunneling microscopes.

The minimal feature describing PSTM, the short-range quasi-static interaction, can be modeled simply by employing the idea of virtual photons with nanometric Compton wavelength, λ_C , and describing the field in terms of the Yukawa potential,

$$\phi(r) \propto \frac{e^{-r/\lambda_C}}{r}. \quad (1)$$

The virtual photon, therefore, has an effective mass due to the coupling of electromagnetic field to the fundamental excitations in the material medium. The model makes it possible to interpret the optical near-field problem as a particle tunneling through the effective

potential barrier between the gap of microscopic dielectrical particles. Compared with the surface plasmon near field microscope [9], the virtual photons employed here may be described in terms of polaritons representing the electromagnetic field coupled to the mechanical vibration in the dielectric medium via induced polarization.

In order to demonstrate the validity of virtual photon picture, the Yukawa potential model is applied for a calculation of evanescent field near a small circular aperture irradiated by propagating light with wavelength, λ , much larger than the aperture radius. Assuming the Compton wavelength of virtual photons equal to the aperture radius, the intensity distribution in the near-field region was estimated simply by taking the gradient of the potential given by integrating the contribution from small surface elements over the aperture using Yukawa potential, as shown in Fig. 2 (a). Figures 2 (b) and (c) show the numerical results for the aperture radius of $\lambda/50$; (b) the intensity distribution on the aperture axis and (c) in three dimensions, respectively. In Fig. 2 (b), the result from the Yukawa potential model (broken line) shows a good agreement with the numerical results (plots) given by Leviatan [7] based on the boundary problem.

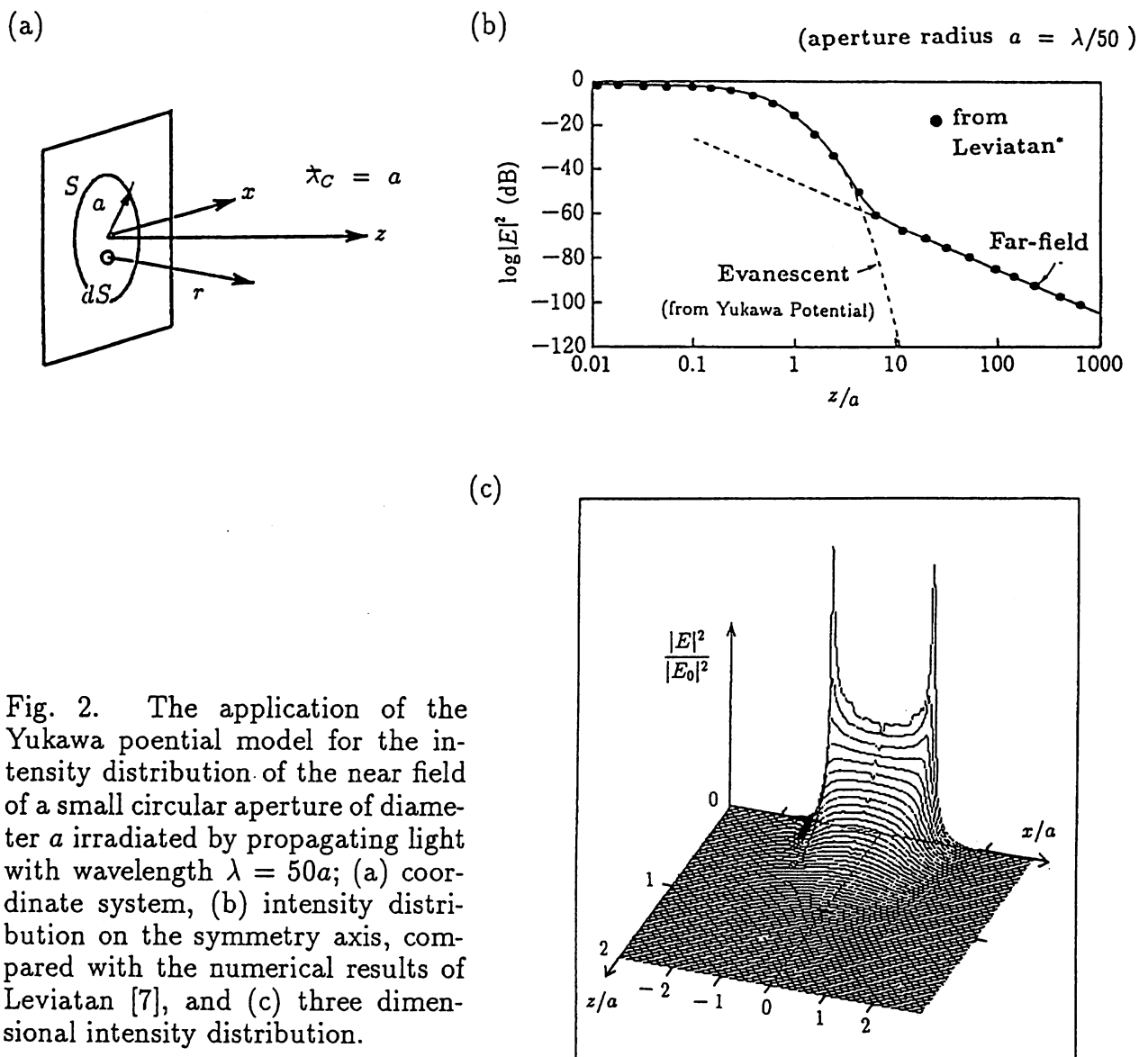


Fig. 2. The application of the Yukawa potential model for the intensity distribution of the near field of a small circular aperture of diameter a irradiated by propagating light with wavelength $\lambda = 50a$; (a) coordinate system, (b) intensity distribution on the symmetry axis, compared with the numerical results of Leviatan [7], and (c) three dimensional intensity distribution.

4. SINGLE ATOM MANIPULATION BY A PSTM PROBE

The resonance interaction of an atom with localized evanescent electromagnetic field will exhibit several remarkable features which cannot be obtained by using ordinary propagating light. First, an atom scattering evanescent photon into propagating photon via resonance absorption and spontaneous emission gets extremely large recoil momentum parallel to the probe-tip surface. The large momentum of the evanescent electromagnetic field is attributed to the mechanical distortion associated with the induced polarization in the dielectric material [10]. Second, the atom feels strong dipole force normal to the tip surface due to rapid decrease of the field intensity in the near-field region. These features altogether result in a mechanical interaction between the atom and the probe-tip, which is analogous to the inter-atomic van der Waals force. A novel technique of manipulating single atom can be realized by using the localized evanescent electromagnetic field produced in the vicinity of the nanometric PSTM probe-tip irradiated by the laser light propagating in the probe, as the reversal process of PSTM.

As a simple consideration on the possibility of single atom manipulation, let us assume that the fiber-probe tip is irradiated by laser light detuned to the red of atomic resonance, as shown in Fig. 3. An atom coming into the evanescent field resonantly absorbs the counterpropagating laser photon due to positive Doppler shift against the red detuning and spontaneously emits a propagating photon. By this process the atom is recoiled strongly

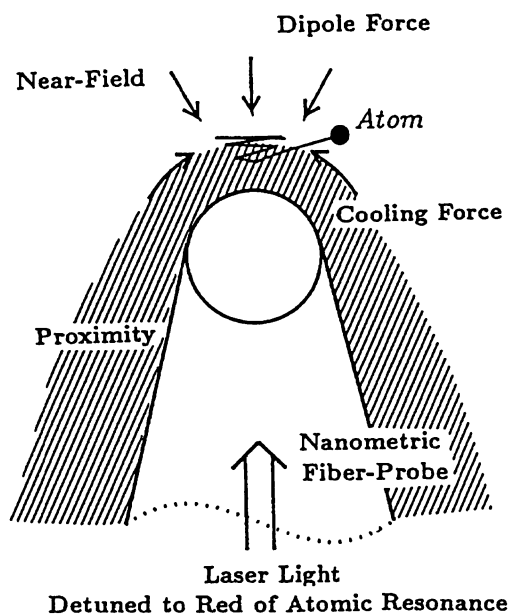


Fig. 3. The resonant interaction of an atom with the localized evanescent field produced at around the extremity of the nanometric optical fiber-probe by the laser light propagating in the probe.

in the direction parallel to the probe surface, since the absorbed momentum of the evanescent photon is much larger than the emitted momentum of the propagating photon, according to the Heisenberg's uncertainty principle. This acts as a cooling force until the momentum of the atom becomes comparable to the recoil momentum. Because of the spatial modulation of the field momentum in its direction, the cooling force accompanies the centrifugal component, which will be compensated by the strong dipole force [11] in the near-field region where the field intensity decreases exponentially. The balance of the centrifugal component of scattering force and the dipole attractive force produces a potential valley along the probe-tip surface. The atom will move back and forth in this po-

tential valley like a pinball trapping in the optical standing-wave. The trapping condition will be achieved when the cooled atomic motion is reversed by each recoil and such scattering occurs several times per passage of the proximity of the probe tip. This condition determines the curvature radius of the probe-tip and trapped atomic temperature.

As an example, in the case of the rubidium D₂-line, the trapping condition is satisfied by a fiber probe with the tip curvature radius ~ 15 nm, and the temperature of trapped atom will be ~ 80 μ K. The laser detuning is assumed to be 10 MHz to the red of the atomic resonance, being larger than the natural linewidth. Such atom may be manipulated from ~ 300 μ K source realized by a laser cooling technique, such as optical molasses [12]. In order to discuss the feasibility of single atom manipulation in detail, the quantum optical analysis of the atomic interaction with localized evanescent field should be required, because the process includes the spontaneous emission as a basic ingredient.

5. CONCLUSION

We have discussed the fundamental process of the PSTM from the view point of the quasi-static short-range electromagnetic interaction, introducing the Yukawa potential model. The model will be useful not only for understanding the PSTM process in terms of generalized framework of the tunneling microscope but also for practical purposes, such as an estimation of the PSTM resolution. This is because the model characterizes the spatial frequency of microscopic sample in terms of the Compton wavelength of the localized field.

Investigating the atomic interaction with localized evanescent field, we have proposed the novel technique of single atom manipulation. The study of the electromagnetic interaction localized in the nanometric region involves lots of interesting problems, concerned with mesoscopic problems, such as the photon localization or localization of the fundamental excitations, cavity QED, tunneling-time, and so on. The PSTM, as well as other types of tunneling microscopes, will serve as a useful technique for the experimental investigation of the novel area of physics.

6. REFERENCES

- 1 U. Dürig et al., *J. Appl. Phys.* **59** (1986) 3318.
- 2 E. Betzig et al., *Appl. Phys. Lett.* **51** (1987) 2088.
- 3 R. C. Reddick et al., *Phys. Rev. B* **39** (1989) 767.
- 4 S. Jiang et al., *Jpn. J. Appl. Phys.* **31** (1992) 2282.
- 5 T. Pangaribuan et al., *Jpn. J. Appl. Phys.* **31** (1992) L1302.
- 6 H. Hori et al., *Tech. Digest of 18th Int. Quantum Electronics Conf.* (1992, Vienna) 48.
- 7 Y. Leviatan, *J. Appl. Phys.* **60** (1986) 1577.
- 8 C. Girard and D. Courjon, *Phys. Rev. B* **40** (1990) 9340.
- 9 M. Specht et al., *Phys. Rev. Lett.* **68** (1992) 476.
- 10 J. P. Gordon, *Phys. Rev. A* **8** (1973) 14.
- 11 J. P. Gordon and A. Ashkin, *Phys. Rev. A* **21** (1980) 1606.
- 12 E. L. Raab et al., *Phys. Rev. Lett.* **59** (1987) 2631.

NANOMETER RESOLUTION PHOTON STM AND SINGLE ATOM MANIPULATION

M. OHTSU, S. JIANG, T. PANGARIBUAN, and M. KOZUMA
Interdisciplinary Graduate School
of Science and Engineering,
Tokyo Institute of Technology,
4259 Nagatsuta, Midori-ku, Yokohama 227, Japan

ABSTRACT. A photon STM was constructed by using a sharpened optical fiber with a radius of curvature of about 1 nm. Nanometer-resolution was achieved to measure biological and other kinds of samples with sub-micron structures. We also proposed a new method to trap a single neutral atom in the evanescent field localized near the fiber probe top.

1. INTRODUCTION

This paper reviews our recent activities on photon scanning tunneling microscopy (PSTM), and is composed of three parts. The first part describes the reliable fabrication technique of nanometric optical fiber probe. Several results of nanometer-resolution imaging are presented in the second part. The last part is to present a possibility of trapping a single neutral atom in the evanescent field emitted from the fiber probe.

2. FABRICATION TECHNIQUE OF FIBER PROBES

Based on the principle of the PSTM, the radius of curvature a and the cone angle θ of the probe, which is used to disturb and detect the evanescent light localized around small particles, must be as small as possible to obtain a high resolution and to avoid picking up low

spatial Fourier frequency components of the evanescent light generated from the substrate. We fabricated an optical fiber probe by using selective chemical etching in a buffered HF solution, whose volume composition is represented as $\text{NH}_4\text{F} : \text{HF} : \text{H}_2\text{O} = X : 1 : 1$. As shown in Figs.1(a) and (b), the minimum of θ realized so far is smaller than 15° , and a was estimated to be about 1 nm.

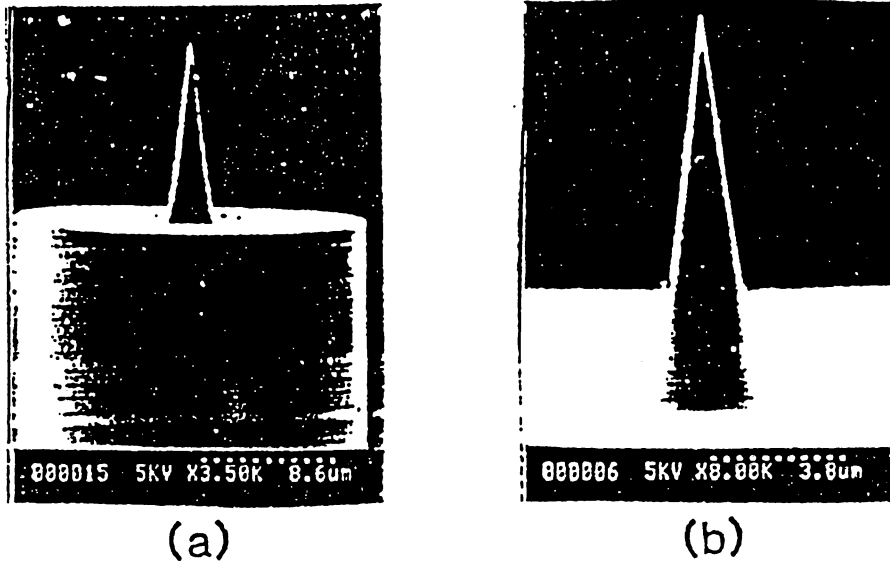


Fig.1 SEM images of the sharpened fiber.(a)and(b) are the images with different magnifications.

The θ can be varied by controlling the compositions of the optical fiber core, cladding, and the buffered HF solution. It was found from the experimental results that θ was a monotonously decreasing function of the X for $X < 6$ and tends to a stationary value for $X > 6$. The stationary values of θ were 100° and 20° for the fibers composed of SiO_2 cladding and Ge-doped SiO_2 core with doping ratios of 3.6 mol% and 23 mol%, respectively [1]. For these fibers, the corresponding normalized refractive index differences between core and cladding were 0.36% and 2.3%, respectively. The probe with the minimum θ shown by Fig. 1 was realized with a special fiber composed of a Ge-doped core and a F-doped cladding, whose normalized refractive index difference was 2.9%. For all fibers, the standard deviation of the cone angle $\Delta\theta$ was kept within 0.5° , which means that the etching process is of high reproducibility. The high reproducibility of our fiber probe fabrication is also demonstrated by Fig.2, in which cone angle and height

differences between two cores of a dual-core fiber are smaller than 0.2° and 20 nm respectively.

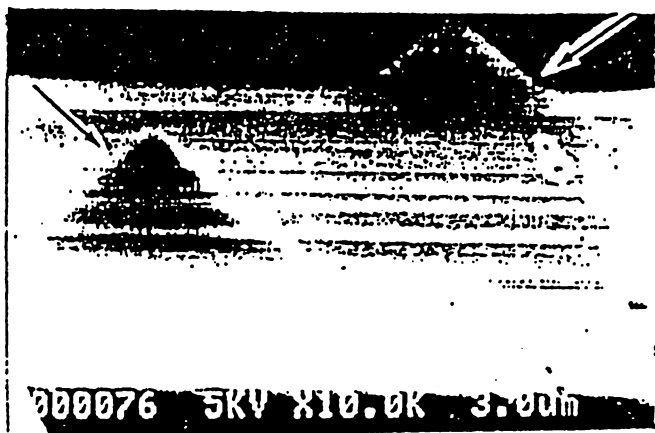


Fig.2 The SEM picture of the sharpened dual-core fiber. The core diameter and separation between two cores are $6\mu\text{m}$ and $40\mu\text{m}$, respectively.

3. EXPERIMENTS OF NANOMETER-RESOLUTION IMAGING

A power-controlled $0.8\mu\text{m}$ wavelength AlGaAs laser was used as a light source in order to construct a reliable and compact system and to take advantage of its wide-band power modulation capability for the fast phase sensitive detection. Direct power modulation was employed for the phase sensitive detection in measuring the evanescent light power which was picked up by the fiber probe and detected by a photo-multiplier. The sample was fixed on an optically flat glass prism to which the laser beam was incident under total reflection condition. A PZT-scanner used for conventional STM or AFM was imported to the present system.

Figure 3(a) shows the exponential decreases of the picked up evanescent light power measured by increasing the probe-prism separation d . 0 nm-point of d was determined by the picked-up power variation as the probe is moved close to the prism. As the probe contacts with the prism, the picked-up power which increases with the increasing of the voltage applied to the PZT will not grow up further. We define such a point as the 0 nm-point for determination of the absolute d . Although the picked up power was on the order of pico-watts, it was high enough for phase sensitive detection. The relationship between θ and the picked up power is shown in Fig.3(b) measured by keeping d constant. From this figure, it can be seen that the picked up power is proportional to $\exp\{-1/\sin(\theta/2)\}$. This proportionality is in

agreement with the theoretically estimated dependence based on the virtual photon model of the localized evanescent field.[2]

We also measured three dimensional profiles by imaging experiments in a constant height mode. The images were: (1) A 9 nm thick SiO₂ thin film[3], (2) a moth-eye optical disk with 300 nm diameter and 80 nm depth pits[4], (3) 80 nm diameter latex particles which were fixed on a glass substrate(see Fig.4) [3], and (4) uncoated bacteriophages T4 (see Figs.5(a) and (b)) [4].

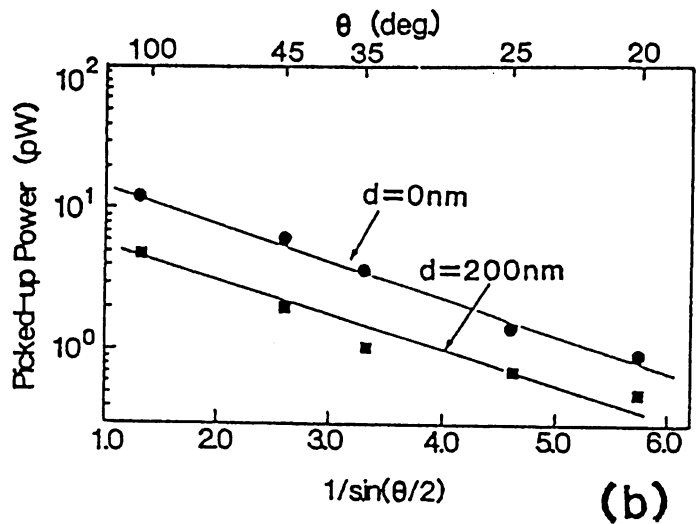
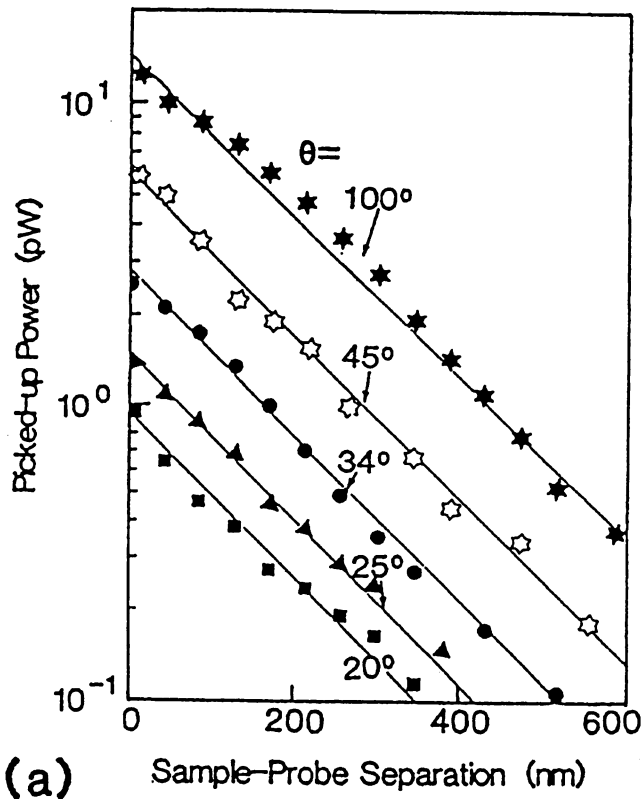


Fig.3 (a) Measured relationship between probe-prism separation d and picked up evanescent light power. The cone angle θ of the fiber probe was used as a parameter. (b) The relationship between θ and the picked up evanescent light power. d was used as a parameter.

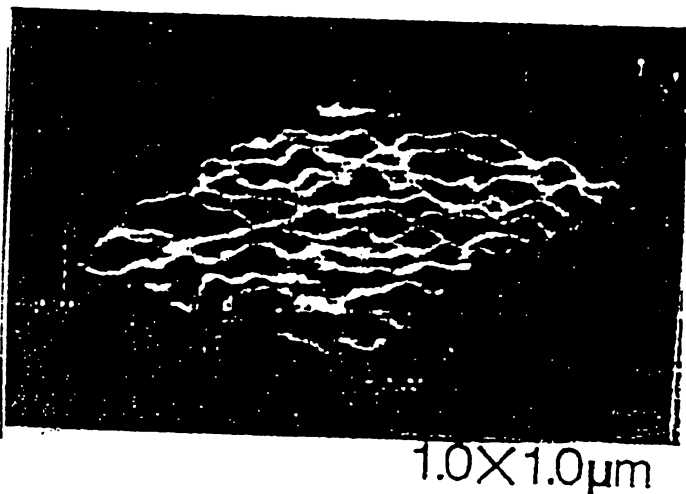


Fig.4 Images of latex particles with diameters of 80nm, which are densely fixed on a prism. The scanning range was $1.0 \mu\text{m} \times 1.0 \mu\text{m}$ [3].

Although the fully quantitative estimation of the resolution has not yet been completed, normal resolution limited by the signal to noise ratio of the PSTM system. (seeing the details in ref.4) was estimated to be 0.5 nm. The lateral resolution given in ref.4 was limited by the pixel size, and it could be improved by optimizing the probe scanning parameter. More fundamental lateral resolution limited by the radius of the curvature of the fiber probe was estimated to be 2 nm. As a quantitative measure to estimate the lateral resolution limited by the radius of the curvature of the fiber probe, we can use the 3-dB spatial frequency cut-off of the picked up evanescent power spectral density.

It should be noted that the signal-to-noise ratio of the evanescent power detection was still 40 dB lower than the detector-noise-limited value[4]. Careful acoustic shielding could improve the signal-to-noise ratio which was mainly limited by the acoustic vibration of the fiber probe, and thus, a resolution improvement up to the atomic level can be expected.

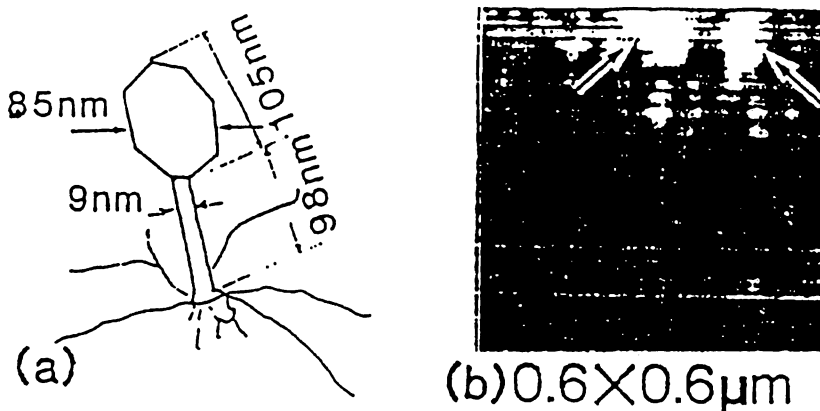


Fig.5 Image of bacteriophage T4[4].

- (a) The structure of T4.
- (b) The image taken by using the fiber probe with a cone angle of 25° . The scanning range was $0.6 \mu\text{m} \times 0.6 \mu\text{m}$.

4. POSSIBILITY OF A SINGLE NEUTRAL ATOM TRAP

Considering a reversal process of the PSTM, we found a possibility of trapping a single neutral atom by an evanescent light which is localized around the nanometric top of a fiber probe[5], although it is impossible if one uses a conventional propagating light[6]. Based on our intuitive virtual photon model, this trapping is

theoretically possible because of the intrinsic properties of the evanescent light localized around the top of the fiber probe, i.e., the evanescent light has a high power density, high spatial power variation, and a large tangential component of the wave vector (for a wavelength λ , it is (λ/a) times larger than that of a conventional propagating light). In other words, it is possible because the photon tunneling process, in general, is associated with a mechanical action and mechanical force between the atom and probe due to the extraordinary large field momentum resulting from its locality.

Figure 6 shows the principle of this trapping. A fiber probe, coated with a metallic thin film except on the top whose radius is smaller than the laser wavelength, is used to emit the evanescent light. An atom coming into this evanescent field resonantly absorbs the counterpropagating laser photon. This is due to a large positive Doppler shift induced by a large tangential component of the evanescent wave vector. After this absorption, the atom spontaneously emits a propagating photon. Since the momentum absorbed by the evanescent photon is much larger than that of the emitted propagating photon, the atom loses its kinetic energy very quickly and is cooled. This large absorbed momentum is attributed to the mechanical distortion associated with the induced polarization in the nanometric fiber probe top.

As a result of this laser cooling process, the atom's momentum becomes comparable to that of the evanescent photon, i.e., the final thermal velocity is inversely

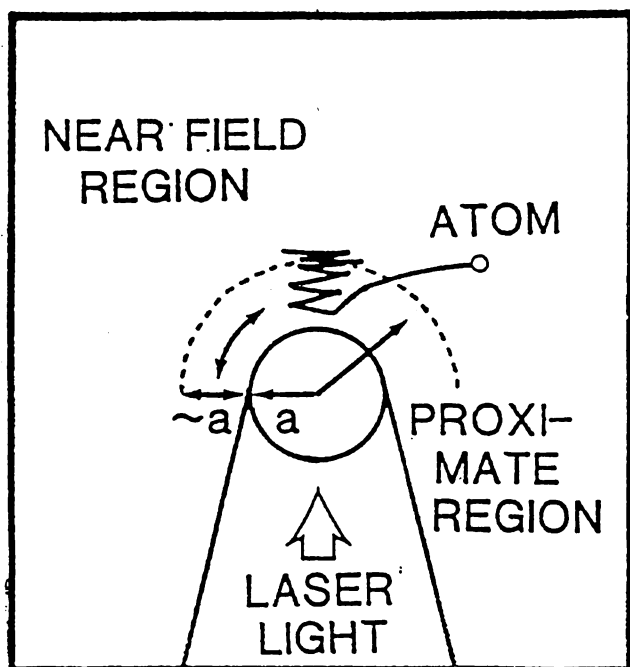


Fig.6 Illustration of the principle of a single neutral atom trapping.

proportional to the curvature radius of the fiber probe, and the atom exhibits a Brownian motion with this velocity along the probe surface. Although the atom is subjected to a centrifugal force and thus being pushed out from the field by this Brownian motion, it also feels an attractive force due to the dipole force induced by the rapidly decreasing power along the normal direction if the laser frequency is red-tuned to the atomic resonance frequency. These features together result in a mechanical interaction between the atom and the probe, which is analogous to an inter-atomic Van der Waals force. As a result of the balance between these two forces, the atom is trapped because it sees a potential minimum at the boundary between the proximate and near-field regions. In other words, this trapping is equivalent to the formation of a diatomic quasi Van der Waals molecule between this atom and an atom at the top of the fiber probe, where the exchange of virtual photons between the two atoms corresponds to the Van der Waals force. Only one atom will be trapped because of the velocity-selective cooling process and of the repulsive force between the atoms in the nanometric volume. Detection of trapped atom is possible by detecting the fluorescence emitted from the atom in the cooling process.

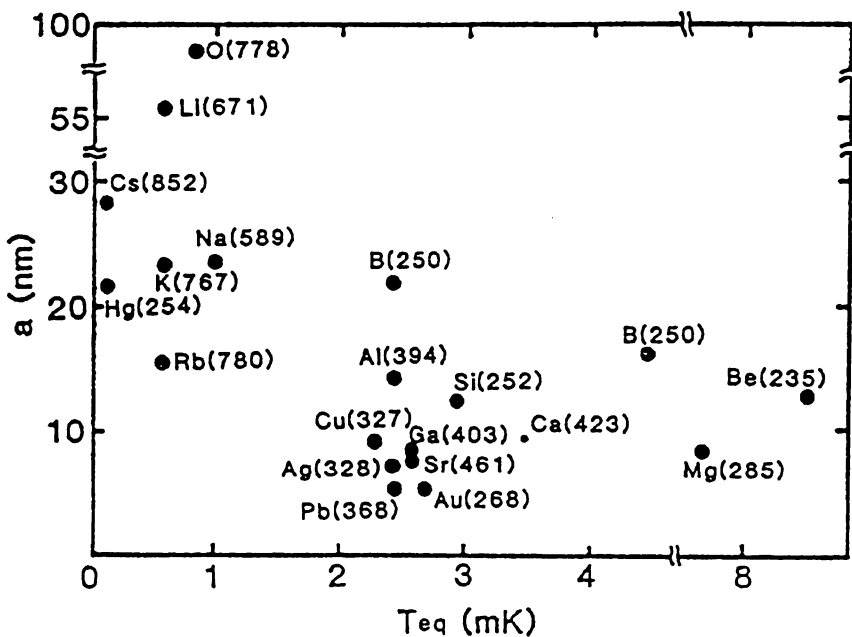


Fig.7 Calculated relationship between the equivalent temperature of the potential depth and the optimum radius of the curvature of the fiber probe. The number attached to each closed circle represents the resonance wavelength (in nanometer unit) of the atomic transition.

Based on the principle of the trapping mentioned above, the atom's momentum has to be equal to the recoil momentum for the purpose of trapping a single atom on the top of the fiber probe. By this requirement, the relation between the equivalent temperature of the potential depth of the trap and the optimum curvature radius of the fiber probe can be calculated. Figure 7 shows the relationship between the equivalent temperature of the potential depth and the optimum radius of curvature of the fiber probe for a variety of atoms. The number attached to each closed circle represents the resonance wavelength (in nanometer unit) of the atomic transition. It can be seen from this figure that the equivalent temperature corresponding to the potential depth is as shallow as several mK for the saturation power of each atomic transition. However, a conventional technique of optical molasses[7] can be employed as a pre-cooling technique to prepare an ultra-cold atomic source in a high vacuum by reducing the equivalent temperature of the molasses atoms to $1 \mu\text{K}$ or even lower. Therefore, it can be expected that an atom can be trapped by this fiber probe by catching the atom falling from this cold molasses. By using this trapping, an optical tweezer for single neutral atoms can be realized. Furthermore, if the trapped atom is brought to the surface of a cold substrate by translating the fiber probe and is accelerated by tuning the laser frequency to the blue, the atom can be fixed at a certain place on the cold substrate by Van der Waals force or other chemical binding forces. By this process, a single atom-level crystal growth is expected. For precise red- and blue-tunings within the accuracy of 1 MHz, coherent and tunable short-wavelength light sources are required. Such sources can be realized by using several semiconductor lasers, LD-pumped solid state lasers, and nonlinear optical crystals. For example, a Peta-Hz tunable range coherent optical frequency sweep generator has been developed by employing semiconductor lasers, high gain and wide bandwidth frequency control techniques, optical phase locking, and nonlinear optical frequency conversions[8].

5. CONCLUSION

By using a sharpened optical fiber with the radius of

curvature of about 1 nm, a photon STM was constructed and a nanometer-resolution imaging was achieved for the biological and other kinds of sub-micron samples. A novel method for trapping a single neutral atom was proposed by using the light pressure of the evanescent light localized around the fiber probe top. For further developments of photon scanning tunneling microscopy and atomic manipulation, careful studies on the concept of massive photon(i.e., the photon interacting with material,), and quantum optical effects (e.g., photon localization, cavity quantum electrodynamics), should be necessary.

REFERENCES

- [1] Pangaribuan, T., Yamada K., Jiang, S., Ohsawa, H. and Ohtsu, M.(1992) 'Reproducible Fabrication Technique of Nanometric Tip Diameter Fiber Probe for Photon Scanning Tunneling Microscope', Jpn. J. Appl. Phys., 31, L1302-L1304
- [2] Hori,H., 'Quantum optical picture of photon STM and proposal of single atom manipulation', the paper appearing in this proceeding
- [3] Jiang, S., Tomita, N., Ohsawa, H. and Ohtsu, M. (1991) 'A Photon Scanning Tunneling Microscope Using an AlGaAs Laser', Jpn. J. Appl. Phys., 30, 2107-2111
- [4] Jiang, S., Ohsawa, H., Yamada, K., Pangaribuan, T., Ohtsu, M., Imai, K. and Ikai, A. (1992) 'Nanometric Scale Biosample Observation Using a Photon Scanning Tunneling Microscope', Jpn. J. Appl. Phys., 31, 2282-2287
- [5] Hori, H., Jiang, S., Ohtsu, M. and Ohsawa, H (1991) 'A Nanometer-Resolution Photon Scanning Tunneling Microscope and Proposal of Single Atom Manipulation', Tech. Digest of the 18th International Quantum Electronics Conference (June 14-19, Vienna) pp.48-49
- [6] Lett, P.D., Phillips, W.D., Rolston, S.L., Tanner, C.E., Watts, R.N., and Westbrook, C.I., (1989), 'Optical molasses', J.Opt. Soc.Am. B, 6, 2084-2107
- [7] Lett, P.D., Watts, R.N., Westbrook, C.I., Phillips, W.D., Gould, P.L. and Metcalf, H.J (1988), 'Observation of Atoms Laser Cooled Below the Doppler Limit', Phys. Rev. Lett., 61, 169-172
- [8] Ohtsu, M. (1992) Highly Coherent Semiconductor Lasers, Artech House, Inc., Boston

tip, where the probe tip can be regarded as a set of dielectric spheres stacked one upon another. Because of the locality of the evanescent field, the interaction is considered to be short-ranged and quasi-static in the sense that retardation effects are not important. This feature makes it possible to describe the localized evanescent field by using the Yukawa potential, $\phi(r) \propto \exp(-r/\lambda_{\text{comp}})/r$, where λ_{comp} is the Compton wavelength characterizing the interaction range. For the evanescent field around a small circular aperture, we have obtained the field distribution by setting λ_{comp} equal to the aperture radius,³ which is consistent with the numerical results based on the conventional boundary problem.⁴

Since Yukawa potential characterizes the interaction by means of quanta having effective mass $mc = \hbar/\lambda_{\text{comp}}$, the present quasi-static short-range electromagnetic interaction can be described as the exchange of virtual photons with an effective mass. This picture corresponds to the fact that the evanescent photon localized in the volume a^3 has an extraordinary large momentum ($\sim \hbar/a$) due to Heisenberg's uncertainty. Therefore it can be assumed that the Compton wavelength is equal to the radius for the case of the evanescent field produced by a dielectric sphere. Also, the momentum conservation for the exchange of virtual photons allows us to assume that

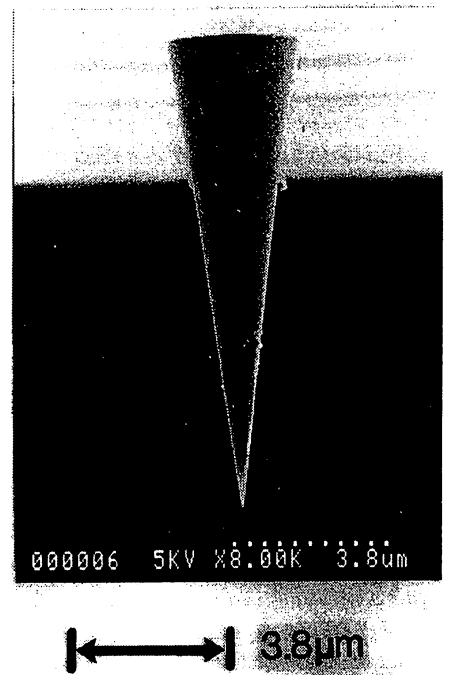
QThH7

Analysis and experimental evaluation of a localized evanescent field by using Yukawa potential

M. Kozuma, S. Jiang, T. Pangaribuan, M. Ohtsu, H. Hori,* *Graduate School at Nagatsuta, Tokyo Institute of Technology, 4259 Nagatsuta, Midori-ku, Yokohama 227, Japan*

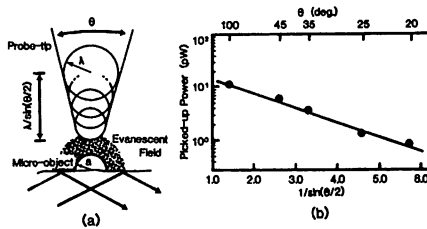
Progress in the selective-etching technique for sharpening an optical-fiber probe (Fig. 1)¹ has brought about the achievement of nanometer resolution in the photon scanning tunneling microscope (photon STM).² This confirms that the evanescent field mediating the object-probe interaction is highly localized in a volume much smaller than λ ,³ where λ is the optical wavelength. We present an intuitive theoretical model for the photon STM process in terms of the short-range quasi-static interaction described by the Yukawa potential.

Figure 2(a) shows schematically the interaction between a microscopic dielectric object with radius a ($\ll \lambda$) and the probe



QThH7 Fig. 1. SEM image of a sharpened optical fiber-probe tip with a cone angle of 15° that was fabricated by selective chemical etching.

THURSDAY

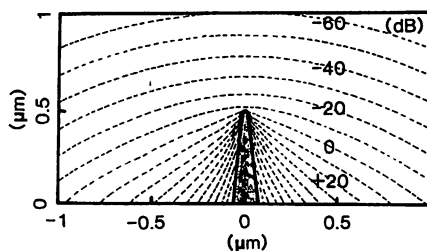


QThH7 Fig. 2. Model for describing the quasi-static short-range interaction between a microscopic object and the probe tip, along with the experimental result. (a) Model of the fundamental process of the photon STM. (b) Efficiency of picking up an evanescent field by a probe tip with a cone angle of θ in the case of measuring an optically flat substrate.

makes it easy to understand the photon STM process in a generalized framework of the tunneling microscopes that includes the STM and the atomic-force microscope.

1. T. Pangaribuan *et al.*, *Jpn. J. Appl. Phys.* **31**, L1302 (1992).
2. S. Jiang *et al.*, *Jpn. J. Appl. Phys.* **31**, 2282 (1992).
3. H. Hori *et al.*, in *Technical Digest of 18th International Quantum Electronics Conference*, Vienna, 1992, p. 48.
4. Y. Leviatan, *J. Appl. Phys.* **60**, 1577 (1986).

**Faculty of Engineering, Yamanashi University, 4-3-11 Takeda, Kofu 400, Japan*



QThH7 Fig. 3. Numerical result of the intensity distribution of the evanescent field around the optical fiber-probe tip with a tip curvature of 5 nm and a cone angle of 15° .

the evanescent field around the micro-object interacts with one of the dielectric spheres of a radius of λ_{comp} in the probe tip.

Since λ_{comp} of the evanescent field on the optically flat substrate is nearly equal to λ , the evanescent field couples most efficiently with the dielectric sphere of a radius of λ in the probe. Therefore it is expected that the efficiency of picking up the evanescent field by a probe tip with a cone angle of θ is proportional to $1/\sin(\theta/2)$, which was experimentally confirmed, as is shown in Fig. 2(b). This result supports the validity of our theoretical assumptions. Fig. 3 shows a numerical result for the field distribution around the probe tip irradiated by laser light propagating inside the fiber probe calculated by this model.

In summary, the present model describes intuitively the quasi-static short-range electromagnetic interaction between microparticles by using the concept of virtual photon tunneling. Such a method also